1978

Prediction of laminar and turbulent flow heat transfer in annular passages

Mujeeb Rehman Malik
Iowa State University

Prediction of laminar and turbulent flow heat transfer in annular passages

by

Mujeeb Rehman Malik

A Dissertation Submitted to the
Graduate Faculty in Partial Fulfillment of
The Requirements for the Degree of
DOCTOR OF PHILOSOPHY

Major: Mechanical Engineering

Approved:

Signature was redacted for privacy.

In Charge of Major Work

Signature was redacted for privacy.

For the Major Department

Signature was redacted for privacy.

For the Graduate College

Iowa State University
Ames, Iowa

1978

TABLE OF CONTENTS

LIST OF TABLES

LIST OF FIGURES

Page

Page

NOMENCLATURE

a	function appearing in model, Eq. (3.8); also exponent of the power law for specific heat
a_1, a_2	empirical constants or functions
A	channel cross sectional area, $\pi(r_2^2 - r_1^2)$
A_1, A_2, A_3	defined in Eqs. (D.5-D.6)
A^+	damping constant for velocity fluctuations
b	function appearing in model, Eq. (3.8)
B	log law constant
B^+	damping constant for temperature fluctuations
c	exponent of wall-to-inlet temperature ratio used to correlate Nusselt number
C_1, C_2, C_D, C_μ	empirical constants or functions
C_{f_w}	wall skin-friction coefficient; see Eq. (2.73)
C_f	overall skin-friction coefficient for the annulus, see Eq. (2.74)
C_m	constant for overall mass conservation
C_p	specific heat
d	height of a parallel wall duct
D_1, D_2	viscous dissipation functions
D_h	hydraulic diameter, $2(r_2 - r_1)$
e	instantaneous value of any quantity
E	Eckert number; see page 32
f	an arbitrary function
f_1	function appearing in Eq. (2.16)

f_p	friction factor; see Eq. (1.4)
f_x	body force in x-direction
f_y	body force in y-direction
F_x	dimensionless body force in x-direction
g	acceleration due to gravity
Gr	Grashof number; see Eq. (4.3).
h	heat transfer coefficient; see Eq. (2.85)
H	enthalpy
H	shape factor, δ^*/θ
k	turbulence kinetic energy per unit mass
K	see Eq. (1.5)
ℓ	mixing length
ℓ_i	mixing length in the wall regions
ℓ_o	mixing length in the outer regions of the shear layers
$\overline{\ell}_o$	average of the outer region mixing lengths
L	turbulent length scale
L*	relaxation length, $C_2 u_m \delta/\overline{u}_\tau$
$\dot{m}$	mass flow rate
n_k	coefficient for diffusion of k
n_T	coefficient for diffusion of heat
n_u	coefficient for momentum diffusion
N	equals (NY+1)
N_k	dimensionless coefficient for diffusion of k
N_T	dimensionless coefficient for diffusion of heat
N_u	dimensionless coefficient for momentum diffusion

N_ϕ	coefficient for diffusion of ϕ
NY	number of Y-grid spacings
p	static pressure
p^+	pressure defect, $(p_0-p)/\rho u_0^2$
P	dimensionless static pressure
Pe	Peclet number, Re Pr
Pr	molecular Prandtl number, $\mu C_p/\lambda$
Pr_k	Prandtl number for the diffusion of k
Pr_T	Prandtl number for turbulent diffusion of heat
PSA,PSB,PSC,PSD PTA,PTB,PTC,PTD	} defined in Appendix E
$\dot{q}$	heat flux
$\dot{Q}$	dimensionless heat flux
r	radial coordinate
r*	radius ratio, r_1/r_2
r_h	hydraulic radius, (r_2-r_1)
r_w^+	dimensionless radius, $r_w u_{\tau_w}/\nu$
R	dimensionless radial coordinate
R_g	gas constant
R_h	dimensionless hydraulic radius
Ra	Rayleigh number; see Eq. (4.2)
Re	Reynolds number based on D_h, $\rho u_b D_h/\mu$
Re_x	Reynolds based on x, $\rho u_b x/\mu$
Re_θ	Reynolds number based on θ, $\rho u_b \theta/\mu$
Re^*	unit Reynolds number, u_m/ν_m

RS	ratio of the successive cross stream spacings near the inner wall
RT	ratio of the successive cross stream spacings near the outer wall
s	guessed value of inner wall shear stress used in the iterative shooting method
S	source term appearing in the model, Eq. (3.8)
$\bar{S}$	finite-difference representation of source term
S_ℓ	"actual" shear layer thickness, see Fig. 2.4
t	time
t_o	reference time
Δt	increment in time
T	absolute temperature
T*	dimensionless temperature
u	axial velocity
u_τ	friction velocity, $\sqrt{\tau_w/\rho}$
u^+	dimensionless velocity, u/u_τ
$\bar{u}_\tau$	characteristic turbulence velocity
U	dimensionless axial velocity
v	radial velocity
$\tilde{v}$	equals $(\bar{\rho}\bar{v}+\overline{\rho' v'})/\bar{\rho}$
v_L	turbulent transport velocity
v_T	characteristic velocity of turbulence, $C_\mu k^{1/2}$
w	circumferential velocity component
x	coordinate along the annulus

x^+	dimensionless distance along the annulus, $x/D_h RePr$
X	dimensionless coordinate along the annulus
Δx_+	$X^{m+1}-X^m$
ΔX_-	X^m-X^{m-1}
y	coordinate normal to the inner wall, $r-r_1$
y_w	distance from the wall, $\lvert r-r_w \rvert$
y_w^+	dimensionless distance from the wall, $y_w u_{\tau_w}/\nu$
Y	dimensionless coordinate normal to the inner wall, $R-R_1$
ΔY_+	$Y_{j+1}-Y_j$
ΔY_-	Y_j-Y_{j-1}
Z_1, Z_2, Z_3, Z_4	constants

Greek symbols:

α	function appearing in Eq. (2.56)
β	coefficient of thermal expansion, $-\frac{1}{\rho}\frac{\partial \rho}{\partial T}\Big\rvert_p$
γ	intermittency factor
δ	boundary layer thickness
δ_{995}	boundary layer thickness defined such that $u(x,\delta) = 0.995\ u_m$
δ^*	displacement thickness
δ_1^*	displacement thickness for the inner wall; see Eq. (2.75)
δ_2^*	displacement thickness for the outer wall; see Eq. (2.76)
δ_k^*	kinematic displacement thickness
Γ	function appearing in Eq. (3.23)

Δ	a measure of extent of transition; see Eq. (2.62)
ε	dissipation rate of turbulence kinetic energy
η	function appearing in Eq. (3.24)
θ	momentum thickness
θ_1	momentum thickness for the inner wall; see Eq. (2.77)
θ_2	momentum thickness for the outer wall; see Eq. (2.78)
λ	thermal conductivity
λ_T	turbulent conductivity
μ	dynamic viscosity
μ_T	turbulent viscosity
ν	kinematic viscosity
ξ	defined in Eq. (2.61)
Π	transformed temperature used in fluid property relations
ρ	density
σ	iteration number
τ	shear stress
ψ	defined in Eq. (A.2)
ϕ	model dependent variable; represents U, T* or $\hat{k}$
$\overline{\phi}$	space-averaged value of ϕ
χ	velocity at the outer wall predicted by the iterative shooting method
Ω	function appearing in Eq. (3.24)

Subscripts:

b	bulk conditions
c	corresponds to the value of a variable in inviscid core region
e	entrance value
fd	fully developed
j	mesh index corresponding to Y
m	refers to radius of maximum velocity
o	refers to radius of zero shear
tr	transition initiation point
t	transition completion point
w	refers to wall value; w = 1,2 for the inner and outer walls respectively
0	refers to bulk value at the inlet
∞	asymptotic value

Superscripts:

m	mesh index corresponding to X
$(\bar{})$	denotes time mean quantity
$(\,)'$	denotes fluctuation component of a quantity
$(\hat{})$	dimensionless quantity

I. INTRODUCTION

A. The Problem

The problem considered in the present study is that of the flow of a Newtonian fluid in an annular passage (Fig. 1.1) whereby heat may be supplied or removed from either or both walls of the passage.

Annular geometries are found in many important engineering applications. Fuel assemblies in nuclear reactors are one such application since annular test sections are often used to evaluate the heat transfer performance of various types of fuel elements. The differences in configuration in this case are often accounted for by use of Hall's transformation [1]. Even when the fuel elements consist of a bundle of rods, it has been shown by Sutherland [2] that the flow around each rod can be approximated as annular flow provided that the pitch/diameter ratio is greater than 1.1 and that there are at least 20 rods per bundle. In addition, the poison rods (which are subjected to high heat flux due to neutron absorption) have annular flow around them since they are contained in guide tubes which form annuli. Other applications of annuli are found in some propulsion systems and in many areas of the thermal process and other industries which utilize fluid flow equipment. In these applications, equipment is often designed to operate in the turbulent flow regime, however, it is possible that laminar flow be employed at low circulation rates, at low power operation, or obtained unintentionally following an accident.

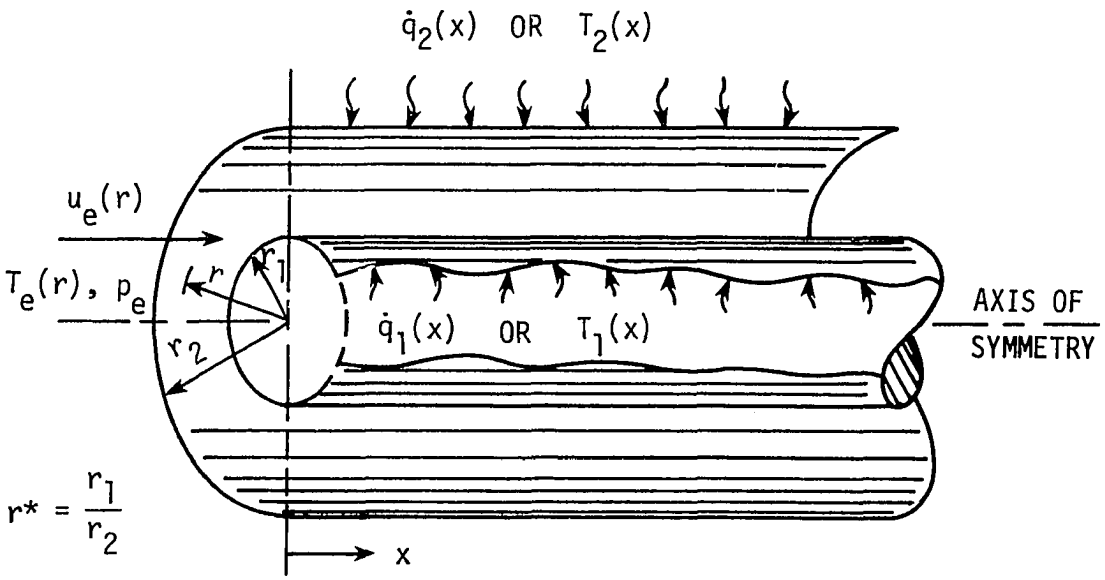

Fig. 1.1. A concentric annular passage

Because of the high temperatures involved in many of these applications, property variations may greatly influence the temperature and velocity distributions. In many situations, predictions based on constant property assumptions do not yield sufficiently accurate results for design purposes. Few, if any, variable property analyses or prediction methods have been proposed to date which appear capable of reliably and accurately treating the variety of possible hydrodynamic and thermal boundary conditions which occur in annular flows.

In the limiting cases of very small and very large radius ratios ($r^* \to 0$ and $r^* \to 1$, respectively), the annular geometry is reduced to the circular pipe and parallel plate channel, respectively. However, in general, annular flow is characterized by markedly asymmetric distribution of the flow parameters. This alone provides enough motivation for a researcher to study this somewhat complicated geometry since several features of the flow structure remain concealed in simple duct flows by virtue of symmetry.

In the present study, a finite-difference method is developed for the prediction of laminar and turbulent heat transfer in straight annular passages whereby the governing partial differential equations for conservation of mass, momentum, and energy are solved numerically. Although this type of computational approach has been used for a number of years [3-5], few definitive studies have been noted (particularly for turbulent flows) whereby predictions have been compared with experimental data for flows in the annular geometry with

heat transfer. The lack of well-tested prediction methods may be partly attributed to the difficulties associated with accurately modeling the turbulent transport mechanism in asymmetric flows where thermal boundary conditions force temperature and velocity profiles to be quite dissimilar. In any event, it would appear unwise to assume that prediction methods and turbulence models applicable to pipe flows would also be satisfactory for the annular geometry without careful verification.

B. Previous Studies in Annular Passages

A brief review of the earlier studies made for laminar and turbulent flow heat transfer is given below.

1. Laminar flow and heat transfer

a. Theoretical work Numerous theoretical studies have been made for flow and heat transfer in annular passages; most of these assumed that the fluid properties were constant. Lamb [6] was the first to solve the hydrodynamic problem to obtain an analytical expression for the fully developed velocity profile. The first known analytical attempt to solve the annulus heat transfer problem was made by Jakob and Rees [7]. For thermally developed flow they were able to integrate the energy equation directly for constant wall heat flux at the inner wall with the outer wall insulated.

Reynolds et al. [8] generalized the problem of constant property heat transfer in annular passages for hydrodynamically developed flow.

They suggested that solutions to problems having rather complex thermal boundary conditions can be obtained just by superimposing a variety of simpler solutions. Four kinds of fundamental solutions were considered necessary to handle most types of boundary conditions. The boundary conditions for these solutions are

1. Fundamental solution of the first kind

   Wall 1 - Uniform wall temperature with a step change occurring at the start of heating.

   Wall 2 - Maintained at inlet temperature.

2. Fundamental solution of the second kind

   Wall 1 - Uniform wall heat flux.

   Wall 2 - Insulated.

3. Fundamental solution of the third kind

   Wall 1 - Uniform wall temperature with a step change occurring at the start of heating.

   Wall 2 - Insulated.

4. Fundamental solution of the fourth kind

   Wall 1 - Uniform wall heat flux.

   Wall 2 - Maintained at inlet temperature.

Since the boundary conditions on Wall 1 and Wall 2 can be interchanged, there are actually a total of eight sets of boundary conditions. Lundberg et al. [9] presented solutions to all four fundamental problems along with their combinations. Their solution for large $x^+(=x/D_h RePr)$ utilized separation of variables and an eigenfunction expansion procedure [10]. For small values of x^+, the above solution converges

very slowly, hence the Lévêque [11] approximation was used near the point of start of heating.

The underlying assumption in the Lévêque method is that since for small x^+ the thermal boundary layer is thin compared to the momentum boundary layer, it can be assumed that the velocity distribution is linear instead of that given by Lamb [6] but having the same slope at the wall. Another assumption in this method is that the effect of curvature is small in the thin thermal boundary layer so that the diffusion term in the energy equation (see next chapter) can be approximated as

$$\frac{1}{r}\frac{\partial}{\partial r}\left(r\lambda\frac{\partial T}{\partial r}\right) \simeq \lambda\frac{\partial^2 T}{\partial r^2}$$

The solutions presented by Lundberg et al. [9] are restricted to constant property flow. Further, it is noted that the concept of superposition suggested in [8] is mathematically invalid for variable property flows since property variation causes the energy equation to become nonlinear.

The problem of simultaneous development of velocity and temperature fields in laminar flow was considered by Heaton et al. [12]. The solution was obtained first for the hydrodynamic problem, and then for the combined hydrodynamic and thermal problem by an integral method. Thermal boundary conditions corresponded to the fundamental solution of second kind. Coney and El-Shaarawi [13-14] presented a finite-difference analysis of the problem with one wall isothermal and the other wall adiabatic. They used an implicit finite-difference

scheme.

Shumway and McEligot [15] were the first to study the problem of variable property heat transfer in laminar flow through an annular passage. They employed an implicit finite-difference method based on the control volume approach used by Bankston and McEligot [4]. Solutions for developing flow with boundary conditions corresponding to all four kinds of fundamental problems were obtained for $r^* = 0.25$. A detailed account of their work is given by Shumway [16].

In all studies mentioned above, only forced flow was considered and buoyancy effects were assumed to be negligible. Sherwin and Wallis [17-19] studied laminar upward and downward flow with the effect of buoyancy employing the Boussinesq approximation (see, e.g., [20]) in which properties are assumed to be constant except for the density in the buoyancy term. They considered both fully developed and developing flow. By assuming a fully developed velocity profile at the entrance, Tanaka and Mitsuishi [21] solved the energy equation using the Crank-Nicolson method [22]. The velocity profile was calculated at each streamwise station by trial and error in order to take account of buoyancy and temperature dependence of viscosity.

A more detailed review of some of the earlier analytical studies for constant property flow and heat transfer is given by Shah and London in [23].

b. Experimental work Heaton et al. [12] took measurements (for $Pr = 0.7$) in the simultaneous velocity and thermal development region in order to compare their predictions with experimental data.

Almost all other experimental work has been for fully developed flow, an account of which can be found in [16].

Sherwin and Wallis [19] obtained limited heat transfer data for combined natural and forced convection in a vertical annulus of $r^* = 0.33$ using water. In the experiment, the inner wall was heated while the outer wall was insulated. They also performed flow visualization studies in order to observe flow reversal near the unheated wall. Okuno and Sugita [24] measured temperature profiles in a vertical annulus ($r^* = 0.3$) in which water was flowing upward. The inner wall was cooled while the outer wall was heated. The range of Reynolds number investigated was from 30 to 200. The flow at the start of heating was fully developed. The radial temperature profiles near the early thermal entrance region showed upward convex curvature near the inner wall. This they attributed to the possible flow reversal near the cooled inner wall.

Maitra and Subba Raju [25] obtained experimental data for a Reynolds number range of 200-1200 and Rayleigh numbers up to 2.5×10^5 for water flowing in an annulus ($r^* = 0.38$) with constant heat flux at the inner wall. Their results show a strong influence of buoyancy on heat transfer.

2. Turbulent flow and heat transfer

a. Theoretical work The theoretical work performed for the hydrodynamic and thermal problem can be grouped according to the assumptions made for simulating turbulent transport of momentum and

heat. According to this classification, three groups can be formed in which the turbulence models employed were one of the following types:

(1) eddy viscosity type models

(2) mixing length models

(3) transport equation models

Most of the analyses made to date fall in the first category as they have, generally, used an assumed distribution for eddy viscosity in modeling turbulence quantities. Also, most of these have been for fully developed flow.

Kays and Leung [26] employed an eddy viscosity distribution in the turbulent core region which was a modification of the proposal made by Reichardt [27] for pipe flow. The modifications were purely empirical and were made to obtain a fit to the measured eddy viscosity. In the laminar sublayers, Kays and Leung used a modification of the eddy viscosity suggested by Deissler [28] for pipe flow. Eddy conductivity was related to eddy viscosity through a turbulent Prandtl number (Pr_T) which was assigned a value of 1 in the laminar sublayers. In the main stream, however, Pr_T was calculated using the Jenkins model [29] and was divided by a constant factor of 1.2 so as to bring the calculated heat transfer results for air in a circular tube into line with the experiments. Their method consisted of solving the ordinary differential equation for a fully developed temperature profile employing a log-law velocity profile which was inconsistent with the assumed eddy viscosity distribution. This inconsistency was allowed in order to avoid zero eddy viscosity at the radius of maximum velocity, r_m. Quarmby and

Anand [30], assuming the same eddy viscosity distribution as suggested by Kays and Leung, presented a solution to the thermal entrance problem using an eigenfunction expansion method. In both of these studies, the location of maximum velocity was assumed to be known a priori and was calculated using the correlation due to Kays and Leung [26],

$$\frac{r_m - r_1}{r_2 - r_m} = r^{*\,0.343} \tag{1.1}$$

Ying [31] calculated fully developed flow and heat transfer in annuli with roughened cores using an eddy viscosity which was prescribed by fitting simple ramp functions to the data of Jonsson and Sparrow [32] on each side of the radius of zero shear which was assumed to be the same as the radius of maximum velocity. This curve fitting allowed a discontinuity in the eddy viscosity at the radius of zero shear, which is unrealistic. His method was based on solving ordinary differential equations for fully developed velocity and temperature profiles using a Runge-Kutta integration technique [33]. Poor results for friction factors and temperature profiles for annuli with rough cores were obtained. Durst [34], later on, improved upon Ying's work and eliminated the discontinuity in the prescribed eddy viscosity. In both of these studies a constant value of $Pr_T(=0.9)$ was used. Lawn and Elliot [35] and Lawn [36] employed Ying's method in their studies.

Levy [37] derived a rather cumbersome expression for the velocity profile in fully developed turbulent annular flow. In his analysis Levy assumed that Reichardt's [27] expression for eddy viscosity in pipe flow was applicable in a modified form to the flow on both sides

of the radius of zero shear which was assumed to be the same as the radius of maximum velocity. The universal mixing length constant (or von Kármán constant), κ, appearing in Reichardt's eddy viscosity expression was assigned a value of 0.4 near the outer wall while for the inner wall, it was allowed to depend upon radius ratio and r_m which was assumed to be known. Roberts [38], essentially following Levy's analysis, obtained a simpler empirical expression for the velocity profile.

One of the earliest attempts to solve for simultaneous growth of hydrodynamic and thermal boundary layers in the entrance region of an annulus is due to Wilson and Medwell [39]. Their analysis employed integral techniques to solve the momentum and energy equations while the eddy viscosity distribution used was based on the suggestion of Levy [37] for fully developed flow. However, κ was assigned a value of 0.4 near both the inner and outer walls. Independently, Lee and Park [40] employed similar techniques to analyze the simultaneous growth of hydrodynamic and thermal boundary layers. Their turbulence model was also similar to that of Wilson and Medwell, the only difference being that κ near the inner wall was allowed to vary in the streamwise direction. In order to be able to calculate κ near the inner wall, the thickness ratio of the developing boundary layers was assumed equal to that of the fully developed flow, an assumption which is generally not true.

No heat transfer study has been noted which falls in the second group, namely the mixing length model approach. The studies which

employed the mixing length model for the hydrodynamic problem include those of Barrow et al. [41], Quarmby [42], and Sharma et al. [43]. All of these studies were for fully developed flow.

Barrow et al. [41] investigated the velocity distribution in fully developed turbulent annular flow using Goldstein's [44] extension of the similarity hypothesis of von Kármán [45]. According to Goldstein, for turbulent flows, the characteristic length, the stress and the rate of transfer of $(r\tau)$ are respectively given by

$$\ell = \kappa \frac{du}{dr} \Big/ \left(\frac{d^2u}{dr^2} - \frac{1}{r} \frac{du}{dr} \right)$$

$$\tau = \rho \ell^2 \left(\frac{du}{dr} \right)^2$$

$$\frac{1}{r} \frac{d}{dr} (r\tau) = \rho \ell^2 \frac{du}{dr} \left(\frac{d^2u}{dr^2} - \frac{1}{r} \frac{du}{dr} \right)$$

Barrow et al. used these equations, along with the assumptions that the radius of maximum velocity for turbulent flow is the same as given by Lamb [6] for laminar flow to obtain integral relations for the velocity defect on both sides of the radius of maximum velocity. Their analysis showed poor agreement with the experimental data on the inside of the radius of maximum velocity.

Quarmby [42] used Deissler's [28] eddy viscosity expression in the sublayers. In the main stream, however, he employed the von Kármán similarity hypothesis which gives characteristic turbulence length scale as

$$\ell = \kappa \frac{du}{dy} \Big/ \frac{d^2u}{dy^2}$$

The shear stress was given as

$$\tau = (\mu + \rho \ell^2 \left|\frac{du}{dy}\right|) \frac{du}{dy}$$

The solution was obtained using a Runge-Kutta technique after several assumptions were made about parameters such as the radius of maximum velocity, the points where the velocity profile was to be matched with the sublayer profiles, and the constants appearing in Deissler's eddy viscosity distribution.

Sharma et al. [43] studied the effect of a rotating core tube on the fully developed turbulent flow through an annulus using a mixing length model whereby the mixing length was assumed to vary linearly with the distance from the walls. Very close to the walls, van Driest's [46] damping function was employed while a constant level of the mixing length was assumed in the central region of the annulus. They used a calculation procedure similar to that described in [3].

Only two studies have been noted which employed turbulence models involving transport equations. Hanjalic [47] solved the transport equations for turbulence kinetic energy, its dissipation rate and shear stress along with the mean momentum equation to obtain a solution for fully developed flow in smooth and rough annuli. He used a modification of the Patankar and Spalding numerical procedure [3].

The very recent work of Heikal et al. [48], which appeared in the literature in the final stages of the present study, employed a two equation (k-ε) turbulence model for the prediction of simultaneously developing hydrodynamic and thermal boundary layers. This analysis

[48], which employed a Crank-Nicolson difference scheme and followed the procedure suggested by Briley [49] for determining streamwise pressure gradient, appears to be quite expensive in terms of computer time. They reported that typically 60 seconds were required on a CDC 7600 which is several times greater than the time required by the calculation scheme to be described in the present study.

Other theoretical studies of turbulent flow in an annulus with or without heat transfer include that of Clump and Kwasnoski [50], Lee [51], Wilson and Medwell [52], Lee and Park [53], and Chung et al. [54]. No study is known to the author which considered variable property turbulent heat transfer.

b. Experimental work Numerous experimental studies have been noted for turbulent flow in annular passages with and without heat transfer. In most of these investigations, gases (generally air) were used as the working fluid. Generally, mean velocity profiles, temperature profiles and Nusselt numbers were measured; however, some investigations also involved measurements of turbulence quantities. Below, an account of the experimental work is given separately in two groups. First, those studies will be discussed which dealt with only the hydrodynamic problem. Secondly, the studies which also involved heat transfer measurements will be described.

Hydrodynamic problem: Rothfus [55] made an extensive survey of the literature to 1948 dealing with friction factors for annular flow and measured both friction factors and velocity distributions for the flow of air in annuli at Reynolds numbers in the transition and

low turbulent range. It is generally believed that the transition Reynolds number for an annulus is about the same as for a circular tube. Lonsdale [56] made velocity measurements for the flow of water in nine vertical annuli whose radius ratio varied from 0.01 to 0.803. His measurements show that the transition Reynolds number for an annulus lies in the range of 2000 to 3000. Knudsen and Katz [57] also suggest a value of about 2000. However, in the entrance region, if the turbulence intensity is low and the inlet is smooth, laminar flow may persist for considerable distance even for Reynolds numbers much greater than 2000. Heaton et al. [12] report that, in a certain annulus, laminar flow was found to remain for 11 times the hydraulic diameter with a Reynolds number of over 29000 with transition occurring a little sooner on the inner wall than on the outer wall.

Brighton and Jones [58] studied fully developed turbulent flow in four annuli ($r^* = 0.0625$, 0.125, 0.375 and 0.562) for a range of Reynolds numbers. They presented mean velocity profiles, friction factors and distributions of three components of turbulence intensity and Reynolds stress.

It was found that for the range of parameters studied, friction factors depend only on Reynolds number and not on radius ratio. The location of maximum velocity was found to be nearer to the inner wall than for laminar flow. Also the zero Reynolds stress and maximum velocity were found to occur at the same point. This last conclusion was contradicted in some later studies. As noted in the discussion of the paper [58], the expression suggested by Kays and Leung [26] for

radius of maximum velocity correlates data of Brighton and Jones within a few percent.

Quarmby [59] presented results of experiments carried out in fully developed turbulent flow in three smooth annuli ($r^* = 0.107$, 0.178 and 0.347) with air as the working fluid and for the Reynolds number range of 6000 to 90,000. His measured velocity profiles did not show a universal logarithmic region except near the outer wall and then only for the smaller radius ratios at the higher Reynolds numbers.

No effect of radius ratio on the friction factor could be identified in Quarmby's study. His data along with results from some earlier investigations lie between the parallel plate correlation,

$$f_p = 0.087 \ (Re)^{-0.25} \tag{1.2}$$

and the well-known Nikuradse correlation for pipe flow,

$$\frac{1}{\sqrt{f_p}} = 4.0 \log (Re \sqrt{f_p}) - 0.40 \tag{1.3}$$

for Reynolds numbers less than about 100,000, while for higher Reynolds numbers the data are close to the latter expression. The friction factor in these correlations is defined as

$$f_p = - \frac{D_h}{2\rho u_b^2} \frac{dp}{dx} \tag{1.4}$$

Lawn [60] and Lawn and Elliot [35] have obtained extensive data for fully developed flow through annuli for three different radius ratios ($r^* = 0.088$, 0.176 and 0.396). Significant deviations from the

universal law of the wall were noticed in the velocity profiles associated with the inner wall except for annulus with $r^* = 0.396$. Also, it was found that the position of zero shear and maximum velocity do not coincide and that the position of zero shear, and not the radius of maximum velocity, can be accurately located by the correlation of Kays and Leung, Eq. (1.1). In the experiment, the position of zero shear was located using the x-wire technique as described in [35].

The structure of the turbulence of fully developed flow through three concentric annuli with small radius ratios ($r^* = 0.0198$, 0.0396 and 0.0998) was investigated by Rehme [61] for a Reynolds number range of $2x10^4 - 2x10^5$. Turbulent shear stresses and all three turbulent intensities were measured. He found that the main difference between symmetrical and asymmetrical flows is that, for the latter, the diffusion of turbulent energy plays an important role and that this is the reason for noncoincidence of the positions of zero shear and maximum velocity. The results of Rehme [62] show a tendency for the zero shear position to be nearer to the inner wall than indicated by the experimental values of Lawn and Elliot [35]. A similar trend was noted for the radius of maximum velocity.

Contrary to most of the earlier investigations, Rehme reports that his results, even for large curvature at the inner wall, do not exhibit differences from the logarithmic velocity profile near the wall, especially for high Reynolds numbers.

Olson and Sparrow [63] carried out static pressure measurements in the entrance region of annuli with water as the working fluid. Both

square and rounded entrances were employed. Later Okiishi [64] undertook an investigation in the entrance region of two annuli ($r^* = 0.344$ and 0.531) with square and rounded entrances. Air was used as a working fluid and developing axial velocity profiles were measured. In both of these studies, laminar-turbulent transition was observed to occur in the rounded entrance annuli.

Lee and Park [53] made some mean flow measurements in the entrance region of four annuli in order to make comparisons with their predictions. Boundary layers were tripped at the entrance so that flow was turbulent right from the beginning.

Thermal problem: Kays and Leung [26] made heat transfer measurements for air in four annuli ($r^* = 0.192$, 0.255, 0.375 and 0.5) with the thermal boundary condition corresponding to the fundamental solution of second kind. The Reynolds number range was from 10,000 up to 160,000. Measurements in the thermal entrance region were taken in order to obtain the fully developed results by extrapolating. Later, Lee and Barrow [65] presented results for fully developed heat transfer from a uniformly heated core tube. The radius ratios studied were 0.258, 0.387 and 0.613 and Reynolds number ranged from 10,000 to 50,000. The results of these authors disagree with reference [26] by as much as 20 percent.

Quarmby [66] obtained results in the thermal entrance region for air flowing in annuli ($r^* = 0.109$, 0.174, 0.347) with a Reynolds number range of 5000 to 270,000. The inner wall was heated uniformly while the outer wall was insulated. Quarmby correlated his data as

$$\log Nu = -K + 0.706 \log Re \tag{1.5}$$

where

$$\log K = 0.1658 + 0.1056 \log r^*$$

Ball and Azer [67] measured velocity and temperature profiles for the flow of air in an annulus of radius ratio 0.25. Eddy viscosity and turbulent Prandtl number distributions were also calculated. Kuzay and Scott [68,69] also measured velocity and temperature profiles in an annulus with $r^* = 0.556$ whereby the outer wall of the annulus was heated. The core tube was allowed to rotate in order to study the effect of rotation on the axial flow and heat transfer. Eddy viscosity and turbulent Prandtl number distributions were calculated using measured velocity and temperature profiles. A detailed description of the experiment and results is given by Kuzay [70].

Furber et al. [71] performed experiments to determine local Stanton numbers and overall pressure drop for two annular channels of radius ratios 0.68 and 0.83. Tests were carried out with helium and nitrogen under high pressures and the effect of variable properties was identified. Dalle Donne and Meerwald [72] used air to study the effect of high heat fluxes on Nusselt number. The radius ratios used were 0.5 and 0.72 and inner heated wall temperatures up to 1000°C were obtained. They correlated their data for Nusselt number as

$$Nu_b = 0.018\, r^{*-0.16}\, Re_b^{0.8}\, Pr_b^{0.4} \left(\frac{T_w}{T_0}\right)^{-0.2} \tag{1.6}$$

Dwyer et al. [73] have obtained data for the fluid dynamics and heat transfer characteristics of mercury in fully developed turbulent flow

through annuli ($r^* = 0.25$, 0.36 and 0.48) with heat supplied at the inner wall only. Reference [73] presents eddy conductivity profiles while the hydrodynamic results have been presented by Hlavac et al. [74] and Dwyer et al. [75]. The heat transfer data referred to in [73] have not been published to date.

Ornatskiy et al. [76] have obtained limited data for heat transfer to water flowing in an annulus under supercritical pressures.

Other heat transfer studies for hydrodynamically developed flow are those of Petukhov and Roizen [77], Michiyoshi et al. [78], and Nyamira and Vilyamas [79].

Relatively few experimental studies have been made for the simultaneous growth of hydrodynamic and thermal boundary layers. Roberts and Barrow [80] obtained local Nusselt number data for two internally heated annuli ($r^* = 0.25$ and 0.476) with air as the working fluid. Lee and Park [40] also obtained data in the entrance region.

Recently, Heikal et al. [48] made measurements of turbulence characteristics, mean flow and heat transfer parameters in the entrance region of an annulus of radius ratio 0.25 over a range of Reynolds number from 13,000 to 190,000. The effect of varying free stream turbulence at the entrance on skin friction and heat transfer was studied. High turbulence intensities at the inlet were seen to produce an increase of friction and heat transfer in the entrance region.

In closing this section on experimental studies in turbulent flow through annular passages it seems appropriate to comment on the general validity of the two correlations (Eqs. (1.5) and (1.6)) presented

for Nusselt number. Table 1.1 gives a comparison of Nusselt numbers for four different radius ratios as predicted by the correlation suggested by Quarmby [66] and that due to Dalle Donne and Meerwald [72]. Comparisons are made for five different Reynolds numbers ranging from 20,000 to 300,000. It can be seen that the predictions of these two correlations, in general, do not agree well; the discrepancy being as large as 29 percent. Quarmby's measurements were made for $r^* = 0.109$, 0.174 and 0.347 while Dalle Donne and Meerwald used $r^* = 0.5$ and 0.72. The two correlations agree more closely at smaller radius ratios, i.e., the range in which Quarmby made his measurements; however, it can be concluded that such correlations cannot be used with a great deal of confidence in a variety of situations. Therefore, a general method for prediction of heat transfer with a wide range of applicability seems quite desirable.

C. Scope of the Present Study

As was indicated earlier, no significant analytical or numerical solution method has been noted to date which appears capable of treating variable property heat transfer in laminar and turbulent flow through annular passages. The major challenge, for turbulent flows, lies in modeling sufficiently accurately the transport of momentum and heat which takes place due to turbulence fluctuations. This seems particularly true for a geometry such as an annular duct because of the asymmetry involved which influence the flow structure. The prediction methods which have been proposed for constant property flows

Table 1.1. Comparison of Nusselt numbers as predicted by the correlation of Quarmby [66] and Dalle Donne and Meerwald [72]

r*	Re	Quarmby	Dalle Donne and Meerwald	% Difference
0.1	20,000	77.2	62.2	+24.1
	50,000	147	129.6	+13.8
	100,000	241	226	+ 6.6
	200,000	392	393	- 0.1
	300,000	523	543	- 3.8
0.25	20,000	59	53.7	+ 9.8
	50,000	113	112	+ 0.8
	100,000	184	195	- 5.6
	200,000	300	339	-11.6
	300,000	400	469	-14.9
0.5	20,000	47.3	48.1	- 1.7
	50,000	90.4	100	- 9.7
	100,000	147	174	-15.5
	200,000	240	304	-20.8
	300,000	320	420	-23.8
0.75	20,000	41.3	45	- 8.3
	50,000	78.8	93.9	-16.1
	100,000	128	163	-21.3
	200,000	210	284	-26.2
	300,000	279	393	-29.1

have generally been applied to specialized situations or have not been well tested and therefore are limited in scope.

In the present study an explicit finite-difference method is developed for the prediction of variable property laminar and turbulent flow heat transfer in annular passages. Both developing and fully developed flows are considered. As for turbulence modeling, the approach has been to identify the simplest turbulence models which will work satisfactorily for predicting both the hydrodynamic and thermal development. While use is made of the mixing length hypothesis to model the Reynolds stress term, $-\overline{\rho u' v'}$, a one-dimensional length scale transport equation is proposed to calculate mixing length in the outer region of the boundary layers. This model predicts correctly the behavior of the interacting merging shear layers in an annular duct. Two other turbulence models are also developed. While one is just a simple modification of the length scale model, the other model employs a transport equation for turbulence kinetic energy.

The present report is organized mainly into five chapters. In Chapter II, the complete mathematical model is developed including turbulence modeling and the assumptions made are clearly identified. The mathematical model is general in that it is applicable to laminar or turbulent flow of any Newtonian fluid. Viscous dissipation and compression work terms are contained in the thermal energy equation while axial conduction is neglected. A brief account of the numerical method developed to solve the mathematical model is given in Chapter III. The finite-difference scheme employed has clear advantages, especially

for variable property flows. Although the scheme is explicit, fairly large streamwise steps can be taken.

In Chapter IV, the validity of the calculation procedure and the proposed turbulence model is tested by comparing the predictions with the available experimental data and the prediction of some other calculation methods. The main conclusions and recommendations are given in Chapter V.

II. ANALYSIS

In this chapter, partial differential equations derivable from basic conservation laws are described and the simplified versions of these equations, both for laminar and turbulent flows, actually to be solved are presented. A turbulence model is developed which utilizes a simplified transport equation for the characteristic mixing length scale in the outer (central) part of the flow. Another model which employs a turbulence kinetic energy transport equation along with the length scale is also described. The effect of large transverse curvature on turbulence and laminar-turbulent transition is also discussed.

Appropriate boundary conditions are provided to complete the mathematical model. Engineering parameters of interest, such as skin-friction coefficient and Nusselt number, are defined in the last section.

A. Governing Partial Differential Equations

1. Geometry and coordinate system

The coordinate system chosen for the present analysis is presented, along with the annular passage, in Fig. 2.1. It is assumed that the annulus is concentric and the flow in it is axisymmetric.

Axial and radial coordinates are denoted by x and r respectively. The domain of calculation is

$$x > 0$$

$$r_1 \leq r \leq r_2$$

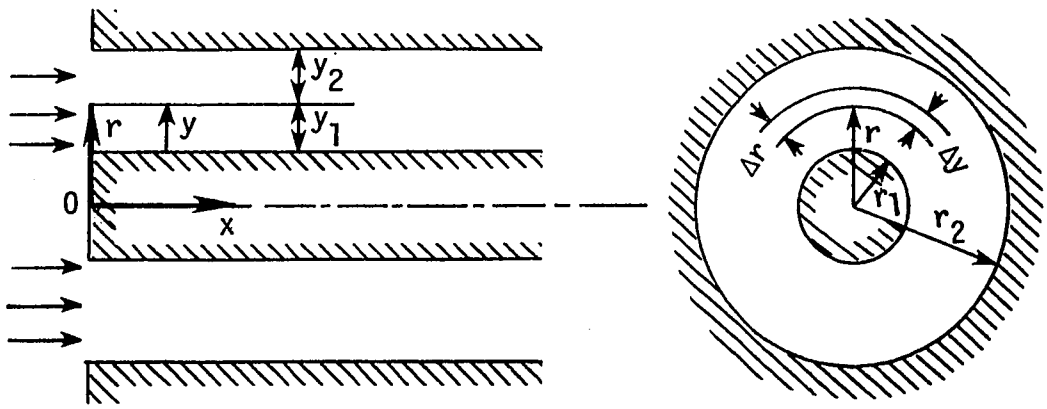

Fig. 2.1. Coordinate system used for the analysis

where

$$0 < \frac{r_1}{r_2} < 1$$

For convenience, another coordinate y can be defined such that

$$y = r - r_1, \quad \frac{\partial}{\partial y} = \frac{\partial}{\partial r}$$

Wall boundary conditions will be specified at y = 0 (inner wall) and $y = r_2 - r_1 = r_h$ (outer wall).

For the reasons which will become obvious later the distance from the walls is defined as

$$y_w = |r - r_w|$$

where w = 1, 2 corresponds to the inner and outer walls of the annulus, respectively.

2. Basic conservation laws

Fluid flow with heat transfer is governed by three basic principles, namely: conservation of mass, momentum, and energy. Governing equations derivable from these principles are described below.

a. Conservation of mass The principle of conservation of mass requires that the Lagrangian derivative of the mass of fluid contained in an element should be zero. This leads to the following partial differential equation, called the continuity equation, for an axisymmetric flow [81]:

$$\frac{\partial \rho}{\partial t} + \frac{\partial}{\partial x}(\rho u) + \frac{1}{r}\frac{\partial}{\partial y}(\rho r v) = 0 \qquad (2.1)$$

b. Conservation of momentum The principle of conservation of momentum, which in effect is an application of Newton's second law of motion to an element of the fluid, together with the constitutive relation for a Newtonian fluid yields the well-known Navier-Stokes equations which for axisymmetric flow are given as [81]

$$\rho\left(\frac{\partial u}{\partial t} + u\frac{\partial u}{\partial x} + v\frac{\partial u}{\partial y}\right) = \frac{1}{r}\frac{\partial}{\partial y}\left(r\mu\frac{\partial u}{\partial y}\right) + \frac{1}{r}\frac{\partial}{\partial y}\left(r\mu\frac{\partial v}{\partial x}\right)$$

$$+ 2\frac{\partial}{\partial x}\left(\mu\frac{\partial u}{\partial x}\right) - \frac{\partial p}{\partial x} + f_x \qquad (2.2)$$

$$\rho\left(\frac{\partial v}{\partial t} + u\frac{\partial v}{\partial x} + v\frac{\partial v}{\partial y}\right) = 2\frac{\partial}{\partial y}\left(\mu\frac{\partial v}{\partial y}\right) + 2\mu\frac{\partial}{\partial y}\left(\frac{v}{r}\right)$$

$$+ \frac{\partial}{\partial x}\left(\mu\frac{\partial v}{\partial x}\right) + \frac{\partial}{\partial x}\left(\mu\frac{\partial u}{\partial y}\right) - \frac{\partial p}{\partial y} + f_y \qquad (2.3)$$

where the terms containing the second viscosity coefficient [82] have been neglected which is exactly the case for constant density flows while, for the variable density case, the neglect of these terms can be justified [83] under the boundary layer approximation to be described in Section A.3.

c. Conservation of energy The principle of conservation of energy amounts to an application of the first law of thermodynamics to a fluid element in motion. This leads to the following partial differential equation, called the energy equation, for an axisymmetric flow [81, 84]:

$$\rho C_p\left(\frac{\partial T}{\partial t} + u\frac{\partial T}{\partial x} + v\frac{\partial T}{\partial y}\right) = \frac{1}{r}\frac{\partial}{\partial y}\left(r\lambda\frac{\partial T}{\partial y}\right) + \frac{\partial}{\partial x}\left(\lambda\frac{\partial T}{\partial x}\right)$$

$$+ D_1 + \beta T\left(\frac{\partial p}{\partial t} + u\frac{\partial p}{\partial x} + v\frac{\partial p}{\partial y}\right) \qquad (2.4)$$

where, internal heat generation and radiative heat transfer have been neglected. The viscous dissipation function D_1 is given as

$$D_1 = \mu\left[2\left\{\left(\frac{\partial v}{\partial y}\right)^2 + \left(\frac{v}{r}\right)^2 + \left(\frac{\partial u}{\partial x}\right)^2\right\} + \left(\frac{\partial v}{\partial x} + \frac{\partial u}{\partial y}\right)^2\right] \qquad (2.5)$$

It can be shown that all terms but one can be neglected in D_1 on the basis of an order of magnitude analysis for boundary layer flows to give the simplified viscous dissipation function as

$$D_1 = \mu\left(\frac{\partial u}{\partial y}\right)^2$$

Eq. (2.4), then, becomes

$$\rho C_p\left(\frac{\partial T}{\partial t} + u\frac{\partial T}{\partial x} + v\frac{\partial T}{\partial y}\right) = \frac{1}{r}\frac{\partial}{\partial y}\left(r\lambda\frac{\partial T}{\partial y}\right) + \frac{\partial}{\partial x}\left(\lambda\frac{\partial T}{\partial x}\right)$$

$$+ \mu\left(\frac{\partial u}{\partial y}\right)^2 + \beta T\left(\frac{\partial p}{\partial t} + u\frac{\partial p}{\partial x} + v\frac{\partial p}{\partial y}\right) \qquad (2.6)$$

β, the coefficient of thermal expansion, appearing in the compression work term is defined as

$$\beta = -\frac{1}{\rho}\frac{\partial \rho}{\partial T}\bigg|_p$$

which, obviously, will be zero for a constant density flow and will equal $\frac{1}{T}$ for an ideal gas.

3. Laminar flows

The equations (2.1-2.3) and (2.6) described in the previous section govern all axisymmetric transient laminar flows. These can be simplified considerably by using Prandtl's boundary-layer approximation [82] which is also frequently referred to as the thin shear layer approximation. This approximation is applicable to the flow in annular passages at all but very small Re as long as the passage is straight or does not have large longitudinal curvature or sudden enlargements or contractions.

In essence, Prandtl's boundary-layer approximation depends on the assumption that gradients of quantities such as u across the principal flow direction x are at least an order of magnitude larger than gradients along x. This assumption permits the neglecting of some terms in Eq. (2.2), while Eq. (2.3) reduces to the statement that, for no cross-stream body forces, pressure is constant in the radial direction. The energy equation, Eq. (2.6), is also simplified under this assumption.

The boundary layer form of the governing equations for steady laminar flows with variable properties can be written as

continuity:

$$\frac{\partial}{\partial x}(\rho u) + \frac{1}{r}\frac{\partial}{\partial y}(\rho r v) = 0 \qquad (2.7)$$

momentum:

$$\rho u \frac{\partial u}{\partial x} + \rho v \frac{\partial u}{\partial y} = \frac{1}{r}\frac{\partial}{\partial y}(r\mu \frac{\partial u}{\partial y}) - \frac{dp}{dx} + f_x \qquad (2.8)$$

energy:

$$\rho C_p u \frac{\partial T}{\partial x} + \rho C_p v \frac{\partial T}{\partial y} = \frac{1}{r} \frac{\partial}{\partial y}(r\lambda \frac{\partial T}{\partial y}) + \mu(\frac{\partial u}{\partial y})^2 + \beta T u \frac{dp}{dx} \qquad (2.9)$$

Neglecting the term $\frac{\partial}{\partial x}(\lambda \frac{\partial T}{\partial x})$ in Eq. (2.9) implies that axial conduction of heat in the fluid is insignificant. This assumption needs some attention. In laminar flow, a measure of the relative magnitudes of heat transfer by convective transport and by molecular diffusion is given by the Peclet number (Pe = RePr). When the Peclet number is large, convective transport is large relative to molecular diffusion and it can be expected that axial conduction will be negligible. Hennecke [85] analyzed the effect of axial conduction on heat transfer in the thermal entrance region of a circular pipe using a fully developed laminar velocity profile whereby the (elliptic)[1] energy equation was solved numerically by a finite-difference method. He found that the influnece of axial conduction was more pronounced in the case of uniform wall temperature than in the case of uniform heat flux and suggested that in the former case, axial conduction may be neglected if Pe > 50 and in the latter if Pe > 10. Schneider [86] employed a slug flow approximation in his analysis along with a constant wall temperature boundary condition and suggested a critical value for Peclet number of 100 under which the effect of axial conduction will become significant.

Nonmetallic (moderate and high Prandtl number) fluids in laminar

---

[1] $\rho C_p u \frac{\partial T}{\partial x} = \frac{1}{r} \frac{\partial}{\partial y}(r\lambda \frac{\partial T}{\partial y}) + \frac{\partial}{\partial x}(\lambda \frac{\partial T}{\partial x})$.

flow will rarely have Peclet numbers less than 100. With liquid metals (low Prandtl number fluids), however, Peclet numbers less than unity are not unexpected and the neglect of axial heat conduction may not be justified. In the present study this effect has been neglected as there is little if any technological interest in the forced convection laminar flow of liquid metals.

It should also be noted that the viscous dissipation term, $\mu(\frac{\partial u}{\partial y})^2$, and compression work, $\beta T u \frac{dp}{dx}$, are kept in the energy equation, Eq. (2.9). Dissipation increases the temperature of the fluid and consequently alters the temperature gradient distribution for heating and cooling in opposite direction. A parallel argument holds for the effects of compression work, which behaves as a thermal energy sink. Usually, viscous dissipation can be regarded as negligible when the Eckert number $E \left(= \frac{u_b^2}{2C_p(T_w - T_b)}\right) \ll 1$; otherwise the viscous dissipation must be taken into account [87]. Madejski [88] has shown that compression work must be taken into account if viscous dissipation is not negligible as both these terms are of the same order and neglect of one will lead to inaccuracies in the predicted temperature profile.

4. Turbulent flows

It is well-known that turbulence is the most complicated kind of fluid motion. Turbulent motion can be assumed to consist of the superposition of eddies of various sizes and vortices with distinguishable upper and lower limits. The upper size limit of the eddies is determined mainly by the characteristic dimension of the flow, whereas the lower

limit is determined by viscosity effects. Within these smallest eddies the flow is of a strong viscous nature, where molecular effects are dominant but still the continuum flow assumption is applicable.

It is generally accepted that turbulence in Newtonian fluids is described by the full Navier-Stokes equations (3-D form of Eqs. (2.2) and (2.3)) which cannot be solved analytically even for simple flow geometries. Any numerical calculation must employ a mesh size smaller than the size of the smallest eddies and the time step used should be much smaller than the turbulent time scale. Such a calculation is far beyond the reach of present day computers. To get an idea about the time required for calculating turbulent flows from the first principles, Emmons [89] considered turbulent flow through a circular pipe of diameter D_h. For Re = 5000, he estimates the computing time for a length equal to 10 D_h to be 100 years. For a large-scale flow, Re = 10^7, he estimates 10^{10} years, or about the age of the universe.

All present day computations of turbulent flows make use of the concept, first adopted by Reynolds [90], that turbulent motion can be decomposed into a mean motion and a fluctuation, or eddying motion. Denoting the time-average of a quantity e by $\bar{e}$ and its fluctuation by e', it can be written that

$$e = \bar{e} + e' \tag{2.10}$$

where

$$\bar{e} = \lim_{\Delta t \to \infty} \frac{1}{\Delta t} \int_{t_o}^{t_o+\Delta t} e(t)dt \tag{2.11}$$

Clearly, the time average is meaningful only if it is independent of t_o; a random process whose time averages are all independent of t_o is called "statistically stationary". Turbulent flow through an annular passage with a constant supply pressure at the inlet is an example of a "statistically stationary" flow.

Using Eq. (2.10), the following relations can be written for velocity components, pressure, density, and temperature:

$$\begin{aligned} u &= \bar{u} + u' \\ v &= \bar{v} + v' \\ p &= \bar{p} + p' \\ \rho &= \bar{\rho} + \rho' \\ T &= \bar{T} + T' \end{aligned} \tag{2.12}$$

Substituting these relations in Eqs. (2.1-2.3) and (2.6), time averaging, and employing the usual boundary layer assumption results in the following set of equations for axisymmetric steady turbulent flow [83]:

<u>continuity</u>:

$$\frac{\partial}{\partial x}(\bar{\rho}\bar{u}) + \frac{1}{r}\frac{\partial}{\partial y}(\bar{\rho} r \tilde{v}) = 0 \tag{2.13}$$

<u>momentum</u>:

$$\bar{\rho}\bar{u}\frac{\partial \bar{u}}{\partial x} + \bar{\rho}\tilde{v}\frac{\partial \bar{u}}{\partial y} = \frac{1}{r}\frac{\partial}{\partial y}\left(r\left(\mu\frac{\partial \bar{u}}{\partial y} - \bar{\rho}\overline{u'v'}\right)\right) - \frac{d\bar{p}}{dx} + f_x \tag{2.14}$$

energy:

$$\bar{\rho}C_p\bar{u}\frac{\partial\bar{T}}{\partial x} + \bar{\rho}C_p\tilde{v}\frac{\partial\bar{T}}{\partial y} = \frac{1}{r}\frac{\partial}{\partial y}(r(\lambda\frac{\partial\bar{T}}{\partial y} - \bar{\rho}C_p\overline{v'T'}))$$

$$+ (\mu\frac{\partial\bar{u}}{\partial y} - \bar{\rho}\overline{u'v'})\frac{\partial\bar{u}}{\partial y} - \beta\bar{T}\bar{u}\frac{d\bar{p}}{x} \qquad (2.15)$$

In the above,

$$\tilde{v} = (\bar{\rho}\bar{v} + \overline{\rho'v'})/\bar{\rho}$$

The terms $-\bar{\rho}\overline{u'v'}$ and $-\bar{\rho}C_p\overline{v'T'}$, appearing in Eqs. (2.14) and (2.15), represent the apparent turbulent shear stress and turbulent heat flux, respectively, and must be modeled using empirical information obtained by studying the behavior of turbulent shear flows. Turbulence modeling will be discussed in the next section.

Again, axial conduction has been neglected in the energy equation as was done in the case of laminar flows. With nonmetallic fluids in turbulent flow, Peclet numbers will generally be very large; with liquid metals, however, Peclet numbers can be as small as 10. Stein [91] states that an examination of Schneider's [86] results suggests that, even with Peclet numbers as small as 10, the loss of accuracy in predicting overall heat transfer rates will not be too serious when axial diffusion is neglected. He extended Schneider's analysis to the uniform wall heat flux boundary condition and concluded that, with this boundary condition, axial heat diffusion can be neglected for all Peclet numbers, except at extremely small length to diameter ratios.

Both viscous dissipation and compression work have been included

in the energy equation. Blanco and Gill [92] studied the importance of these terms and concluded that the contribution of dissipation and compression work to the temperature distribution in gaseous flow is significant unless the Eckert number is very small. The net effect of dissipation alone in constant density flows and of dissipation and compression work in variable density flows is that of increasing the heat flux when the fluid is hotter than the wall, and decreasing it when the fluid is cooler than the wall. They suggest that including dissipation only in the energy equation (for variable density flows) will lead to inaccuracies in the temperature distribution. Consequently, both terms have been employed in the present study.

B. Turbulence Modeling

1. Physics of turbulent flow in an annular passage

Figure 2.2 schematically depicts the flow configuration in an annulus. For the present, it can be assumed that the flow is turbulent at the inlet and that the effect of inlet shape can be neglected. This effect will be discussed in Section B.7.

Three flow regimes can be identified in Fig. 2.2. Region I is the initial length where the two "external like" boundary layers interact with the inviscid core; this region is also known as the "displacement interaction" region [93] because the blocking effect of the growing wall boundary layers affects the flow speed in the inviscid core. For short passages, this may be the only flow regime. A much more complex inter-

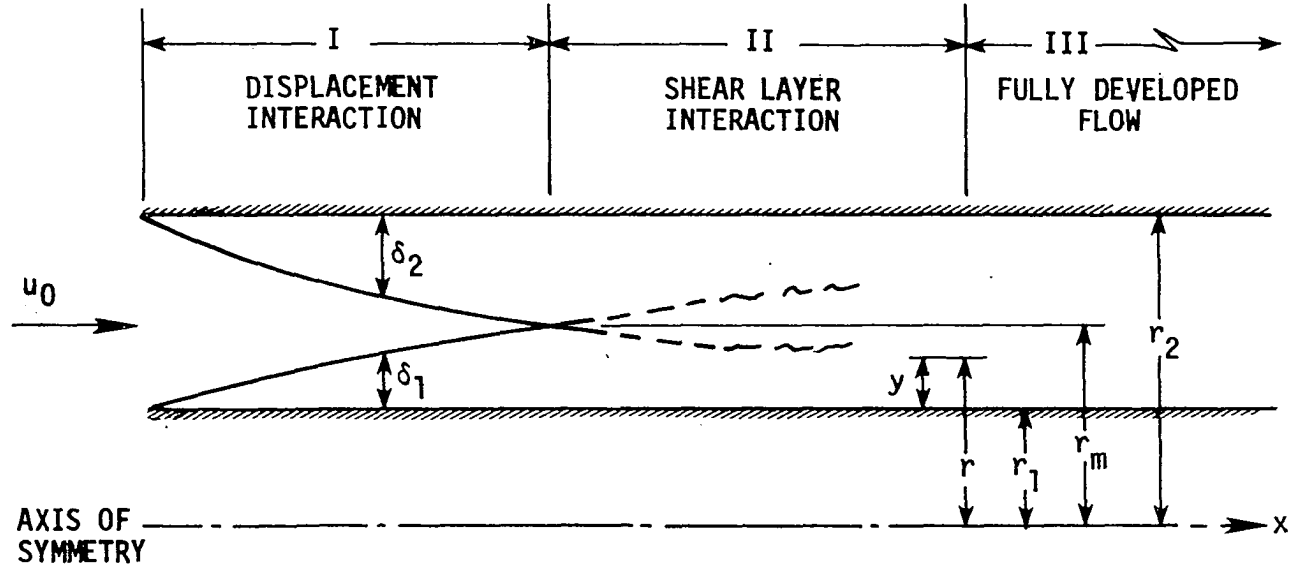

Fig. 2.2. A schematic of the turbulent flow in the entrance region of an annulus showing three flow regimes

action starts to occur at the beginning of region II, the "shear layer interaction" region. Stress containing eddies of one sign penetrate into the shear layer of opposite sign and this penetration grows before a mutual balance is established which characterizes fully developed flow, Region III. It should be noted that, in an annular duct, the position where the shear stress changes sign may not be the same as the position where the velocity gradient changes sign which makes the situation in the region of interaction between the two shear layers obviously more complicated as compared to that in a symmetrical duct flow.

Fully developed flow is unique to internal flows and it is, by definition, a flow type that is independent of the inlet or outlet states and one where conditions are statistically identical at each axial position. The flow in an annular duct becomes fully developed after about 50 hydraulic diameters from the entrance. Region II can be considered as a "transition region" as, in it, the flow undergoes a transition from an "external like flow" (Region I) to "fully developed flow" (Region III).

It will be useful for the discussion in the following sections to introduce some of the terminology commonly used in the turbulent flow literature. Fig. 2.3 shows a typical mean velocity distribution across a turbulent boundary layer. It is the usual practice to treat a turbulent boundary layer as a composite layer consisting of inner and outer regions, as shown in the figure.

The inner region of a turbulent boundary layer is much smaller than

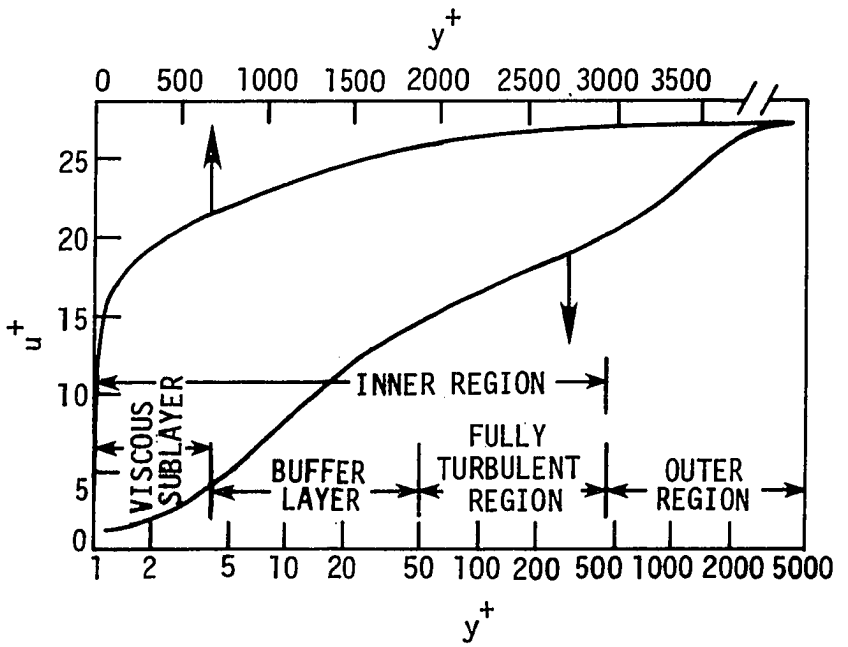

Fig. 2.3. Semilogarithmic and linear plots of mean velocity distribution across a typical turbulent boundary layer

the outer region, with a thickness of about 10 to 20% of the entire boundary layer thickness. It is generally assumed that the mean velocity distribution in this region is completely determined by the wall shear τ_w, density ρ, viscosity μ, and the distance y from the wall. It is given by the following expression known as the "law of the wall":

$$u^+ = \frac{u}{u_\tau} = f_1(y^+) \tag{2.16}$$

Here $u_\tau = (\tau_w/\rho)^{1/2}$ is a parameter having the dimensions of velocity, and called the friction velocity. The parameter y^+ is a Reynolds number defined as $y^+ = yu_\tau/\nu$. u^+ and y^+ are known as law of the wall coordinates.

The inner region can be divided into three layers as indicated in Fig. 2.3: (1) the viscous sublayer, (2) the buffer layer, and (3) the fully turbulent region.

In the viscous sublayer, the stresses are mainly viscous, since turbulent fluctuations, like mean velocities, become zero at the wall. The predominantly viscous region is neither uniform according to time nor according to distance along the wall. If one measures the instantaneous velocity profile instead of the time-mean profile the sublayer is revealed to have a spatial and time-dependent flow structure [94], "continuously disturbed by small-scale velocity fluctuations of low magnitude and periodically disturbed by fluid elements which [penetrate] into this region from positions further removed from the wall" [95].

However, at any section a time-mean value of the thickness of the region may be distinguished which at the most extends to $y^+ \simeq 4$. In this region, mean velocity varies linearly with the distance from the wall, i.e.,

$$u^+ = y^+ \tag{2.17}$$

hence the name "linear sublayer" is also used sometimes for this region.

In the region $y^+ > 4$ in Fig. 2.3, the effect of viscosity on the flow decreases gradually with increasing distance from the wall. Ultimately, a region is reached where the flow is completely turbulent and the effects of molecular viscosity on the shear-stress-producing eddies are small. The intermediate region, where the total stress is partly viscous and partly turbulent, is called the buffer layer (it is sometimes called the transitional region which should not be confused with the standard laminar-turbulent boundary layer transition). In general, the thickness of either the viscous sublayer or the buffer layer is quite small in comparison with that of the fully turbulent region. The buffer layer roughly lies in the range $4 < y^+ < 50$. The velocity profile in the fully turbulent region ($y^+ > 50$) of the inner layer can generally be given as

$$u^+ = \frac{1}{\kappa} \log y^+ + B \tag{2.18}$$

where κ and B are constants.

The outer region of a turbulent boundary layer contains 80-90% of

the boundary layer thickness (see Fig. 2.3). This region is characterized by large eddies which contribute at least 50% to the turbulent energy associated with the u- and v-fluctuations and about 80% to the Reynolds stress [96]. Whether the large eddies arise in the outer layer because of some form of interfacial instability near the edge of the boundary layer [97], or result from the ejection of bursts from the inner region [98], or both, is still an open question.

In case of turbulent flow through an annular passage, two inner regions can be identified associated with the two walls of the passage. Also in Region I of the flow (Fig. 2.2), there are two corresponding outer regions. In Regions II and III, where the two shear layers have merged, the central core region may also be considered as an outer region as it is composed of the outer regions of the two shear layers. In the discussion to follow, "outer region", "central core region", or simply "central region" will be synonymous.

2. Apparent turbulent viscosity and conductivity

Time averaging of the Navier-Stokes equations results in a second order symmetric tensor for the apparent turbulent stresses known as Reynolds stresses. These must be specified before the governing equations can be solved for the mean velocity distribution. Proper weighting of the Navier-Stokes equations before time averaging will give exact "transport" equations for the Reynolds stresses. However, additional unknowns appear in these equations and therefore the set of equations must be closed by empirical assumptions.

In the flow configuration under study, only one of the six stress components, namely $-\bar{\rho}\overline{u'v'}$, is of significance. The exact equation for the transport of $-\bar{\rho}\overline{u'v'}$ contains additional unknown quantities. Hanjalic and Launder [99] developed a model involving two additional transport equations, one for turbulence kinetic energy and another for its dissipation rate, along with the transport equation for $-\bar{\rho}\overline{u'v'}$ whereby some of the terms appearing in the equations were modeled empirically. The main objection to such an approach is that the terms appearing in the shear stress transport equation are less understood than the shear stress itself. Also, three more PDE's have to be solved in addition to the basic conservation equations which means a significant increase in the computation cost. It is, therefore, always wise to develop turbulence models which are less complicated, and thus less expensive, for the practical calculation of turbulent flows.

The simplest and currently most common modeling approach follows a concept originally advanced by Boussinesq in 1877 (see, e.g., [100]), that the turbulent shearing stress can be related to the rate of mean strain as

$$-\bar{\rho}\overline{u'v'} = \mu_T \frac{\partial \bar{u}}{\partial y} \tag{2.19}$$

where μ_T is an apparent turbulent (or eddy) viscosity yet to be defined. The implied assumption in Eq. (2.19) is that the stress~strain law for time-averaged turbulent flows is of the same form as that for a Newtonian fluid in laminar motion.

In a circular pipe or parallel plate duct, the velocity profile is symmetric about the centerline and shear stress also goes to zero there. In an asymmetric flow (asymmetry may be due to difference in curvature, like in a smooth annulus, or due to a difference in surface roughness), however, there is no reason to believe that radius of maximum velocity and that of zero shear will coincide; measurements [35,61] have shown that these two are not the same.

Any turbulence model involving the turbulent viscosity concept, Eq. (2.19), is inherently incapable of differentiating between the maximum velocity and zero shear radius. However, the discrepancy between the two radii only becomes significant for very small radius ratios and even in those cases it is possible to predict overall flow characteristics quite accurately. Exact knowledge of the radius of zero shear is not very crucial for the present method, which employs Eq. (2.19), since it will not be used to calculate wall shear stresses, nor is the proposed turbulence model tied to it in any direct sense contrary to the case of some of the earlier eddy viscosity models [26,39].

As suggested by Prandtl [101] in 1925, turbulent viscosity can be interpreted by analogy with kinetic theory of gases in general sense as

$$\mu_T = \rho v_T \ell \tag{2.20}$$

where v_T and ℓ can be thought of as characteristic velocity and length scales, respectively. These scales must be expected to vary from place

to place, and to have values influenced by the particular pattern and velocity of the mean flow.

For heat transfer calculations, a modeled equation for the transport of $-\bar{\rho}C_p\overline{v'T'}$ can be developed. However, such an attempt is considered unnecessary for nonbuoyant flows [102]. The term $-\bar{\rho}C_p\overline{v'T'}$ represents an additional transport of heat which is caused by the turbulent motion and can be modeled by assuming that this transport is of diffusive type so that the Fourier's law applies, i.e.,

$$-\bar{\rho}C_p\overline{v'T'} = \lambda_T \frac{\partial \bar{T}}{\partial y} \tag{2.21}$$

where λ_T is an apparent turbulent (or eddy) conductivity which can be related to turbulent viscosity μ_T by defining a turbulent Prandtl number such as

$$Pr_T = \frac{\mu_T C_p}{\lambda_T} \tag{2.22}$$

In general, the turbulent Prandtl number may vary throughout the flow, although quite accurate results can be obtained by using a constant value of Pr_T. Further discussion on Pr_T will be found later in a separate section.

3. Length scale transport equation model

One of the simplest ways to calculate the turbulent viscosity is through Prandtl's mixing length hypothesis as a consequence of which $\nu_T = \ell\left|\frac{\partial \bar{u}}{\partial y}\right|$ in Eq. (2.20) so that

$$\mu_T = \rho\ell^2\left|\frac{\partial \bar{u}}{\partial y}\right| \tag{2.23}$$

where ℓ, the mixing length, is yet to be specified. Physically, ℓ can be interpreted as the transverse distance over which lumps of fluid can maintain their original momentum.

It is generally believed that the mixing length in the inner region of a turbulent boundary layer varies linearly with distance y from the wall. This is confirmed by experiments [103] and can also be justified by dimensional reasoning [104,105]. In the regions very close to the walls, however, turbulent fluctuations are damped due to viscous effects which can be taken into account by use of van Driest's hypothesis [46]. Therefore, for the two "inner regions" of an annular duct, mixing length can be specified as

$$\ell_{i,w} = \kappa y_w [1-\exp(-y_w^+/A^+)] \tag{2.24}$$

Here w = 1,2 corresponds to inner and outer wall of the annulus respectively and κ is von Kármán constant taken to be 0.41 while A^+ is a damping constant having a value of 26. Whether or not κ and A^+ are affected by large transverse curvature will be discussed later.

In the outer region of a turbulent boundary layer, the mixing length remains approximately constant and can be specified as

$$\ell_o = C_1 L \tag{2.25}$$

Where C_1 is a constant and L is a characteristic length scale of turbulence yet to be specified. It can be assumed to be equal to the local shear layer thickness for flows which are changing slowly so that the dynamics of turbulent fluctuations can "track" the development of

the mean velocity profile. For that case $C_1 \simeq 0.085$. Pletcher [106] and many others have successfully used such a model for the prediction of turbulent boundary layers. However, this model is based on the implicit neglect of the transport terms which, in general, can not be justified.

In the outer region, the length scale transported from upstream is significant since the large eddies which characterize that region travel a streamwise distance of several shear-layer thicknesses in their life-times. The rate at which large eddy structure changes, which determines changes in the length scale, is often quite slow relative to the mean flow development. So L, in Eq. (2.25), can be assumed to lag δ (shear layer thickness) in a manner controlled by the relaxation time for the large eddy structure, which is assumed to be proportional to $\delta/\bar{u}_\tau$ where $\bar{u}_\tau$ is a characteristic turbulence velocity. If it is further assumed that fluid in the outer part of the boundary layer travels at velocity u_m, the streamwise distance traversed by the flow during the relaxation time is $L^* = C_2 u_m \delta/\bar{u}_\tau$. A rate equation can be developed by assuming that L will tend towards δ according to

$$\frac{dL}{dx} = \frac{\delta - L}{L^*}$$

or

$$u_m \frac{dL}{dx} = \frac{\bar{u}_\tau}{C_2}\left(\frac{\delta - L}{\delta}\right)$$

By a proper choice of C_2, this can also be written as

$$u_m \frac{dL}{dx} = \frac{u_\tau}{C_2} \left(\frac{\delta - L}{\delta}\right) \tag{2.26}$$

where u_τ is the friction velocity.

It can be shown that the above equation is a one-dimensional ($\frac{\partial}{\partial y} = 0$) specialization of a more general transport equation for length scale such as the one proposed by Bradshaw [107]:

$$\underset{\text{advection}}{\frac{DL}{Dt}} = \underset{\text{generation}}{a_1 L \frac{\partial \bar{u}}{\partial y}} \quad \underset{\text{diffusion}}{- \frac{\partial}{\partial y}(v_L L)} \quad + \underset{\text{destruction}}{a_2 (-\overline{u'v'})^{1/2}}$$

where v_L is a turbulent transport velocity.

By assuming that at a certain streamwise station a uniform level of length scale exists in the outer region so that $\frac{\partial L}{\partial y} = 0$, and that diffusion of length scale can be neglected leads to the following equation for steady flow if it is further assumed that fluid in the outer region moves with a velocity of u_m:

$$u_m \frac{dL}{dx} = a_1 L \frac{\partial \bar{u}}{\partial y} + a_2 (-\overline{u'v'})^{1/2} \tag{2.27}$$

Now when $\frac{dL}{dx} = 0$ (i.e., when the turbulence and the mean flow are in local equilibrium), Eq. (2.27) reduces to

$$L = -\left(\frac{a_2}{a_1}\right) (-\overline{u'v'})^{1/2} / \left(\frac{\partial \bar{u}}{\partial y}\right)$$

Writing this value of L as δ and rearranging gives the following relation between a_1 and a_2:

$$a_1 = -a_2 (-\overline{u'v'})^{1/2} / \left(\delta \frac{\partial \bar{u}}{\partial y}\right) \tag{2.28}$$

Equation (2.27), then, becomes

$$u_m \frac{dL}{dx} = a_2(-\overline{u'v'})^{1/2} \left(\frac{\delta-L}{\delta}\right)$$

Now, by proper choice of C_2, $a_2(-\overline{u'v'})^{1/2}$ can be replaced by u_τ/C_2 if a lumped value of $(-\overline{u'v'})^{1/2}$ is taken in the outer region, so that

$$u_m \frac{dL}{dx} = \frac{u_\tau}{C_2}\left(\frac{\delta-L}{\delta}\right)$$

which is the same as Eq. (2.26).

a. Determination of C_1 and C_2 Consider turbulent flow in the entrance region of a parallel plate duct as shown in Fig. 2.4. A turbulence model, such as $\ell_o = 0.085\ S_\ell$ (with $S_\ell = \delta$), can describe the flow quite accurately in the region where the shear layers have not merged since the flow is more like an external boundary layer flow under favorable pressure gradient which has been calculated previously very successfully by a simple mixing length model [106]. However, such a model is unable to correctly describe the interaction of the two shear layers if $S_\ell = \delta$, where $\delta = \frac{d}{2}$ is taken as the "apparent" shear layer thickness after they merge. As stated in Section B.1, eddies from one shear layer penetrate into the other and the interaction grows as the flow tends towards its fully developed state. Although the phenomenon is intermittent, it can be assumed that the shear layers grow into each other as shown in Fig. 2.4. If the "actual" shear layer thickness, S_ℓ, is known, then the model $\ell_o = 0.085\ S_\ell$ ($S_\ell \neq \delta$) can be used to describe quite accurately the shear layer interaction

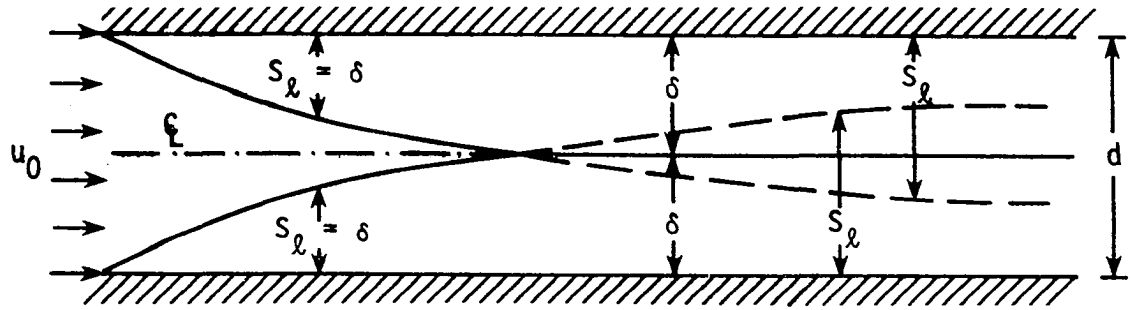

Fig. 2.4. Flow configuration in the entrance region of a parallel wall duct showing shear layer interaction

which causes the centerline velocity overshoot. Dean (see [108]), by a boundary layer sampling technique, observed that the interaction in a parallel plate duct is confined to within $\pm 0.2d$ of the centerline. This means that, in the fully developed state,

$$S_{\ell} \simeq 1.4\delta$$

therefore

$$\ell_o \simeq 0.085 \times 1.4\delta \simeq 0.12\delta \tag{2.29}$$

Now, in the fully developed state ($\frac{dL}{dx} = 0$), $L = \delta$ from Eq. (2.26); so from Eqs. (2.25) and (2.29) $C_1 = 0.12$.

Two forms for C_2 were considered; $C_2 = 0.92$ and $C_2 = 0.92\ \delta/L$. The latter choice gave slightly better results and was adopted. The restriction imposed for determination of the constant 0.92 was that ℓ_o/δ should remain of the order of 0.085 in the "displacement-interaction" region.

Once C_1 and C_2 are known, Eqs. (2.25) and (2.26), for the shear layers in an annular passage, can be written as

$$\ell_{o,w} = 0.12\ L_w \tag{2.30}$$

and

$$u_m \frac{dL_w}{dx} = 1.09\ u_{\tau_w} \left[\frac{L_w}{\delta_w} - \left(\frac{L_w}{\delta_w}\right)^2\right] \tag{2.31}$$

where w = 1,2 corresponds to the inner and outer wall of the annulus respectively.

The switch between inner and outer region models is made whenever $\ell_{o,w} \leq \ell_{i,w}$.

The mixing length given by Eq. (2.30) will eventually become discontinuous at the radius of maximum velocity after the growing boundary layers have merged as they tend towards the fully developed state. To overcome this, an average of the outer length scale ($\bar{\ell}_o = (\ell_{o,1}+\ell_{o,2})/2$) predicted for the flow along each wall was used for the central core region after the viscous layers had merged. This implies that in the fully developed state ($\frac{dL}{dx} = 0$), the mixing length in the "outer" region will be given as

$$\bar{\ell}_o = 0.12(r_2-r_1)/2 \tag{2.32}$$

The model described in Eqs. (2.23), (2.24), (2.30) and (2.31) will be seen to predict most hydrodynamic features of the annular flow quite accurately. Pletcher [109] has utilized a similar model, with $C_2 = 0.8\ \delta/L$, for calculation of flows containing regions of recirculation using an inverse finite-difference method to solve the boundary layer equations; but in that application δ was defined as δ_{99}, whereas in the present method it is defined as δ_{995} (the distance from the wall where $u = 0.995\ u_m$), partially accounting for the difference in the numerical constant.

The scheme suggested by Pletcher [110] to take account of the low Reynolds number effect is employed for some distance downstream of the entrance. When the low Reynolds number effect becomes negligible, a switch is made to the length scale transport model.

4. Bridging

It should be noted that after the boundary layers have merged, Eq. (2.23) will give zero turbulent viscosity at the radius of maximum velocity ($\frac{\partial u}{\partial y} = 0$). This implies zero turbulent conductivity there, which is unrealistic when asymmetric thermal boundary conditions exist; use of this model will likely lead to an inaccurate prediction of the temperature profile. This shortcoming, however, is not associated only with this model; Bradshaw's shear layer interaction model [111], for example, will also predict zero turbulent heat transport at the radius of zero shear.

An improvement in the predicted temperature distribution has been noted for fully developed flow when the turbulent viscosity (thus, the turbulent conductivity) profile predicted by Eq. (2.23) is "bridged" just by assuming a linear distribution between the peaks (see Fig. 4.12). Similar schemes for treating the eddy viscosity near the point of zero velocity gradient in the wall mixing zone of a wall jet have been suggested by Pai and Whitelaw [112] and by Dvorak [113]. In the latter study, a cosine fairing was used for the eddy viscosity. No studies of this type have been noted to date for annular flows.

5. Turbulence kinetic energy equation model

A more general remedy for the problem of predicting unrealistically small values of μ_T (thus, λ_T) in the central core can be provided by assuming $v_T = C_\mu k^{1/2}$ in Eq. (2.20), so that

$$\mu_T = C_\mu \bar{\rho} k^{1/2} \ell \tag{2.33}$$

where k is turbulence kinetic energy defined as

$$k = \frac{1}{2}(\overline{u'^2 + v'^2 + w'^2})$$

An exact transport equation for turbulence kinetic energy for axisymmetric boundary layer flows, derivable from the Navier-Stokes equations, is of the following form [83]:

$$\bar{\rho}\bar{u}\frac{\partial k}{\partial x} + \bar{\rho}\tilde{v}\frac{\partial k}{\partial y} = \frac{1}{r}(r\mu\frac{\partial k}{\partial y}) - \frac{1}{r}\frac{\partial}{\partial y}(r(\bar{\rho}\overline{v'k'} + \overline{v'p'})) - \bar{\rho}\overline{u'v'}\frac{\partial \bar{u}}{\partial y} - D_2 \tag{2.34}$$

In the above equation, the turbulent (kinetic and pressure) diffusion term can be modeled as given in [114], i.e.,

$$-\frac{1}{r}\frac{\partial}{\partial y}(r(\bar{\rho}\overline{v'k'} + \overline{v'p'})) = \frac{1}{r}\frac{\partial}{\partial y}(r\frac{\mu_T}{Pr_k}\frac{\partial k}{\partial y})$$

where Pr_k is turbulent Prandtl number for the diffusion of k.

The generation term, $-\bar{\rho}\overline{u'v'}\frac{\partial \bar{u}}{\partial y}$, is modeled by use of Eq. (2.19) and is given by

$$-\bar{\rho}\overline{u'v'}\frac{\partial \bar{u}}{\partial y} = \mu_T(\frac{\partial \bar{u}}{\partial y})^2$$

The dissipation term, D_2, is modeled as

$$D_2 = C_D \bar{\rho} k^{3/2}/\ell$$

The modeled form of the turbulence kinetic energy, then, is

$$\bar{\rho}\bar{u}\frac{\partial k}{\partial x} + \bar{\rho}\tilde{v}\frac{\partial k}{\partial y} = \frac{1}{r}\frac{\partial}{\partial y}\left(r\left(\mu + \frac{\mu_T}{Pr_k}\right)\frac{\partial k}{\partial y}\right) + \mu_T\left(\frac{\partial \bar{u}}{\partial y}\right)^2 - C_D\bar{\rho}k^{3/2}/\ell \quad (2.35)$$

The above equation is valid only where flow is fully turbulent. For that reason, the boundary conditions for Eq. (2.35) are not specified at the walls where flow is largely influenced by laminar viscosity. Instead, they are specified at some distance from the walls. The boundary conditions employed were

$$k(x,y_w^+) = -\bar{\rho}\overline{u'v'}(x,y_w^+)/C_D^{2/3} \quad (2.36)$$

A value of $y_w^+ \simeq 60$ is suggested.

The above boundary conditions follow from a specialization of Eq. (2.35) under the usual assumption that in the fully turbulent region near the wall the generation and dissipation terms balance one another and the Prandtl's mixing length formula, Eq. (2.23), holds in that region.

Two more boundary conditions for k are needed in Region I (Fig. 2.2) as the method to be described in Chapter III treats the two shear layers separately in that region. These are

$$k(x,\delta_1) = k(x,\delta_2) = \left(\frac{u_m}{u_0}\right)^2 k_0 \quad (2.37)$$

where k_0 is the free stream turbulence kinetic energy specified at the inlet.

An initial distribution of k is provided by initially using Eq. (2.23) up to some distance downstream of the inlet where the low Reynolds number modification [110] is no longer needed and then assuming

that the turbulent viscosity predicted by both Eqs. (2.23) and (2.33) are equal, i.e.,

$$k(\text{initial}) = \ell^2 \left|\frac{\partial \bar{u}}{\partial y}\right|^2 / C_\mu^2 \tag{2.38}$$

The length scale needed in Eq. (2.33) is provided by using the model described in Section B.3.

a. Determination of constants In the regions where the k variation is small so that convective and diffusion terms can be neglected, Eq. (2.35) reduces to

$$\mu_T \left(\frac{\partial \bar{u}}{\partial y}\right)^2 = C_D \bar{\rho} k^{3/2} / \ell$$

But, from Eqs. (2.23) and (2.33),

$$\mu_T \left(\frac{\partial \bar{u}}{\partial y}\right)^2 = \frac{(-\bar{\rho}\overline{u'v'})^2}{\mu_T} = \frac{(-\bar{\rho}\overline{u'v'})^2}{C_\mu \bar{\rho} k^{1/2} \ell}$$

therefore,

$$\frac{(-\bar{\rho}\overline{u'v'})^2}{C_\mu \bar{\rho} k^{1/2} \ell} = C_D \bar{\rho} k^{3/2} / \ell$$

or

$$-\frac{\overline{u'v'}}{k} = (C_\mu C_D)^{1/2} \tag{2.39}$$

In fully developed pipe flow, it has been found experimentally that over a considerable portion of the radius,

$$\frac{-\overline{u'v'}}{k} \simeq 0.3$$

So,

$$C_\mu C_D = 0.09 \tag{2.40}$$

Now from Eqs. (2.19) and (2.23),

$$-\bar{\rho}\overline{u'v'} = \bar{\rho}\ell^2\left|\frac{\partial \bar{u}}{\partial y}\right| \frac{\partial \bar{u}}{\partial y}$$

or

$$-\overline{u'v'} = \frac{\bar{\rho}\ell^2\left|\frac{\partial \bar{u}}{\partial y}\right|\bar{\rho}\ell^2\frac{\partial \bar{u}}{\partial y}}{\bar{\rho}^2\ell^2}$$

or

$$\mu_T^2 = \bar{\rho}^2\ell^2(-\overline{u'v'})$$

or

$$\mu_T = \bar{\rho}\ell(-\overline{u'v'})^{1/2}$$

Comparing this with Eq. (2.33) gives

$$C_\mu = \left(\frac{-\overline{u'v'}}{k}\right)^{1/2}$$

So from Eq. (2.39),

$$C_\mu = (C_\mu C_D)^{1/4}$$

or, from Eq. (2.40),

$$C_\mu = (0.09)^{1/4} = 0.548 \tag{2.41}$$

Also,

$$C_D = \frac{0.09}{C_\mu} = 0.164 \tag{2.42}$$

Pr_k, turbulent Prandtl number for diffusion of k, was assigned a value of 1.47 which has earlier been used for turbulent flow in parallel

plate channels as given in [115].

6. Turbulent Prandtl number

Turbulent Prandtl number was defined in a previous section as

$$Pr_T = \frac{\mu_T C_p}{\lambda_T} \tag{2.22}$$

A strict application of the Reynolds analogy by assuming that heat and momentum are transferred by the same process, leads to a turbulent Prandtl number of unity. However, experiments frequently show that Pr_T, in general, varies throughout the flow and also depends upon molecular Prandtl number. The literature discusses the value of Pr_T at great length (see, e.g., Reynolds [116]) without definite conclusions. Any model developed for the prediction of turbulent Prandtl number has to rely upon experiments in order to determine the empirical constants. The dilemma is that the experiments do not agree among themselves and no consensus exists, at least for the region very close to the wall, about the variation of Pr_T across a shear layer.

Two methods are generally used to calculate turbulent Prandtl number from the measurable quantities namely $\bar{u}$, $\bar{T}$, $-\overline{u'v'}$ and $-\overline{v'T'}$. These are described below briefly in order to develop an appreciation for the uncertainty involved in the determination of Pr_T even if the quantities measured were of sufficient accuracy.

a. The eddy correlation method From Eqs. (2.19) and (2.21):

$$\frac{\overline{u'v'}}{\overline{v'T'}} = \frac{\mu_T C_p}{\lambda_T} \frac{\frac{\partial \bar{u}}{\partial y}}{\frac{\partial \bar{T}}{\partial y}}$$

Using the definition of Pr_T from Eq. (2.23), this gives

$$Pr_T = \frac{\overline{u'v'}}{\overline{v'T'}} \frac{\frac{\partial \bar{T}}{\partial y}}{\frac{\partial \bar{u}}{\partial y}} \tag{2.43}$$

It can be seen that the process of determining Pr_T will involve differentiation of experimentally determined profiles of $\bar{u}$ and $\bar{T}$ which is not very straightforward. The uncertainty involved will be particularly large when the gradients are small; for example near the edge of a flat plate boundary layer or near the radius of maximum velocity in an annulus.

b. Integration method Total (laminar and turbulent) shear stress and heat flux can be written as

$$\tau = (\mu+\mu_T)\frac{\partial \bar{u}}{\partial y}$$

$$\dot{q} = -(\lambda+\lambda_T)\frac{\partial \bar{T}}{\partial y}$$

These two equations can be rearranged to give

$$\mu_T = \tau/\frac{\partial \bar{u}}{\partial y} - \mu$$

$$\lambda_T = -\dot{q}/\frac{\partial \bar{T}}{\partial y} - \lambda$$

So that,

$$Pr_T = \frac{\mu_T C_p}{\lambda_T} = C_p \left\{ \frac{\tau / \frac{\partial \bar{u}}{\partial y} - \mu}{-\dot{q} / \frac{\partial \bar{T}}{\partial y} - \lambda} \right\} \tag{2.44}$$

Here, again, $\frac{\partial \bar{u}}{\partial y}$ and $\frac{\partial \bar{T}}{\partial y}$ can be determined by numerical differentiation of $\bar{u}$ and $\bar{T}$ profiles respectively. In order to determine τ and $\dot{q}$, Eqs. (2.14) and (2.15) will have to be integrated (after they have been closed using the assumptions given in Eqs. (2.19) and (2.21)). For the case of fully developed annular flow, the momentum equation (2.14) can be written as

$$\frac{1}{r} \frac{\partial}{\partial r}(r\tau) = \frac{d\bar{p}}{dx}$$

Integration gives

$$\tau(r) = -\frac{1}{2} \frac{d\bar{p}}{dx}\bigg|_{fd} \left(\frac{r_m^2 - r^2}{r}\right) \tag{2.45}$$

where r_m, the radius of maximum velocity, can be determined from the measured velocity profile or by direct measurement of shear stress at one of the walls forming the annulus.

The energy equation (2.15) can be written as (after neglecting viscous dissipation and compression work)

$$\frac{1}{r} \frac{\partial}{\partial r}(r\dot{q}) = \bar{\rho} C_p \bar{u} \frac{\partial \bar{T}}{\partial x}$$

Integrating this, $\dot{q}$ can be written as

$$\dot{q}(r) = \frac{1}{r} \int_{r_1}^{r} \bar{\rho} C_p \bar{u} r \frac{\partial \bar{T}}{\partial x} \, dr$$

If the constant heat flux boundary condition is applied at one of the walls then, on full development,

$$\frac{\partial \overline{T}}{\partial x} = \left.\frac{\partial \overline{T}}{\partial x}\right|_b$$

Therefore, for constant $\overline{\rho}$ and C_p,

$$\dot{q}(r) = \frac{\overline{\rho} C_p}{r} \left.\frac{d\overline{T}}{dx}\right|_b \int_{r_1}^{r} \overline{u} r dr \qquad (2.46)$$

The integral appearing in the above equation can be evaluated using numerical techniques. Generally, numerical integration schemes are quite accurate while numerical differentiation schemes (needed to evaluate $\frac{\partial \overline{u}}{\partial y}$, $\frac{\partial \overline{T}}{\partial y}$) are not.

The experimental studies made to date have employed both eddy correlation and integration method for determining turbulent Prandtl number. There is fair amount of agreement among these studies on that the turbulent Prandtl number attains a value of 0.9 in the fully turbulent part of the inner region of a shear layer. Rotta [117], based on the measurements of Ludwieg [118] and Johnson [119], has suggested following formula for Pr_T across a flat plate boundary layer:

$$Pr_T = 0.9 - 0.4(y/\delta)^2 \qquad (2.47)$$

According to this formula, the value of turbulent Prandtl number is fairly uniform near the wall but falls to 0.5 at the edge of the layer. The reduction in Pr_T as the edge is approached was also observed by Blom [120] in his investigation of a flat plate boundary layer. For channel and pipe flow studies, the results are not so conclusive.

A number of experiments show a gradual reduction in Pr_T toward the centerline while others show quite the reverse (see, e.g., Kestin and Richardson [121]).

The results of Kuzay and Scott [69] and Ball and Azer [67] for an annular duct show a decrease in turbulent Prandtl number as the radius of maximum velocity is approached. These results might have been influenced by large uncertainties associated with the calculation of Pr_T in this region; however, one would expect a small value ($\simeq$0.7) of Pr_T since a "wake like flow" exists near the maximum velocity radius and, in fact, a value of $Pr_T = 0.7$ is commonly used for free shear flows [122].

At present, there seems to be no consensus about the value of turbulent Prandtl number very near the wall, say, $y^+ < 50$. Kuzay and Scott [69] report that very close to the wall Pr_T has a low value (0.4 to 0.6). Measurements of Ball and Azer [67] and Blom [120] seem to confirm this conclusion. However, data taken at Stanford University (see Kays and Moffat [123]) shows that turbulent Prandtl number goes well above unity very close to the wall.

How the wall value of Pr_T affects the models proposed for turbulent Prandtl number can be shown by considering Cebeci's model [124]. Cebeci, by applying van Driest's concept [46] to temperature fluctuations, proposed following model for turbulent Prandtl number:

$$Pr_T = \frac{\kappa[1-\exp(-y^+/A^+)]}{\kappa_h[1-\exp(-y^+/B^+)]} \tag{2.48}$$

where B^+ is a damping constant for temperature fluctuations and κ_h is mixing length constant for heat.

At the wall, Pr_T is given by

$$(Pr_T)_w = \frac{\kappa}{\kappa_h} \frac{B^+}{A^+} \tag{2.49}$$

Note that as y^+ becomes larger the exponential terms in Eq. (2.48) approach zero. The turbulent Prandtl number then becomes

$$(Pr_T)_\infty = \frac{\kappa}{\kappa_h} \tag{2.50}$$

In the logarithmic region, $Pr_T \simeq 0.9$. So that,

$$\frac{\kappa}{\kappa_h} = 0.9 \tag{2.51}$$

Now from Eqs. (2.49) and (2.51), for $A^+ = 26$,

$$B^+ = 28.9(Pr_T)_w \tag{2.52}$$

For a wall value of turbulent Prandtl number more than unity, say 1.5,

$$B^+ = 43.4 \tag{2.53}$$

If $(Pr_T)_w = 0.6$ (the upper limit of the value suggested by Kuzay and Scott), then

$$B^+ = 17.3 \tag{2.54}$$

The two values of B^+ given by Eqs. (2.53) and (2.54) are significantly different and if used in Eq. (2.48) will give drastically different variation of turbulent Prandtl number near the wall.

In view of the absence of reliable data, a constant value of

$Pr_T = 0.9$ is used throughout this study unless otherwise mentioned. Generally, this value gives sufficiently accurate predictions of heat transfer. This seems to suggest that

> . . . if ignorance prevails for a long time about something in which many are interested, it is often an indication that exact knowledge is not necessary; for otherwise a false assumption would bring such startling divergences between predictions and experiments that its falsity would be at once apparent [114].

7. Transverse curvature effect

In flow through annuli of very small radius ratios, the boundary layer developing around the core is relatively thick, i.e., δ_1/r_1 is large, which may affect the turbulence structure causing the heat transfer and skin friction to be different from that predicted by the usual turbulence models due to changes in the turbulence structure itself not accounted for by the models.

The effect of transverse curvature on axisymmetric turbulent boundary layers has been studied theoretically and experimentally in many investigations [125-130]. In a thick axisymmetric boundary layer, Rao [125] argued that the logarithmic law in the classical two-dimensional coordinates does not hold since the constant stress layer is no longer present. He proposed that the logarithmic law of the wall in axisymmetric flow around a cylinder of radius r_1 should be taken as

$$u^+ = \frac{1}{\kappa} \log(r_1^+ \log \frac{r}{r_1}) + B \qquad (2.55)$$

where κ and B are as defined earlier but may have different values. Rao and Keshavan [126] undertook an experimental investigation of axisymmetric turbulent boundary layers in zero pressure gradient and concluded that both κ and B are not universal constants. Afzal and Narasimha [128], however, expressed skepticism about the validity of the conclusion drawn in [126] as the flow may not have been in the fully turbulent state in some of those experiments. They (Afzal and Narasimha) further argued that a logarithmic law in classical two-dimensional coordinates does exist and that only B is a nonuniversal constant.

Huffman and Bradshaw [129] show by data analysis that the viscous sublayer is more strongly affected by transverse wall curvature than is the rest of the inner region. This will suggest that only B (or equally van Driest's damping constant A^+, as B depends on A^+) is significantly affected by transverse curvature, a conclusion which is in line with the findings of Afzal and Narasimha. Huffman and Bradshaw do not suggest any explanation for the apparent curvature effect except that it is a real effect of curvature on the sublayer.

Cebeci [130], using Rao's log law coordinates [125], suggested a modified mixing length distribution for the inner region. He, however, stated that this modification did not change the results (velocity profiles, skin friction) from those obtained by the usual mixing length distribution. According to him, the real effect comes by the use of a variable α in his eddy viscosity distribution for the

outer region, i.e.,

$$\mu_T \text{ (outer)} = \alpha \bar{\rho} u_m \delta_k^* \tag{2.56}$$

where δ_k^* is the kinematic displacement thickness, and the α function includes any intermittency effects or Reynolds number dependence as given in [130]. In view of the discussion presented above, however, it is hard to believe that transverse curvature will significantly affect the outer region eddy viscosity. Such a model seems particularly inappropriate for the use in annular passages.

Experimental investigation of turbulent flow in annuli of very small radius ratios have been performed by Brighton and Jones [58], Lawn and Elliot [35], and Rehme [62]. Both of the former investigations indicate that the velocity at the edge of the sublayer on the inner wall falls below the universal logarithmic velocity profile. This evidence suggests that transverse curvature does affect the sublayer. According to Rheme [62], however, his results did not exhibit any difference from the usual logarithmic velocity profile near the inner wall, even for large curvature.

It is assumed here that the sublayer thickness around the inner wall of the annulus decreases as the curvature increases. This is because the sublayer on a convex surface seems more likely to be influenced by the fluid elements which penetrate into it periodically from positions further removed from the wall as opposed to the sublayer on a concave surface. In other words, large convex curvature helps turbulent eddies tear apart the viscous sublayer so that the effective

time-mean thickness is decreased. A measure of the sublayer thickness is A^+, the van Driest's damping constant. On the basis of the available data of various authors [35,58], A^+ was assumed to differ from its value of 26 for the inner wall, in the case of small radius ratios, according to:

$$A^+ = 26(r^*)^{0.1} \tag{2.57}$$

A similar approach was used by Hanjalic [47] to account for the transverse curvature effect in calculating fully developed flow in an annulus of $r^* = 0.088$ using a three equation differential model of turbulence. In the calculation procedure of Patankar and Spalding [2], which he employed, the near wall boundary conditions are determined by use of "wall functions". In order to calculate the velocity boundary condition near the inner wall, the constant B in Eq. (2.18) was modified which is equivalent to modifying A^+ as done in the present study.

8. Laminar-turbulent transition

The boundary layer in the entrance region of a duct depends, along with other factors, upon the shape of the entrance. In a rounded entrance, (see Fig. 2.5), the boundary layers will generally start as laminar, even though the duct Reynolds number is high enough to characterize turbulent flow, and will undergo a transition to turbulent flow at some distance downstream of the entrance. In a square-edged entrance (Fig. 2.5) a small separated flow region may even exist, as

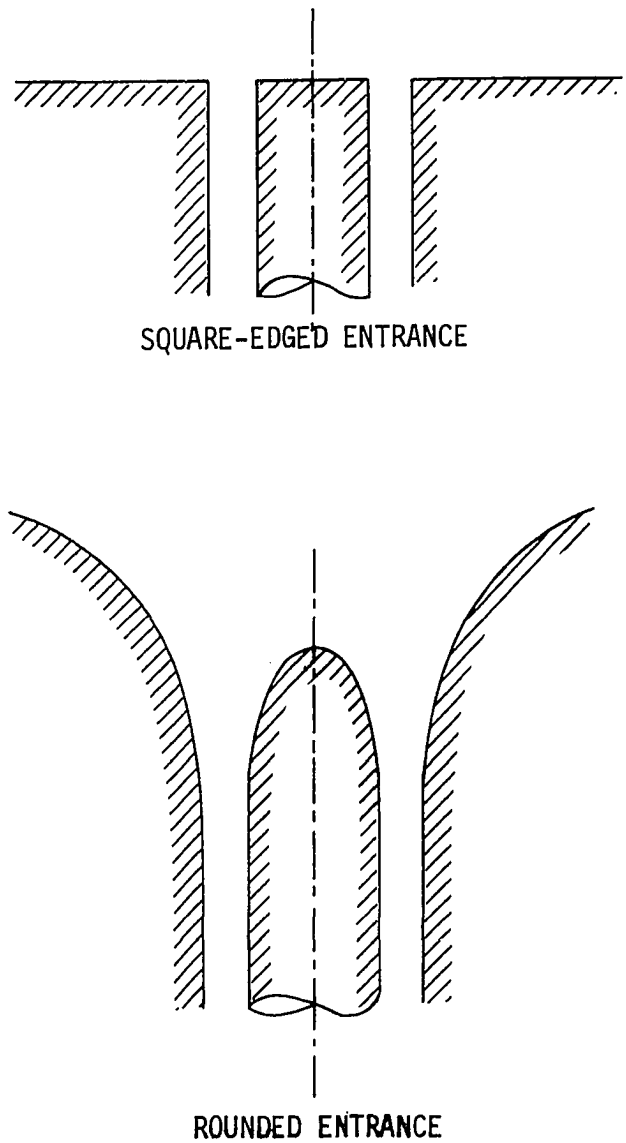

Figure 2.5. Two possible entrance shapes

was observed by Olson and Sparrow [63].

In some of the experiments with which the present predictions will be compared in Chapter IV, the boundary layers were tripped at the entrance so that the flow was turbulent from the beginning. However, trips may not be present in practical circumstances and one would like to be able to predict the flow under actual conditions which may involve laminar-turbulent transition.

Considerable interest has been shown in the stability of laminar shear flows and the eventual transition from a laminar state to a turbulent state of fluid motion because of the fundamental importance of being able to make a realistic prediction of where and if transition will occur in a given configuration under a given environment. The location of the point of transition depends upon many factors such as, Reynolds number, the streamwise pressure gradient, free stream turbulence, the curvature and roughness of the surface, the surface temperature, etc. Several correlations have been suggested for the relatively simple case of two-dimensional constant property boundary layers. One such correlation is given by Cebeci et al. (see [83]) as

$$Re_{\theta,tr} = 1.174\left(1 + \frac{22400}{Re_x}\right)Re_x^{0.46} \qquad (2.58)$$

for $1 \times 10^5 \leq Re_x \leq 40 \times 10^6$.

The above correlation was not found suitable for prediction of the onset of transition in the configuration under study. Transition in internal flows, perhaps, largely depends upon the shape of the entrance

and it becomes difficult to predict it's initiation point by use of a general correlation.

In some calculation procedures (see, for example, Cebeci and Chang [131]), the experimental location of transition is used. This point is often taken as the point of minimum Stanton number obtained from heat transfer measurements. It should be noted, however, that the actual transition process begins somewhat upstream of the location where the wall heat transfer shows an upward trend. In STAN5 (A Program for Numerical Computation of Two-Dimensional Internal/External Boundary Layer Flows), Crawford and Kays [132] assumed that transition will occur whenever $Re_\theta = 200$. Cebeci and Chang [131] used a value of critical $Re_\theta = 320$ for pipe flow whenever the experimental transition location was not available.

The transition region is characterized by the appearance of turbulent "spots" outside of which the flow still remains laminar. While moving downstream, these spots grow and merge with one another until the flow becomes fully turbulent. These spots were identified first by Emmons [133] and the existence of them in the boundary layer flow has been confirmed experimentally by Schubauer and Klebanoff [134] and others. The calculation of flow through the transition region can be made by use of an intermittency function γ which was first introduced by Emmons such that $\gamma = 0$ for fully laminar flow and $\gamma = 1$ for fully turbulent flow. If μ_T is the turbulent viscosity in the fully turbulent flow, then the effective turbulent viscosity in the

transition region can be calculated as

$$(\mu_T)_{tr} = \gamma\mu_T \tag{2.59}$$

In the present study, the Dhawan and Narasimha correlation [135] for γ, which was obtained by using the source density function of Emmons [133], was used. According to this the intermittency function, γ, in the streamwise direction is

$$\gamma = 1-\exp(-0.412\ \xi^2) \tag{2.60}$$

where

$$\xi = \frac{x-x_{tr}}{\Delta} \tag{2.61}$$

for $x_{tr} \geq x \geq x_t$ and Δ is a measure of the extent of the transition taken as

$$\Delta = x\Big|_{\Delta=0.75} - x\Big|_{\Delta=0.25} \tag{2.62}$$

according to [135].

x_t, in the above, is the location where transition is complete (or flow becomes fully turbulent). This location can be given by the following approximate relation:

$$\frac{Re_{x,t}}{Re_{x,tr}} \simeq 2 \tag{2.63}$$

Another correlation for determining the extent of transition region, which is incorporated in the present computer code, is that due to Dhwan and Narasimha [135] and can be reduced to

$$x_t = x_{tr} + 5.0\ Re^*(Re_{x,tr})^{0.8} \tag{2.64}$$

where Re^* is the local unit Reynolds number, u_m/ν_m.

C. Complete Mathematical Model

1. Governing equations

Under the assumptions given in Eqs. (2.19) and (2.21), Eqs. (2.13-2.15) have the same form as Eqs. (2.7-2.9) which apply to laminar flow. So the model equations, both for laminar and turbulent flow, can be written as

continuity equation:

$$\frac{\partial}{\partial x}(\rho u) + \frac{1}{r}\frac{\partial}{\partial y}(r\rho v) = 0 \tag{2.65}$$

momentum equation:

$$\rho u \frac{\partial u}{\partial x} + \rho v \frac{\partial u}{\partial y} = \frac{1}{r}\frac{\partial}{\partial y}(r n_u \frac{\partial u}{\partial y}) - \frac{dp}{dx} + f_x \tag{2.66}$$

where n_u, the coefficient for momentum diffusion, is given as

$n_u = \mu$ for laminar flows

and

$n_u = \mu + \mu_T$ for turbulent flows

energy equation:

$$\rho C_p u \frac{\partial T}{\partial x} + \rho C_p v \frac{\partial T}{\partial y} = \frac{1}{r}\frac{\partial}{\partial y}(r n_T \frac{\partial T}{\partial y}) + n_u(\frac{\partial u}{\partial y})^2 + \beta T u \frac{dp}{dx} \tag{2.67}$$

where n_T, the coefficient for diffusion of heat, is given as

$$n_T = \lambda \text{ for laminar flows}$$

and

$$n_T = \lambda + \lambda_T \text{ for turbulent flows}$$

In the above, $u = \bar{u}$, $v = \tilde{v}$, $p = \bar{p}$, $T = \bar{T}$ and $\rho = \bar{\rho}$ for turbulent flows.

Note that Eqs. (2.65) and (2.67) have four unknowns, namely, u, v, p, and T after the properties of the fluid have been specified. An additional equation, therefore, is needed which, for confined flows, is specified through the requirement that, for no blowing or suction through the walls, overall mass flow should be conserved, i.e.,

$$\dot{m} = \int_A \rho u dA = 2\pi \int_0^{r_h} \rho u r dy = \text{constant} \tag{2.68}$$

This equation will be used to determine $\frac{dp}{dx}$ as described in the next chapter.

2. Boundary conditions

To complete the mathematical model, appropriate boundary conditions need to be specified which for the present geometry are given as

$$u(x,0) = u(x,r_h) = 0$$

i.e., no slip at the walls,

$$v(x,0) = v(x,r_h) = 0,$$

i.e., no blowing or suction through the walls, and

$$T(x,0) = T_1(x),\ T(x,r_h) = T_2(x);$$

where $T_1(x)$ and $T_2(x)$ are the specified wall temperature distributions, or

$$\dot{q}(x,0) = \dot{q}_1(x),\ \dot{q}(x,r_h) = \dot{q}_2(x); \tag{2.69}$$

where $\dot{q}_1(x)$ and $\dot{q}_2(x)$ are the specified wall heat flux distributions, or a combination of these.

Also,

$$u(0,y) = u_e(y)$$

$$p(0,y) = p_e$$

$$T(0,y) = T_e(y) \tag{2.70}$$

Boundary conditions are not needed at the downstream end of the duct. This is a consequence of the use of the boundary layer approximation which has rendered the governing equations parabolic in nature. Eqs. (2.65-2.70), thus, present the complete mathematical model for laminar and turbulent flow and heat transfer in axisymmetric annular passages.

3. Fluid properties

The properties of the fluid, namely, density, viscosity, thermal conductivity, and specific heat, are, in general, assumed to vary with temperature and pressure. Their values need to be specified before the set of governing equations can be solved. Specific property relations used in the present study will be given in Appendix F.

D. Engineering Parameters

It seems appropriate to define the engineering parameters of interest for the annular geometry since some of these differ from the well-known definitions for flat plate or tube flow.

1. Shear stress

Shear stress at any point in the flow can be determined by

$$\tau = (\mu+\mu_T)\frac{\partial u}{\partial y} \tag{2.71}$$

where $\mu_T = 0$ in laminar flow. In case of turbulent flow, the laminar contribution to the shear stress away from the walls is negligibly small. At the walls, however, turbulent viscosity vanishes and wall shear stress can be calculated as

$$\tau_w = \mu_w \left.\frac{\partial u}{\partial y}\right|_w \tag{2.72}$$

2. Skin-friction coefficient

Skin-friction coefficients at the two walls are defined as

$$C_{f_w} = \frac{\tau_w}{1/2\ \rho_b u_b^{\,2}} \tag{2.73}$$

where w = 1,2 corresponds to the inner and outer wall respectively.

An overall skin-friction coefficient for the annulus can be defined as

$$C_f = \frac{C_{f_2} + r^* C_{f_1}}{1+r^*} \tag{2.74}$$

3. Displacement thickness

The displacement thickness, δ^*, is a measure of the mass flow defect due to the presence of viscous boundary layer. It is defined as the distance which the inviscid flow would need to be displaced from the wall to yield the same flow rate as in the actual flow with the boundary layer included. For the shear layer on the inner wall, it can be given as

$$(\delta_1^*+r_1)^2-r_1^2 = 2\int_{r_1}^{r_1+\delta_1}(1-\frac{\rho u}{\rho_m u_m})rdr$$

or

$$\delta_1^* = \sqrt{r_1^2+\int_{r_1}^{r_1+\delta_1}(1-\frac{\rho u}{\rho_m u_m})rdr}-r_1 \qquad (2.75)$$

Similarly for outer shear layer, the displacement thickness can be given as

$$r_2^2-(r_2-\delta_2^*)^2 = 2\int_{r_2-\delta_2}^{r_2}(1-\frac{\rho u}{\rho_m u_m})rdr$$

or

$$\delta_2^* = r_2-\sqrt{r_2^2-2\int_{r_2-\delta_2}^{r_2}(1-\frac{\rho u}{\rho_m u_m})rdr} \qquad (2.76)$$

4. Momentum thickness

The momentum thickness, θ, is defined as the thickness of a layer of reference velocity fluid carrying a momentum flow rate equal to the momentum defect caused by the presence of boundary layer. For the inner shear layer, the momentum thickness can be given by the following

relation:

$$(\theta_1+r_1)^2-r_1^2 = 2\int_{r_1}^{r_1+\delta_1} \frac{u}{u_m}(1 - \frac{\rho u}{\rho_m u_m})rdr$$

or

$$\theta_1 = \sqrt{r_1^2 + 2\int_{r_1}^{r_1+\delta_1} \frac{u}{u_m}(1 - \frac{\rho u}{\rho_m u_m})rdr}-r_1 \qquad (2.77)$$

For the outer shear layer, the momentum thickness is given as

$$r_2^2-(r_2-\theta_2)^2 = 2\int_{r_2-\delta_2}^{r_2} \frac{u}{u_m}(1 - \frac{\rho u}{\rho_m u_m})rdr$$

or

$$\theta_2 = r_2-\sqrt{r_2^2-2\int_{r_2-\delta_2}^{r_2} \frac{u}{u_m}(1 - \frac{\rho u}{\rho_m u_m})rdr} \qquad (2.78)$$

5. Bulk mean temperature

The bulk temperature at any cross section can be calculated once the bulk enthalpy at that location is known. The bulk enthalpy is defined as

$$H_b = \frac{\int_A \rho u H dA}{\int_A \rho u dA} \qquad (2.79)$$

Now

$$dH = C_p dT \qquad (2.80)$$

The equality sign in the above equation holds exactly for a perfect gas; while for any other fluid, it holds only approximately.

Integration of Eq. (2.80) reduces it to

$$H-H_0 = \int_{T_0}^{T} C_p dT \tag{2.81}$$

If functional dependence of C_p is known, then an explicit relation between T and H can be obtained. Assuming, for example, that C_p varies as

$$\frac{C_p}{C_{p_0}} = \left(\frac{T}{T_0}\right)^a \tag{2.82}$$

Equation (2.81) can be reduced to:

$$H-H_0 = \frac{C_{p_0}}{T_0^a} \int_{T_0}^{T} T^a dT$$

or

$$H = H_0 + \frac{C_{p_0} T_0}{(a+1)} \left[\left(\frac{T}{T_0}\right)^{a+1} - 1\right] \tag{2.83}$$

This relation can be substituted into Eq. (2.79) to determine the bulk enthalpy from the calculated temperature profile.

Eq. (2.83) can be rearranged as

$$T = T_0\left[1 + \frac{(a+1)(H-H_0)}{C_{p_0} T_0}\right]^{\frac{1}{(a+1)}}$$

Bulk temperature, $T = T_b$, can be calculated when $H = H_b$, i.e.,

$$T_b = T_0\left[1 + \frac{(a+1)(H_b-H_0)}{C_{p_0} T_0}\right]^{\frac{1}{(a+1)}} \tag{2.84}$$

6. Heat transfer coefficient

The heat transfer coefficient is defined as

$$h = \frac{\dot{q}_w}{T_w - T_b} \tag{2.85}$$

where, for the case of specified wall temperature, $\dot{q}_w$ is calculated as

$$\dot{q}_w = \lambda_w \left.\frac{\partial T}{\partial y}\right|_w \tag{2.86}$$

The Nusselt number is a useful nondimensional parameter for heat transfer at the wall and is defined as

$$Nu = \frac{hD_h}{\lambda_b} \tag{2.87}$$

Another useful nondimensional parameter for wall heat transfer is the Stanton number which is defined as

$$St = \frac{h}{\rho_b u_b C_{p_b}} \tag{2.88}$$

III. NUMERICAL METHOD

This chapter describes the numerical method used to solve the governing partial differential equations. The finite-difference scheme employed is a modification of the explicit Dufort-Frankel [136] method which allows fairly large streamwise steps. A computer code, "ANNULUS", is developed which is introduced in the last section.

A. Nondimensional Form of the Governing Equations

It is generally useful to write the governing equations in dimensionless form before attempting to obtain a solution. In the present study, the variables are nondimensionalized as follows:

$$U = \frac{u}{u_0}, \quad V = \frac{v}{v_0}, \quad P = \frac{p}{\rho_0 u_0^2}, \quad X = \frac{\rho_0 u_0 x}{\mu_0}, \quad Y = \frac{\rho_0 u_0 y}{\mu_0},$$

$$R = \frac{\rho_0 u_0 r}{\mu_0}, \quad T^* = \frac{C_{p_0} T}{u_0^2}, \quad \dot{Q} = \frac{\dot{q}}{\rho_0 u_0^3}, \quad F_x = \frac{f_x \mu_0}{\rho_0^2 u_0^3},$$

$$\hat{\rho} = \frac{\rho}{\rho_0}, \quad \hat{C}_p = \frac{C_p}{C_{p_0}}, \quad \hat{\beta} = \frac{u_0^2 \beta}{C_{p_0}}, \quad N_u = \frac{n_u}{\mu_0}, \quad N_T = \frac{n_T}{\mu_0 C_{p_0}}$$

The governing equations [Eqs. (2.65-2.68)] then become

$$\frac{\partial}{\partial X}(\hat{\rho}U) + \frac{1}{R}\frac{\partial}{\partial Y}(R\hat{\rho}V) = 0 \tag{3.1}$$

$$\hat{\rho}U\frac{\partial U}{\partial X} + \hat{\rho}V\frac{\partial U}{\partial Y} = \frac{1}{R}\frac{\partial}{\partial Y}(RN_u\frac{\partial U}{\partial Y}) - \frac{dP}{dX} + F_X \tag{3.2}$$

$$\hat{\rho}\hat{C}_p U \frac{\partial T^*}{\partial X} + \hat{\rho}\hat{C}_p V \frac{\partial T^*}{\partial Y} = \frac{1}{R}\frac{\partial}{\partial Y}(RN_T \frac{\partial T^*}{\partial Y}) + N_u(\frac{\partial U}{\partial Y})^2 + \beta T^* U \frac{dP}{dX} \tag{3.3}$$

$$\int_0^{R_h} \hat{\rho} U R dY = \text{Constant} \tag{3.4}$$

The nondimensional boundary and initial conditions are:

Boundary conditions:

$$U(X,0) = U(X,R_h) = V(X,0) = V(X,R_h) = 0$$

and

$$T^*(X,0) = T_1^*(X),\ T^*(X,R_h) = T_2^*(X)$$

or

$$\dot{Q}(X,0) = \dot{Q}_1(X),\ \dot{Q}(X,R_h) = \dot{Q}_2(X)$$

or a combination of these. (3.5)

Initial conditions:

$$U(0,Y) = U_e(Y)$$

$$P(0,Y) = P_e$$

$$T^*(0,Y) = T_e^*(Y) \tag{3.6}$$

The turbulence kinetic energy equation (2.34) can also be nondimensionalized, if used, as follows:

$$\hat{\rho} U \frac{\partial \hat{k}}{\partial X} + \hat{\rho} V \frac{\partial \hat{k}}{\partial Y} = \frac{1}{R}\frac{\partial}{\partial Y}(RN_k \frac{\partial \hat{k}}{\partial Y}) + (N_u - \hat{\mu})(\frac{\partial U}{\partial Y})^2 - C_D \hat{\rho}\hat{k}^{3/2}/\hat{\ell} \tag{3.7}$$

where

where

$$\hat{k} = \frac{k}{u_0^2}, \quad \hat{\mu} = \frac{\mu}{\mu_0}, \quad \hat{\ell} = \frac{\rho_0 u_0}{\mu_0},$$

$$N_k = \frac{n_k}{\mu_0} = (\mu + \frac{\mu_T}{Pr_k})/\mu_0$$

Note that Eqs. (3.2), (3.3) and (3.7) all have the same form. If ϕ stands for U, T* or $\hat{k}$, then any one of these equations can be modeled as

$$a\frac{\partial \phi}{\partial X} + b\frac{\partial \phi}{\partial Y} = \frac{1}{R}\frac{\partial}{\partial Y}(RN_\phi \frac{\partial \phi}{\partial Y}) + S \tag{3.8}$$

where a, b, N_ϕ and S are, in general, functions of X, Y and ϕ.

B. Finite-Difference Formulation

The model equation, Eq. (3.8), is parabolic in nature, so a marching finite-difference method can be employed. The present analysis has made use of an explicit three level finite-difference scheme of the Dufort-Frankel [136] type which has earlier been used for predicting flow in wall boundary layers [137], circular pipe [138] and jet flow [139]. This scheme does not have severe stability constraints and permits the use of fairly large streamwise steps.

1. The difference equations

Fig. 3.1 shows the finite-difference grid utilized in the present calculation method. The mesh size generally varies throughout the flow. The finite-difference form of Eq. (3.8) for a variable grid can be

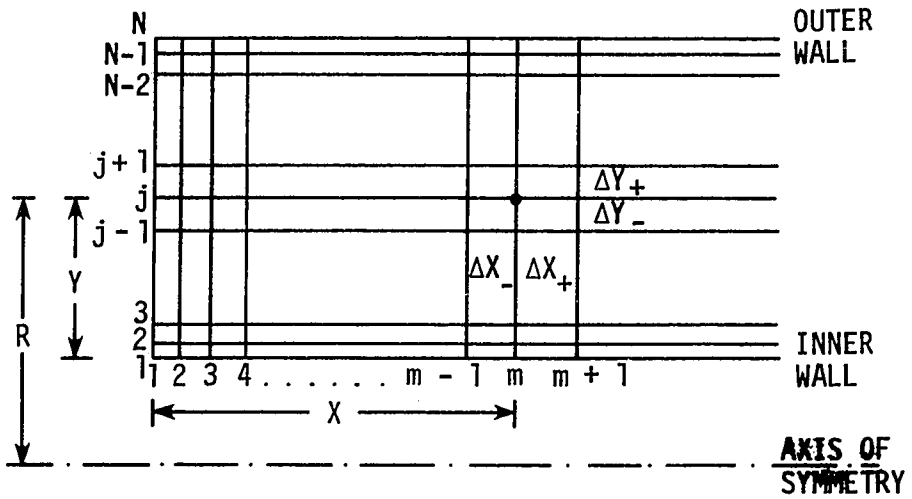

Fig. 3.1. Finite-difference grid

written as

$$a_j^m \frac{\phi_j^{m+1}-\phi_j^{m-1}}{\Delta X_+ + \Delta X_-} + b_j^m \frac{\phi_{j+1}^m - \phi_{j-1}^m}{\Delta Y_+ + \Delta Y_-}$$

$$= \frac{2}{R_j(\Delta Y_+ + \Delta Y_-)} \left[R_{j+1/2} N_{j+1/2}^m \frac{(\phi_{j+1}^m - \bar{\phi}_j^m)}{\Delta Y_+} \right.$$

$$\left. - R_{j-1/2} N_{j-1/2}^m \frac{(\bar{\phi}_j^m - \phi_{j-1}^m)}{\Delta Y_-} \right] + \bar{S}_j^m \qquad (3.9)$$

where

$$(\ )_{j+1/2} = [(\ )_j + (\ )_{j+1}]/2$$

$$(\ )_{j-1/2} = [(\ )_j + (\ )_{j-1}]/2$$

and

$$\bar{\phi}_j^m = \frac{\Delta X_+ \phi_j^{m-1} + \Delta X_- \phi_j^{m+1}}{\Delta X_+ + \Delta X_-} \qquad (3.10)$$

Special consideration needs to be given to the source term, $\bar{S}_j^m$. In the case of the momentum equation (3.2), it is written as

$$\bar{S}_j^m = - \frac{P^{m+1} - P^{m-1}}{\Delta X_+ + \Delta X_-} + F_{x_j}^m \qquad (3.11)$$

while for energy equation (3.3), it is written as

$$\bar{S}_j^m = N_{u_j}^m \left(\frac{U_{j+1}^m - U_{j-1}^m}{\Delta Y_+ + \Delta Y_-} \right)^2 + \hat{\beta} T_j^{*m} U_j^m \frac{P^{m+1} - P^{m-1}}{\Delta X_+ + \Delta X_-} \qquad (3.12)$$

In the case of the turbulence kinetic energy equation (3.7), the finite-difference representation of the source term was not as straight-

forward because of the presence of $\hat{k}^{3/2}$ in the dissipation term. At first, $\bar{S}_j^m$ was written as

$$\bar{S}_j^m = (N_{u_j}^m - \hat{\mu})\left(\frac{U_{j+1}^m - U_{j-1}^m}{\Delta Y_+ + \Delta Y_-}\right)^2 - C_D \hat{\rho}_j^m \hat{k}_j^{m\,3/2}/\hat{\ell}_j^m$$

This representation, however, caused the solution to become unstable when $\hat{k}^{3/2}$ was evaluated at $(\ )_j^m$. Note that in the diffusion term, $\hat{k}_j^m$ (also U_j^m and T_j^{*m} in the momentum and energy equation respectively) is taken to be the weighted average of $\hat{k}_j^{m+1}$ and $\hat{k}_j^{m-1}$ to avoid instability as is required by the Dufort-Frankel differencing. The same remedy can be used for the dissipation term but, then, $\hat{k}_j^{m+1}$ will be nonlinear and an iterative solution will be required at each grid point which will increase the computational cost considerably. In order that a noniterative solution still be possible, the dissipation term in $\bar{S}_j^m$ was represented as

$$-C_D\hat{\rho}\hat{k}^{3/2}/\hat{\ell} = -C_D\hat{\rho}\hat{k}^{1/2}\hat{k}/\hat{\ell}$$

$$= -C_D\hat{\rho}_j^m\left(\frac{\Delta Y_+ \hat{k}_{j-1}^m + \Delta Y_- \hat{k}_{j+1}^m}{\Delta Y_+ + \Delta Y_-}\right)^{1/2}\left(\frac{\Delta X_+ \hat{k}_j^{m-1} + \Delta X_- \hat{k}_j^{m+1}}{\Delta X_+ + \Delta X_-}\right)/\hat{\ell}_j^m \qquad (3.13)$$

This provided a stable solution (see the next section for details on stability analysis). It will be shown in Appendix C that the above representation of the dissipation term is mathematically consistent.

The finite-difference form of the continuity equation (3.1), employed in the present solution method, is given as

$$R_{j+1/2}\frac{(\hat{\rho}^{m+1}_{j+1}U^{m+1}_{j+1}-\hat{\rho}^{m-1}_{j+1}U^{m-1}_{j+1}+\hat{\rho}^{m+1}_{j}U^{m+1}_{j}-\hat{\rho}^{m-1}_{j}U^{m-1}_{j})}{2(\Delta X_{+}+\Delta X_{-})}$$

$$+\frac{R_{j+1}\hat{\rho}^{m+1}_{j+1}V^{m+1}_{j+1}-R_{j}\hat{\rho}^{m+1}_{j}V^{m+1}_{j}}{\Delta Y_{+}}=0 \qquad (3.14)$$

2. Consistency, stability and convergence

Consistency and stability are both major concerns arising in the use of finite-difference methods. It is only when these conditions are satisfied that there is a hope of obtaining a converged solution, according to Lax's equivalency theorem (see, e.g., Roache [140]). Convergence here means that the solution to the finite-difference equations approaches the true solution to the partial differential equations having the same initial and boundary conditions.

Consistency deals with the degree to which the finite-difference equations approximate the partial differential equations. The difference between a partial differential equation and its finite-difference representation is known as truncation error. A finite-difference scheme is said to be consistent if the truncation error vanishes as the mesh is refined. Consistency is generally studied by expanding the dependent variables in Taylor series and observing the difference between the partial differential equations and the finite-difference representation. It will be shown in Appendix C that the finite-difference representation, Eq. (3.9), of the model equation (3.8) is mathematically consistent.

Stability is a very important consideration since even the very best finite-difference schemes in terms of truncation error can be unstable and hence give a solution which is entirely different from that of the partial differential equations, rendering the results useless. The essence of stability is that round off errors, or errors from any other source, do not grow as the solution is advanced. No general theory exists for the stability analysis of nonlinear partial differential equations. For linear PDE's, the theory of Von Neumann (see e.g., Richtmyer and Morton [141]) can generally be applied in order to obtain stability restriction on the axial step size. Madni [139] applied this theory to study the stability of Dufort-Frankel formulation of the nonlinear boundary layer equations by treating the coefficients of the convective terms locally as constants. The stability criterion developed thereby is for "local" stability as the coefficients can be considered constant only in a small neighborhood of each grid point; but if the requirement is checked at each grid point then it can be reasoned that an instability could not originate.

Following the analysis given in [139], the stability constraint for Eq. (3.9) can be given as, with $\Delta Y_+ \simeq \Delta Y_- = \Delta Y$,

$$\Delta X_+ \leq \min_{j=2,N-1} \left[\frac{a_j^m \, \Delta Y}{\left| b_j^m + \frac{N_{\phi_{j+1}}^m - N_{\phi_{j-1}}^m}{2\Delta Y} \right|} \right] \tag{3.15}$$

This restriction, however, is valid only if the source term in Eq. (3.8) is not a function of ϕ. In case of turbulence kinetic energy

equation, this is not the case as S contains $\hat{k}^{3/2}$ in the dissipation term. The Dufort-Frankel scheme was always found to be unstable whenever $\hat{k}^{3/2}$ was written as $(\hat{k}_j^m)^{3/2}$. This should have not been unexpected since the finite-difference scheme (Eq. (3.9)) is unstable if in the diffusion term $\bar{\phi}_j^m$ is taken equal to ϕ_j^m instead of the expression given in Eq. (3.10). Averaging over (m+1, m-1) was the idea originated by Dufort and Frankel [136] which made the central difference scheme stable. In order to obtain a stable representation for the turbulence kinetic energy equation, $\hat{k}^{3/2}$ appearing in the dissipation term was written as

$$\left(\frac{\Delta Y_- \hat{k}_{j+1}^m + \Delta Y_+ \hat{k}_{j-1}^m}{\Delta Y_+ + \Delta Y_-}\right)^{1/2}\left(\frac{\Delta X_+ \hat{k}_j^{m+1} + \Delta X_- \hat{k}_j^{m-1}}{\Delta X_+ + \Delta X_-}\right)$$

With this modification, the solution of the kinetic energy equation was always stable as long as the condition given in Eq. (3.15) was satisfied for the momentum equation. A rigorous stability analysis for the finite-difference representation of the turbulence kinetic energy equation was therefore not warranted.

C. Solution Procedure

As the finite-difference formulation employed is explicit in nature, unknown quantities at the (m+1) level can be calculated just by using the known values at the (m-1) and (m) levels. A complete flow diagram will be presented at the end of this section. First, some of the important features of the program are described.

1. ΔY-Grid

Before the calculation can be started, the ΔY-grid should be carefully specified. For laminar flows, an evenly spaced grid has been found to be satisfactory in most cases. However, for flows where steep gradients might exist near the walls, of which high Prandtl number flow with variable properties is an example, an unequal grid will be desirable with the smallest ΔY used nearest the walls. The present method includes the option of using unequal grid spacing for laminar flows.

For turbulent flows where at least one point whould lie in the viscous sublayer, a variable grid is a must if the calculation scheme is to be of any practical value. In the present analysis, the annular gap is divided into NY unequal spacings; NY/2 on each side of the radius of maximum velocity which is estimated by using the Kays and Leung correlation, Eq. (1.1). The knowledge of the radius of maximum velocity, however, is not essential and the grid can be generated arbitrarily without knowing its location a priori.

A very small value ΔY is specified nearest the walls so that the first point outwards from the walls will lie within the viscous sublayer ($y^+<4$). The cross stream spacing increases in a geometric progression away from the walls towards the radius of maximum velocity such that

$$\Delta Y_{j+1} = RS \times \Delta Y_j; \text{ (for the inner wall), } j = 1,2,3... \qquad (3.16)$$

and

$$\Delta Y_{j-1} = RT \times \Delta Y_j \text{ (for the outer wall), } j=N, N-1, N-2, ... \qquad (3.17)$$

A value of RS and RT between 1.05-1.15 has been found suitable.

Since the thickness of the boundary layers on the walls of an annulus is generally (except for large radius ratios) quite different, specifying an equal number of grid points on each side of the radius of maximum velocity will result in a large sudden change in ΔY at R_m. The ΔY-grid in the central region was therefore altered arbitrarily in these cases in order to smooth out this discontinuity.

While 70-100 cross stream grid spacings were needed to fill the annular gap for turbulent flows, 50 spacings were found sufficient for laminar flow calculations.

2. Initial profiles

For hydrodynamically developing flow, a uniform velocity profile is specified at the inlet. However, if the flow is fully developed and laminar, the initial velocity profile is specified using the analytical expression obtained by Lamb [6]:

$$U = 2\left[\frac{R_2^2-R^2-2R_m^2\ln(R_2/R)}{R_2^2+R_1^2-2R_m^2}\right] \tag{3.18}$$

where R_m, radius of maximum velocity for laminar flow, is given by

$$R_m^2 = \frac{R_2^2-R_1^2}{2\ln(R_2/R_1)} \tag{3.19}$$

It was found necessary to use double precision on the IBM 360/158 in order to obtain axial velocity profiles for large radius ratios,

using Eqs. (3.18) and (3.19).

For turbulent heat transfer cases which require hydrodynamically developed flow as an initial condition, the momentum equation (3.2) can be solved first to obtain a fully developed velocity profile. Alternatively, Eq. (3.2) can be specialized to a fully developed form and solved as an ordinary differential equation. This was done for cases where a mixing length model was used. In that case, Eq. (3.2) can be reduced to the following set of ordinary differential equations:

$$\psi = \frac{dU}{dY} \tag{3.20}$$

and

$$\frac{d\psi}{dY} = \frac{\frac{dP}{dX} - \frac{\hat{\mu}\psi}{R} - \left(\frac{\hat{\rho}\hat{\ell}^2}{R} + 2\hat{\rho}\hat{\ell}\,\frac{d\hat{\ell}}{dY}\right)|\psi|\psi}{(\hat{\mu}+2\hat{\rho}\hat{\ell}^2|\psi|)} \tag{3.21}$$

with

$$U(0) = U(R_h) = 0 \tag{3.22}$$

which was solved by use of a fourth order Runge-Kutta procedure using an iterative "shooting" method to satisfy the boundary condition at the outer wall.

More details on the derivation of the Equations (3.20-3.21) and the solution procedure will be given in Appendix A.

In all the test runs made, the initial temperature profiles were assumed to be uniform; however, any initial temperature distribution can be specified.

The Dufort-Frankel method which was employed in the present study

is a three level differencing scheme (see Fig. 3.1) requiring information at the (m-1) and mth levels. In order to start the solution, therefore, the initial profiles are yet to be specified at mth level. This is done by using a simple explicit method (see Appendix B) for one step before the calculations are started using Dufort-Frankel method.

3. Solution of the finite-difference equations

The solution of the finite-difference equations can be initiated after the cross stream grid has been specified and initial profiles of the dependent variables are known at two upstream locations. Equation (3.9) then can be written in terms of known quantities at the (m-1) and mth levels as

$$\phi_j^{m+1} = \Gamma_j(X,Y,\phi_j^{m-1},\phi_{j-1}^{m},\phi_j^{m},\phi_{j+1}^{m}) \tag{3.23}$$

Since Γ_j in general is a known function at all j's, ϕ_j^{m+1} can be calculated. In case of momentum Equation (3.2), however, Γ_j contains the pressure, p^{m+1}, which needs to be determined before the momentum equation can be solved explicitly for U_j^{m+1}. The pressure can be determined from the global conservation of mass constraint, Eq. (3.4), in a fashion described below.

Equation (3.9), for $\phi = U$, can be written in the following form:

$$U_j^{m+1} = \eta_j(X,Y,U_j^{m-1},U_{j-1}^{m},U_{j+1}^{m}) + P^{m+1}\,\Omega_j(X,Y,U_j^{m}) \tag{3.24}$$

where η_j and Ω_j are known functions.

Now from Eq. (3.4),

$$\int_0^{R_h} \hat{\rho} U R dY = \text{constant} = C_m$$

where the constant C_m is known once the mass flow rate is specified.

The above equation can be written, using Eq. (3.24), as

$$\int_0^{R_h} \hat{\rho}_j^m U_j^{m+1} R_j dY = \int_0^{R_h} \hat{\rho}_j^m \eta_j R_j dY + P^{m+1} \int_0^{R_h} \hat{\rho}_j^m \Omega_j R_j dY = C_m$$

or

$$P^{m+1} = \left(C_m - \int_0^{R_h} \hat{\rho}_j^m \eta_j R_j dY \right) \Big/ \int_0^{R_h} \hat{\rho}_j^m \Omega_j R_j dY \tag{3.25}$$

Strictly speaking, $\hat{\rho}$ appearing in the above equation (3.25) should be evaluated at (m+1)th level. But for small streamwise density variations, the above formulation provides satisfactory results. Integrals appearing in Eq. (3.25) can be evaluated numerically using Simpson's rule which is given in Appendix D for a variable grid.

Once P^{m+1} is known, Eq. (3.24) can be used to calculate U^{m+1} for all j. For developing flows, the program treats the boundary layers growing on the two walls separately until they merge, thus saving unnecessary calculations in the inviscid core region. The velocity in that region is obtained using Euler's equation:

$$\hat{\rho} U \frac{\partial U}{\partial X} = - \frac{dP}{dX} \tag{3.26}$$

which is written in the finite-difference form as

$$\hat{\rho}_c^m U_c^m \frac{U_c^{m+1} - U_c^{m-1}}{\Delta X_+ + \Delta X_-} = - \frac{P^{m+1} - P^{m-1}}{\Delta X_+ + \Delta X_-} \tag{3.27}$$

where the subscript c refers to the values of the variables in the inviscid core region.

Since P^{m+1} is known, U_c^{m+1} can be calculated from the above equation. In Region I of Fig. 2.2, Eq. (3.14) is solved out from each wall until $\frac{U_j^{m+1}}{U_c^{m+1}} \geq 0.995$. Alternatively, the momentum equation can be solved across the annular gap starting from one wall and proceeding to the other; however, computing out from each wall saves computer time by reducing the number of grid points at which the full equations need to be solved. After the boundary layers have merged, the momentum equation is solved across the annular gap starting at the inner wall. A similar procedure is employed to solve the turbulence kinetic energy equation.

It was found necessary to solve the continuity equation (3.14) starting from both walls towards the central region of the annulus. If instead, the continuity equation is solved starting from one wall, say the inner wall, then the values predicted for the cross stream velocity near the outer wall were generally too large very near the inlet which affects the predicted shear stress and heat transfer coefficient at the outer wall. Likewise, near the inlet large V values were predicted near the inner wall if the solution is started at the outer wall. No completely satisfactory explanation could be found to this effect although the differences in the numerical integration schemes used in enforcing the global and pointwise conservation of mass are suspected of contributing to the observed phenomenon.

When both walls are heated, the energy equation is solved in the entire annular gap starting at the inner wall. However, if only one wall is heated, then the energy equation is solved only near the heated wall. The edge of the thermal boundary layer is determined by the requirement that the difference in calculated temperatures at two adjacent cross stream stations be very small. However, it was found necessary to solve the energy equation across the entire annulus after the thermal boundary layer had penetrated well within the viscous boundary layer of the unheated wall because of the difficulty of numerically distinguishing the edge of the growing thermal boundary layer.

After the governing equations have been solved, engineering parameters of interest such as wall shear stress and heat transfer coefficient can be calculated. The wall derivatives required for this purpose are evaluated employing polynomial fits to the U and T* profiles. More details on the evaluation of wall derivatives can be found in Appendix E.

A computer code, "ANNULUS", has been developed to solve the finite-difference form of the governing equations. Fig. 3.2 gives the flow diagram which illustrates briefly the solution procedure employed in ANNULUS. A listing of the computer code is given in Appendix G.

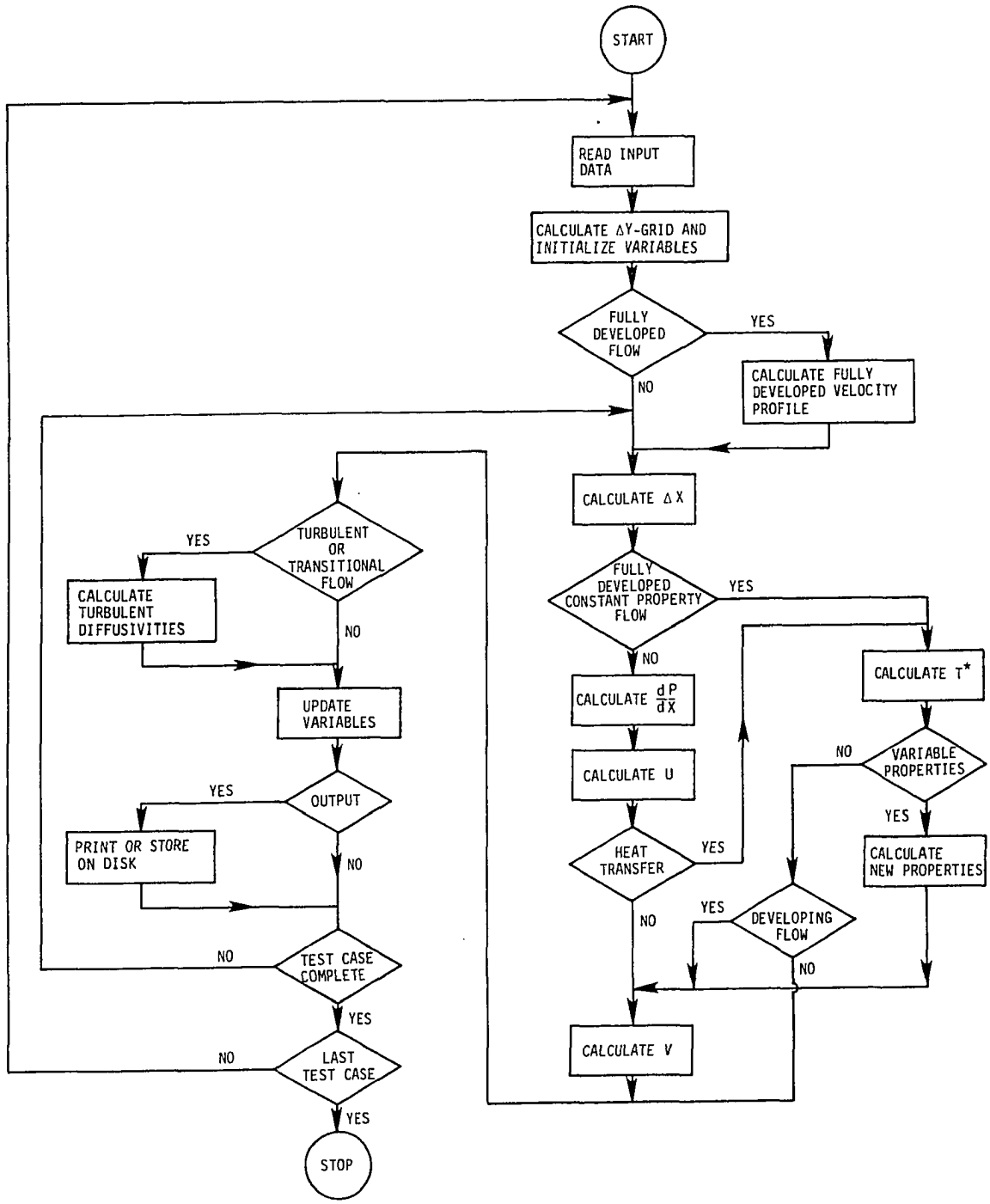

Figure 3.2. Flow chart for the computer code "ANNULUS"

IV. RESULTS AND DISCUSSION

The finite-difference method developed has been applied to predict laminar and turbulent flows with and without heat transfer. Comparisons have been made with the available experimental data and the predictions of the other methods in order to establish the validity of the present calculation method and the proposed turbulence models.

A. Laminar Flow and Heat Transfer

1. Forced convection

Some constant property test cases have been run in order to establish the validity of the proposed finite-difference method. Very limited experimental data are available in the literature for laminar flow heat transfer in annular passages. Comparisons have been made therefore with the predictions of Shumway and McEligot [15] for flow of air in an annulus (with $r^* = 0.25$) using an implicit finite-difference procedure.

Fig. 4.1 and 4.2 show the predicted axial pressure drop and the friction parameter $f_p Re$ respectively. It can be seen that the agreement between the predictions of the present explicit method and the implicit method of [15] is excellent.

Fig. 4.3 shows the predicted Nusselt numbers on the inner and outer wall of the annulus for simultaneously developing flow and heat transfer with thermal boundary conditions corresponding to the fundamental solution of first kinds. Fig. 4.4 gives the Nusselt number for the inner

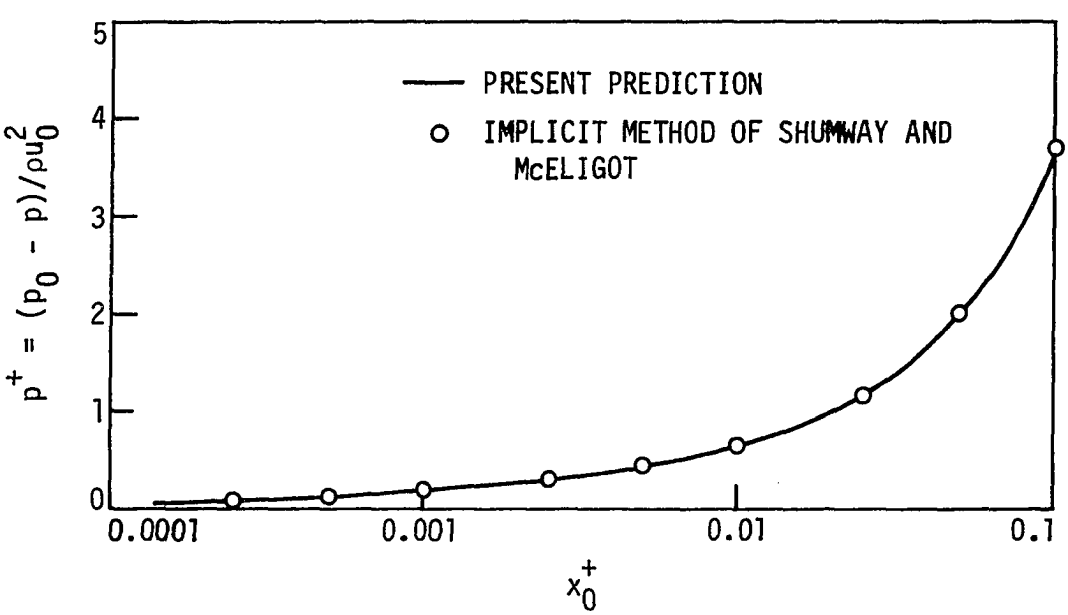

Fig. 4.1. Pressure defect in laminar flow through an annulus ($r^* = 0.25$)

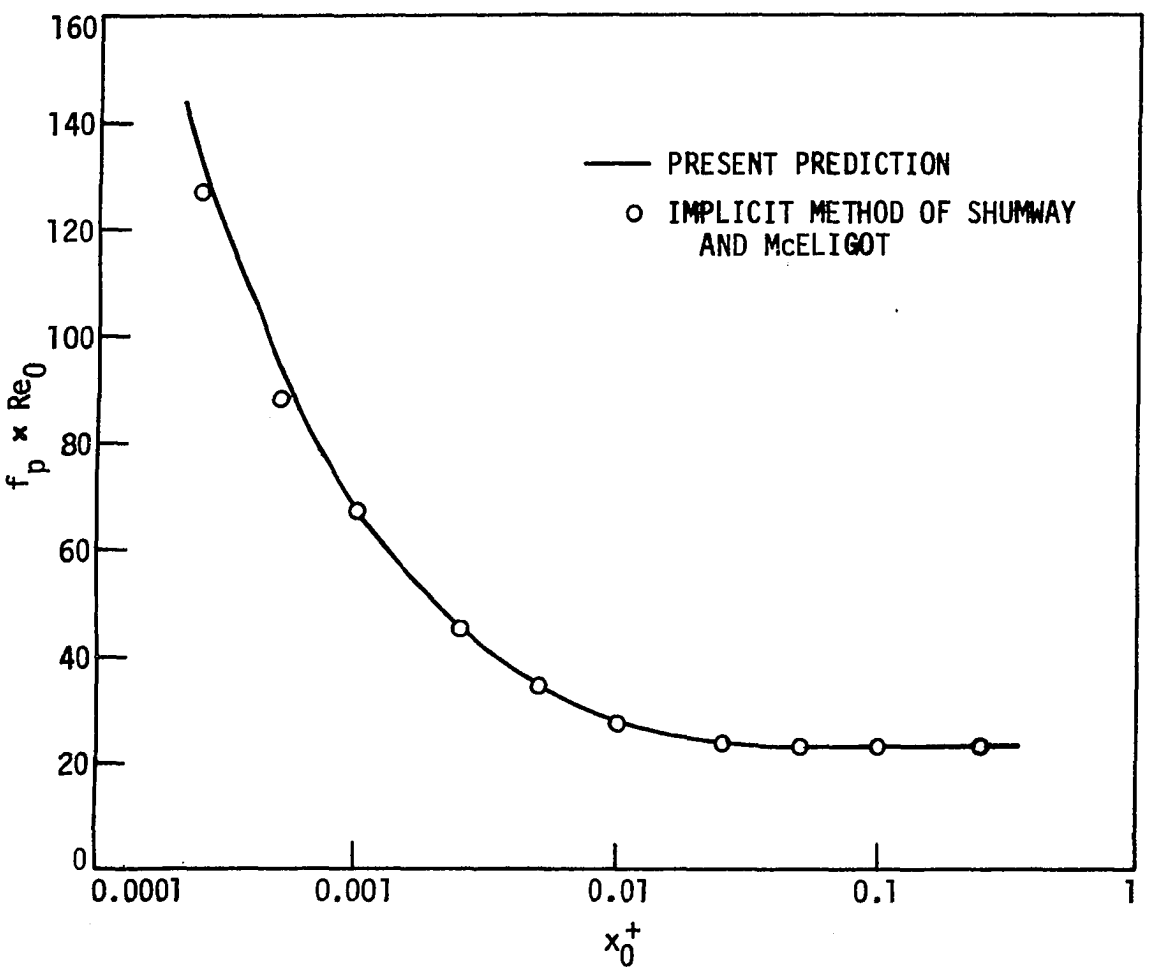

Fig. 4.2. Variation of friction factor parameter f_pRe in the entrance region of an annulus ($r^* = 0.25$)

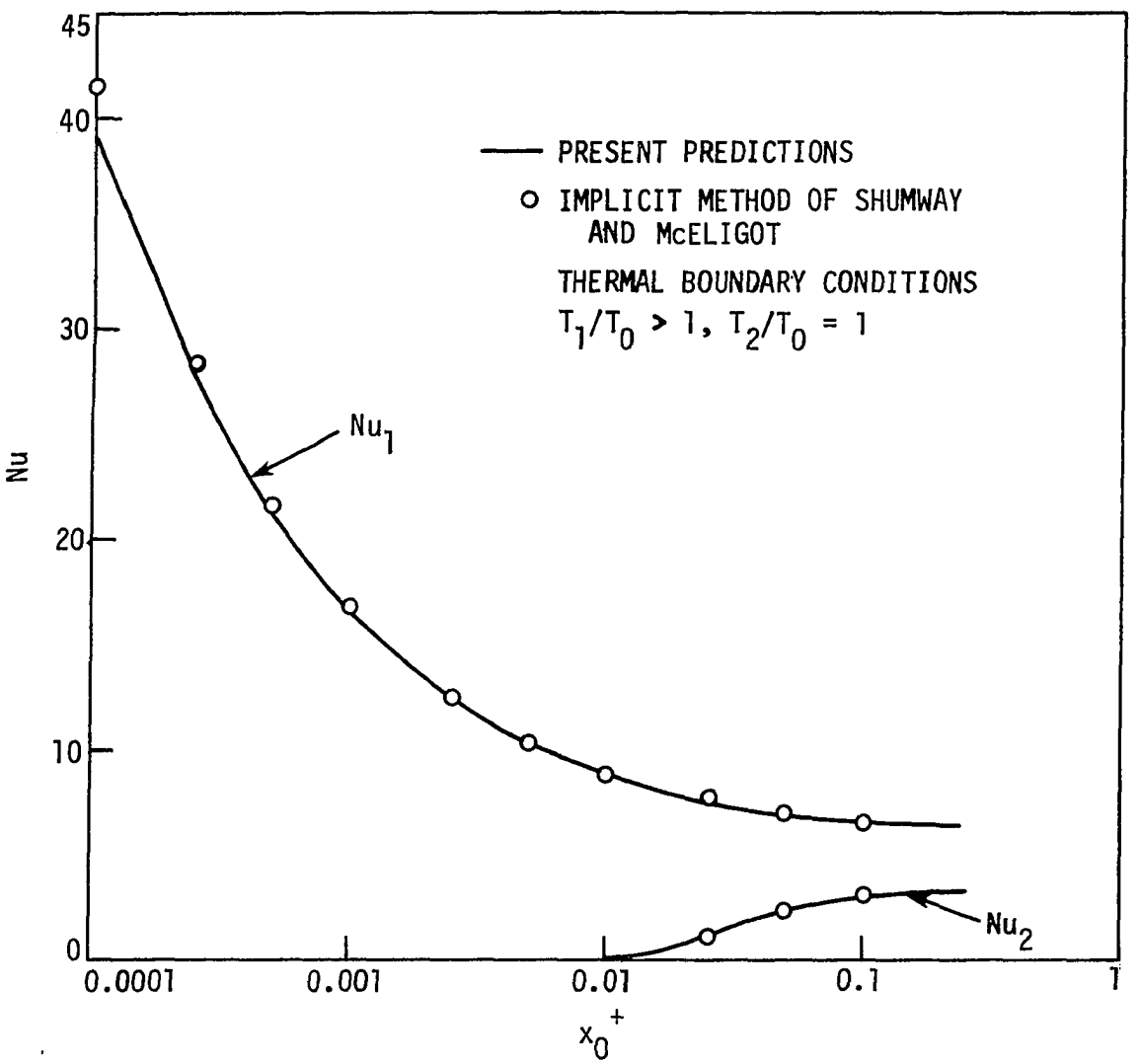

Fig. 4.3. Variation of Nusselt number for hydrodynamically developing flow through an annulus ($r^* = 0.25$)

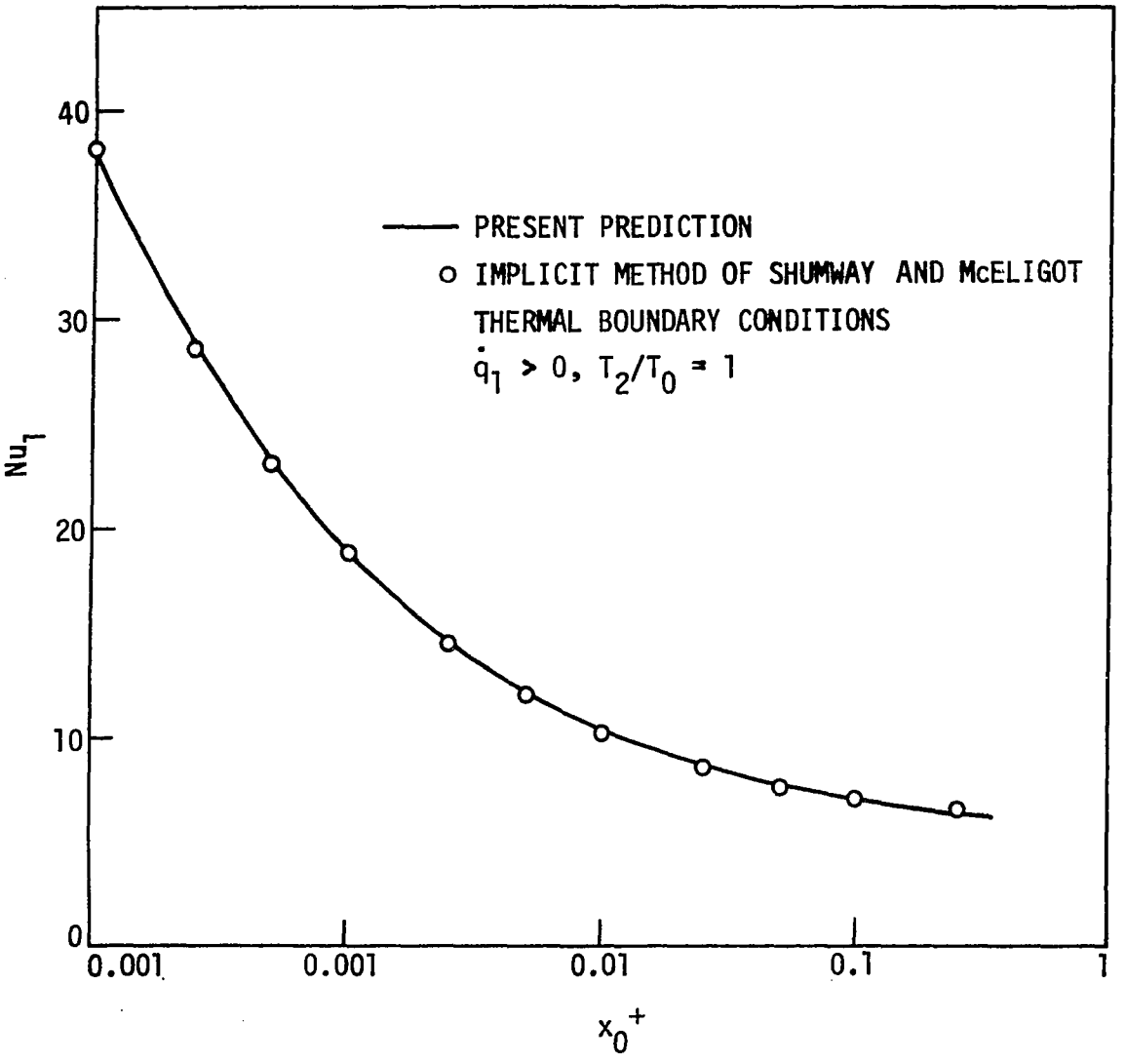

Fig. 4.4. Variation of Nusselt number for hydrodynamically developed flow through an annulus (r* = 0.25)

wall for fully developed flow at the inlet with thermal boundary conditions corresponding to the fundamental solution of fourth kind. Both of these figures indicate that the present results are in good agreement with the predictions of [15]. Several other comparisons were also made which are not shown here. It can thus be concluded that the predictions of the explicit finite-difference method proposed in the present study are reliable. It was also found that the weighted average over (m-1) and (m+1)th levels (see Eq. (3.10)), instead of simple averaging, used in the diffusion term of Eq. (3.9) helps in the energy balance and permits larger streamwise steps to be taken.

2. Combined forced and free convection in asymmetrically heated vertical ducts

Heating (or cooling) may affect the flow pattern in a duct because of the induced density gradients. For a horizontal duct, there even may be secondary flows rendering the assumption of axisymmetry, employed in the present study, invalid. However, for a vertical duct the flow still remains axisymmetric because the body forces in this case are parallel to the main flow direction. The present method can be applied to study this flow configuration since the body force term f_x is retained in the momentum equation (2.8). Here a problem is studied where the flow is in an upward direction in a vertical annular duct. In that case,

$$f_x = -\rho g \tag{4.1}$$

Two test cases were run; one for the flow of water using the Boussinesq approximation with properties of the water assumed constant and a second case for flow of ethylene glycol where all properties were varied. The properties of ethylene glycol used are given in Appendix F. In the calculations, only one wall was heated (uniform heat flux) while the other was assumed to be insulated and the flow was assumed to be fully developed at the inlet.

Figure 4.5 shows the predicted Nusselt number variation along an annular duct of radius ratio 0.38. The experimental data of Maitra and Subba Raju [25] for upward flow of water in an annulus ($r^* = 0.38$) is also shown along with the constant property prediction (buoyancy neglected) of Lundberg et al. [9] which is for $r^* = 0.4$. The data of [25] is shown for two different Rayleigh numbers where this non-dimensional parameter was defined as

$$Ra = \frac{\beta g \rho^2 C_p D_h^4 \frac{dT_w}{dx}}{k\mu} \tag{4.2}$$

Apparently the experimental values of Ra shown in the Fig. 4.5 are the "fully developed" values since Ra will be expected to vary in the thermal entrance region according to Eq. (4.2). The reported value of Ra for the present prediction is the fully developed value. It can be seen that neglecting buoyancy underpredicts Nusselt number. This is because in upward flow the buoyant forces are in the direction of main flow causing an increased flow near the heated wall which enhances heat transfer. The apparent tail up behavior of experimental Nusselt number for higher Rayleigh numbers at $x_0^+ \simeq 0.02$ might be linked

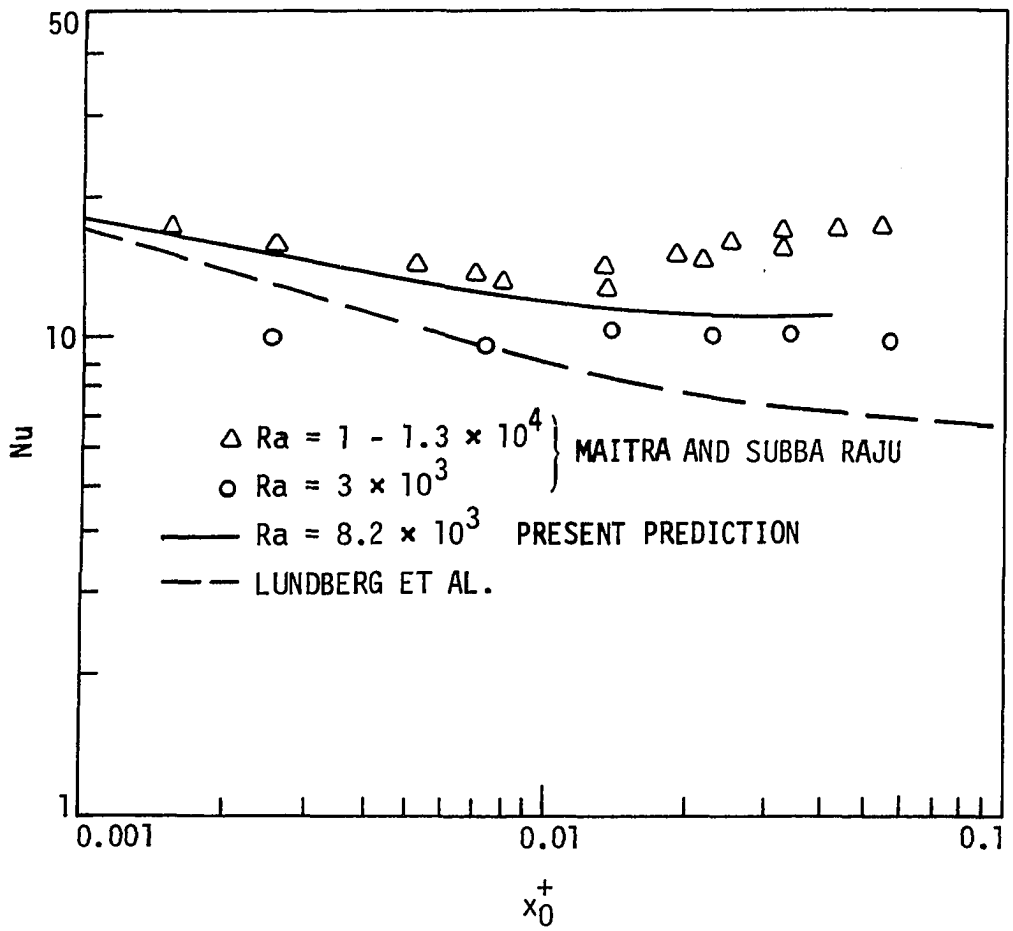

Fig. 4.5. Effect of buoyancy on heat transfer in a vertical annulus ($r^* = 0.38$) with upflow of water (inner wall heated uniformly)

to the onset of instability to be discussed below.

Axial velocity profiles at four different streamwise locations, including the one at the start of heating, are shown in Fig. 4.6. It can be seen that the velocities near the heated wall increase while they decrease near the unheated wall because of density variations in the fluid. This results in increased radial flow (see Fig. 4.7) along the duct. The increased velocities near the heated surface are the main cause of higher Nusselt number as compared to that predicted with only forced flow. At some streamwise station, the radial flow increases to such an extent that local flow reversal occurs near the outer unheated wall. This flow instability may eventually lead to an unsteady flow if a sufficient length of duct is available for the disturbance to grow. For a particular fluid, the location of flow reversal depends upon Gr, Re and x/D_h. For the present case, flow reversal occurred at $x_0^+ \simeq 0.02$ which coincides with the tail-up behavior of the experimental Nusselt number. This leads one to suspect that flow mechanism downstream of the onset of reversal is such that further increases in heat transfer might occur.

The tail-up behavior was not predicted in the present calculation. This is perhaps because the properties of the fluid were assumed constant except the density appearing in the buoyancy term. In another test run made for upward flow of ethylene glycol in an annulus of $r^* = 0.99$, properties were varied. Ethylene glycol, which has a high Prandtl number, is often used as a model fluid for transformer cooling. Its viscosity is a strong function of temperature and it was thought that a

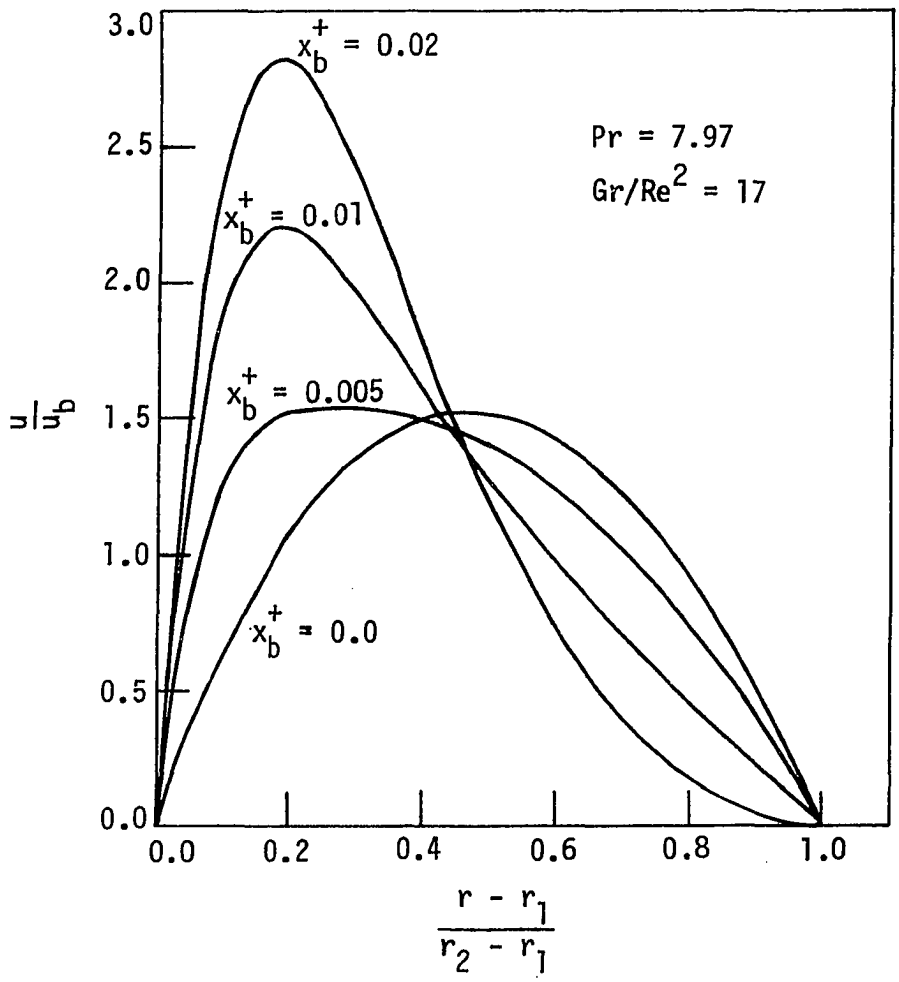

Fig. 4.6. Distortion of axial velocity profile due to buoyancy in upward flow through an annulus ($r^* = 0.38$)

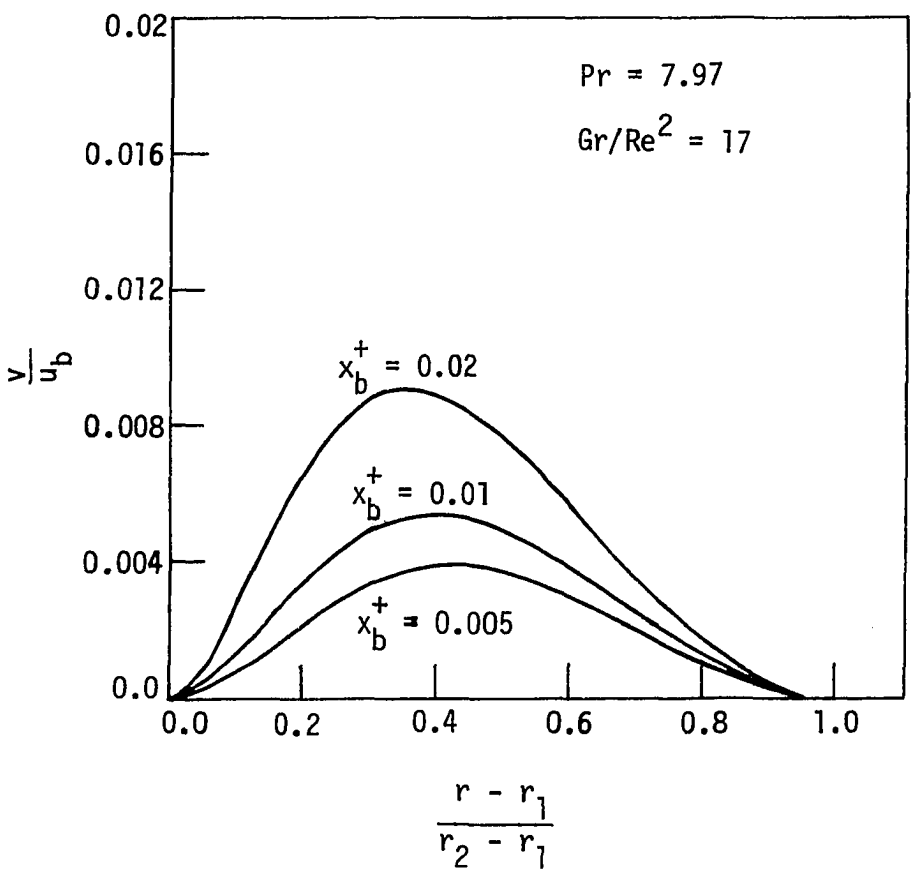

Fig. 4.7. Buoyancy-induced radial flow in an annulus (r* = 0.38)

constant property solution will not yield accurate results. Figure 4.8 shows the Nusselt number variation for two different heat fluxes, one being almost four times the other. At the lower heat flux, flow reversal did not occur in the length of the duct studied (see Figs. 4.9 and 4.10 for velocity and temperature profiles respectively). The Nusselt numbers are compared for this heat flux with the data of Joshi (see [142]) taken in a high aspect ratio rectangular duct with one wall heated. The predictions are within the scatter of the data. At the higher heat flux, the flow reversal was predicted near the unheated wall at $x_b^+ \simeq 0.013$ and a tail-up behavior of Nusselt number was also predicted. For flows of this type it is believed that all the properties need to be taken as variable in order to predict the heat transfer characteristics accurately.

Figure 4.11 shows the variation of the parameter $C_f Re_b$ for two different heat fluxes. The parameter is scaled by a factor of 24; its value for isothermal flow in a parallel wall duct. It can be seen that the streamwise location where outer wall shear stress goes to zero (the onset of reverse flow) is determined by Gr/Re^2. Earlier investigations for upward flow of water in a vertical tube [143] and in a vertical annulus [19] have used Gr/Re as a parameter. But it is this author's feeling that Gr/Re^2 is a better correlation parameter, at least for ethylene glycol, since Gr/Re varies along the duct, because of strong viscosity variations, while Gr/Re^2 does not if Grashof number is defined as

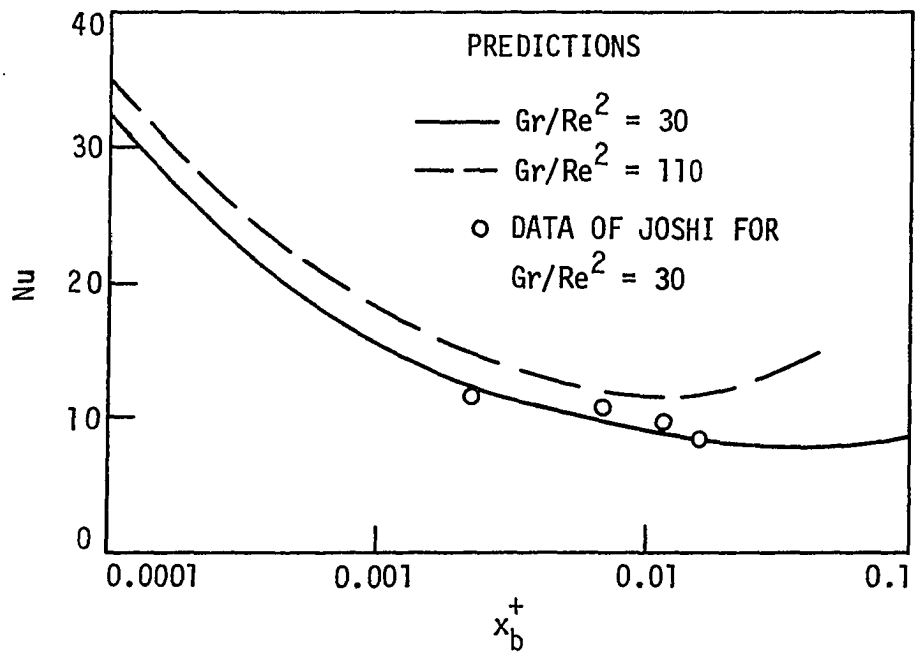

Fig. 4.8. Predicted Nusselt numbers for upward flow of ethylene glycol in a large radius ratio annular duct ($r^* = 0.99$); comparison with the data of Joshi taken in a plane duct with one wall heated

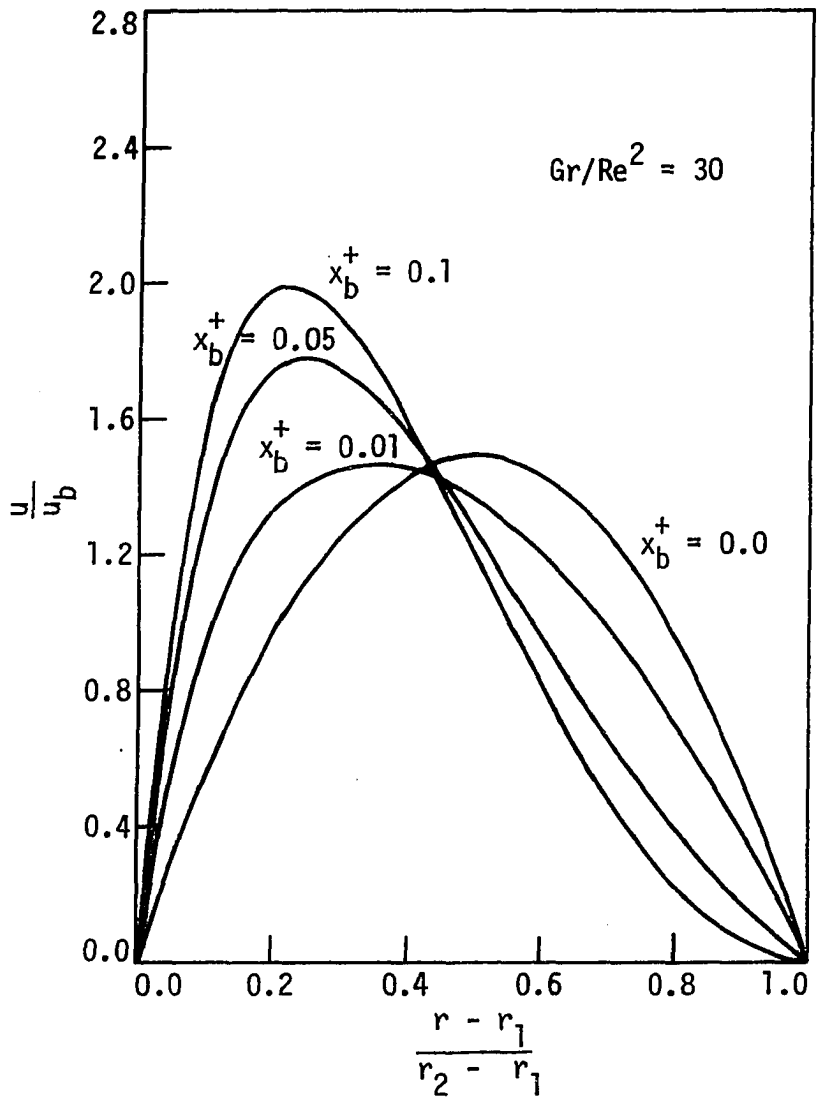

Fig. 4.9. Predicted axial velocity profiles for flow of ethylene glycol in an asymmetrically heated annulus ($r^* = 0.99$)

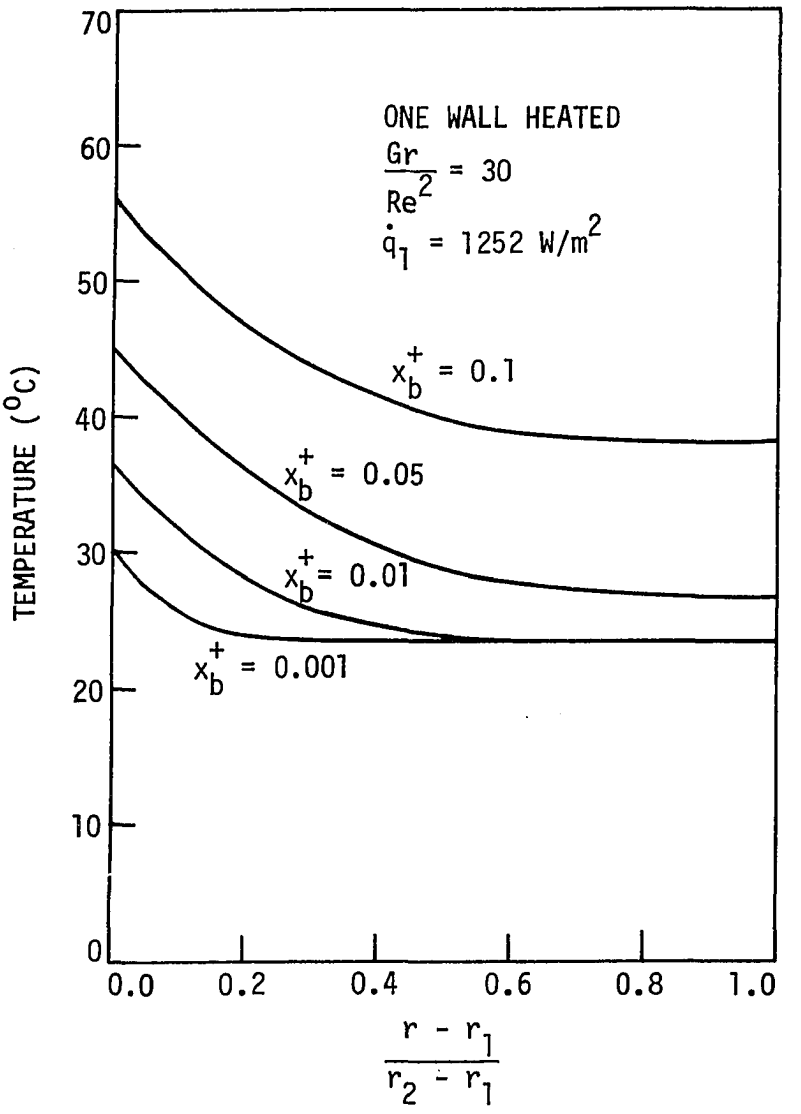

Fig. 4.10. Predicted temperature profiles for flow of ethylene glycol in an annulus (r* = 0.99)

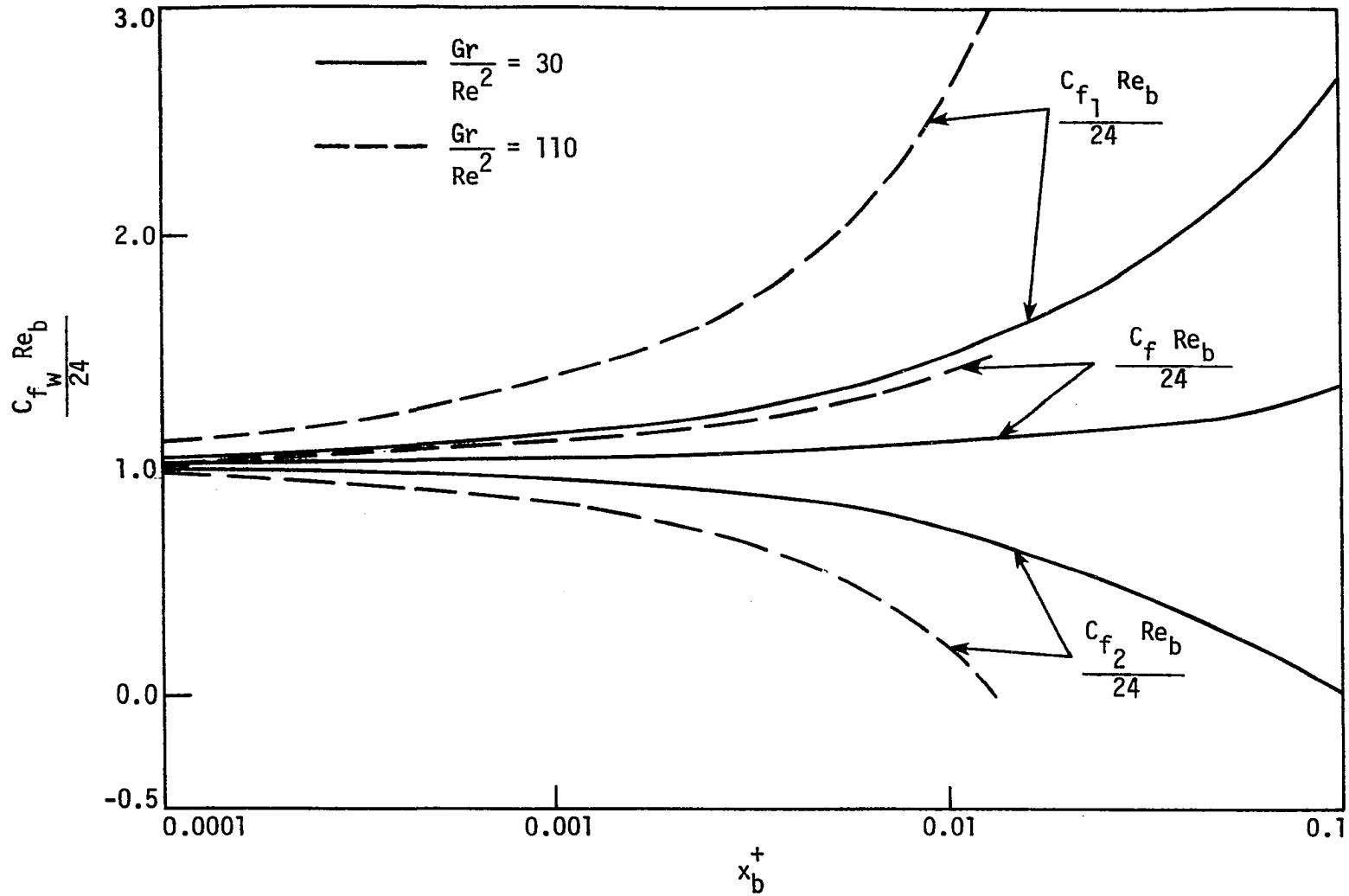

Figure 4.11. Effect of buoyancy on skin-function parameter for upward flow of ethylene glycol in an asymmetrically heated annulus (r* = 0.99)

$$Gr = \frac{\beta g \rho^2 D_h^4 \dot{q}_1 r_1}{\lambda \mu^2 (r_1+r_2)} \tag{4.3}$$

Scheele and Hanratty [143] studied the effect of natural convection on the stability of flow in a vertical pipe. They noted that velocities near the heated wall increase while they decrease near the centerline and that the flow first becomes unstable when the velocity profiles develop points of inflexion. Transition to unsteady flow involves the gradual growth of small disturbances and whether or not transition occurs depends upon the length of the tube.

B. Turbulent Flow and Heat Transfer

Comparisons with experimental data and the predictions of other calculation methods were made to show the validity of the proposed turbulence models and the calculation procedure. In all the calculations, buoyancy effects were neglected since these are expected to be small in turbulent flows. However, buoyancy effects may become significant at lower Reynolds numbers. Some studies [144-146] have shown that the apparent effect of buoyancy on turbulent heat transfer is in an opposite sense to that found in laminar flows; i.e., in upward turbulent flow, heating causes a deterioration in heat transfer coefficient while the reverse is true for downward flow. For ease of discussion, the three turbulence models evaluated will be referred to as:

1) Model A: Length scale equation model.

2) Model B: Bridging.

3) Model C: Turbulence kinetic energy model with length scale.

Before discussing the hydrodynamic and heat transfer results, some sample turbulent viscosity profiles, as predicted by the models, are presented below.

Figure 4.12 compares the fully developed turbulent viscosity profile predicted by Model A with the measurements of Ball and Azer [67] and of Jonsson and Sparrow [32]. The numerical method employed in the present study utilizes a value of μ_T in the difference scheme which has been averaged over three grid points to enhance numerical stability. This partially explains why the predicted turbulent viscosity at the radius of maximum velocity, though small, is nonzero. The concept of linear bridging (Model B) is also demonstrated in the figure. Figure 4.13 compares the turbulent viscosity profiles predicted by Models A, B, and C for an annulus of $r^* = 0.25$.

1. Hydrodynamic results

To test the turbulence models, calculations were first made for an annulus of $r^* = 0.99$ (which approximates a parallel wall duct) because of the lack of experimental data for developing annular flows. Figure 4.14 shows mean velocity profiles at two streamwise stations as predicted by Model A. The predictions seem to compare fairly well with the experimental data of Dean [147] taken in a high aspect ratio rectangular duct. The symmetry of the predicted profiles shows that

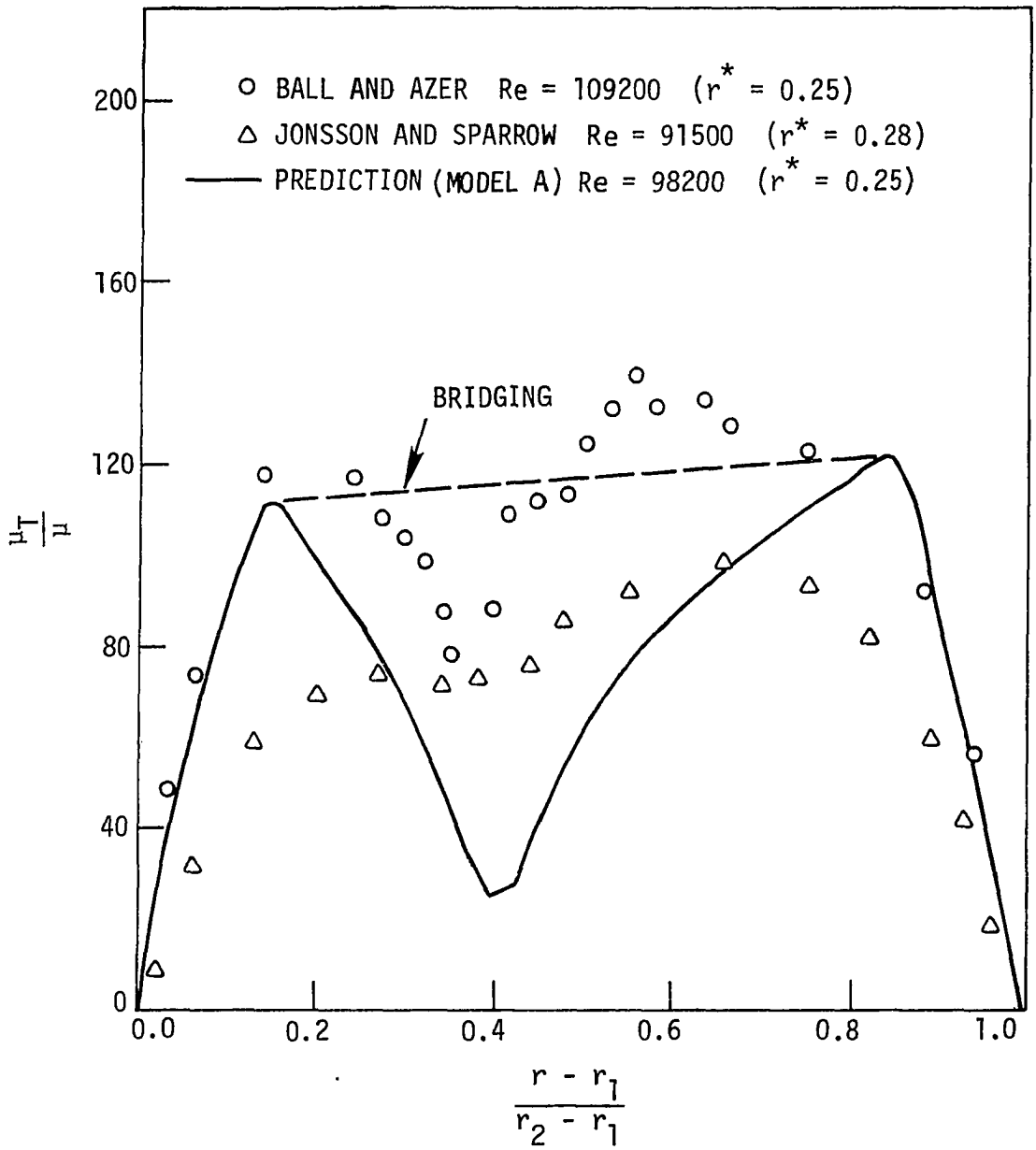

Fig. 4.12. Predicted and measured distribution of turbulent viscosity in fully developed flow through an annulus

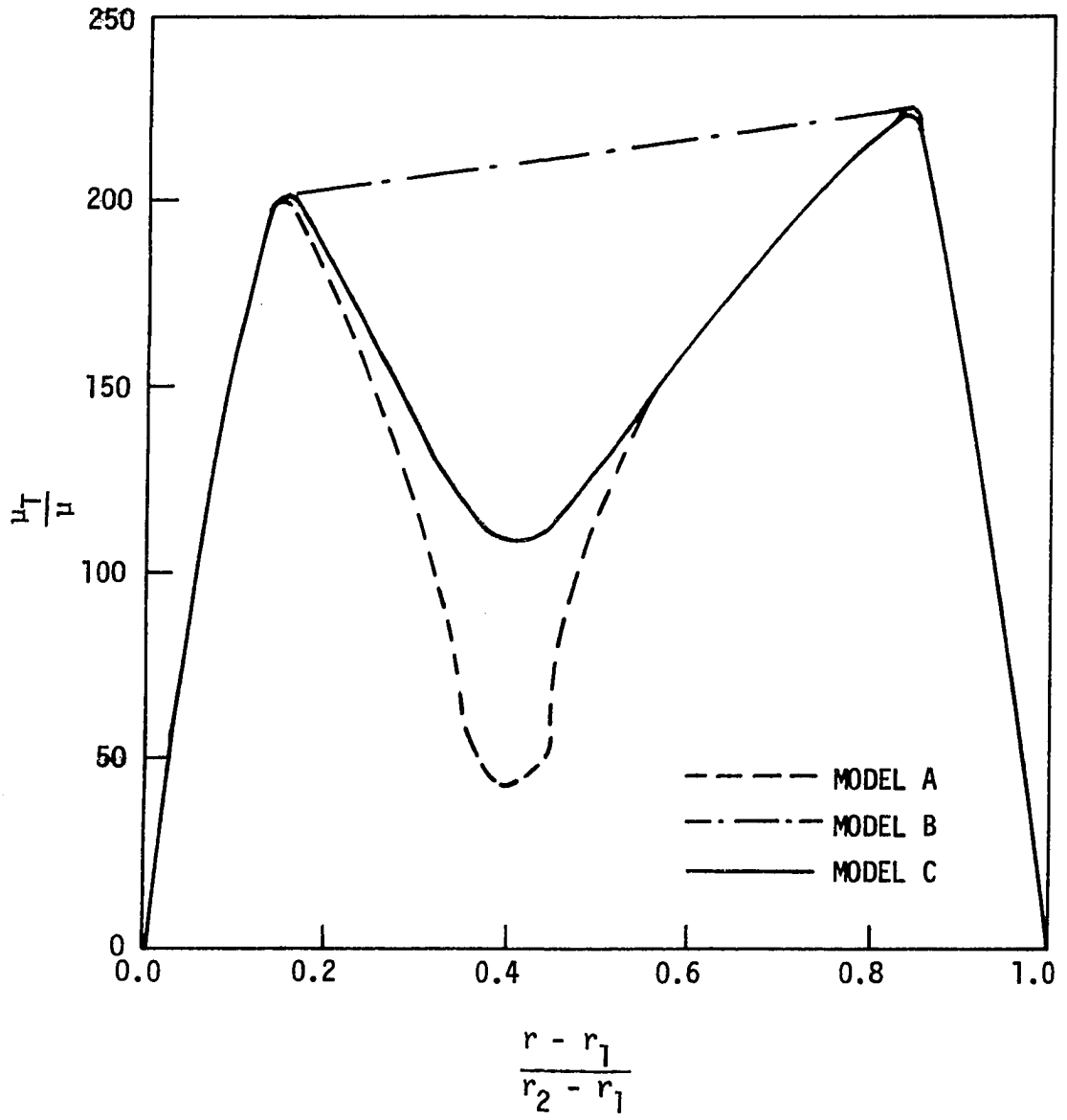

Fig. 4.13. Predicted fully developed turbulent viscosity profiles in an annulus ($r^* = 0.25$) for $Re = 1.9 \times 10^5$

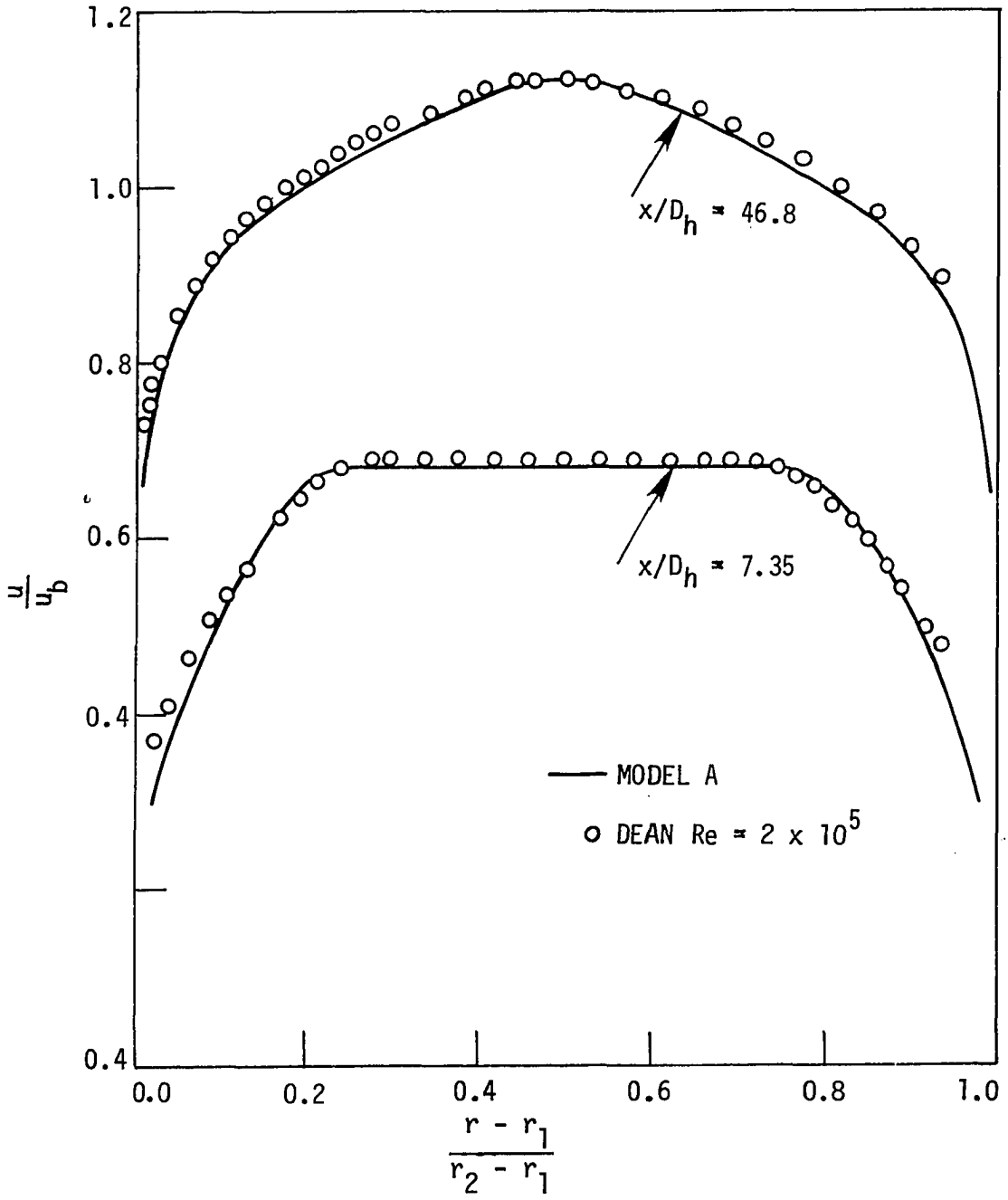

Fig. 4.14. Predicted velocity profiles in an annulus (r* = 0.99); comparison with measurements of Dean in a plane duct

$r^* = 0.99$ is a good approximation for the parallel plate duct. Velocity profiles as predicted by Model A at two streamwise stations are drawn on "law of the wall" coordinates in Fig. 4.15. The experimental data of Dean is also shown in the figure. The predicted slope and the intercept of the logarithmic region compares fairly well with his data. The predicted shear stress profiles at two streamwise stations are compared with Dean's data in Fig. 4.16. Predictions based on shear layer interaction model proposed by Bradshaw et al. [111] and given by Dean [147] are also shown.

Figure 4.17 shows the development of the boundary layers on the two walls of the duct where δ_{995} has been used to represent the edge of the boundary layer. In the present calculations, a uniform velocity profile was assumed at the inlet. The discrepancy between the predictions and Dean's data [147] at the lower values of x/D_h suggests that the uniform velocity assumption does not match experimental conditions existing at the inlet of the duct and that the flow might have been partially developed in his experiment. The present predictions suggest that the two shear layers begin to merge after about $x/D_h = 16$.

Figure 4.18 shows the comparison made between the predictions of Model A for an annulus of $r^* = 0.99$ with the measurements of Dean [147] and Byrne et al. [148] for centerline velocity development in a high aspect ratio rectangular duct. The proposed length scale model predicts the velocity "overshoot" in fair agreement with Dean's data. The

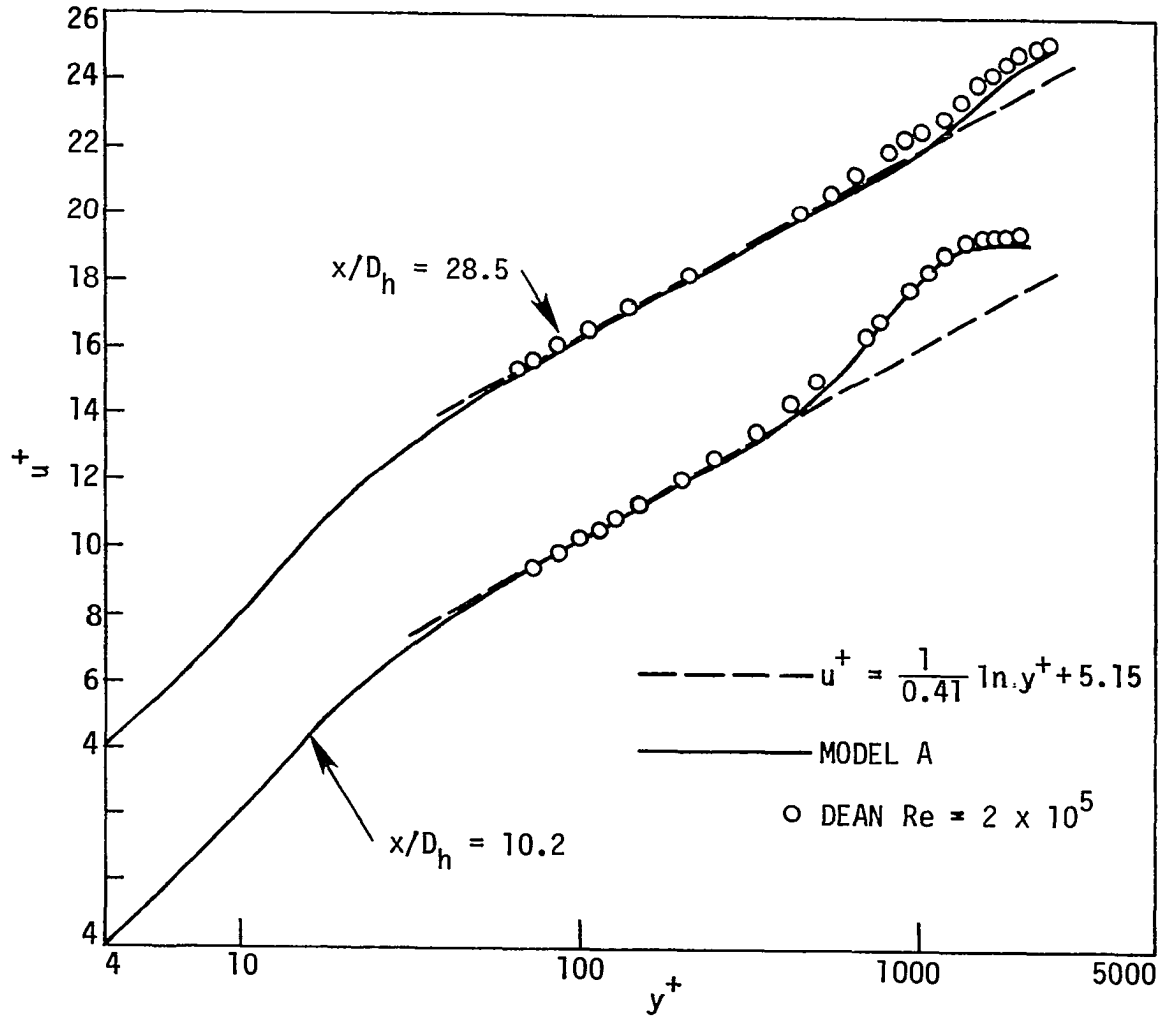

Fig. 4.15. Predicted and measured velocity profiles on law of the wall coordinates

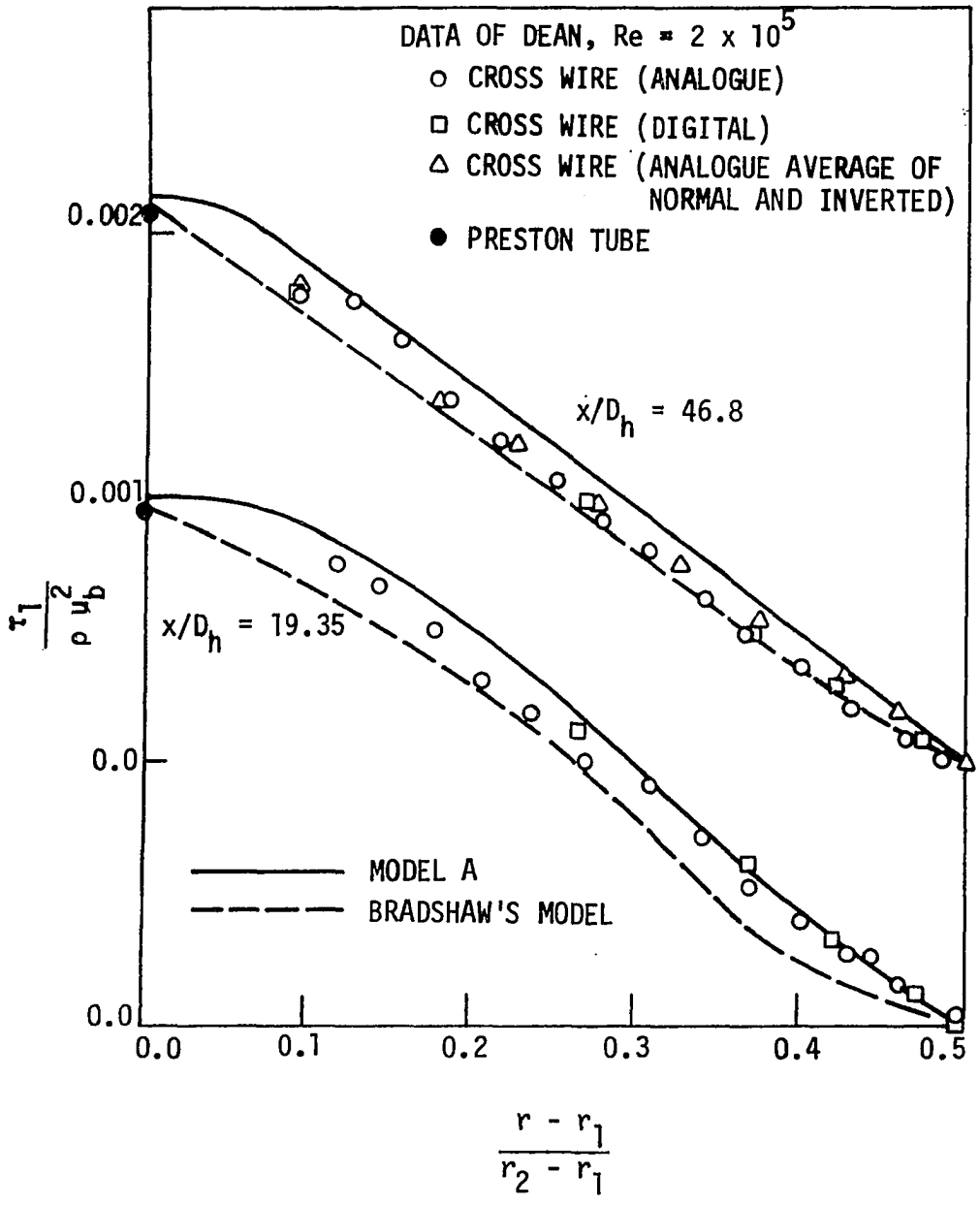

Fig. 4.16. Predicted and measured shear stress profiles

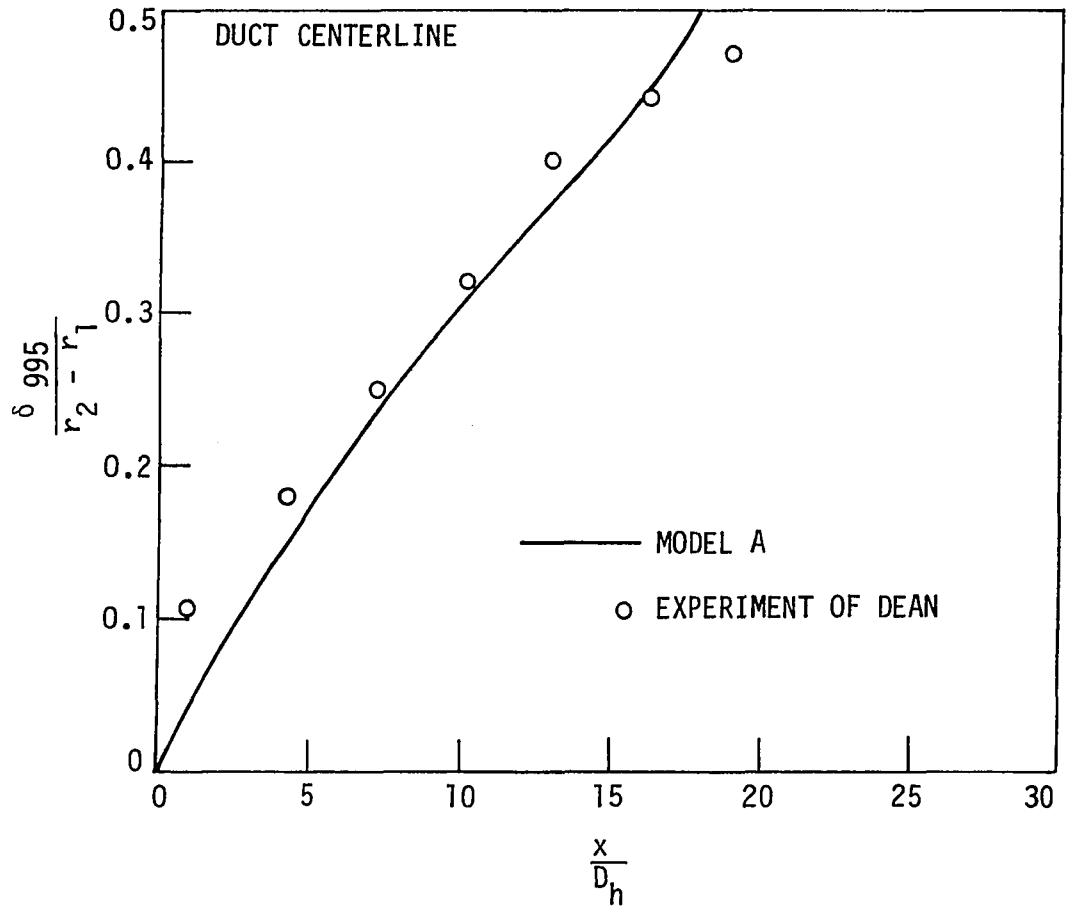

Fig. 4.17. Predicted and measured boundary layer growth in the entrance region of a plane duct

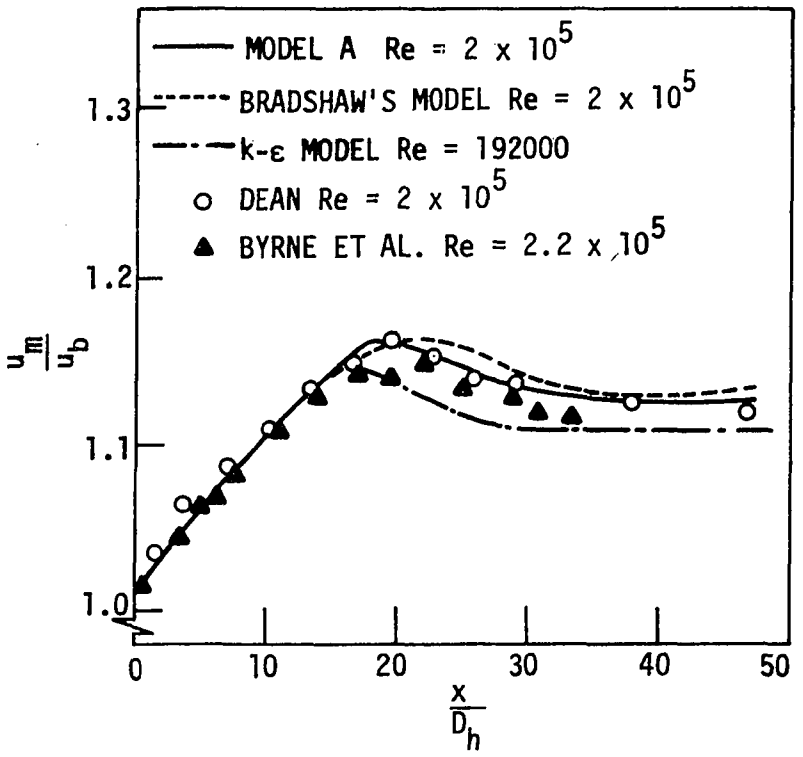

Fig. 4.18. Maximum velocity development in an annulus (r* = 0.99) compared with the results for a parallel wall duct

overshoot in the velocity is a consequence of the interaction between the shear layers and this was also observed in the data of Barbin and Jones [149] for pipe flow. The same phenomenon will be expected in annuli. Okiishi [64] noted that ". . . the velocities near the radius of maximum velocity decreased with axial distance in portions of [the] annulus . . ." with $r^* = 0.531$. Model A predicts this overshoot in annuli. Predictions based on the shear layer interaction model proposed by Bradshaw et al. [111] and that of the k-ε model as reported by Stephenson [150] are also shown.

Comparison with the data of Comte-Bellot [151] for centerline velocity development is made in Fig. 4.19. Predictions of Emery and Gessner [152] and Cebeci et al. [153] are also shown. It is interesting to note that the present results are similar to that of [152] which employed an algebraic formulation of the mixing length with 12 constants. In both cases, calculations were started assuming a uniform profile at the inlet. This was not the case in the actual experiment. Results of [153] seem to compare better with the experimental results, but it should be noted that their predictions are based on matched initial conditions at $x/D_h = 10$ (Fig. 4.19). Figure 4.20 shows predictions of velocity development at four different cross stream locations (including the centerline) in a parallel wall duct. Experimental data of Byrne et al. [148] and predictions of k-ε model as reported by Stephenson [150] are also given. The present predictions generally compare better with the experimental data. It can be

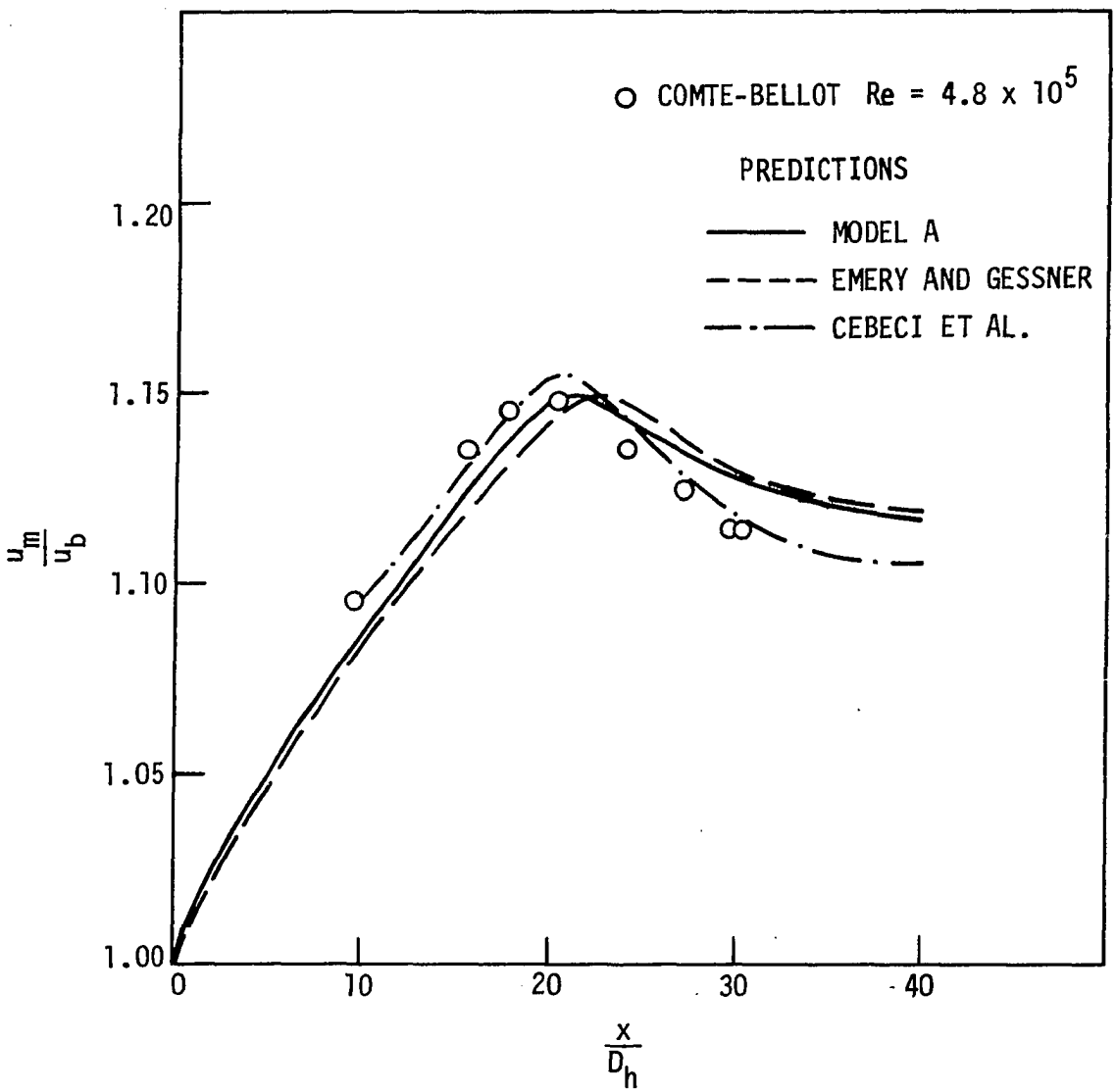

Fig. 4.19. Maximum velocity development in an annulus (r* = 0.99) compared with the results for a parallel wall duct

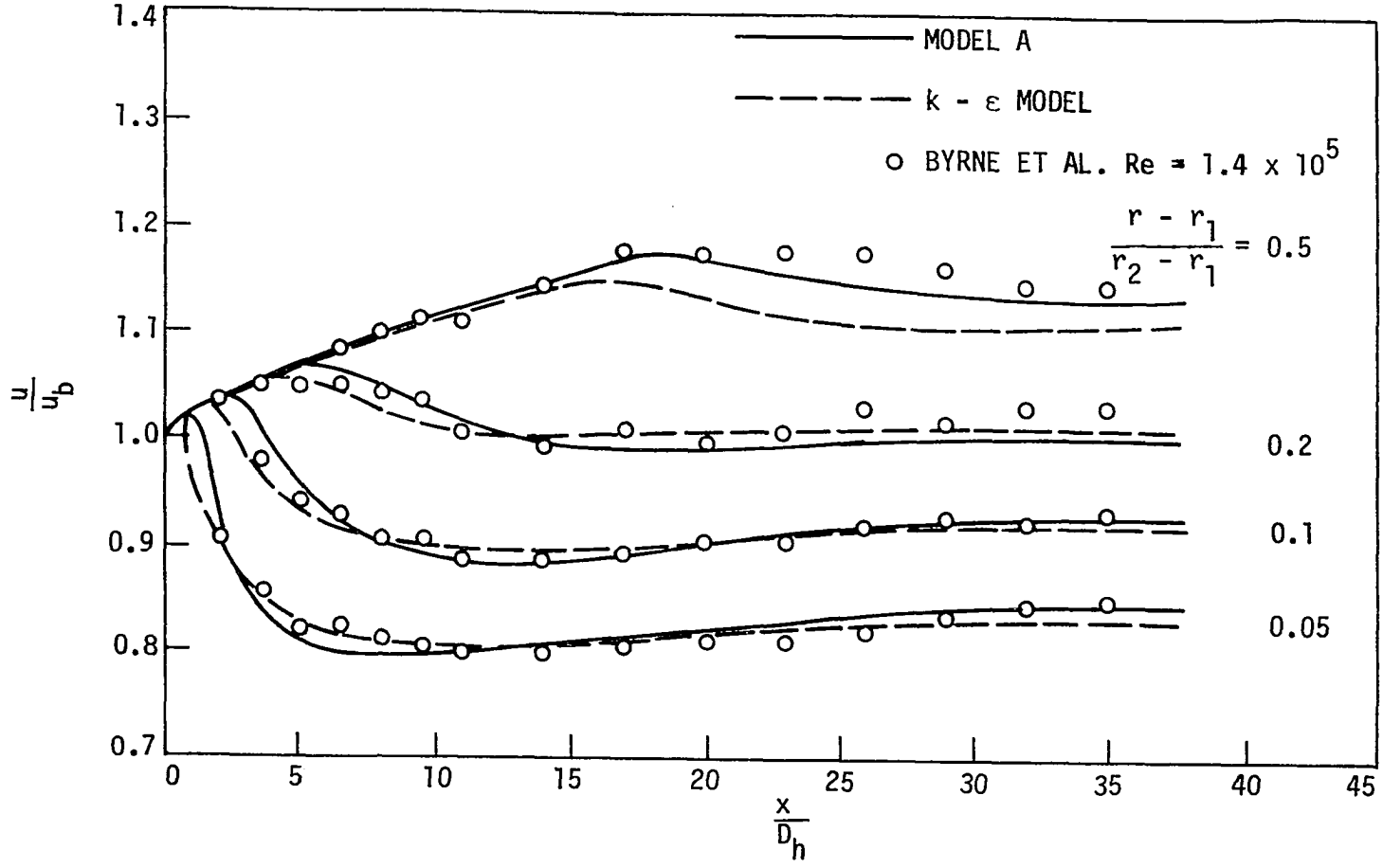

Fig. 4.20. Velocity development in the entrance region of an annulus (r* = 0.99)

concluded that nonmonotonic development of centerline velocity in a plane duct is well-predicted by the proposed length scale transport model.

Prediction of flow development by Model A is further tested by the comparisons shown in Figs. 4.21-4.23 for displacement and momentum thicknesses. In general, the present predictions are in fair agreement with the experimental data and compare better than the predictions of some of the more complicated turbulence models. It should be noted that the predictions using Bradshaw's model [111] were initiated at $x/D_h = 13.25$ using the measured velocity profile at this station. This applies to all the results labeled as "Bradshaw's model".

In Fig. 4.24 the present predictions for skin friction coefficients are compared with the data of Dean [147] and Byrne et al. [148], along with the predictions of [111] and [150]. The wall shear stress values in [148] were evaluated by indirect means involving velocity profile integration via the momentum integral equation, while Dean employed a Preston tube which is a more direct means of measuring wall shear stress. It is therefore reasonable to expect that Dean's experimental results are more reliable of the two. This conclusion can be further justified by noting that values of τ_w based on the momentum integral equation exhibit unacceptable tail-up behavior when $x/D_h > 30$. The predictions of Model A are generally in good agreement with Dean's results.

The effect of bridging (Model B) on flow development was also studied. In these cases, the turbulent viscosity profile was bridged

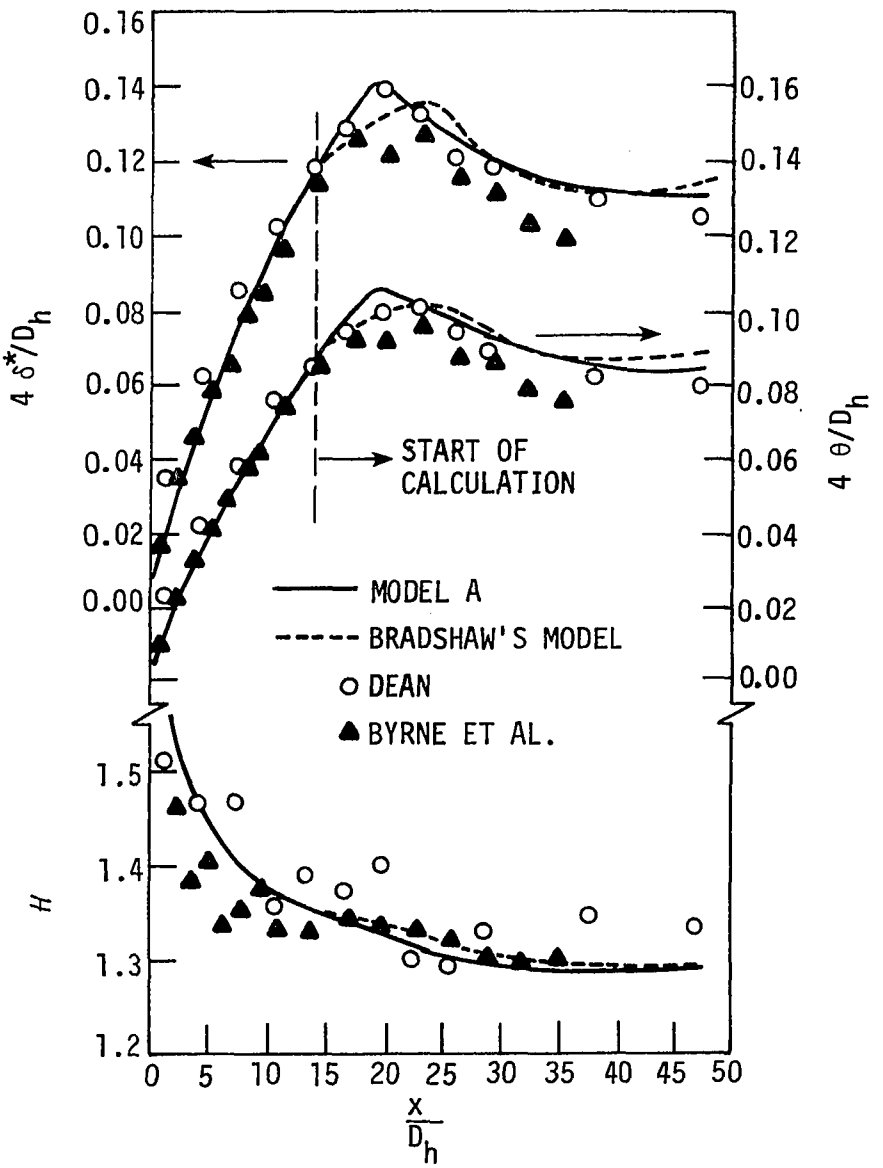

Fig. 4.21. Predicted displacement and momentum thicknesses along with shape factors for an annulus (r* = 0.99) compared with the results for a parallel wall duct

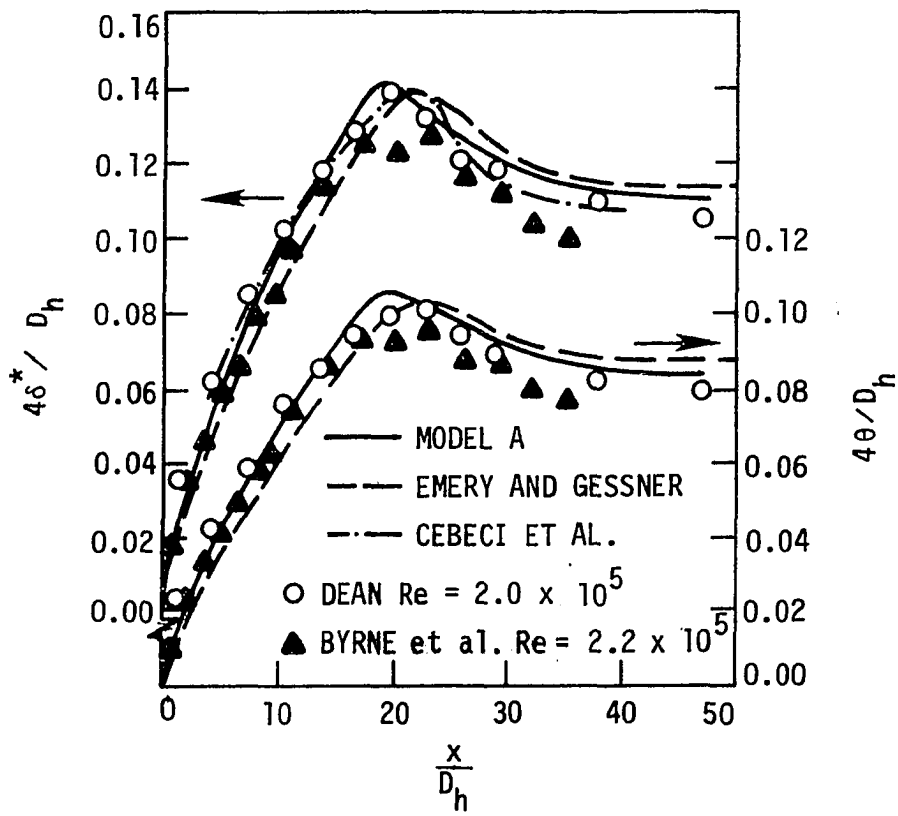

Fig. 4.22. Displacement and momentum thicknesses in the entrance region of an annulus (r* = 0.99)

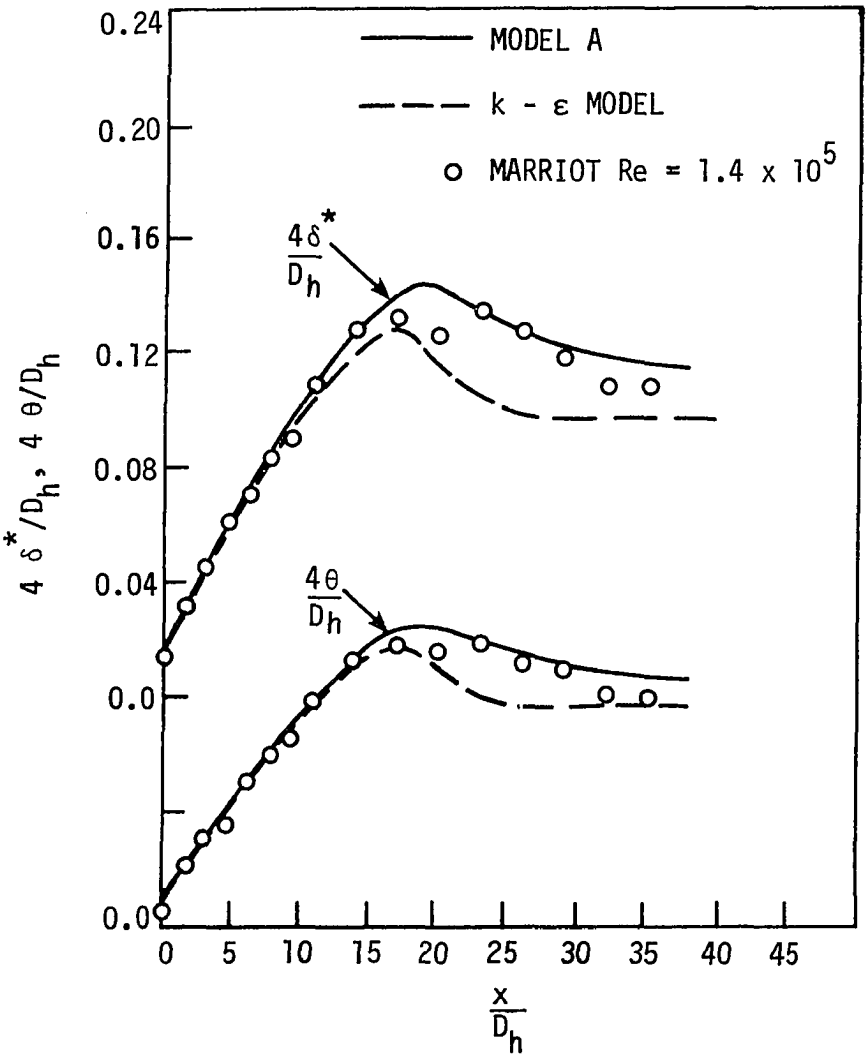

Fig. 4.23. Displacement and momentum thicknesses in an annulus (r* = 0.99)

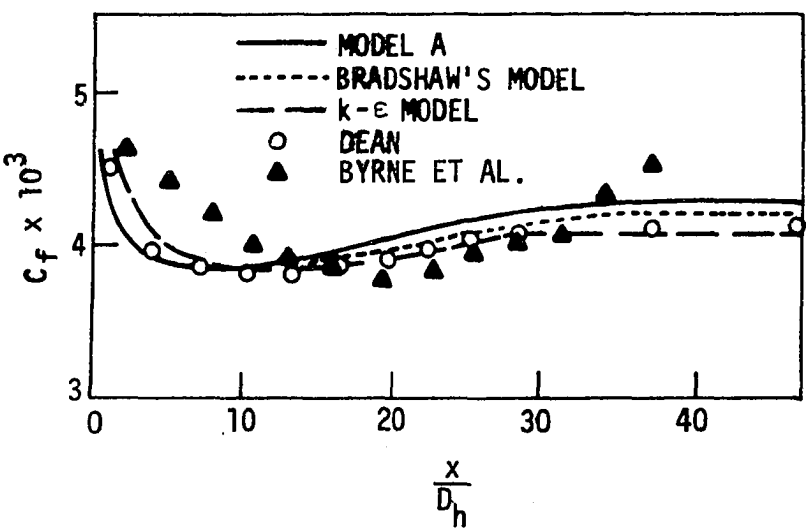

Fig. 4.24. Predicted distribution of skin-friction coefficient in an annulus ($r^* = 0.99$) compared with the results for a parallel wall duct

right after the shear layers had merged. Figure 4.25 shows the centerline velocity development as predicted by Model B. The experimental data of [147] and [148] along with the prediction of Model A are also shown. A sudden drop in the centerline velocity is observed when bridging is used in this manner which cannot be justified. Similar behavior is observed for displacement thickness and momentum thickness (see Fig. 4.26). It can be concluded, therefore, that linear briding is not appropriate for hydrodynamic development. However, it will be shown later that for fully developed flow, it is a good approximation.

Calculations were also made using the turbulence kinetic energy equation model (Model C). Figure 4.27 shows predicted turbulence kinetic energy profiles as compared to the data of Comte-Bellot [151]. Her data were taken in a high aspect ratio rectangular duct. In the present calculation which is for $r^* = 0.99$, a free stream turbulence level of 0.02% was specified at the inlet.

The predicted mean velocity distribution is shown in Fig. 4.28 along with the data of Comte-Bellot. The present predictions compare very well with her data. Calculations were also made using Model A. The predictions of Model A (not shown) were too close to that of Model C to draw on the figure. It can be concluded that for hydrodynamic development, at least, employing a turbulence kinetic energy equation has no real advantage and that the length scale transport model predicts the flow development sufficiently accurately.

Figure 4.29 shows the predicted variation of inner and outer wall

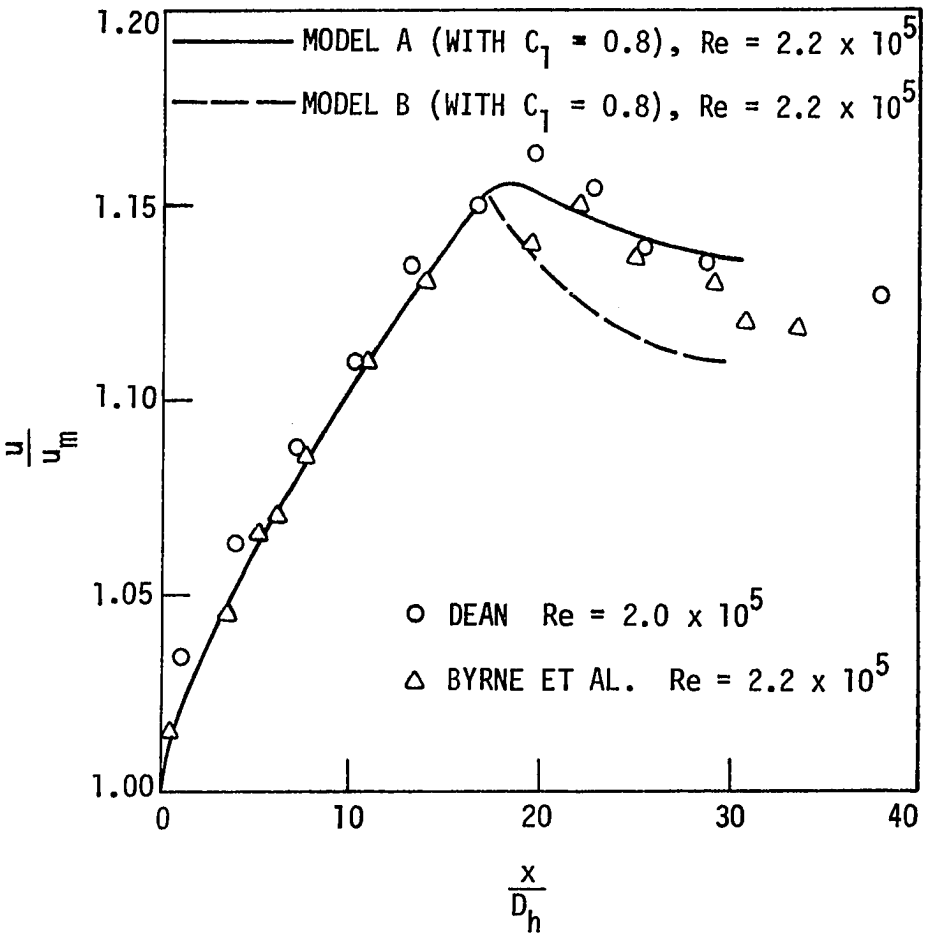

Fig. 4.25. Effect of bridging on maximum velocity development in an annulus (r* = 0.99)

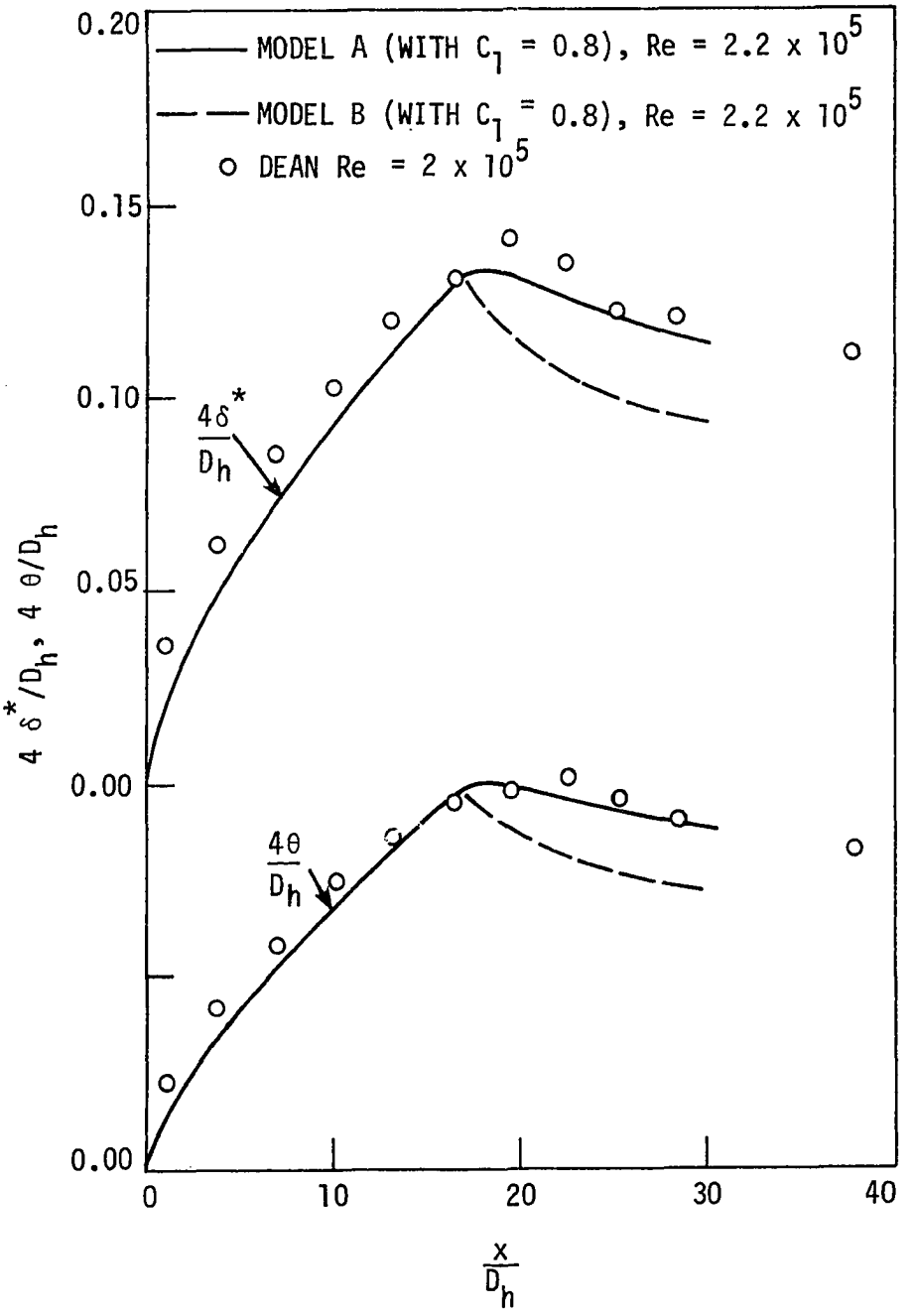

Fig. 4.26. Effect of bridging on displacement and momentum thickness in an annulus (r* = 0.99)

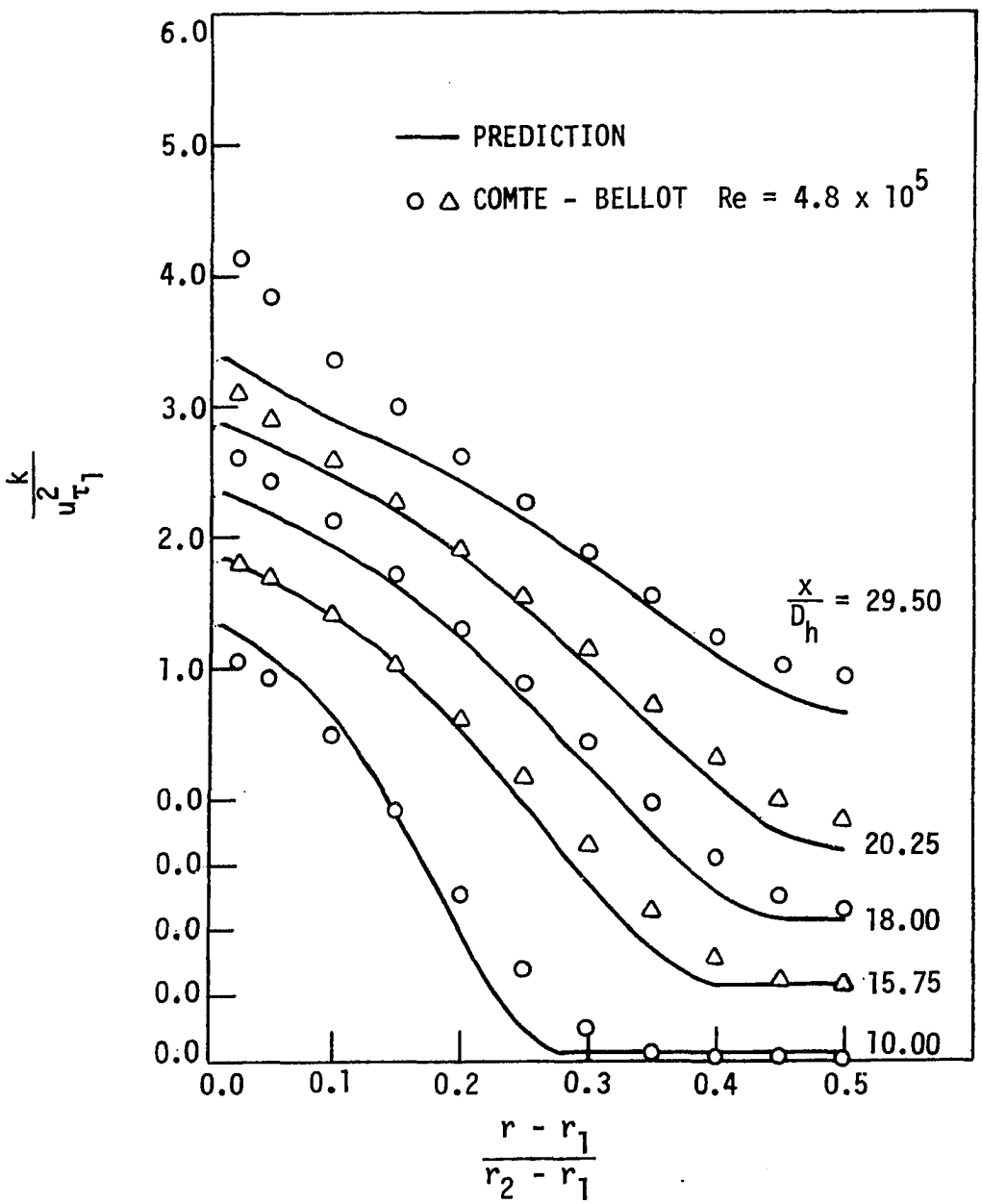

Fig. 4.27. Predicted turbulence kinetic energy profiles in an annulus (r* = 0.99); comparison with measurements of Comte-Bellot in a plane duct

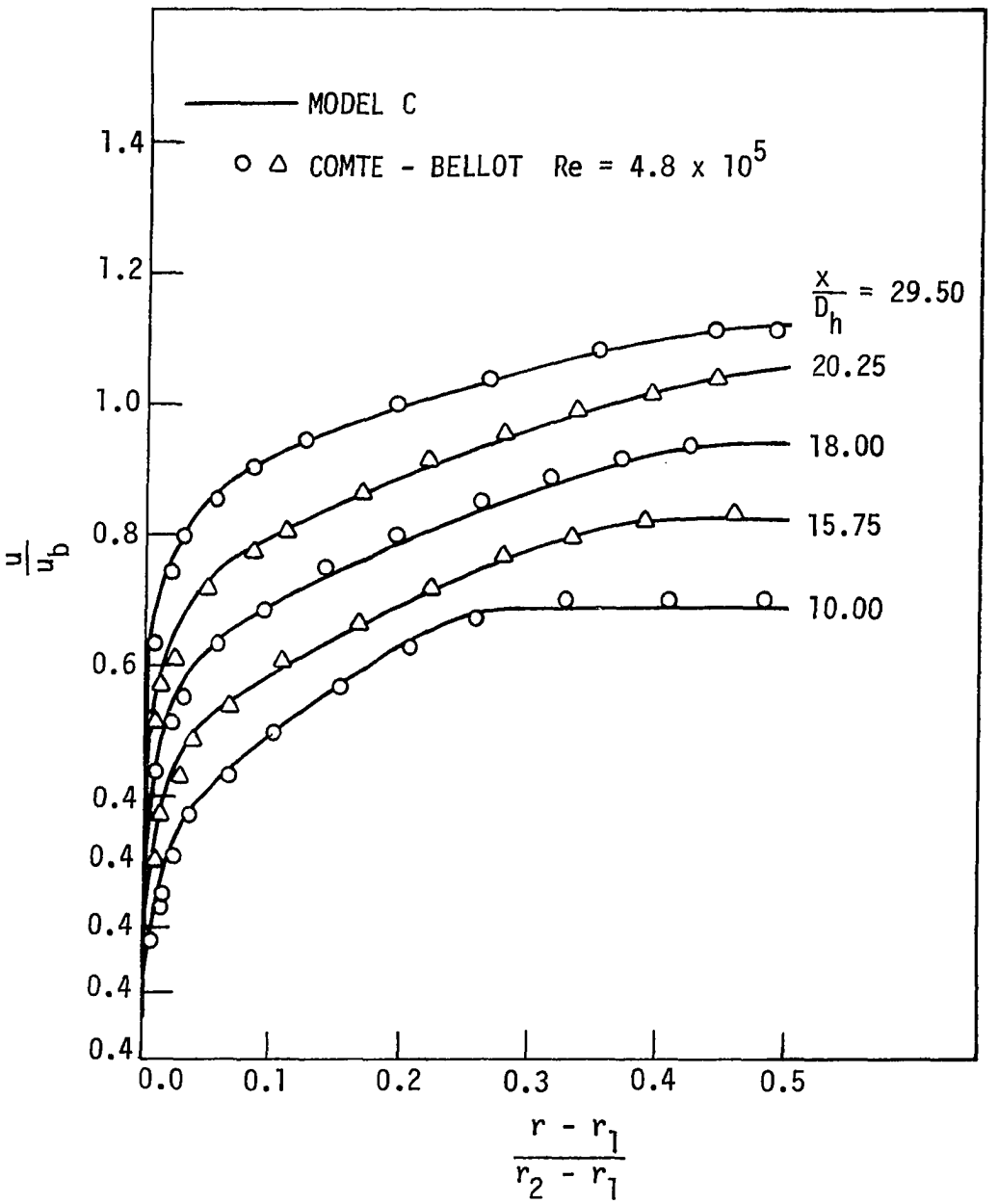

Fig. 4.28. Predicted velocity profiles in an annulus (r* = 0.99); comparison with measurements of Comte-Bellot in a plane duct

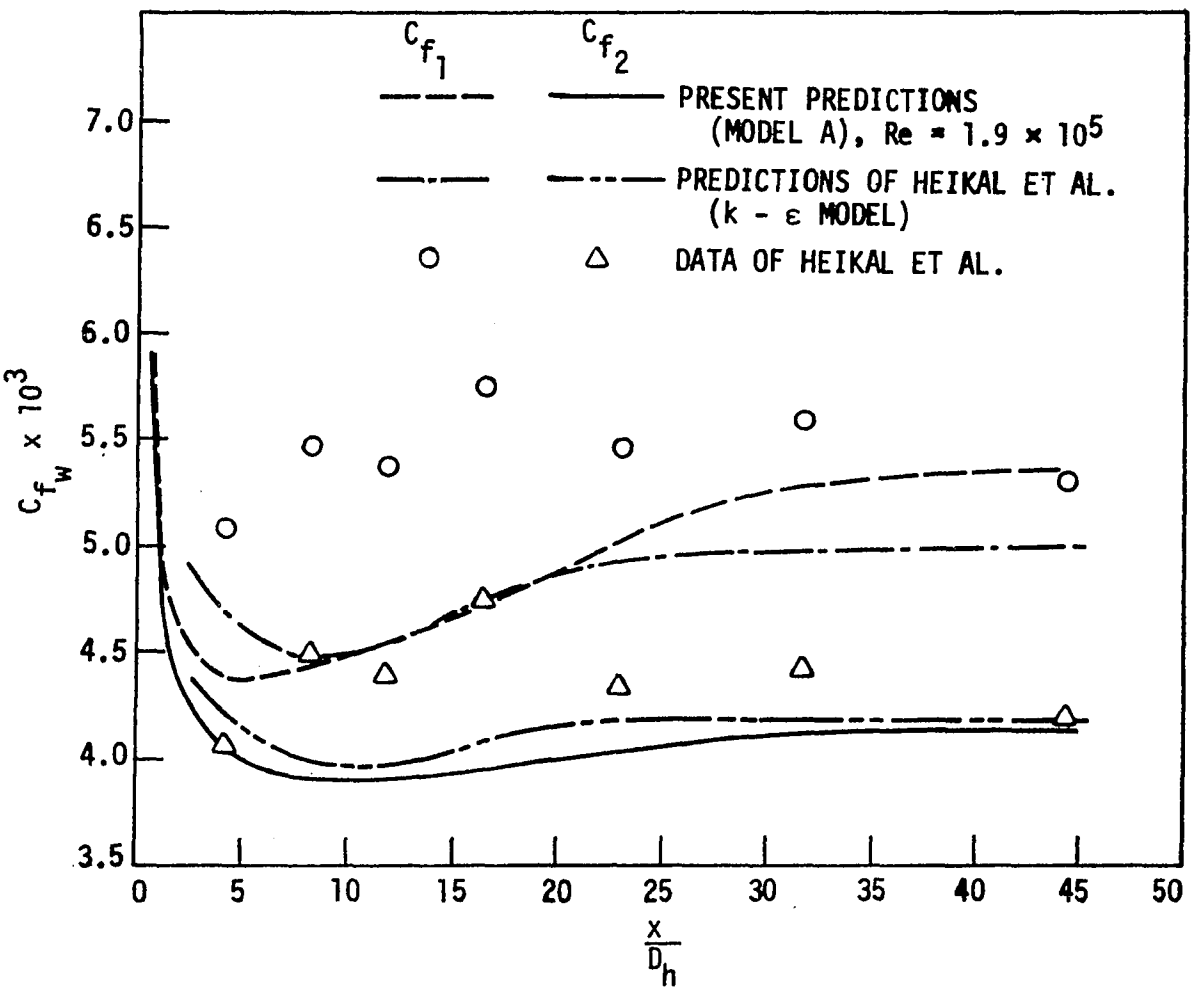

Fig. 4.29. Distribution of skin-friction coefficients along the walls of an annulus (r* = 0.25)

skin-friction coefficients along an annular duct ($r^* = 0.25$). The experimental data of Heikal et al. [48] using a Preston tube and their predictions using the k-ε model are also shown. The variation predicted by Model A is qualitatively similar to that of the k-ε model and the fully developed values are well-predicted. The measured skin-friction coefficients in the entrance region are somewhat higher than the calculated values. The variation of measured skin friction in the entrance region suggests that Heikal's experiment is not a representative test case for a developing turbulent flow in an annulus with uniform flow at the inlet and that laminar-turbulent transition might have taken place in the entrance region. The mismatch of the inlet conditions between the experiment and the calculation is further suggested by the comparisons shown in Figs. 4.30 and 4.31 for turbulence kinetic energy profiles at four streamwise stations. The predicted and measured profiles do not compare well in the entrance region but the agreement becomes better farther downstream.

The predicted variation of mean velocity at particular radii along the duct is compared in Fig. 4.32 with the experimental data of Heikal et al. and predictions using the k-ε model. All results are for a free stream turbulence level of 0.02% at the inlet. The calculations of Heikal et al. [48] were started as laminar and a switch to turbulent flow calculation was made at a particular "boundary-layer thickness Reynolds number" (not mentioned). They do not give any reason as to why this was necessary.

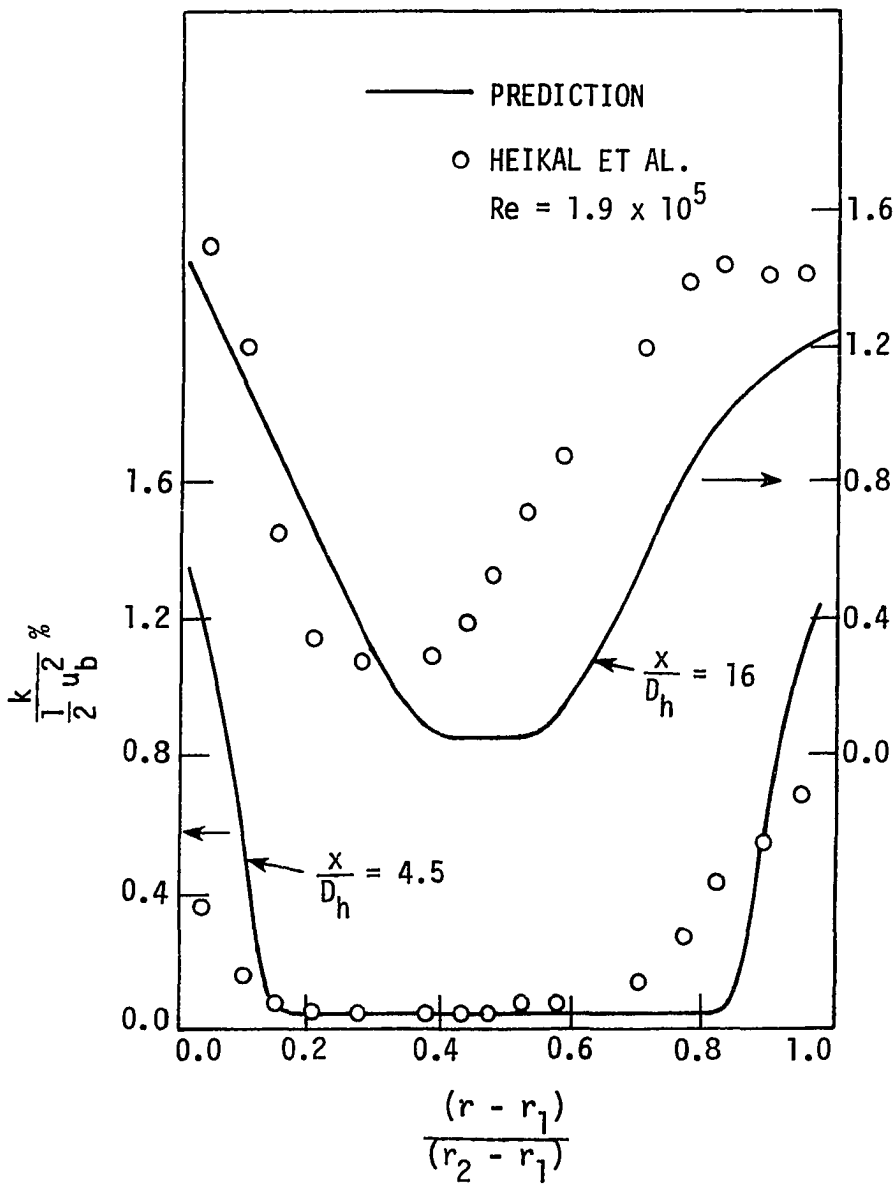

Fig. 4.30. Turbulence kinetic energy profiles in an annulus (r* = 0.25)

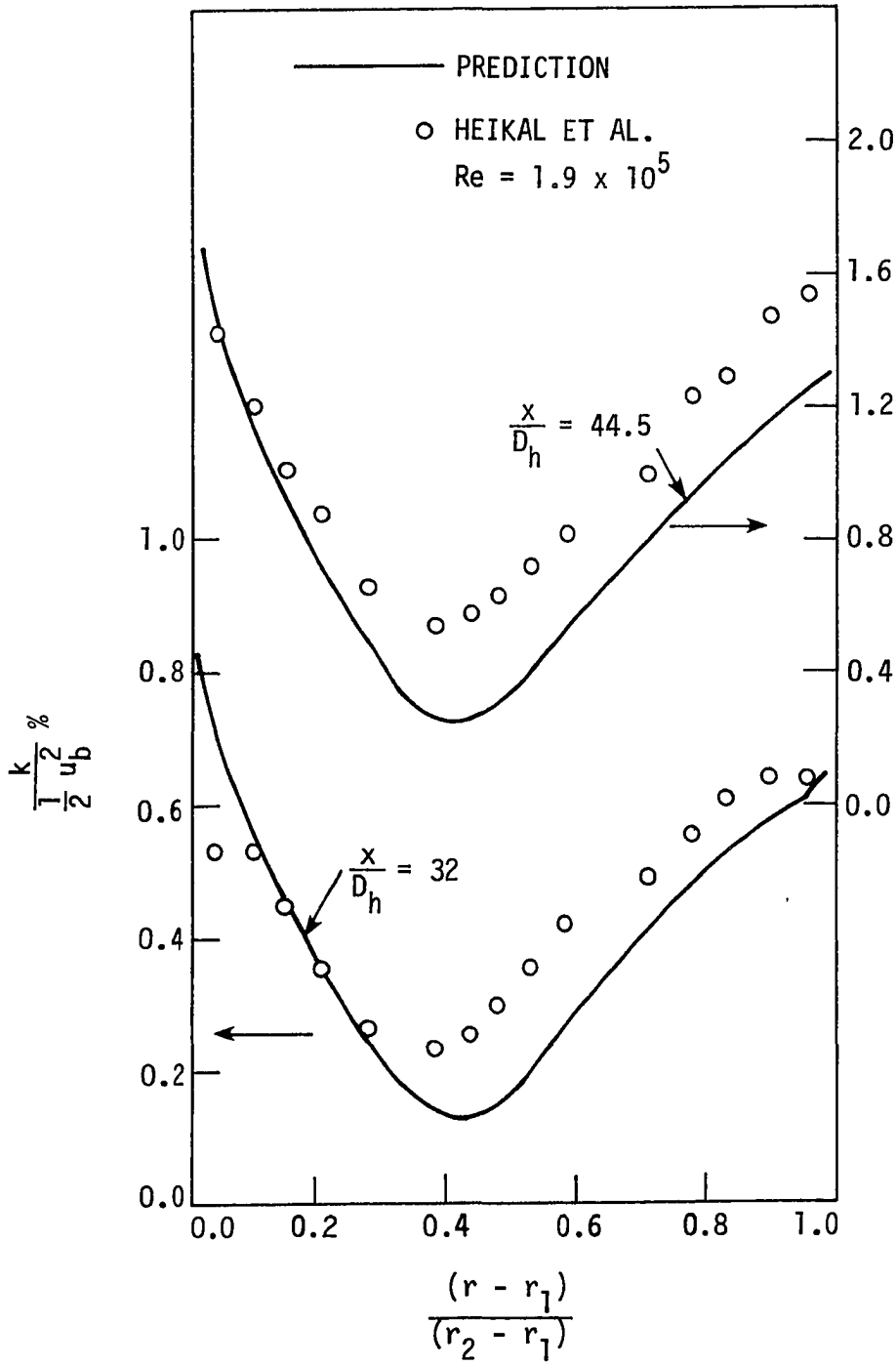

Fig. 4.31. Turbulence kinetic energy profiles in an annulus (r* = 0.15)

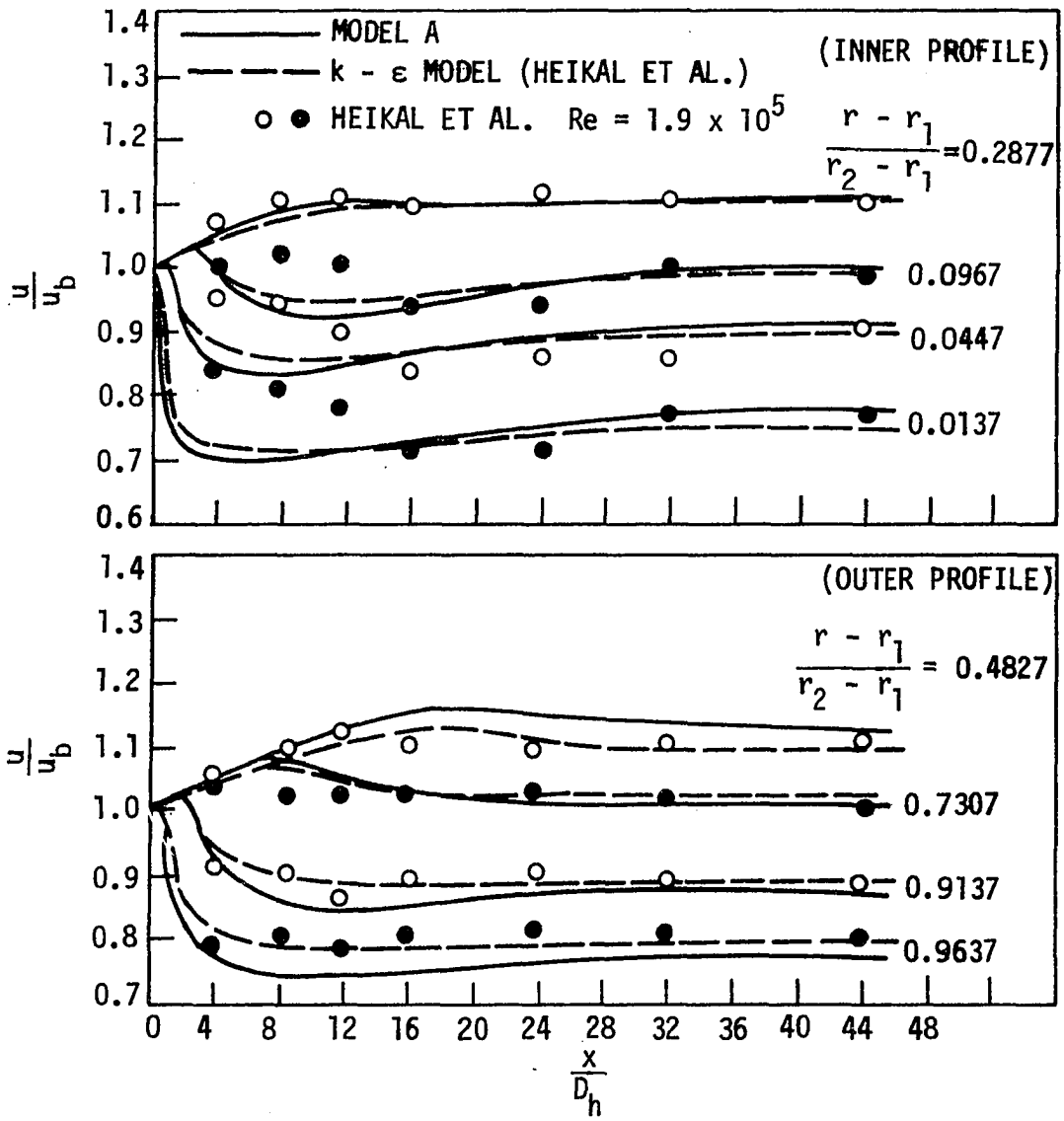

Fig. 4.32. Velocity development in an annulus (r* = 0.25)

Figure 4.33 shows the fully developed velocity profile in an annulus of radius ratio 0.556 predicted by Model A along with the experimental data of Kuzay [70]. Another such comparison is made for an annulus of radius ratio 0.25 where predictions were made using both Models A and B and are compared with the data of Ball and Azer [67] in Fig. 4.34. Predictions of Model B seem to be only slightly better than those of Model A. Reynolds stress profiles were also calculated for an annulus of $r^* = 0.25$ using Models A and C. In Figs. 4.35 and 4.36 these profiles are compared at two streamwise locations ($x/D_h = 32, 44.5$) with the experimental data of Heikal et al. [48]. The predicted profiles are within the scatter of the experimental data and the difference between the predictions of Model A and C is negligible. The reason for this negligible difference is that, from Eq. (2.19), shear stress is zero whenever $\frac{\partial \bar{u}}{\partial y} = 0$ even if μ_T is not zero there. So improvements in the turbulent viscosity profile provided by Model C have little effect on the Reynolds stress profile. This further confirms the conclusion arrived at earlier that Model A predicts the flow development in ducts sufficiently accurately and no more sophistication in the turbulence model is needed for such flows.

Another comparison between the predictions of Models A, B, and C is given in Table 4.1 where the predicted fully developed shear stresses at the inner and outer wall are compared with the experimental data of Kuzay [70] taken in an annulus of radius ratio 0.556. Kuzay evaluated shear stress by three methods namely,

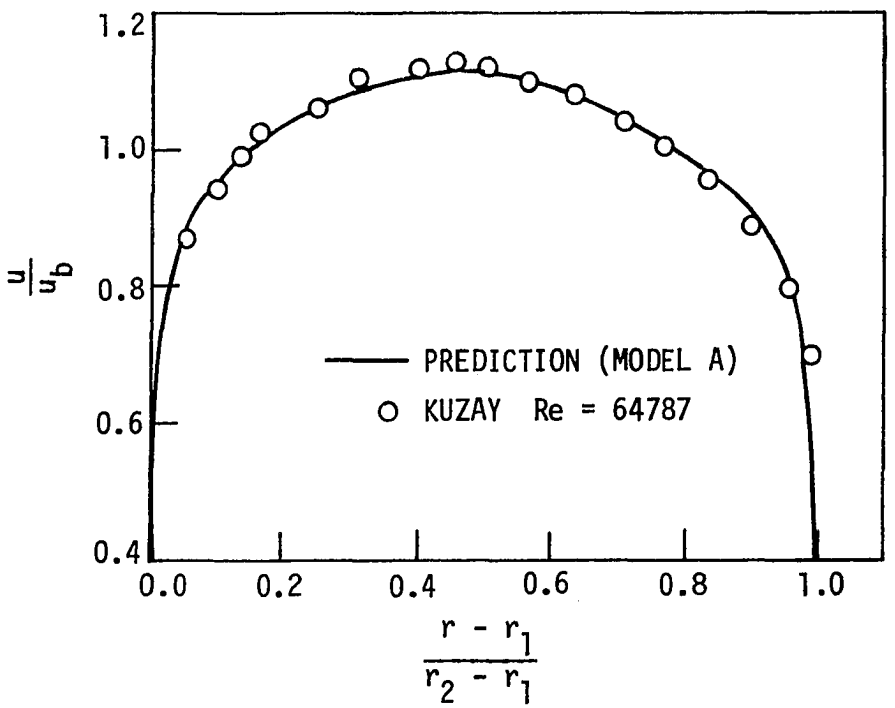

Fig. 4.33. Fully developed velocity profile in an annulus (r* = 0.556)

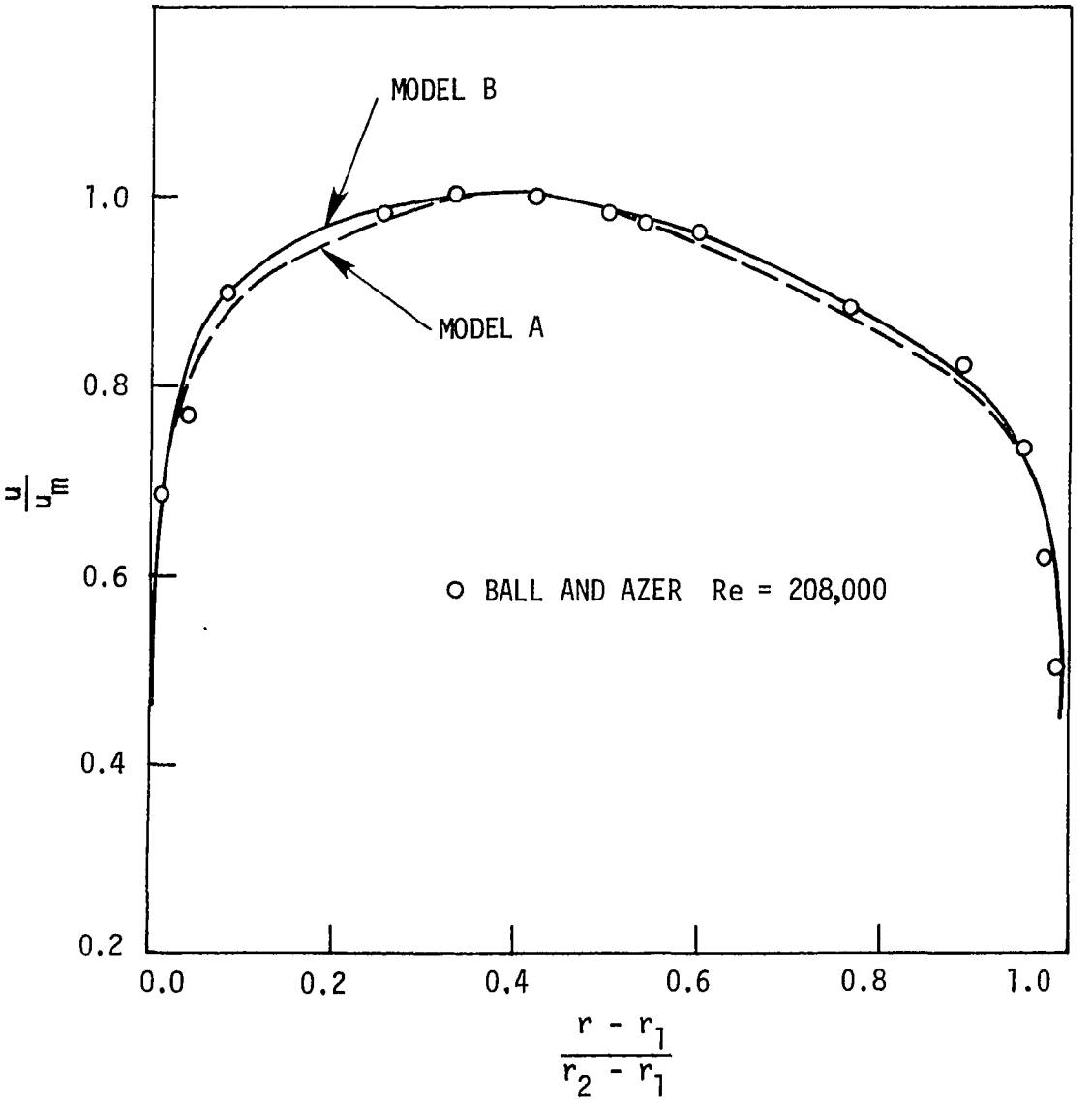

Fig. 4.34. Fully developed velocity profile in an annulus (r* = 0.25)

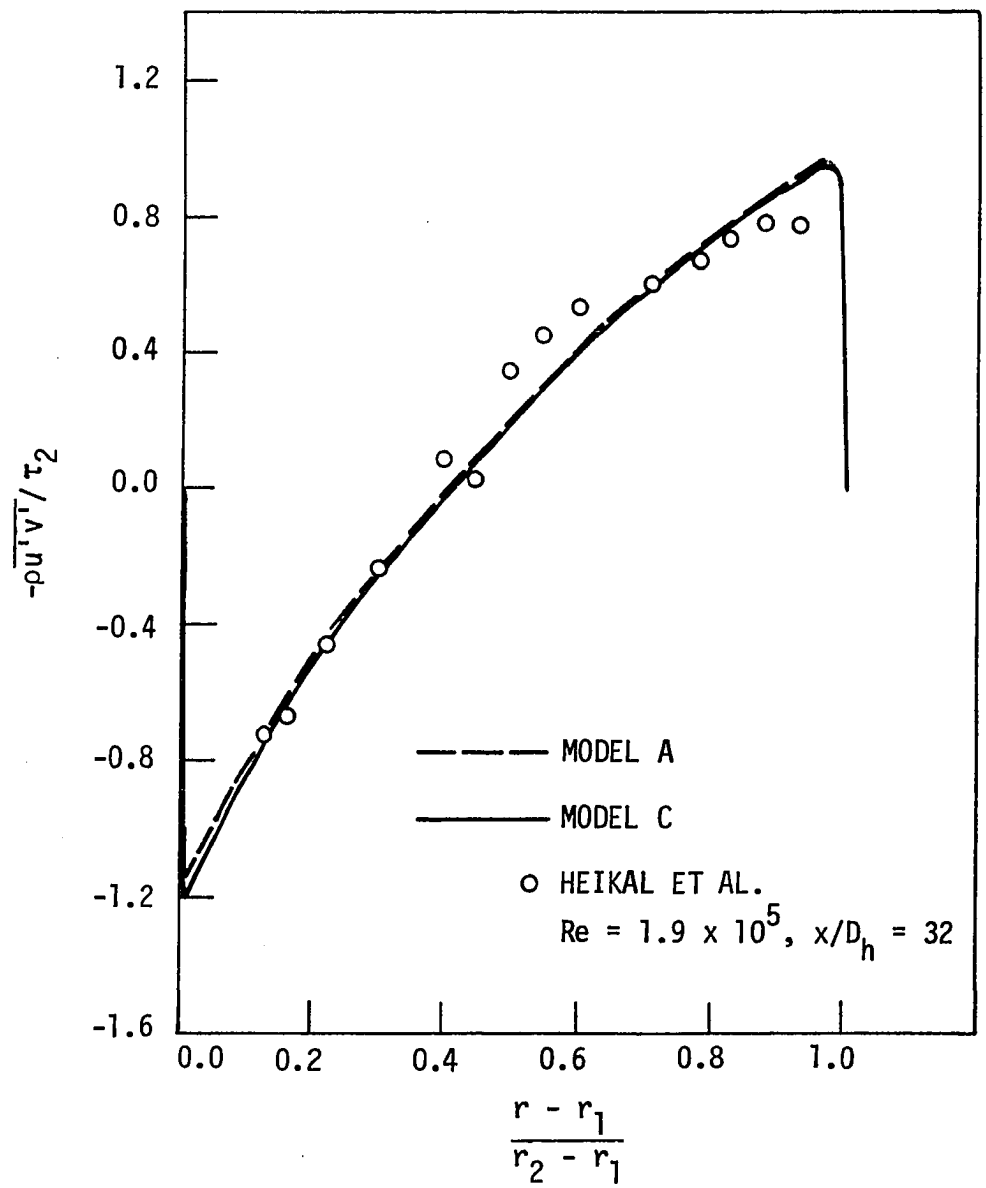

Fig. 4.35. Reynolds stress profile in an annulus (r* = 0.25)

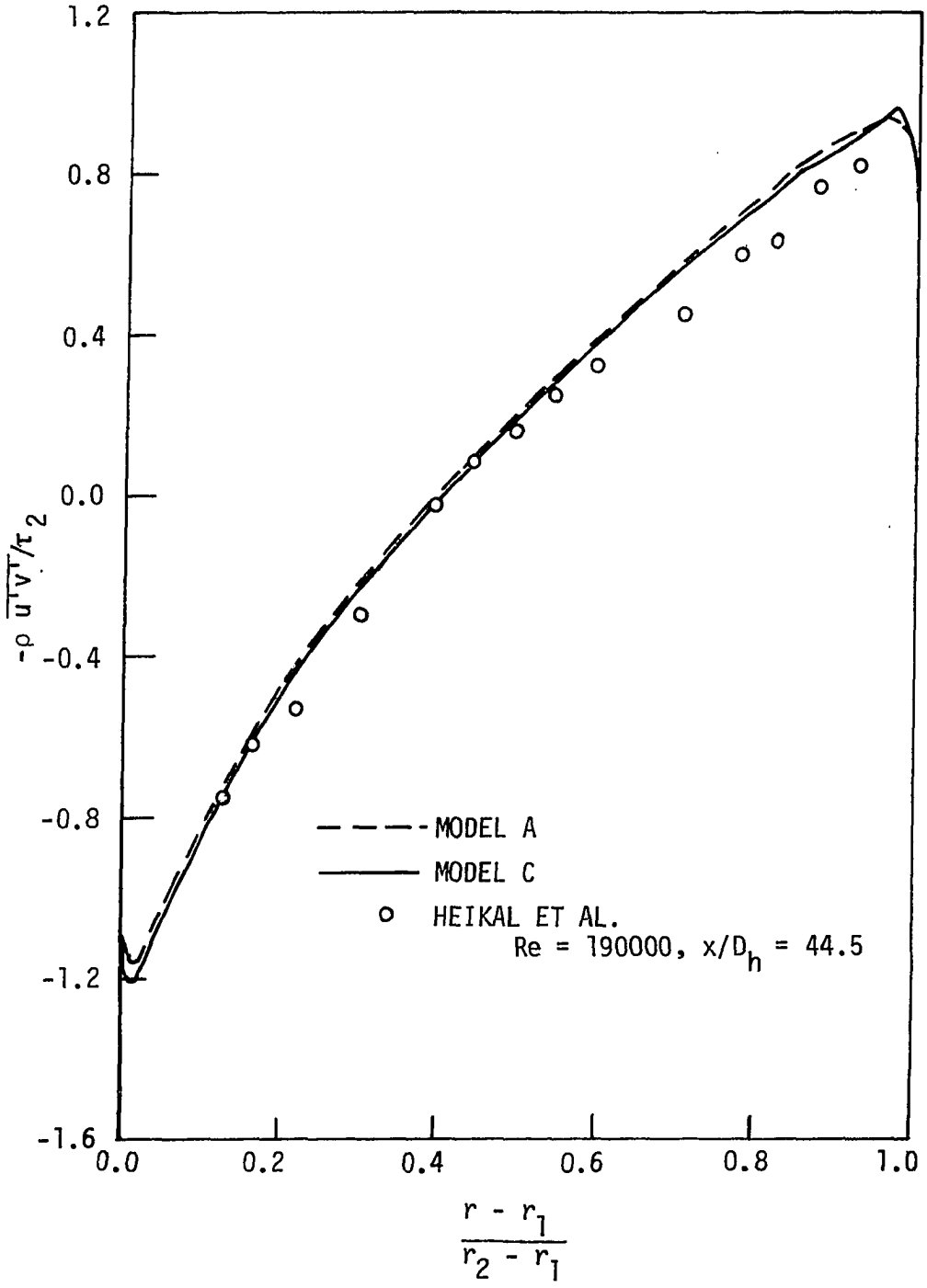

Fig. 4.36. Reynolds stress profile in an annulus (r* = 0.25)

Table 4.1. Predicted inner and outer wall shear stresses in an annulus (r* = 0.556) as compared to the data of Kuzay [70]

Method	τ_1 Newtons/m^2	τ_2 Newtons/m^2	Effective stress $= \frac{\tau_2+r^*\tau_1}{1+r^*}$ Newtons/m^2
Measurements Re = 33156			
Force balance	0.1968	0.1798	0.1860
Clauser plot	0.2077	0.1626	0.1790
Preston tube	0.2222	0.1926	0.2033
Predictions Re = 32285			
Model A	0.2204	0.1863	0.1987
Model B	0.2226	0.1913	0.2027
Model C	0.2189	0.1857	0.1977

1) Fully developed region force balance between the wall and the radius of zero shear.

2) Clauser plot technique.

3) Preston tube method.

The present predictions are closest to the values measured by Preston tube. While the use of Preston tubes to measure wall shear in annular passages has been a matter of controversy [154-156], it is reasonable to assume that for this radius ratio (r* = 0.556) the

results given by it will be reliable.

Figure 4.37 shows the predicted inner and outer wall velocity profiles drawn on the "law of the wall" coordinates, as compared with the results of Lawn and Elliot [35] for $r^* = 0.396$. At this radius ratio the predictions agree quite well with their data and seem to suggest that a universal logarithmic region with Patel's [157] suggested constants exists near each wall. However, at very small radius ratios, it has been suggested that the universal log law does not hold at least near the inner wall. For such cases, a modification in the turbulence model was suggested earlier in order to account for large transverse curvature (see Eq. (2.57)). Calculations with and without the curvature correction were made for an annulus ($r^* = 0.088$) and are shown in Fig. 4.38. It can be seen that with the proposed modification in the damping constant, A^+, the predictions agree well with the data of [35]. Table 4.2 gives the values predicted for the radius of zero shear and the ratio of shear stresses for the same annulus using the transverse curvature correction. The present predictions are for $Re = 2.37 \times 10^5$. Results of Lawn and Elliot [35] are also given in the table.

2. Thermal results

Heat transfer calculations were also made both for simultaneously developing hydrodynamic and thermal boundary layers and for cases where the flow was hydrodynamically fully developed at the inlet.

Figure 4.39 shows the predicted Stanton number for an annulus

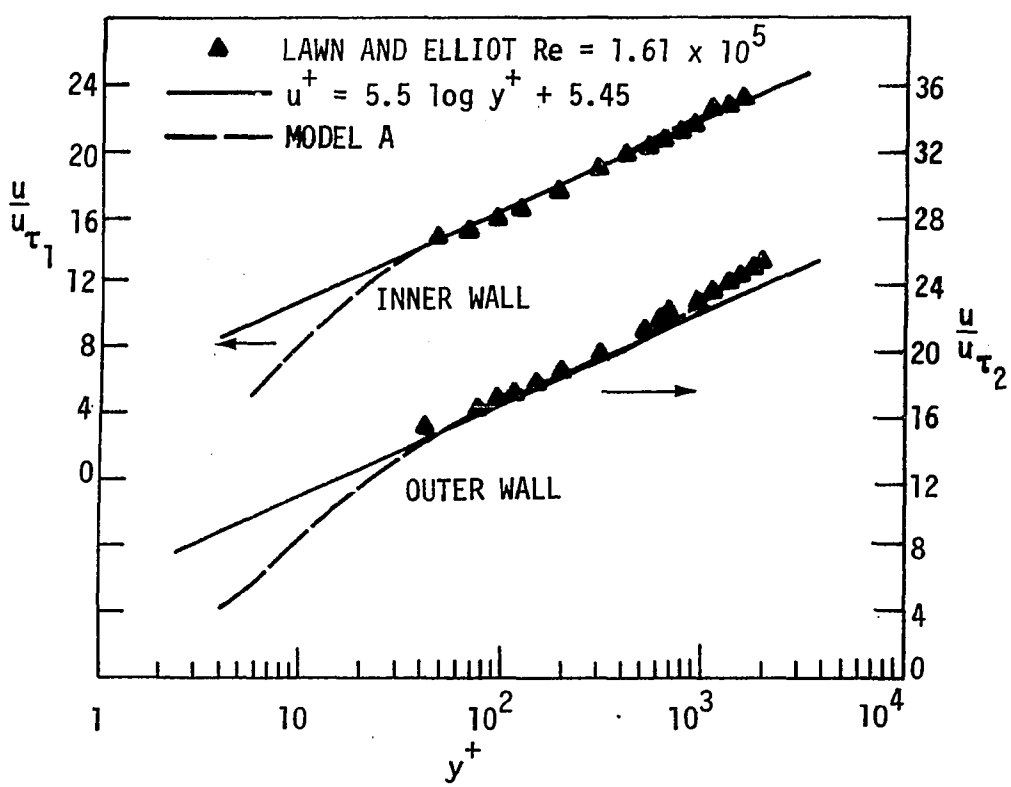

Fig. 4.37. Velocity distribution on law of the wall coordinates ($r^* = 0.25$)

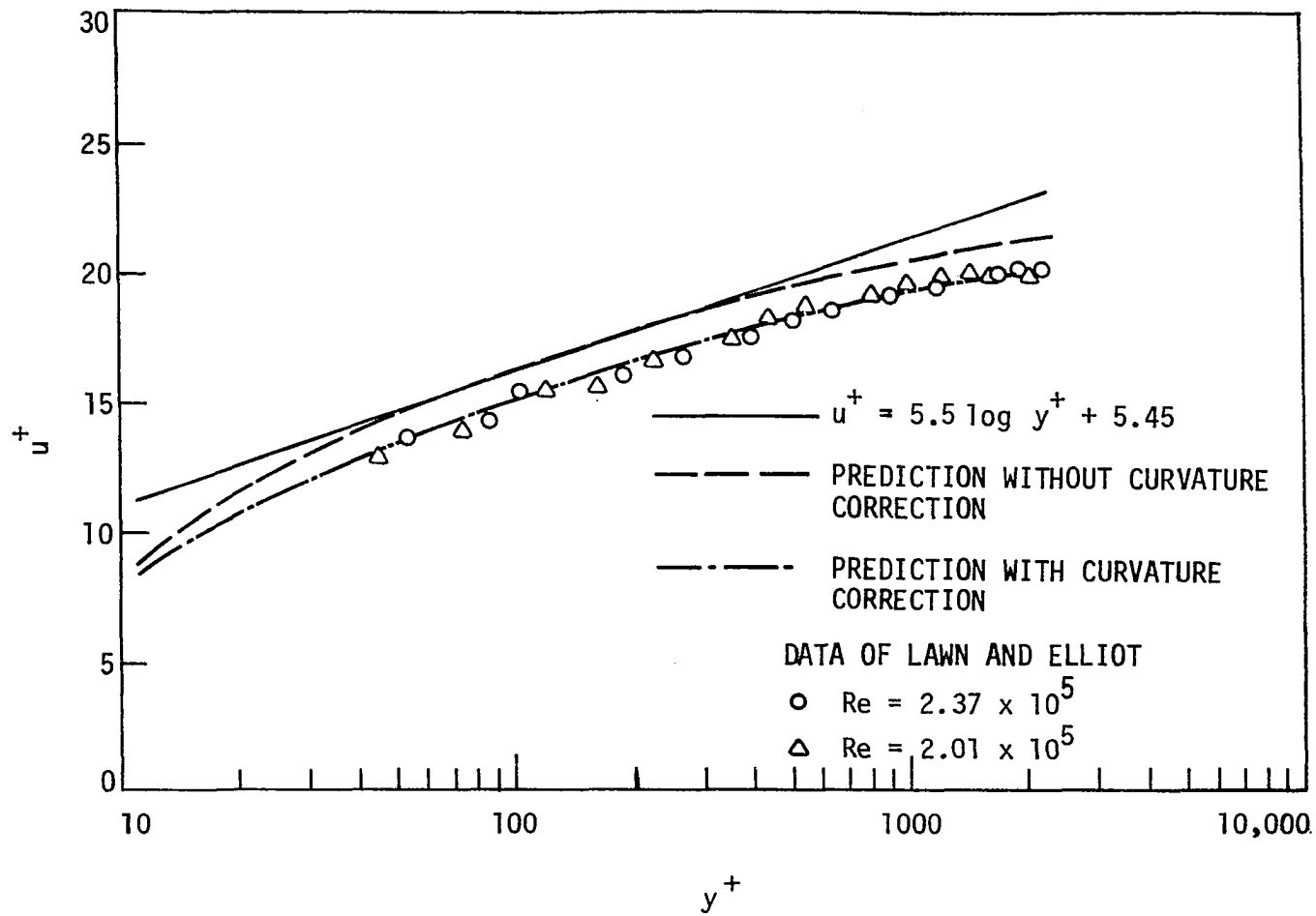

Fig. 4.38. Velocity distribution near the inner wall of an annulus (r* = 0.088); prediction Re = 2.37×10^5

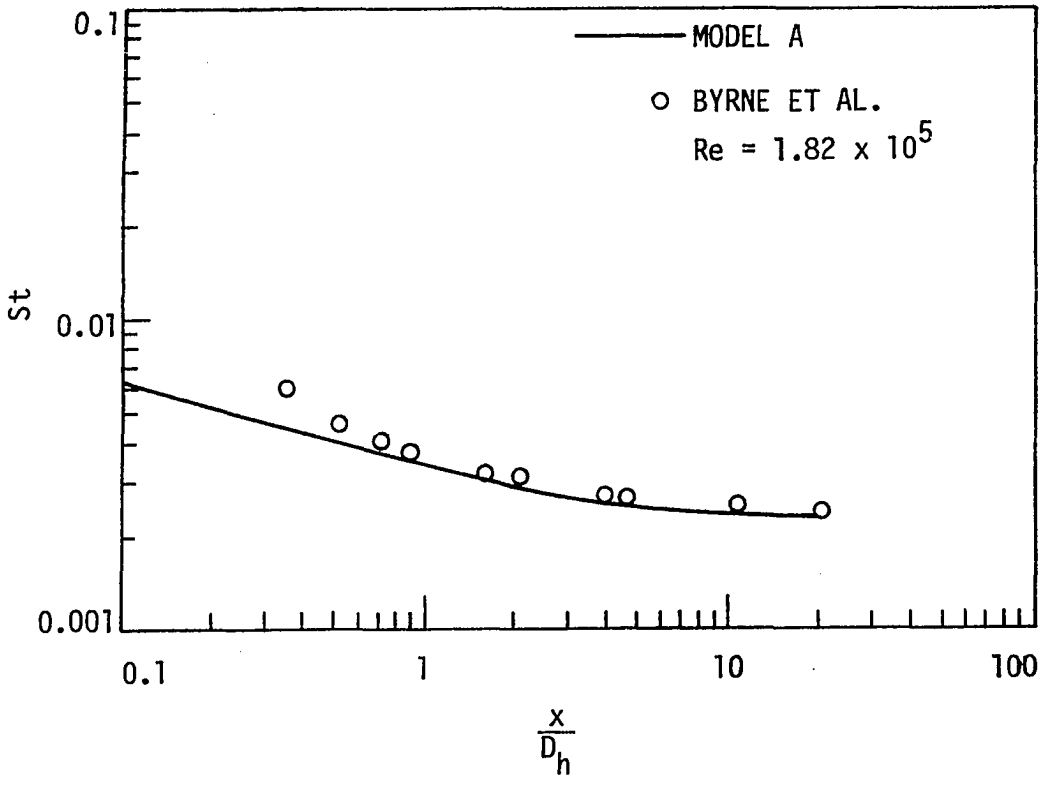

Fig. 4.39. Prediction of Stanton number for hydrodynamically developing flow in an annulus ($r^* = 0.99$) with one wall heated; comparison with measurements of Byrne et al. in a plane duct

Table 4.2. Predicted (Model A with curvature correction) and measured [35] values of some parameters for an annulus with $r^* = 0.088$

Method	$\frac{r_o}{r_2}$	$\frac{\tau_1}{\tau_2}$	$(\frac{\tau_1}{\frac{1}{2}\rho u_b^2})/C_f$	$(\frac{\tau_2}{\frac{1}{2}\rho u_b^2})/C_f$
Measurements	0.362 ± 0.0031	1.61	1.532 ± 0.028	0.952 ± 0.01
Predictions	0.3623	1.603	1.529	0.953

($r^* = 0.99$) as compared to the data of Byrne et al. [148] taken in the entrance region of a parallel passage with one wall heated. A constant heat flux boundary condition was assumed in the calculations which were made using Model A. The predicted Stanton number is in good agreement with the data except very near the entrance where the differences are exaggerated by using a log-log plot. The reason for this discrepancy near the inlet is that in the experiment of Bryne et al., heating started at a small distance downstream of the inlet while the present calculations were made by assuming that the heating started at the inlet. Another thermal computation was made with an unheated starting length ($x/D_h = 0.3$) to approximate Byrne's experimental conditions. The results are shown in Fig. 4.40 along with the data of [148]. It can be clearly seen that the predictions are greatly

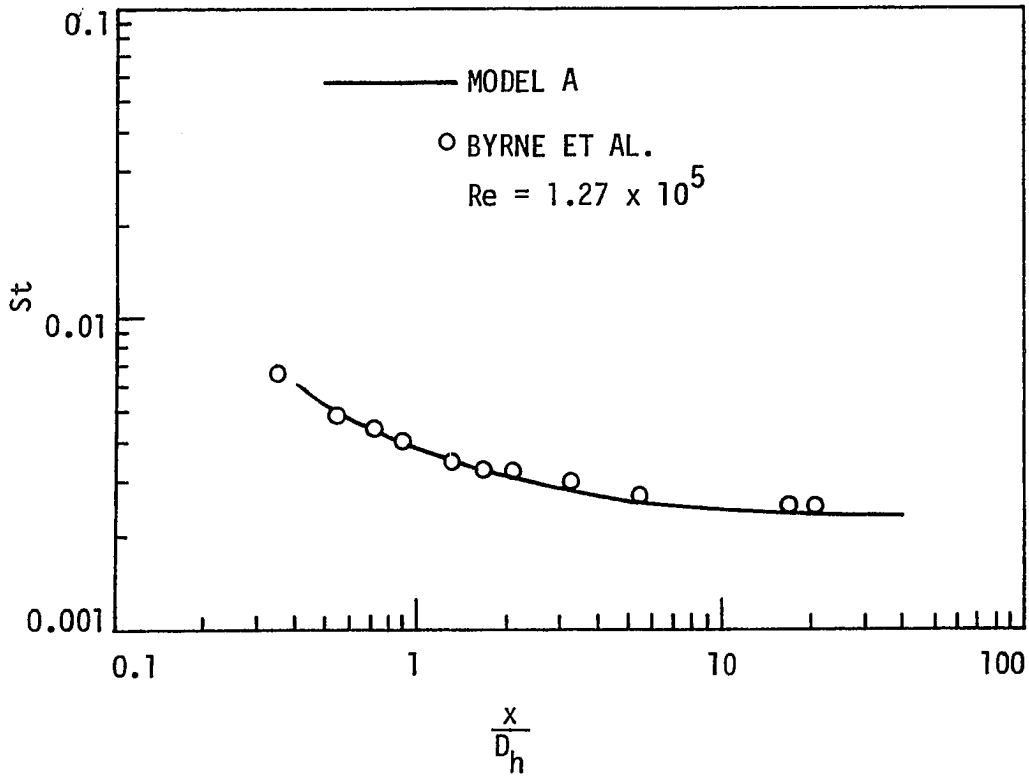

Fig. 4.40. Prediction of Stanton number for hydrodynamically developing flow in an annulus ($r^* = 0.99$); thermal calculations started at $x/D_h = 0.3$

improved by matching the initial conditions existing in the experiment. The predicted Reynolds analogy factor is shown in Fig. 4.41 and is compared with the data of Byrne et al. The present predictions were made with a constant turbulent Prandtl number of 0.9.

The predicted variation of Nusselt number in the entrance region of an annulus ($r^* = 0.476$) is compared in Fig. 4.42 with the data of Roberts and Barrow [80] at two different Reynolds numbers. Predictions were made using Models A and C. Since both predictions were nearly identical, only the results from Model C are shown. The predicted value of fully developed Nusselt number at the higher Reynolds number is about 15% higher than that given in [80]. The fully developed value given by the correlation suggested by Dalle Donne and Meerwald [72] (see Eq. (1.6)) agrees with the present predictions. Calculations were also made (for the higher Reynolds number) using a variable turbulent Prandtl number, similar to that given in Eq. (2.48) with a wall value of 1.5, and a significant improvement between the predictions and the data of Roberts and Barrow was noted. However, improved agreement with data from just one experimental study was not seen as sufficient justification for adopting the more complex Pr_T model, especially in view of the discussion provided in Section B.6 of Chapter II. A constant value of $Pr_T = 0.9$ seems to simulate most of the cases tested in this study.

The effect of bridging on Stanton number is shown in Fig. 4.43 where the predictions are compared with the experimental data of Furber

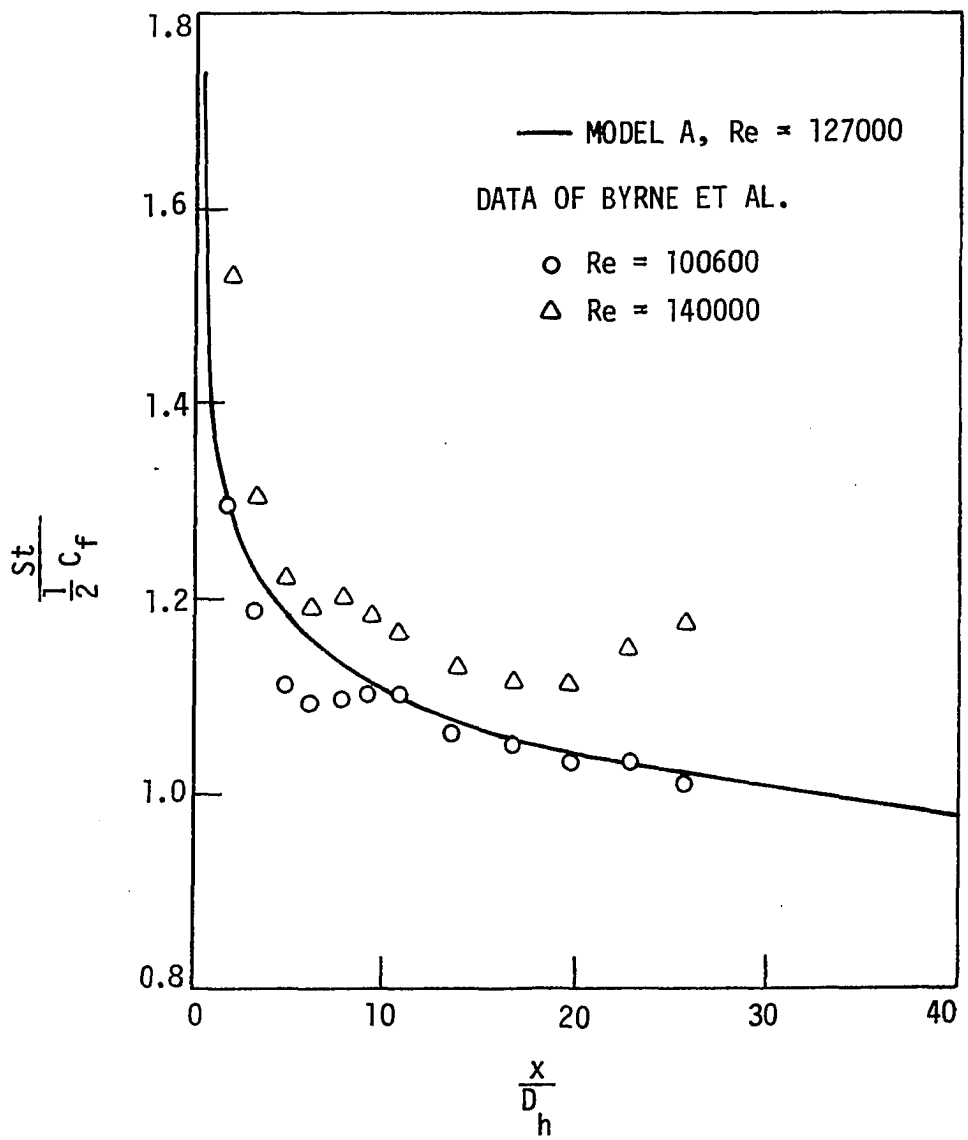

Fig. 4.41. Reynolds analogy factor in an annulus (r* = 0.99) with inner wall heated

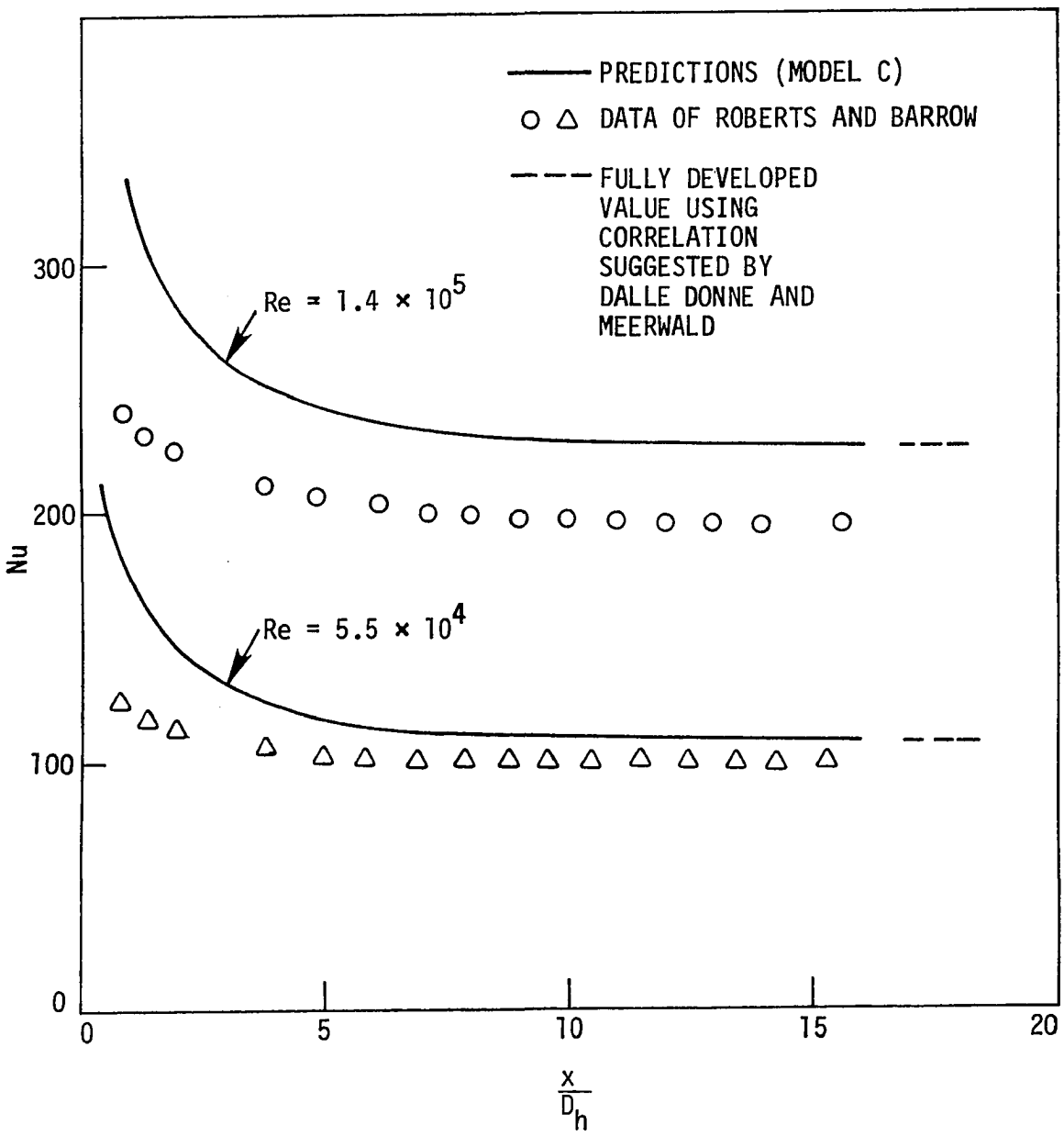

Fig. 4.42. Nusselt number distribution for hydrodynamically developing flow in an annulus (r* = 0.476); inner wall heated

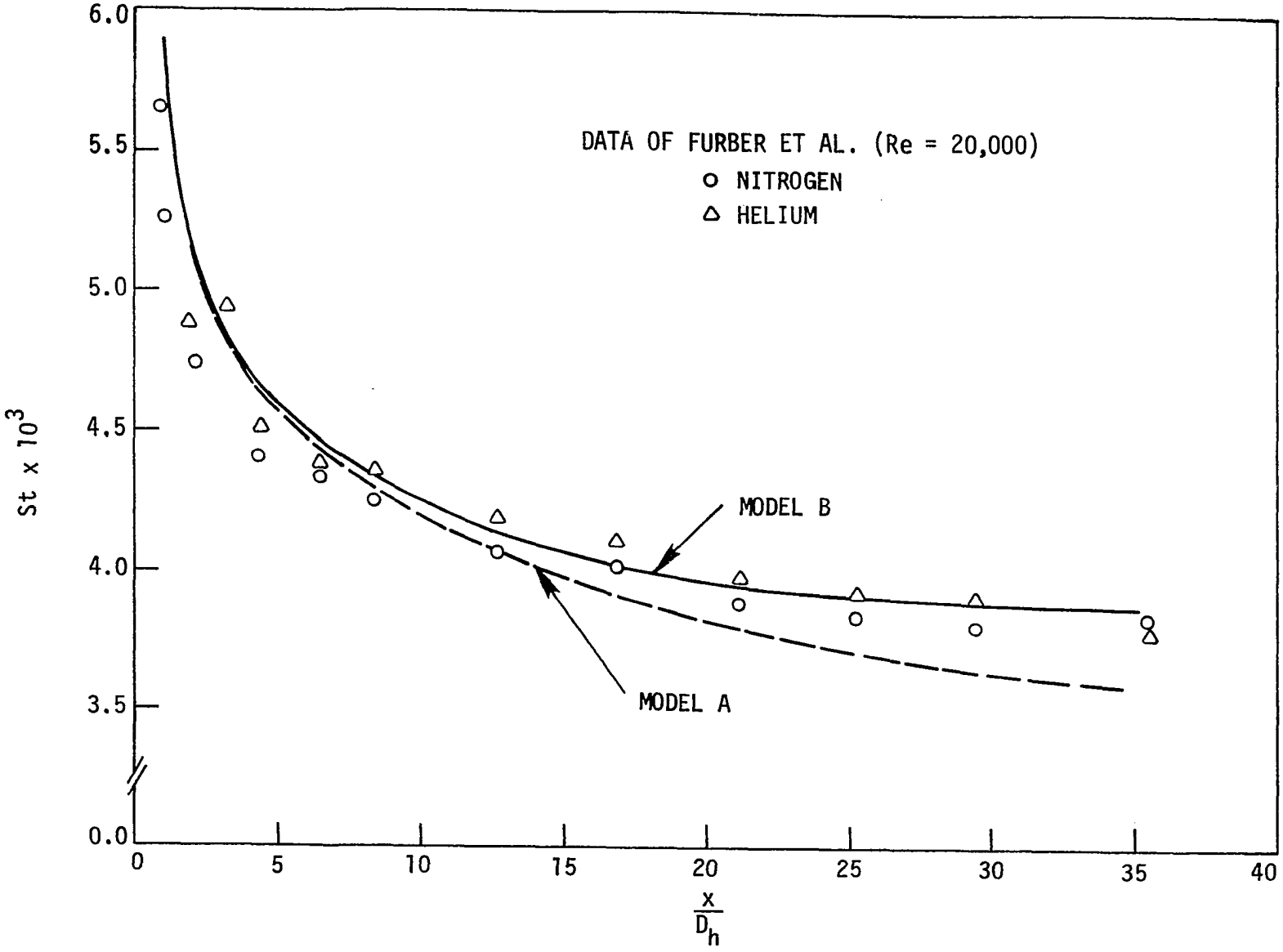

Fig. 4.43. Local Stanton number for hydrodynamically developed flow in an annulus (r* = 0.68); inner wall heated

et al. [71] taken in an annulus (r* = 0.68) for flows of both nitrogen and helium at high pressure. The thermal boundary conditions were those of constant heat flux at the inner wall and an insulated outer wall. The flow was hydrodynamically developed at the start of heating. The present calculations are for Re = 20,000 and have made use of the properties of nitrogen given in Appendix F. The fully developed Stanton number with bridging seems to be about 8% higher than that without bridging. The difference, however, decreases with Reynolds number. Predictions of Model C, though not shown, are expected to lie between that of Models A and B. In Table 4.3, fully developed Stanton numbers obtained for an annulus (r* = 0.556) with outer wall heated are given. It can be seen that the difference between the predictions of Models A and B reduces with Reynolds number and the prediction of Model C lies in between that of Model A and B.

Table 4.3. Predicted fully developed Stanton numbers for an annulus (r* = 0.556) with the outer wall heated

Model	St	
	Re = 32285	Re = 64131
A	0.002907	0.002514
B	0.003103	0.002661
C	0.002938	0.002657

Figure 4.44 compares the predicted Stanton number with the measurements of Furber et al. [71] at Re = 10^5. The thermal boundary conditions were the same as mentioned before and only Model A was used. The agreement between the predictions and the data seems encouraging and suggests that a turbulent Prandtl number of 0.9 can give sufficiently accurate predictions of wall heat transfer. Figure 4.45 shows the effect of varying heat flux on Stanton number. Again the present predictions (Model A) compare fairly well with the data of [71]. The predictions show that the Stanton number is reduced by about 18% if T_w/T_b is varied from 1.0 to 2.0. The source of the properties of nitrogen used in the present calculations has already been mentioned.

Dalle Donne and Meerwald [72] also studied the effect of variable properties on Nusselt number and correlated their data as given in Eq. (1.6). They suggested that heat transfer coefficients can be better correlated with T_w/T_0 instead of T_w/T_b because in the former choice, the exponent c of the temperature ratio does not depend upon x/D_h after a certain length required for the temperature profile to become fully developed. Dalle Donne and Meerwald, based on the data taken in two annuli, suggested that the exponent c = -0.2. Calculations were made using Model A for the annulus with r* = 0.5. A fully developed velocity profile was assumed at the inlet. The results at two streamwise locations (x/D_h = 40.3, 56.5) are shown separately in Figs. 4.46 and 4.47 along with the experimental data of [72] at these locations. It can be seen that present predictions give a value of c = -0.31 as

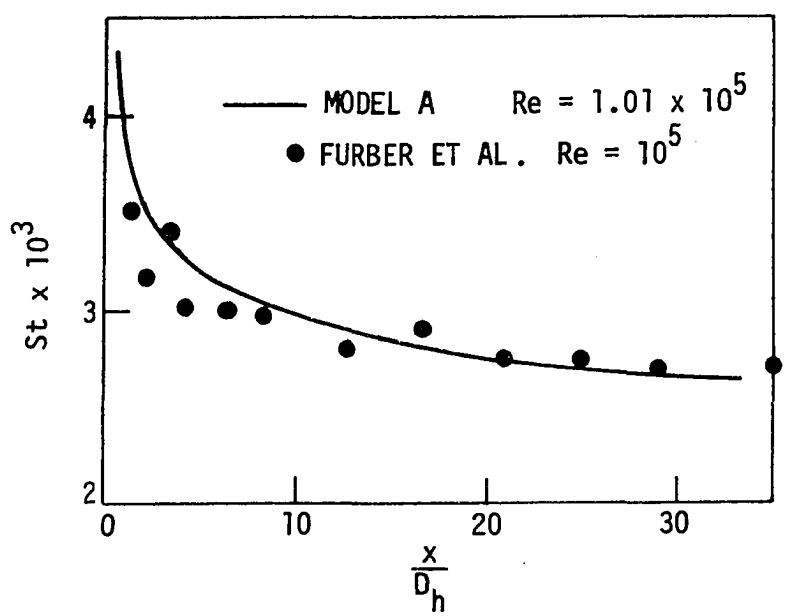

Fig. 4.44. Local Stanton number for hydrodynamically developed flow in an annulus (r* = 0.68); inner wall heated

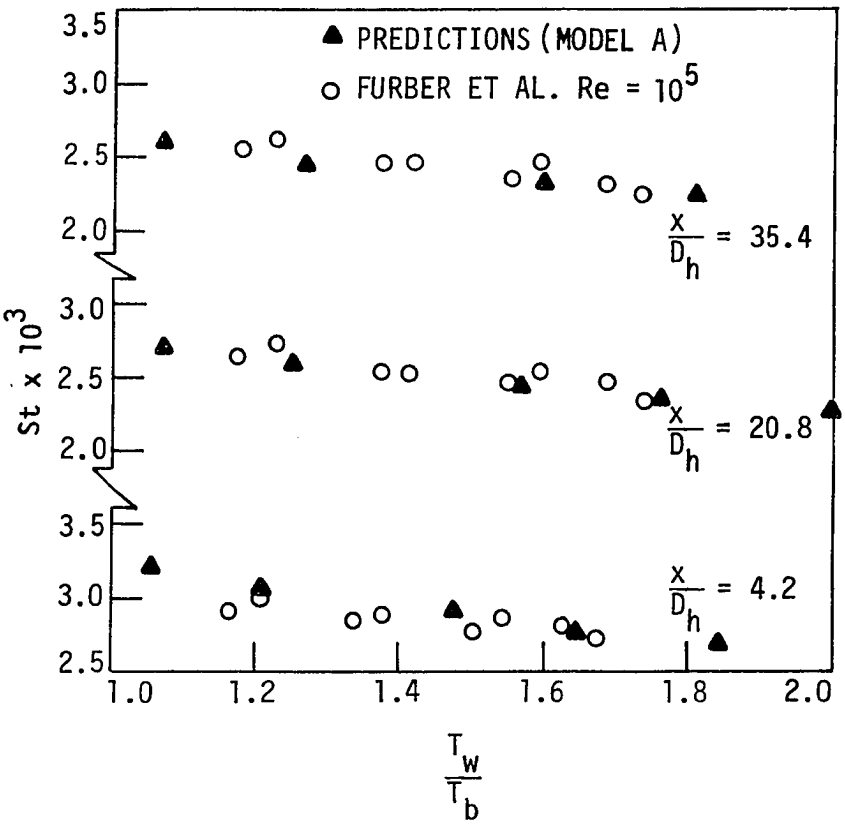

Fig. 4.45. Effect of wall-to-bulk temperature ratio on Stanton number for flow of nitrogen through an annulus ($r^* = 0.68$) with inner wall heated

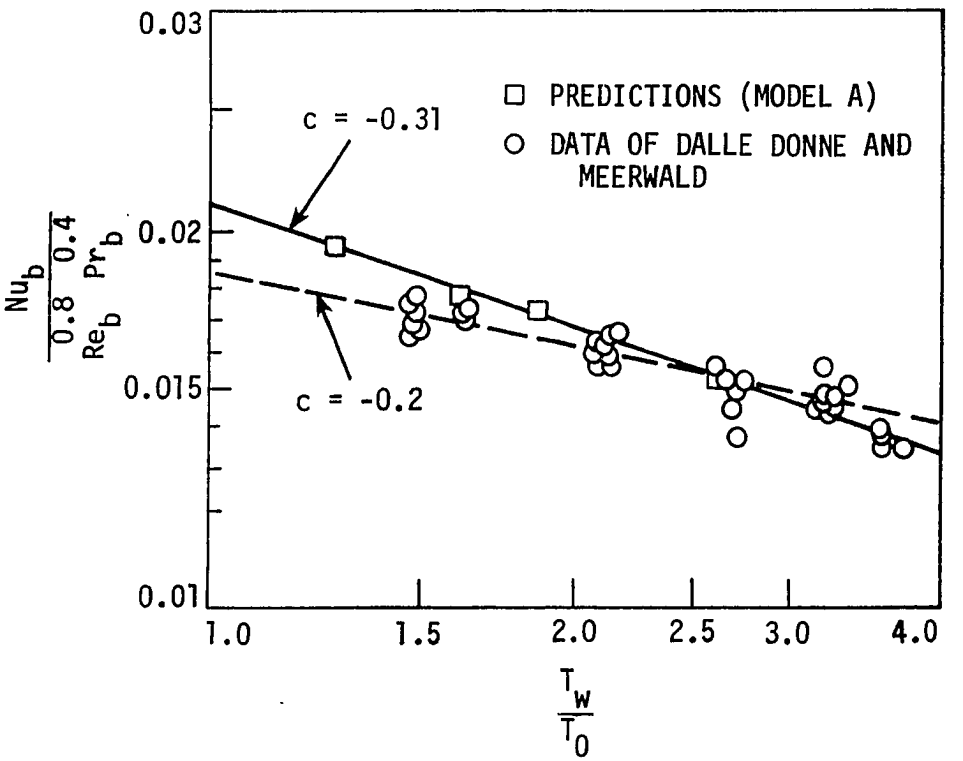

Fig. 4.46. Correlation of heat transfer with wall-to-inlet temperature ratio for flow of air through an annulus ($r^* = 0.5$), $x/D_h = 40.3$

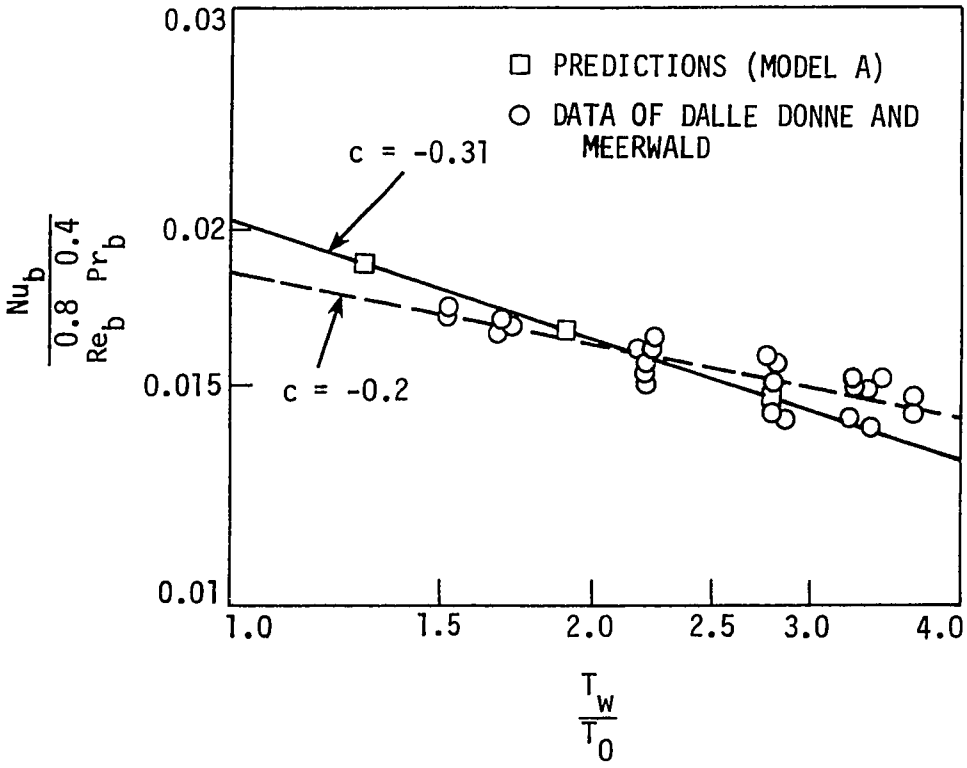

Fig. 4.47. Correlation of heat transfer with wall-to-inlet temperature ratio for flow of air through an annulus ($r^* = 0.5$), $x/D_h = 56.5$

against -0.2 suggested by Dalle Donne and Meerwald. Earlier, Dalle Donne and Bowditch [158] and Dalle Donne [159] had suggested different values of c for a tube: -0.255 for a tube with a long entrance length, and -0.304 for a tube with short entrance length. Also quite a wide range of values of c has been suggested in the literature (see, e.g., [72]) when heat transfer is correlated with T_w/T_b. So the value of -0.31 predicted in the present calculations should be considered as within the typical scatter of data.

Figure 4.48 shows the temperature profile at 14.4 hydraulic diameters downstream of the start of heating, compared to the data of Ball and Azer [67]. Their data were taken in an annulus ($r^* = 0.25$) using constant heat flux at the inner wall, with the outer wall insulated. The temperature profile predicted by Model A does not compare well with the measurements [67], while the comparison is seen to be improved by bridging (Model B) the turbulent viscosity and, thus, the turbulent conductivity profile. Figures 4.49 and 4.50 show the comparison between all three models and the experimental data of Kuzay [70] at two different Reynolds numbers. In this experiment, an unheated length of 15 hydraulic diameters was followed by a heated length of 36 diameters (outer wall heated). These experimental conditions were matched in the predictions. It can be seen from Figs. 4.49 and 4.50 that Model A predicts an unrealistically large temperature gradient in the region of maximum velocity because of the very small eddy conductivity predicted there. Both Models B and C offer

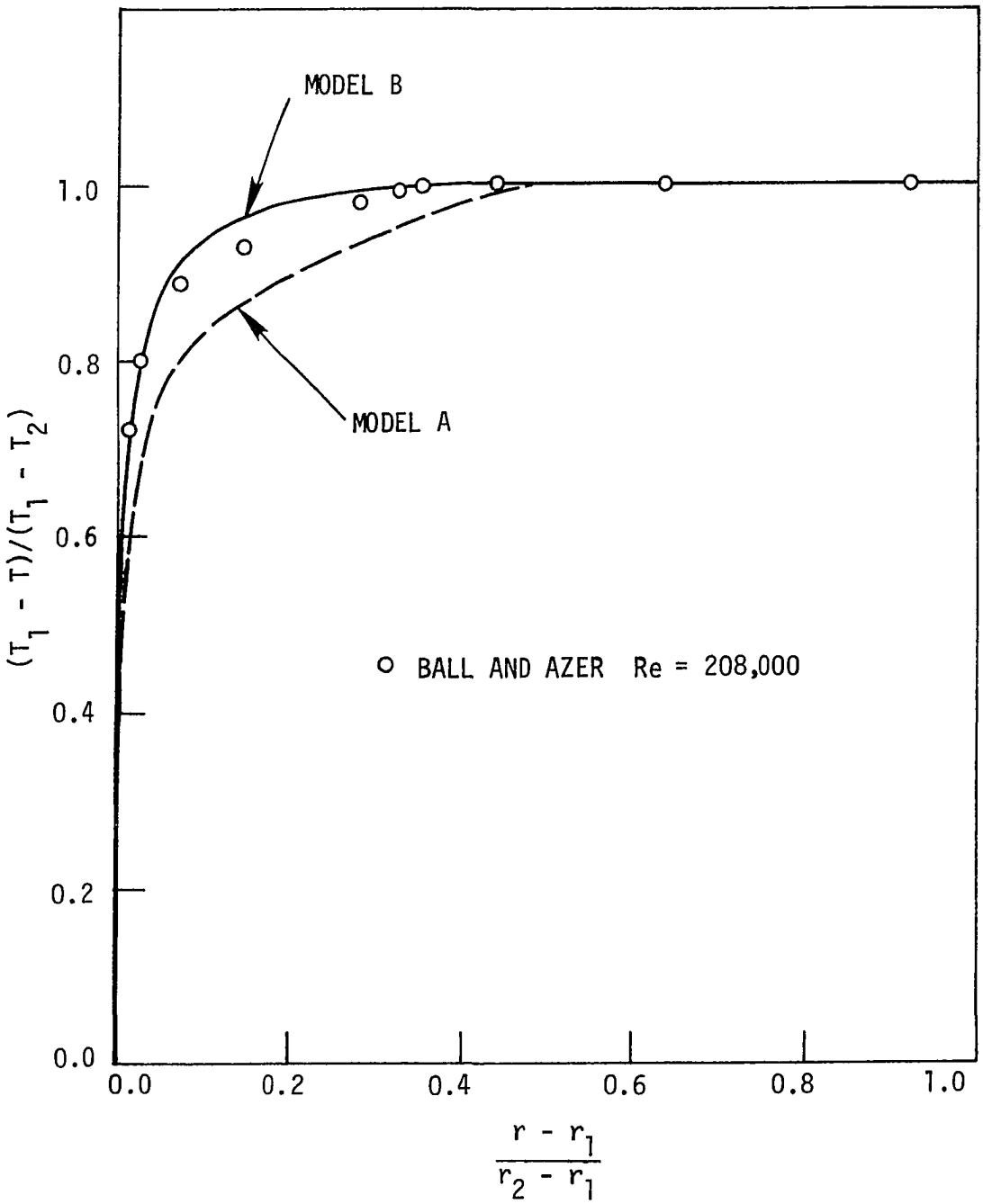

Fig. 4.48. Predicted temperature profile (Re = 215,000) for flow of air through an annulus ($r^* = 0.25$) compared with the data of Ball and Azer at 14.4 diameters downstream of the start of heating

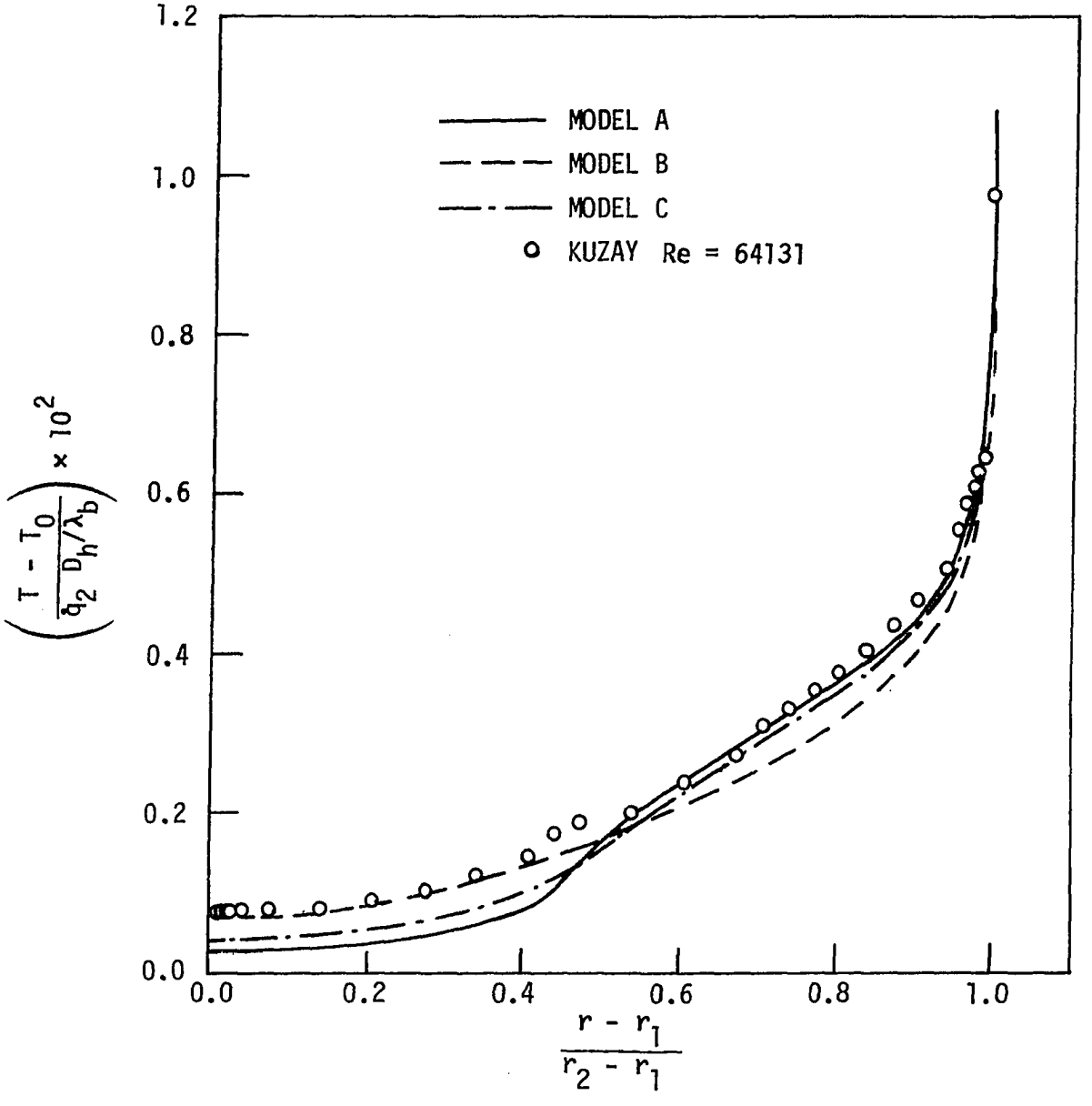

Fig. 4.49. Predicted temperature profiles for flow of air through an annulus ($r^* = 0.556$) compared with the data of Kuzay at 33 diameters downstream of the start of heating

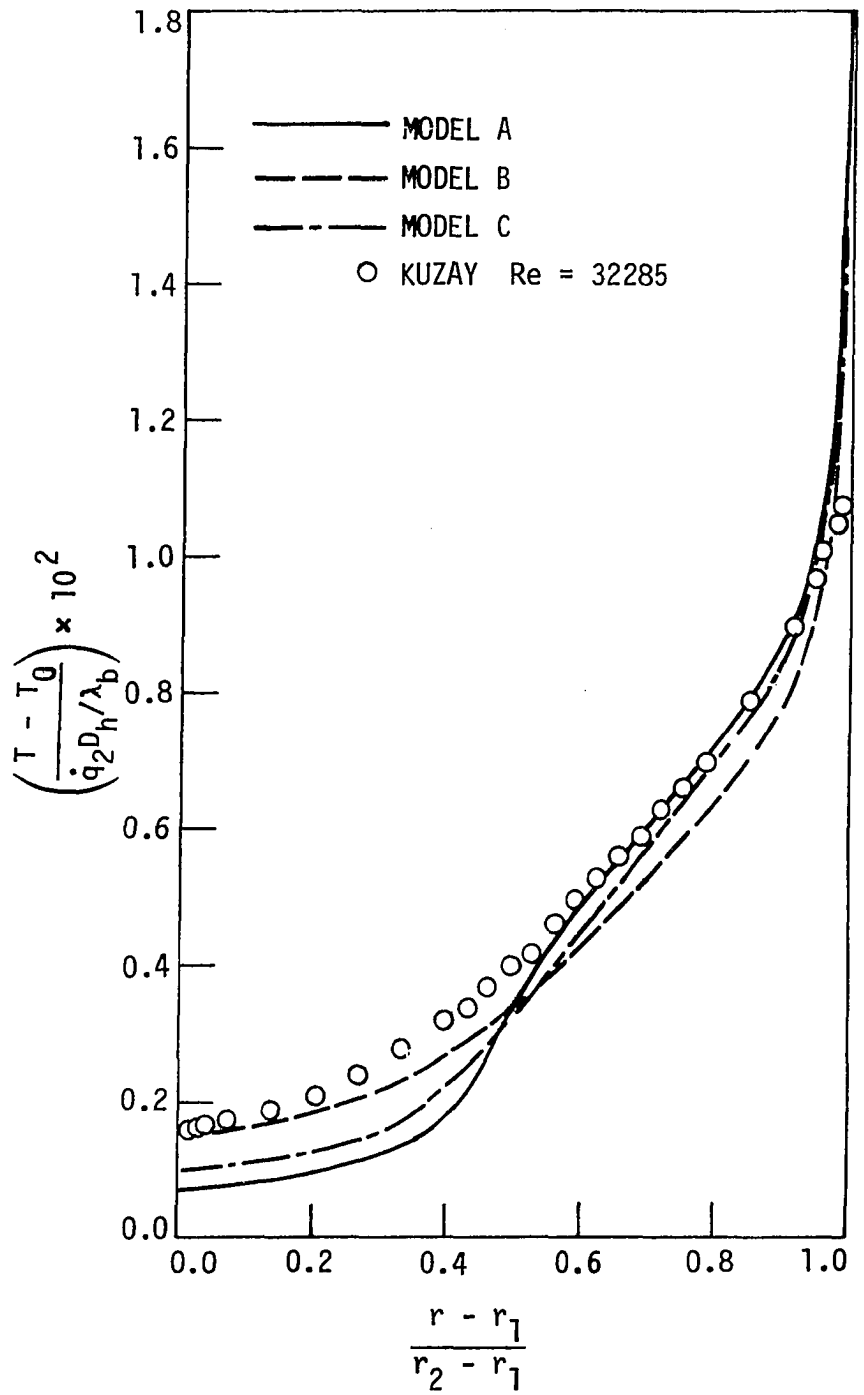

Fig. 4.50. Predicted temperature profiles for flow of air through an annulus (r* = 0.556) compared with the data of Kuzay at 33 diameters downstream of the start of heating

improvement to the predicted temperature profile. In another test run (Re = 64131) with Model C, a variable turbulent Prandtl number similar to that given in Eq. (2.47) was used in order to provide a small value of Pr_T near the radius of maximum velocity. The predicted temperature profile by this procedure fell in between the predictions of Models B and C with $Pr_T = 0.9$.

V. CONCLUSIONS

An explitic finite-difference method for the prediction of variable property laminar and turbulent convective heat transfer in straight annular passages has been developed. The calculation scheme was evaluated for the following flow regimes:

1) Laminar constant property flow

2) Laminar vertical buoyant flow

3) Turbulent flow with and without heat transfer

A major part of this study was devoted to the development and evaluation of turbulence models for interacting shear layers. A first-order ordinary differential equation for the transport of length scale was proposed. Consideration was also given to the effects of large transverse curvature and variations in the turbulent Prandtl number. Comparisons were made with the available experimental data to test the turbulence models and the calculation procedure.

The following major conclusions are noted:

1) The proposed finite-difference method is reliable. This was tested by applying it to relatively simple case of laminar forced convection. Good agreement with the available results in the literature was observed both for the variation of pressure gradient and Nusselt number.

2) The calculation scheme provides an economical means for obtaining predictions for reasonably complicated flows in annuli. None of the test cases reported in this study required more than 160 seconds

on an ITEL AS/5 and most were run in less than 100 seconds.

3) In the calculations made for laminar vertical buoyant flows, it was found that the effect of natural convection on heat transfer was significant. Thus, this effect should be included in any such calculation. In asymmetrically heated ducts, the velocity profile given by Eq. (3.18) is distorted greatly due to density gradients which results in eventual flow reversal near the unheated wall. The location where the shear stress on the unheated wall goes to zero may be taken as the location of the onset of flow instabilities. Gr/Re^2 is believed to be a suitable correlation parameter for the prediction of this location.

4) The transport of turbulence length scale in the outer region of a shear layer is an important consideration for any turbulent flow calculation where the flow is rapidly changing. The proposed length scale equation appears to model this transport satisfactorily. The observed nonmonotonic development of centerline velocity and other flow parameters in a plane duct is well-predicted by this model.

5) The proposed correlation for the damping constant A^+ simulates the effect of large transverse curvature in agreement with the experimental data.

6) A turbulent Prandtl number of 0.9 generally gave good results for Stanton number for the test cases considered in the present study.

7) The temperature profiles predicted by use of the length scale model have large gradients in the central core region because of

very small values of turbulent conductivity predicted there. An improvement in the predicted temperature profiles was noted when the predicted turbulent conductivity profile was linearly bridged between the peaks. The use of the turbulence kinetic energy equation along with the length scale also resulted in an improved temperature profile.

8) Property variations do appear to have a significant effect on the heat transfer coefficient, and the present calculation method is seen to predict these effects in reasonable agreement with experimental data. The predictions (made for flow of air with inner wall heated) show that Nusselt number can be correlated with wall-to-inlet temperature ratio using an exponent of -0.31.

In future research, the effect of large and small molecular Prandtl number on turbulent Prandtl number may be studied if experimental data becomes available. Further research may also be directed towards the prediction of flow in annular diffusers. The present method can be modified for that purpose by incorporating appropriate changes in the coordinates used.

VI. REFERENCES

1. Hall, W. B. "Heat Transfer in Channels Having Rought and Smooth Surfaces." J. Mechanical Engineering Science 4(1962): 287-291.

2. Sutherland, W. A. "Experimental Heat Transfer in Rod Bundles." Heat Transfer in Rod Bundles, pp. 104-138. New York: ASME, 1968.

3. Patankar, S. V. and Spalding, D. B. Heat and Mass Transfer in Boundary Layers. London: Intertext Books, 1970.

4. Bankston, C. A. and McEligot, D. M. "Turbulent and Laminar Heat Transfer to Gases with Variable Properties in the Entry Region of Circular Ducts." Int. J. Heat Mass Transfer 13(1970):319-344.

5. Nelson, R. M. and Pletcher, R. H. "An Explicit Scheme for the Calculation of Confined Turbulent Flows with Heat Transfer." Proc. 1974 Heat Transfer and Fluid Mechanics Institute, pp. 154-170. Stanford: Stanford University Press, 1974.

6. Lamb, H. Hydrodynamics, 6th ed. New York: Dover Publications, 1932.

7. Jakob, M. and Rees, K. A. "Heat Transfer to a Fluid in Laminar Flow Through an Annular Space." Trans. AIChE 37(1941): 619-648.

8. Reynolds, W. C., Lundberg, R. E. and McCuen, P. A. "Heat Transfer in Annular Passages. General Formulation of the Problem for Arbitrarily Prescribed Wall Temperatures or Heat Fluxes." Int. J. Heat Mass Transfer 6(1963):483-493.

9. Lundberg, R. E., McCuen, P. A. and Reynolds, W. C. "Heat Transfer in Annular Passages. Hydrodynamically Developed Laminar Flow with Arbitrarily Prescribed Wall Temperatures or Heat Fluxes." Int. J. Heat and Mass Transfer 6 (1963): 495-529.

10. Siegel, R., Sparrow, E. M. and Hallman, T. M. "Steady Laminar Heat Transfer in a Circular Tube with Prescribed Wall Heat Flux." Applied Scientific Research 7A (1958):386-392.

11. Lévêque, M. A. "Les Lois de la Transmission de Chaleur par convection." Annals Mines 13(1928):201-299.

12. Heaton, H. S., Reynolds, W. C. and Kays, W. M. "Heat Transfer in Annular Passages. Simultaneous Development of Velocity and Temperature Fields in Laminar Flow." Int. J. Heat Mass Transfer 7 (1963):763-781.

13. Coney, J. E. R. and El-Shaarawi, M. A. I. "Finite-Difference Analysis for Laminar Flow Heat Transfer in Concentric Annuli with Simultaneously Developing Hydrodynamic and Thermal Boundary Layers." Int. J. Numerical Methods in Engineering 9 (1975):17-38.

14. Coney, J. E. R. and El-Shaarawi, M. A. I. "Developing Laminar Radial Velocity Profiles and Pressure Drop in the Entrance Region of Concentric Annuli." Nuclear Science and Engineering 57 (1975):169-174.

15. Shumway, R. W. and McEligot, D. M. "Heated Laminar Gas Flow in Annuli with Temperature Dependent Transport Properties." Nuclear Science and Engineering 46 (1971):394-407.

16. Shumway, R. W. "Variable Properties Laminar Gas Flow Heat Transfer and Pressure Drop in Annuli." EMMT Lab TR 3, The University of Arizona, Tucson, Arizona.

17. Sherwin, K. and Wallis, J. D. "A Study of Laminar Convection for Flow Down Vertical Annuli." Instn. Mechanical Engineers Thermodynamics and Fluid Mechanics Group Convention. Proc. Instn. Mechanical Engineers 182 (Pt. 3H) (1967-68):330-335.

18. Sherwin, K. and Wallis, J. D. "A Theoretical Study of Combined Natural and Forced Laminar Convection for Developing Flow Down Vertical Annuli." Heat Transfer 1970, Vol. 4, Paper NC 3.9. Amsterdam: Elsevier Publishing Company, 1970.

19. Sherwin, K. and Wallis, J. D. "Combined Natural and Forced Laminar Convection for Upflow Through Heated Vertical Annuli." Heat and Mass Transfer by Combined Forced and Natural Convection, pp. 1-5. London: Instn. of Mechanical Engineers, 1972.

20. Gebhart, B. Heat Transfer. New York: McGraw-Hill Book Company, 1971.

21. Tanaka, M. and Mitsuishi, N. "Numerical Solutions for Laminar Heat Transfer in Concentric Annuli." Heat Transfer, Japanese Research 3(1974):69-79.

22. Crank, J. and Nicolson, P. "A Practical Method for Numerical Evaluation of Solutions of Partial Differential Equations of the Heat Conduction Type." Proc. Cambridge Philosophical Society 43 (1947):50-67.

23. Shah, R. K. and London, A. L. "Laminar Flow Forced Convection Heat Transfer and Flow Friction in Straight and Curved Ducts - A Summary of Analytical Solutions." Department of Mechanical Engineering, Stanford University, Technical Report No. 75, 1971.

24. Okuno, M. and Sugita, J. "Heat Transfer in Thermal Entrance Section for Fully Developed Upward Flow in a Vertical Annulus." Heat Transfer, Japanese Research 3 (1974): 81-86.

25. Maitra, D. and Subba Raju, K. "Combined Free and Forced Convection Laminar Heat Transfer in a Vertical Annulus." J. Heat Transfer 97 (1975):135-137.

26. Kays, W. M. and Leung, E. Y. "Heat Transfer in Annular Passages - Hydrodynamically Developed Turbulent Flow with Arbitrarily Prescribed Heat Flux." Int. J. Heat Mass Transfer 6 (1963): 537-557.

27. Reichardt, H. "Vollständige Darstellung der turbulenten Geschwindigkeitsverteilung in glatten Leitungen." Zeitschrift für angewandte Mathematik und Mechanik 31 (1951):208-219.

28. Deissler, R. G. "Analysis of Turbulent Heat Transfer, Mass Transfer, and Fluid Friction in Smooth Tubes at High Prandtl and Schmidt Numbers." NACA Report 1210, 1955.

29. Jenkins, R. "Variation of the Eddy Conductivity with Prandtl Modulus and its Use in Prediction of Turbulent Heat Transfer Coefficients." Proc. 1951 Heat Transfer and Fluid Mechanics Institute, pp. 147-158. Stanford: Stanford University Press, 1951.

30. Quarmby, A. and Anand, R. K. "Turbulent Heat Transfer in the Thermal Entrance Region of Concentric Annuli with Uniform Wall Heat Flux." Int. J. Heat Mass Transfer 13 (1970): 395-411.

31. Ying, W. M. "A Theoretical Method of Predicting Heat Transfer and Friction Factor in Annuli with Roughened Core Tubes." M.S. Thesis, Imperial College, London, 1967.

32. Jonsson, V. K. and Sparrow, E. M. "Turbulent Diffusivity for Momentum in Concentric Annuli." J. Basic Engineering 88 (1966):550-552.

33. Johnson, L. W. and Riess, R. D. Numerical Analysis. Reading, Mass.: Addison-Wesley Publishing Co., 1977.

34. Durst, F. "On Turbulent Flow Through Annular Passages with Smooth and Rough Cores." M.S. Thesis, Imperial College, London, 1968.

35. Lawn, C. J. and Elliot, C. J. "Fully Developed Turbulent Flow Through Concentric Annuli." C.E.G.B. Report RD/B/N1878, 1971.

36. Lawn, C. J. "The Use of an Eddy Viscosity Model to Predict the Heat Transfer and Pressure Drop Performance of Roughened Surfaces." Int. J. Heat Mass Transfer 17 (1974):421-428.

37. Levy, S. "Turbulent Flow in an Annulus." J. Heat Transfer 89 (1967):25-31.

38. Roberts, A. "A Comment on the Turbulent Flow Velocity Profile in a Concentric Annulus." Int. J. Heat Mass Transfer 10 (1967):709-712.

39. Wilson, N. W. and Medwell, J. O. "An Analysis of the Developing Turbulent Hydrodynamic and Thermal Boundary Layers in an Internally Heated Annulus." Paper No. 70-HT-9, ASME, 1970.

40. Lee, Y. and Park, S. D. "Developing Turbulent Flow and Heat Transfer in Concentric Annuli." Trans. CSME 1 (1972): 13-24.

41. Barrow, H., Lee, Y. and Roberts, A. "The Similarity Hypothesis Applied to Turbulent Flow in an Annulas." Int. J. Heat Mass Transfer 8 (1965):1499-1505.

42. Quarmby, A. "An Analysis of Turbulent Flow in Concentric Annuli." Applied Scientific Research 19 (1968): 250-273.

43. Sharma, B. I., Launder, B. E. and Scott, C. J. "Computation of Annular, Turbulent Flow with Rotating Core Tube." J. Fluids Engineering 98 (1976):753-758.

44. Goldstein, S. "The Similarity Theory of Turbulence, and Flow Between Parallel Planes and Through Pipes." Proc. Royal Society of London A159 (1937):473-496.

45. von Kármán, T. "Mechanical Similitude and Turbulence." NACA Tech. Memo No. 611, 1931.

46. van Driest, E. R. "On Turbulent Flow Near a Wall." J. Aeronautical Sciences 23 (1956):1007-1011, 1036.

47. Hanjalic, K. "Prediction of Turbulent Flow in Annular Ducts with Differential Transport Model of Turbulence." Wärme- und Stoffübertragung 7 (1974):71-78.

48. Heikal, M. R. F., Walklate, P. J. and Hatton, A. P. "The Effect of Free Stream Turbulence Level on the Flow and Heat Transfer in the Entrance Region of an Annulus." Int. J. Heat and Mass Transfer 20 (1977):763-771.

49. Briley, R. W. "Numerical Method for Predicting Three-Dimensional Steady Viscous Flow in Ducts." J. Computational Physics 14 (1974):8-28.

50. Clump, C. W. and Kwasnoski, D. "Turbulent Flow in Concentric Annuli." AIChE Journal 14 (1968):164-168.

51. Lee, Y. "Turbulent Heat Transfer from the Core Tube in Thermal Entrance Regions of Concentric Annuli." Int. J. Heat Mass Transfer 11 (1968):509-522.

52. Wilson, N. W. and Medwell, J. O. "An Analysis of Heat Transfer for Fully Developed Turbulent Flow in Concentric Annuli." J. Heat Transfer 90 (1968):43-50.

53. Lee, Y. and Park, S. D. "Developing Turbulent Flow in Concentric Annuli: An Analytical and Experimental Study." Wärme-und Stoffübertragung 4 (1971):156-166.

54. Chung, B. T. F., Thomas, L. C. and Pang, Y. "A Surface Rejuvenation Model for Turbulent Heat Transfer in Annular Flow with High Prandtl Numbers." J. Heat Transfer 100 (1978):92-97.

55. Rothfus, R. R. "Velocity Distribution and Fluid Friction in Concentric Annuli." Ph.D. Thesis, Carnegie Institute of Technology, 1948.

56. Lonsdale, T. "The Flow of Water in the Annular Space Between Two Coaxial Cylindrical Pipes." Philosophical Magazine 46 (1923):163-169.

57. Knudsen, J. G. and Katz, D. L. Fluid Dynamics and Heat Transfer. New York: McGraw-Hill Book Company, 1958.

58. Brighton, J. A. and Jones, J. B. "Fully Developed Turbulent Flow in Annuli." J. Basic Engineering 86 (1964):835-844.

59. Quarmby, A. "An Experimental Study of Turbulent Flow Through Concentric Annuli." Int. J. Heat Mass Transfer 9 (1967): 205-221.

60. Lawn, C. J. "Application of the Turbulence Energy Equation to Fully Developed Flow in Simple Ducts - Figures and Figure Captions." C.E.G.B. Report RD/B/1575(C), 1970.

61. Rehme, K. "Turbulence Measurements in Smooth Concentric Annuli with Small Radius Ratios." J. Fluid Mechanics 72 (1975): 189-206.

62. Rehme, K. "Turbulent Flow in Smooth Concentric Annuli with Small Radius Ratios." J. Fluid Mechanics 64 (1974):263-287.

63. Olson, R. M. and Sparrow, E. M. "Measurements of Turbulent Flow Development in Tubes and Annuli with Square or Rounded Entrances." AIChE Journal 9 (1963):766-770.

64. Okiishi, T. H. "Fluid Velocity Profile Development for Turbulent Flow in Smooth Annuli." Ph.D. Thesis, Iowa State University, Ames, Iowa, 1965.

65. Lee, Y. and Barrow, H. "Turbulent Flow and Heat Transfer in Concentric and Eccentric Annuli." Paper 12, Thermodynamics and Fluid Mechanics Convention, Cambridge, 1964.

66. Quarmby, A. "Some Measurements of Turbulent Heat Transfer in the Thermal Entrance Region of Concentric Annuli." Int. J. Heat Mass Transfer 10 (1967):267-276.

67. Ball, H. D. and Azer, N. Z. "Experimental Investigation of Eddy Diffusivities of Air in Turbulent Annular Flow," Proc. 1972 Heat Transfer and Fluid Mechanics Institute, pp. 19-38. Stanford: Stanford University Press, 1972.

68. Kuzay, T. M. and Scott, C. J. "Turbulent Heat Transfer Studies in Annulus with Inner Cylinder Rotation." ASME Paper No. 75-WA/HT-55, 1975.

69. Kuzay, T. M. and Scott, C. J. "Turbulent Prandtl Numbers for Fully Developed Rotating Annular Axial Flow of Air." ASME Paper No. 76-HT-36, 1976.

70. Kuzay, T. M. "Turbulent Heat and Momentum Transfer Studies in an Annulus with Rotating Inner Cylinder." Ph.D. Thesis, University of Minnesota, Minneapolis, Minnesota, 1973.

71. Furber, B. N., Appleby, G. G. and Facer, R. I. "Forced Convection Heat Transfer in an Annulus." Heat Transfer 1974, Vol. 2, pp. 155-159. Japan: JSME, 1974.

72. Dalle Donne, M. and Meerwald, E. "Heat Transfer and Friction Coefficients for Turbulent Flow of Air in Smooth Annuli at High Temperatures." Int. J. Heat Mass Transfer 16 (1973): 787-809.

73. Dwyer, O. E., Hlavac, P. J. and Nimmo, B. G. "Eddy Diffusivity of Heat Transfer in the Radial Direction for Turbulent Flow of Mercury in Annuli." Int. J. Heat Mass Transfer 20 (1977): 141-151.

74. Hlavac, P. J., Nimmo, B. G. and Dwyer, O. E. "Experimental Study of Effect of Wetting on Turbulent Flow of Mercury in Annuli." Int. J. Heat Mass Transfer 15 (1972):2611-2631.

75. Dwyer, O. E., Hlavac, P. T. and Nimmo, B. G. "Effect of Wetting on Friction Factors for Turbulent Flow of Mercury in Annuli." J. Fluids Engineering 98 (1976):113-116.

76. Ornatskiy, A. P., Glushchenko, L. F. and Gandzyuk, O. F. "An Experimental Study of Heat Transfer in Externally Heated Annuli at Supercritical Pressures." Heat Transfer - Soviet Research 4 (1972):25-29.

77. Petukhov, B. S. and Roizen, L. I. "An Experimental Investigation of Heat Transfer in a Turbulent Flow of Gas in Tubes of Annular Section." High Temperature 1 (1963):373-380.

78. Michiyoshi, I., Mitani, S. and Takahashi, O. "Turbulent Heat Transfer to High Temperature Gas in Concentric Annulus." Int. Chemical Engineering 10 (1970):146-149.

79. Nyamira, M. A. and Vilyamas, Yu. V. "Heat Transfer from Cylindrical and Helical Rods in an Annular Channel to a Turbulent Air Stream with Variable Physical Properties." Int. Chemical Engineering 16 (1976):412-417.

80. Roberts, A. and Barrow, H. "Turbulent Heat Transfer to Air in the Vicinity of the Entry of an Internally Heated Annulus." Proc. Instn. Mechanical Engineers 182 (Pt. 3H) (1967-68):268-276.

81. Rohsenow, W. M. and Hartnett, J. P. Handbook of Heat Transfer. New York: McGraw-Hill Book Company, 1973.

82. Schlichting, H. Boundary Layer Theory, 6th ed. New York: McGraw-Hill Book Company, 1968.

83. Cebeci, T. and Smith, A. M. O. Analysis of Turbulent Boundary Layers. New York: Academic Press, 1974.

84. Chao, B. T. "Selected Topics on Convective Heat Transfer." In Lectures on Advanced Heat Transfer, pp. 1-24. Edited by B. T. Chao. University of Illinois Press, 1969.

85. Hennecke, D. K. "Heat Transfer by Hagen-Poiseuille Flow in the Thermal Development Region with Axial Conduction." Wärme-und Stoffübertragung 1 (1968):177-184.

86. Schneider, P. J. "Effect of Axial Fluid Conduction on Heat Transfer in the Entrance Regions of Parallel Plates and Tubes." Proc. 1956 Heat Transfer and Fluid Mechanics Institute, pp. 41-57. Stanford: Stanford University Press, 1956.

87. Tyagi, V. P. "Laminar Forced Convection of a Dissipative Fluid in a Channel." J. Heat Transfer 88 (1966):161-169.

88. Madejski, J. "Temperature Distribution in Channel Flow with Friction." Int. J. Heat Mass Transfer 6 (1963): 49-51.

89. Emmons, H. W. "Critique of Numerical Modeling of Fluid Mechanics Phenomena." Annual Review of Fluid Mechanics 2 (1970): 15-36.

90. Reynolds, O. "On the Dynamical Theory of Incompressible Viscous Fluids and the Determination of the Criterion." Philosophical Transactions of the Royal Society of London 186 (1895): 123-164.

91. Stein, R. P. "Liquid Metal Heat Transfer." Advances in Heat Transfer 3 (1966):101-174.

92. Blanco, J. A. and Gill, W. N. "Effect of Dissipation and Compression Work on the Eddy Conductivity Calculated from Experimental Temperature Data for Gases." AIChE Journal 17 (1971):940-946.

93. Johnston, J. P. "Internal Flows." Turbulence (Topics in Applied Physics, Vol. 12), pp. 109-169. Edited by P. Bradshaw, Heidelberg: Springer, 1976.

94. Kline, S. J. and Runstadler, P. W. "Some Preliminary Results of Visual Studies of the Flow Model of the Wall Layers of the Turbulent Boundary Layer." J. Applied Mechanics 26 (1959):166-170.

95. Corino, E. R. and Brodkey, R. S. "A Visual Investigation of the Wall Region in Turbulent Flow." J. Fluid Mechanics 37 (1969):1-30.

96. Blackwelder, R. F. and Kovasznay, L. S. G. "Time Scales and Correlations in a Turbulent Boundary Layer." Physics of Fluids 15 (1972):1545-1554.

97. Kovasznay, L. S. G., Kibens, V. and Blackwelder, R. F. "Large-Scale Motion in the Intermittent Region of a Turbulent Boundary Layer." J. Fluid Mechanics 41 (1970):283-325.

98. Antonia, R. A. and Atkinson, J. D. "Use of a Pseudo-Turbulent Signal to Calibrate an Intermittency Measuring Circuit." J. Fluid Mechanics 64 (1974):679-699.

99. Hanjalic, K. and Launder, B. E. "A Reynolds Stress Model of Turbulence and Its Application to Asymmetric Shear Flows." J. Fluid Mechanics 52 (1972):609-638.

100. Hinze, J. O. Turbulence. New York: McGraw-Hill Book Company, 1959.

101. Prandtl, L. "Bericht über Untersuchungen zue ausgebildeten Turbulenz." Zeitschrift für angewandte Mathematik und Mechanik 5 (1925):136-139.

102. Bradshaw, P. (Appendix by Patel, V. C.) "The Strategy of Calculation Methods for Complex Turbulent Flows." Imperial College Aero Report 73-05, August 1973.

103. Klebanoff, P. S. "Characteristics of Turbulence in a Boundary Layer with Zero Pressure Gradient." NACA Tech. Note 3178, 1954.

104. Bradshaw, P. "The Understanding and Prediction of Turbulent Flow." Aeronautical Journal 76 (1972):403-418.

105. Townsend, A. A. "Equilibrium Layers and Wall Turbulence." J. Fluid Mechanics 11 (1961):97-120.

106. Pletcher, R. H. "Prediction of Transpired Turbulent Boundary Layers." J. Heat Transfer 96 (1974):89-94.

107. Bradshaw, P. "Turbulence Research - Progress and Problems." Proc. 1976 Heat Transfer and Fluid Mechanics Institute, pp. 128-139. Stanford: Stanford University Press, 1976.

108. Dean, R. B. and Bradshaw, P. "Measurements of Interacting Turbulent Shear Layers in a Duct." J. Fluid Mechanics 78 (1976):641-676.

109. Pletcher, R. H. "Prediction of Incompressible Turbulent Separating Flow." To be published in ASME J. Fluids Engineering.

110. Pletcher, R. H. "Prediction of Turbulent Boundary Layers at Low Reynolds Numbers." AIAA Journal 14 (1976):696-698.

111. Bradshaw, P., Dean, R. B. and McEligot, D. M. "Calculation of Interacting Turbulent Shear Layers: Duct Flow." J. Fluids Engineering 95 (1973):214-219.

112. Pai, B. R. and Whitelaw, J. H. "The Prediction of Wall Temperature in the Presence of Film Cooling." Imperial College, Heat Transfer Section Report EHT/TN/A/22, 1970.

113. Dvorak, F. A. "Calculation of Turbulent Boundary Layers and Wall Jets Over Curved Surfaces." AIAA Journal 11 (1973): 517-524.

114. Launder, B. E. and Spalding, D. B. Mathematical Models of Turbulence. New York: Academic Press, 1972.

115. Spalding, D. B. "Turbulence Models." (3rd Issue). Imperial College, Heat Transfer Section Report HTS/76/17, 1977.

116. Reynolds, A. J. "The Prediction of Turbulent Prandtl and Schmidt Numbers." Int. J. Heat Mass Transfer 18 (1975): 1055-1069, 1975.

117. Rotta, J. C. "Temperaturverteilungen in Der Turbulenten Grenzschicht an Der Ebenen Platte." Int. J. Heat Mass Transfer 7 (1964):215-228.

118. Ludwieg, H. "Bestimmung des Verhaltnisses der Austauschköffizienten für Warme and Impuls bei turbulenten Grenzschlichten." Zeitschrift für Flugwissenschaften 4 (1956):73-81.

119. Johnson, S. D. "Velocity and Temperature Fluctuation Measurements in a Turbulent Boundary Layer Downstream of a Stepwise Discontinuity in Wall Temperature." J. Applied Mechanics 26 (1959):325-336.

120. Blom, J. "Experimental Determination of the Turbulent Prandtl Number in a Developing Temperature Boundary Layer", Heat Transfer 1970, Vol. 2, Paper FC 2.2. Amsterdam: Elsevier Publishing Company, 1970.

121. Kestin, J. and Richardson, P. D. "Heat Transfer Across Turbulent Incompressible Boundary Layers." Int. J. Heat Mass Transfer 6 (1963):147-189.

122. Hwang, S. S. and Pletcher, R. H. "Prediction of Buoyant Turbulent Jets and Plumes in a Cross Flow." Heat Transfer 1978, Vol. 1, pp. 109-114. Washington, D.C.: Hemisphere Publishing Corporation, 1978.

123. Kays, W. M. and Moffat, R. J. "The Behavior of Transpired Turbulent Boundary Layers." In Studies in Convection, Vol. 1: Theory, Measurement and Application. London: Academic Press, 1975.

124. Cebeci, T. "A Model for Eddy Conductivity and Turbulent Prandtl Number." J. Heat Transfer 95 (1973):227-234.

125. Rao, G. N. V. "The Law of the Wall in a Thick Axisymmetric Turbulent Boundary Layer." J. Applied Mechanics 34 (1967):237-238.

126. Rao, G. N. V. and Keshavan, N. R. "Axisymmetric Turbulent Boundary Layers in Zero Pressure-Gradient Flows." J. Applied Mechanics 39 (1972):25-32.

127. White, F. M. "An Analysis of Axisymmetric Turbulent Flow Past a Long Cylinder." J. Basic Engineering 94 (1972): 200-206.

128. Afzal, N. and Narasimha, R. "Axisymmetric Turbulent Boundary Layer Along a Circular Cylinder at Constant Pressure." J. Fluid Mechanics 74 (1976):113-128.

129. Huffman, G. D. and Bradshaw, P. "A Note on von Kármán Constant in Low Reynolds Number Turbulent Flows." J. Fluid Mechanics 53 (1972):45-60.

130. Cebeci, T. "Eddy Viscosity Distribution in Thick Axisymmetric Turbulent Boundary Layers." J. Fluids Engineering 95 (1973): 319-326.

131. Cebeci, T. and Chang, K. C. "A General Method for Calculating Momentum and Heat Transfer in Laminar and Turbulent Duct Flows." Numerical Heat Transfer 1 (1978):39-68.

132. Crawford, M. E. and Kays, W. M. "STAN5 - A Program for Numerical Computation of Two-Dimensional Internal/External Boundary Layer Flows." Report No. HMT-23. Stanford University, Stanford, Calif., 1975.

133. Emmons, H. W. "The Laminar-Turbulent Transition in a Boundary Layer - Part I." J. Aerospace Sciences 18 (1951):235-246.

134. Schubauer, G. B. and Klebanoff, P. S. "Contributions on the Mechanics of Boundary-Layer Transition." NACA Report 1289, 1956.

135. Dhawan, S. and Narasimha, R. "Some Properties of Boundary Layer Flows During the Transition from Laminar to Turbulent Motion." J. Fluid Mechanics 3 (1958):418-436.

136. Dufort, E. C. and Frankel, S. P. "Stability Conditions in the Numerical Treatment of Parabolic Differential Equations." Mathematical Tables Aid Computation 7 (1953):135-152.

137. Pletcher, R. H. "On a Finite-Difference Solution for the Constant-Property Turbulent Boundary Layer." AIAA Journal 7 (1969):305-311.

138. Nelson, R. M. "An Explicit Finite Difference Analysis for Developing Turbulent Internal Flows with Heat Transfer and Property Variations." M.S. Thesis, Iowa State University, Ames, Iowa, 1972.

139. Madni, I. K. "A Finite-Difference Analysis of Turbulent, Axisymmetric, Buoyant Turbulent Jets and Plumes." Ph.D. Thesis, Iowa State University, Ames, Iowa, 1975.

140. Roache, P. J. Computational Fluid Dynamics. Albuquerque: Hermosa Publishers, 1976.

141. Richtmyer, R. D. and Morton, K. W. Difference Methods for Initial-Value Problems. New York: Wiley (Interscience), 1967.

142. Joshi, S. D. and Bergles, A. E. "Heat Transfer in Cooling Channels of Power Transformers." Affiliate Research Program in Electrical Power, Annual Report. ISU-ERI-Ames-78287 (1978):7.1-7.15.

143. Scheele, G. F. and Hanratty, T. J. "Effect of Natural Convection on Stability of Flow in a Vertical Pipe." J. Fluid Mechanics 14 (1962):244-256.

144. Easby, J. P. "The Effect of Buoyancy on Flow and Heat Transfer for a Gas Passing Down a Vertical Pipe at Low Turbulent Reynolds Numbers." Int. J. Heat Mass Transfer 21 (1978):791-801.

145. Axcell, B. P. and Hall, W. B. "Mixed Convection to Air in a Vertical Pipe." Heat Transfer 1978, Vol. 1, pp. 37-42. Washington, D.C.: Hemisphere Publishing Corporation, 1978.

146. Jackson, J. D. and Hall, W. B. "Influences of Buoyancy on Heat Transfer to Fluids Flowing in Vertical Tubes Under Turbulent Conditions." Turbulent Forced Convection in Channels and Rod Bundles, Proc. NATO Advanced Study Institute. Washington, D.C.: Hemisphere Publishing Corporation, 1978.

147. Dean, R. B. "Interaction of Turbulent Shear Layers in Duct Flow." Ph.D. Thesis, London University, 1972.

148. Byrne, J., Hatton, A. P. and Mariott, P. G. "Turbulent Flow and Heat Transfer in the Entrance Region of a Parallel Wall Passage." Proc. Instn. Mechanical Engineers 184 (1969-70):697-712.

149. Barbin, A. R. and Jones, J. B. "Turbulent Flow in the Inlet Region of a Smooth Pipe." J. Basic Engineering 85 (1963):29-34.

150. Stephenson, P. L. "A Theoretical Study of Heat Transfer in Two-Dimensional Turbulent Flow in a Circular Pipe and Between Parallel and Diverging Plates." Int. J. Heat Mass Transfer 19 (1976):413-423.

151. Comte-Bellot, G. "Turbulent Flow Between Parallel Walls." Ph.D. Thesis, University of Grenoble, France, 1963. (Also available as ARC 31 609).

152. Emery, A. F. and Gessner, F. B. "The Numerical Prediction of the Turbulent Flow and Heat Transfer in the Entrance Region of a Parallel Plate Duct." J. Heat Transfer 98 (1976): 594-600.

153. Cebeci, T., Hirsh, R. S. and Chang, K. C. Discussion on "The Numerical Prediction of the Turbulent Flow and Heat Transfer in the Entrance Region of a Parallel Plate Duct." J. Heat Transfer 99 (1977):693-694.

154. Quarmby, A. "On the Use of the Preston Tube in Concentric Annuli." J. Royal Aeronautical Society 71 (1967):47-49.

155. Quarmby, A. "On the Use of the Preston Tube in Concentric Annuli." Reply to a Comment by H. G. Lyall. J. Royal Aeronautical Society 71 (1967):865-866.

156. Patel, V. C. "On the Use of the Preston Tube in Concentric Annuli." J. Royal Aeronautical Society 73 (1969): 602-603.

157. Patel, V. C. "Calibration of the Preston Tube and Limitations on its use in Pressure Gradients." J. Fluid Mechanics 23 (1965):185-208.

158. Dalle Donne, M. and Bowditch, F. H. "Local Heat Transfer and Average Friction Coefficients for Subsonic Laminar, Transitional and Turbulent Flow of Air in a Tube at High Temperature." Nuclear Engineering 8 (1963):20-29.

159. Dalle Donne, M. "High Temperature Gas Heat Transfer in Tubes." Trans. ANS 7 (1964):506-507.

160. Tables of Thermal Properties of Gases, NBS Circular 564. Washington, D.C.: U.S. Government Printing Office, 1955.

161. Hong, S. W. "Laminar Flow Heat Transfer in Ordinary and Augmented Tubes." Ph.D. Thesis, Iowa State University, Ames, Iowa, 1974.

VII. ACKNOWLEDGMENTS

This work was supported by the Engineering Research Institute, Iowa State University, through funds provided by the National Science Foundation under Grant ENG 74-22193. Part of the work was done while the author was visiting in the Department of Aeronautics, Imperial College, London, England.

Several people have helped me in completing this study. My special thanks go to my advisor, Professor Richard H. Pletcher, for his invaluable suggestions and continuous encouragement in the course of this study. Professor Arthur E. Bergles also made several helpful suggestions for which I am grateful. Thanks are also due to Professors William J. Cook, Donald F. Young and Harry J. Weiss for their encouragement and guidance. I am grateful to Mr. Peter Bradshaw for making it possible for me to visit Imperial College and use computational facilities there.

Last, but certainly not least, I wish to express my gratitude to my parents, Mr. and Mrs. Malik Saif-ur-Rehman, who always showed faith in my dreams and did their best to help those dreams come true. This dissertation is dedicated to them.

VIII. VITA

The author was born on November 14, 1951, in Rabwah, Pakistan. He completed his high school education at Talim-ul-Islam College, Rabwah, in 1968 and was awarded a "National Talent Scholar Gold Medal." He was also awarded a scholarship from Saigol Foundation of Pakistan to study at the West Pakistan University of Engineering and Technology, Lahore, where he received, with distinction, the degree of Bachelor of Science in Mechanical Engineering in 1973. Later in 1975, he received his Master's Degree in Mechanical Engineering from the University of Toronto, Canada, where he also served as a Teaching Assistant. He matriculated at Iowa State University in September, 1975, and has been working as a Research Assistant since then. He was an Academic Visitor in the Department of Aeronautics, Imperial College, London, from September 1976 to February 1977.

IX. APPENDIX A: FULLY DEVELOPED TURBULENT VELOCITY PROFILE

For fully developed flow, nondimensional momentum equation (3.2) can be reduced to:

$$\frac{1}{R}\frac{d}{dY}[RN_u\frac{dU}{dY}] = \frac{dP}{dX}$$

After substituting for N_u, this becomes:

$$\frac{1}{R}\frac{d}{dY}[R(\hat{\mu}+\hat{\rho}\hat{\ell}^2|\frac{dU}{dY}|)\frac{dU}{dY}] = \frac{dP}{dX}$$

or

$$\frac{1}{R}(\hat{\mu}+\hat{\rho}\hat{\ell}^2|\frac{dU}{dY}|)\frac{dU}{dY} + (\hat{\mu}+\hat{\rho}\hat{\ell}^2|\frac{dU}{dY}|)\frac{d^2U}{dY^2}$$

$$+ \hat{\rho}\hat{\ell}^2\frac{dU}{dY}\frac{d}{dY}(|\frac{dU}{dY}|) + 2\hat{\rho}\hat{\ell}\frac{d\hat{\ell}}{dY}\frac{dU}{dY}|\frac{dU}{dY}| = \frac{dP}{dX} \qquad (A.1)$$

If

$$\psi = \frac{dU}{dY} \qquad (A.2)$$

Then, Eq. (A.1) can be written as

$$(\hat{\mu}+\hat{\rho}\hat{\ell}^2|\psi|)\frac{d\psi}{dY} + \hat{\rho}\hat{\ell}^2\psi\frac{d}{dY}(|\psi|)$$

$$= \frac{dP}{dX} - \frac{\hat{\mu}\psi}{R} - (\frac{\hat{\rho}\hat{\ell}^2}{R} + 2\hat{\rho}\hat{\ell}\frac{d\hat{\ell}}{dY})\psi|\psi| \qquad (A.3)$$

Now

$$\psi\frac{d}{dY}(|\psi|) = |\psi|\frac{d\psi}{dY}$$

Therefore, Eq. (A.3) becomes

$$(\hat{\mu}+2\hat{\rho}\hat{\ell}^2|\psi|)\frac{d\psi}{dY} = \frac{dP}{dX} - \frac{\hat{\mu}\psi}{R} - (\frac{\hat{\rho}\hat{\ell}^2}{R} + 2\hat{\rho}\hat{\ell}\,\frac{d\hat{\ell}}{dY})\psi|\psi|$$

or

$$\frac{d\psi}{dY} = \frac{\frac{dP}{dX} - \frac{\hat{\mu}\psi}{R} - (\frac{\hat{\rho}\hat{\ell}^2}{R} + 2\hat{\rho}\hat{\ell}\,\frac{d\hat{\ell}}{dY})\psi|\psi|}{(\hat{\mu}+2\hat{\rho}\hat{\ell}^2|\psi|)} \tag{A.4}$$

Equations (A.2) and (A.4) form a set of two first order ordinary differential equations which can be solved to obtain a fully developed turbulent velocity profile. The equations contain the pressure gradient term, dP/dX, which in principle needs to be guessed or otherwise specified in order to obtain a velocity profile consistent with the specified Reynolds number (or mass flow rate). Rather than proceeding with this on a trial and error basis, it was found advantageous to relate the pressure gradient to the friction factor according to Eq. (1.4), which in nondimensional terms can be written as

$$f_p = -(R_2-R_1)\frac{dP}{dX} \tag{A.5}$$

where the friction factor was determined using the parallel wall duct correlation, Eq. (1.2),

$$f_p = 0.087\ Re^{-0.25} \tag{A.6}$$

So that,

$$\frac{dP}{dX} = -0.087/((R_2-R_1)Re^{0.25}) \tag{A.7}$$

The set of Equations (A.2) and (A.4) can now be solved using an appropriate integration technique. The known boundary conditions for the problem are:

$$U(0) = 0 \tag{A.8}$$

$$U(R_h) = 0 \tag{A.9}$$

In order that the integration can be stepped off using the Runge-Kutta method (which is employed in the present study), a value of $\psi(0)$ is needed which is unknown. This requires that an iterative shooting method be used. If the shear stress at the inner wall, $\psi(0)$, is denoted by

$$\psi(0) = s \tag{A.10}$$

and the velocity obtained at the outer wall as a result of solving the initial value problem, specified by Eqs. (A.2), (A.4) and (A.8), by

$$U(R_h) = \chi(s) \tag{A.11}$$

then, the problem is to find s such that,

$$\chi(s) = 0 \tag{A.12a}$$

The secant method (see, e.g., [33]) was used to obtain the converged value of s. For initial estimates of s^0 and s^1, a successive relation can be written as

$$s^{\sigma+2} = s^{\sigma+1} - \frac{s^{\sigma+1}-s^{\sigma}}{\chi(s^{\sigma+1})-\chi(s^{\sigma})}\chi(s^{\sigma+1}), \sigma = 0,1,2... \tag{A.12b}$$

Convergence has been observed to be quite fast if the first two estimates are made such that $\chi(s^0)$ and $\chi(s^1)$ are of opposite sign. The iteration was terminated when $\chi(s^\sigma) < 0.0001$. It generally took 7 to 20 iterations to meet this criteria.

After the converged solution is obtained, the Reynolds number is calculated. If this does not match the desired Re, $\frac{dP}{dX}$ must be corrected and the whole procedure repeated again. The correction procedure has not been necessary to date since the Re computed has always been within 4% of the desired value which has been considered a close enough match for the present studies.

The subroutine used for generating the fully developed turbulent velocity profile was first developed on a University of London computer CDC 6600. When the subroutine was later run on the ISU-IBM 360/158, it was found necessary to use double precision.

X. APPENDIX B: THE SIMPLE EXPLICIT FINITE-DIFFERENCE SCHEME

Since the Dufort-Frankel scheme, employed in the present study requires information at two upstream locations, a simple explicit method is used for the first step to start the solution.

Finite-difference equations:

The simple explicit form of the model Equation (3.8) is

$$a_j^m \frac{\phi_j^{m+1}-\phi_j^m}{\Delta X_+} + b_j^m \frac{\phi_j^m-\phi_{j-1}^{m*}}{\Delta Y_-} = \frac{2}{R_j(\Delta Y_+ + \Delta Y_-)}\left[R_{j+1/2}\, N_{\phi_{j+1/2}}^m \frac{(\phi_{j+1}^m-\phi_j^m)}{\Delta Y_+}\right.$$

$$\left. - R_{j-1/2}\, N_{\phi_{j-1/2}}^m \left(\frac{\phi_j^m-\phi_{j-1}^m}{\Delta Y_-}\right)\right] + \bar{S}_j^m \qquad \text{(B.1)}$$

where the source term for the momentum equation is written as

$$S_j^m = -\frac{P^{m+1}-P^m}{\Delta X_+} + F_{x_j}^m$$

P^{m+1} is determined by using the overall mass flow constraint as in the case of Dufort-Frankel equations.

In case of ϕ=U with b_j^m as negative, the starred term is written as

$$b_j^m\left(\frac{\phi_{j+1}^m-\phi_j^m}{\Delta Y_+}\right)$$

The simple explicit form of the continuity equation is given as

$$R_{j+1/2}\frac{\hat{\rho}^{m+1}_{j+1}U^{m+1}_{j+1} - \hat{\rho}^{m}_{j+1}U^{m}_{j+1} + \hat{\rho}^{m+1}_{j}U^{m+1}_{j} - \hat{\rho}^{m}_{j}U^{m}_{j}}{2\Delta X_{+}}$$

$$+\frac{R_{j+1}\hat{\rho}^{m+1}_{j+1}V^{m+1}_{j+1} - R_{j}\hat{\rho}^{m}_{j}V^{m}_{j}}{\Delta Y_{+}} = 0 \qquad \text{(B.2)}$$

Stability constraint on step size:

The Von Neuman analysis, when applied to Eq. (B.1), reveals the following constraint:

$$\Delta X_{+} \leq \frac{a^{m}_{j}}{\left[\frac{|b^{m}_{j}|}{\Delta Y_{-}} + \frac{R_{j+1/2}N\phi_{j+1/2}}{2R_{j}\Delta Y_{+}(\Delta Y_{+}\Delta Y_{-})} + \frac{R_{j-1/2}N\phi_{j-1/2}}{2R_{j}\Delta Y_{-}(\Delta Y_{+}+\Delta Y_{-})}\right]} \qquad \text{(B.3)}$$

XI. APPENDIX C: CONSISTENCY OF DUFORT-FRANKEL EQUATIONS

In order to show that Eq. (3.9) is a consistent representation of the model Equation (3.8), the following Taylor series expansions about the point (m,j) (see Fig. 3.1) can be written:

$$\phi_j^{m+1} = \phi_j^m + \left(\frac{\partial\phi}{\partial X}\right)_j^m X_+ + \left(\frac{\partial^2\phi}{\partial X^2}\right)_j^m \frac{\Delta X_+^2}{2} + \left(\frac{\partial^3\phi}{\partial X^3}\right)_j^m \frac{\Delta X_+^3}{6} + \left(\frac{\partial^4\phi}{\partial X^4}\right)_j^m \frac{\Delta X_+^4}{24} + \ldots \tag{C.1}$$

$$\phi_j^{m-1} = \phi_j^m - \left(\frac{\partial\phi}{\partial X}\right)_j^m \Delta X_- + \left(\frac{\partial^2\phi}{\partial X^2}\right)_j^m \frac{\Delta X_-^2}{2} - \left(\frac{\partial^3\phi}{\partial X^3}\right)_j^m \frac{\Delta X_-^3}{6} + \left(\frac{\partial^4\phi}{\partial X^4}\right)_j^m \frac{\Delta X_-^4}{24} - \ldots \tag{C.2}$$

$$\phi_{j+1}^m = \phi_j^m + \left(\frac{\partial\phi}{\partial Y}\right)_j^m \Delta Y_+ + \left(\frac{\partial^2\phi}{\partial Y^2}\right)_j^m \frac{\Delta Y_+^2}{2} + \left(\frac{\partial^3\phi}{\partial Y^3}\right)_j^m \frac{\Delta Y_+^3}{6} + \left(\frac{\partial^4\phi}{\partial Y^4}\right)_j^m \frac{\Delta Y_+^4}{24} + \ldots \tag{C.3}$$

$$\phi_{j-1}^m = \phi_j^m - \left(\frac{\partial\phi}{\partial Y}\right)_j^m \Delta Y_- + \left(\frac{\partial^2\phi}{\partial Y^2}\right)_j^m \frac{\Delta Y_-^2}{2} - \left(\frac{\partial^3\phi}{\partial Y^3}\right)_j^m \frac{\Delta Y_-^3}{6} + \left(\frac{\partial^4\phi}{\partial Y^4}\right)_j^m \frac{\Delta Y_-^4}{24} - \ldots \tag{C.4}$$

Using Eqs. (C.1) and (C.2), $\frac{\partial\phi}{\partial X}$ can be written as

$$\left(\frac{\partial\phi}{\partial X}\right)_j^m = \frac{\phi_j^{m+1}-\phi_j^{m-1}}{\Delta X_+ + \Delta X_-} - \left(\frac{\partial^2\phi}{\partial X^2}\right)_j^m \frac{\Delta X_+ - \Delta X_-}{2}$$

$$- \left(\frac{\partial^3\phi}{\partial X^3}\right)_j^m \frac{\Delta X_+^3 + \Delta X_-^3}{6(\Delta X_+ + \Delta X_-)} + \ldots \qquad \text{(C.5)}$$

where the first term on the right hand side is the finite-difference representation of $\frac{\partial\phi}{\partial X}$ used in Eq. (3.9). So the truncation error is

$$\text{T.E.} = -\left(\frac{\partial^2\phi}{\partial X^2}\right)_j^m \frac{\Delta X_+ - \Delta X_-}{2} - \left(\frac{\partial^3\phi}{\partial X^3}\right)_j^m \frac{\Delta X_+^3 + \Delta X_-^3}{6(\Delta X_+ + \Delta X_-)} + \ldots \qquad \text{(C.6)}$$

It can be seen that for equal grid the truncation error is of $0[(\Delta X)^2]$ and for unequal grid it will be of $0(\Delta X_+)$. However, it should be noted that for boundary layer flows $\frac{\partial^2\phi}{\partial X^2} << 1$ which makes the representation of $\frac{\partial\phi}{\partial X}$ better than of $0(\Delta X_+)$ even for unequal grid.

In a similar fashion it can be shown that the representation for $\frac{\partial\phi}{\partial Y}$ is first order accurate for unequal grid while it becomes second order accurate for equal grid.

Using Eqs. (C.1-C.4), $\frac{\partial^2\phi}{\partial Y^2}$ can be written as

$$\left(\frac{\partial^2\phi}{\partial Y^2}\right)_j^m = \frac{2}{\Delta Y_+ + \Delta Y_-}\left[\frac{1}{\Delta Y_+}\left(\phi_{j+1}^m - \frac{\Delta X_-\phi_j^{m+1} + \Delta X_+\phi_j^{m-1}}{\Delta X_+ + \Delta X_-}\right)\right.$$

$$\left. - \frac{1}{\Delta Y_-}\left(\frac{\Delta X_-\phi_j^{m+1} + \Delta X_+\phi_j^{m-1}}{\Delta X_+ + \Delta X_-} - \phi_{j-1}^m\right)\right] - \left(\frac{\partial^3\phi}{\partial Y^3}\right)_j^m \frac{\Delta Y_+ - \Delta Y_-}{3}$$

$$- \left(\frac{\partial^4\phi}{\partial Y^4}\right)_j^m \frac{\Delta Y_+^3 + \Delta Y_-^3}{12(\Delta Y_+ + \Delta Y_-)} + \left(\frac{\partial^2\phi}{\partial X^2}\right)_j^m \frac{\Delta X_+\Delta X_-}{\Delta Y_+\Delta Y_-} + \left(\frac{\partial^4\phi}{\partial X^4}\right)_j^m \frac{(\Delta X_+^3 - \Delta X_-^3)\Delta X_+\Delta X_-}{12\Delta Y_+\Delta Y_-} - \ldots \qquad \text{(C.7)}$$

It can be seen that the truncation error for an unequal grid is of $0(\Delta Y_+)$ and $0[(\frac{\Delta X_+}{\Delta Y_+})^2]$. Thus the finite-difference formulation of $\frac{\partial^2\phi}{\partial Y^2}$ is consistent only if ΔX_+ goes to zero faster than ΔY_+. In order to make practical computations, however, ΔX_+ should be much larger than ΔY_+; in the present calculations, $\frac{\Delta X_+}{\Delta Y_+} >> 1$ was used and numerical results compared well with the experiments and other implicit calculations. The reason why the Dufort-Frankel scheme still provides an exceptionally good approximation to the governing partial differential equations perhaps lies in the fact that the entire term consists of $(\frac{\partial^2\phi}{\partial X^2})_j^m \frac{\Delta X_+\Delta X_-}{\Delta Y_+\Delta Y_-}$ and for boundary layer flows $\frac{\partial^2\phi}{\partial X^2}$ is negligibly small.

Since the truncation error vanishes when $\Delta X_+ \to 0$, $\Delta Y_+ \to 0$, it is concluded that the finite-difference representation, Eq. (3.9), is consistent.

Due to stability considerations, $\hat{k}^{3/2}$ appearing in the dissipation term of the turbulence kinetic energy Equation (3.7) was modeled as [Eq. (3.13)]:

$$(\hat{k}_j^m)^{3/2} = \left(\frac{\Delta Y_-\hat{k}_{j+1}^m+\Delta Y_+\hat{k}_{j-1}^m}{\Delta Y_++\Delta Y_-}\right)^{1/2}\left(\frac{\Delta X_-\hat{k}_j^{m+1}+\Delta X_+\hat{k}_j^{m-1}}{\Delta X_++\Delta Y_-}\right)$$

It will now be shown that the weighted average, both in X and Y directions, used to represent k_j^m is also mathematically consistent.

Using the Taylor series expansions in X-direction, Eqs. (C.1) and (C.2), for $\hat{k}=\phi$,

$$\hat{k}_j^m = \frac{\Delta X_- \hat{k}_j^{m+1} + \Delta X_+ \hat{k}_j^{m-1}}{\Delta X_+ + \Delta X_-} - \left(\frac{\partial^2 \phi}{\partial X^2}\right)_j^m \frac{\Delta X_+ \Delta X_-}{2}$$

$$- \left(\frac{\partial^3 \phi}{\partial X^3}\right)_j^m \frac{\Delta X_+ \Delta X_-}{6}(\Delta X_+ - \Delta X_-) - \ldots \qquad \text{(C.8)}$$

which shows that the truncation error is of $0[(\Delta X_+)^2]$.

Now for Y-direction averaging, from Eqs. (C.3) and (C.4), for $\hat{k}=\phi$,

$$\hat{k}_j^m = \frac{\Delta Y_- \hat{k}_{j+1}^m + \Delta Y_+ \hat{k}_{j-1}^m}{\Delta Y_+ + \Delta Y_-} - \left(\frac{\partial^2 \phi}{\partial Y^2}\right)_j^m \frac{\Delta Y_+ \Delta Y_-}{2}$$

$$- \left(\frac{\partial^3 \phi}{\partial Y^3}\right)_j^m \frac{\Delta Y_+ \Delta Y_-}{6}(\Delta Y_+ - \Delta Y_-) - \ldots \qquad \text{(C.9)}$$

Here also the truncation error is of $0[(\Delta Y_+)^2]$. So the representation of $(\hat{k}_j^m)^{3/2}$ given in Eq. (3.13) is mathematically consistent.

XII. APPENDIX D: SIMPSON'S RULE FOR AN UNEQUAL GRID

The problem under consideration is the numerical integration of a function $f(Y)$ over the interval $[Y_1, Y_3]$. Let $Y_1 = -\Delta Y_-$, $Y_2 = 0$ and $Y_3 = \Delta Y_+$. A quadrature formula can be developed for

$$\int_{-\Delta Y_-}^{\Delta Y_+} f(Y)dY, \text{ such that}$$

$$A_1 f(Y_1) + A_2 f(Y_2) + A_3 f(Y_3) = \int_{-\Delta Y_-}^{\Delta Y_+} f(Y)dY \tag{D.1}$$

where $f(Y_1)$, $f(Y_2)$ and $f(Y_3)$ are the nodal values of the function $f(Y)$, and A_1, A_2, A_3 are weights which depend on the grid spacing.

Eq. (D.1) is exact if $f(Y) = 1$, or $f(Y) = Y$, or $f(Y) = Y^2$, so

$$A_1 + A_2 + A_3 = \int_{-\Delta Y_-}^{\Delta Y_+} 1\, dy = \Delta Y_+ + \Delta Y_- \tag{D.2}$$

$$-A_1\Delta Y_- + A_3\Delta Y_+ = \int_{-\Delta Y_-}^{\Delta Y_+} Y\, dY = \frac{(\Delta Y_+)^2-(\Delta Y_-)^2}{2} \tag{D.3}$$

$$A_1(\Delta Y_-)^2 + A_3(\Delta Y_+)^2 = \int_{-\Delta Y_-}^{\Delta Y_+} Y^2\, dy = \frac{(\Delta Y_+)^3+(\Delta Y_-)^3}{3} \tag{D.4}$$

Multiplying Eq. (D.3) by ΔY_- and then adding Eq. (D.4) to it results in:

$$A_3\Delta Y_+(\Delta Y_+ + \Delta Y_-) = \left[\frac{(\Delta Y_+)^3+(\Delta Y_-)^3}{3} + \frac{\Delta Y_-((\Delta Y_+)^2-(\Delta Y_-)^2)}{2}\right]$$

Noting that

$$(\Delta Y_+)^3+(\Delta Y_-)^3 = (\Delta Y_+ + \Delta Y_-)^3 - 3\Delta Y_+\Delta Y_-(\Delta Y_+ + \Delta Y_-)$$

the above equation can be written as

$$A_3 = \frac{1}{\Delta Y_+}\left[\frac{(\Delta Y_+ + \Delta Y_-)^2}{3} - \Delta Y_+ \Delta Y_- + \frac{\Delta Y_-(\Delta Y_+ - \Delta Y_-)}{2}\right]$$

or

$$A_3 = \frac{\Delta Y_+ + \Delta Y_-}{\Delta Y_+}\left[\frac{\Delta Y_+ + \Delta Y_-}{3} - \frac{\Delta Y_-}{2}\right] \tag{D.5}$$

Multiplying Eq. (D.2) by ΔY_- and then adding Eq. (D.3) to it results in:

$$A_2 \Delta Y_- + A_3(\Delta Y_+ + \Delta Y_-) = \frac{(\Delta Y_+)^2 - (\Delta Y_-)^2}{2} + \Delta Y_+ \Delta Y_- + \Delta Y_-^2 = \frac{(\Delta Y_+ + \Delta Y_-)^2}{2}$$

or

$$A_2 = \frac{(\Delta Y_+ + \Delta Y_-)^2}{2\Delta Y_-} - A_3 \frac{\Delta Y_+ + \Delta Y_-}{\Delta Y_-} \tag{D.6}$$

Now from Eq. (D.2)

$$A_1 = (\Delta Y_+ + \Delta Y_-) - A_2 - A_3 \tag{D.7}$$

Once A_1, A_2, A_3 have been determined, Eq. (D.1) can be used to integrate f(Y).

XIII. APPENDIX E: EVALUATION OF WALL DERIVATIVES

The shear stress and heat transfer at the walls (Eqs. (2.72) and (2.86)) are directly proportional to the gradients of axial velocity and temperature evaluated at the walls, respectively. Three schemes for evaluating wall derivatives were tested: a straight line fit between the wall and the first point out or a second and third degree polynomial fit using three and four points, respectively. The second degree curve, though found suitable for laminar flows, did not give satisfactory results for turbulent flows. The first and third degree polynomial fits gave, in general, satisfactory results; the former was found particularly suitable for turbulent flows where the first calculation point is very near the wall as the nondimensional velocity is known to be very nearly linear with the distance.

The computer code calculates wall derivatives using both the straight line and third degree polynomial fits. For the straight line fit, the wall slope is (see Fig. 3.1)

$$\left.\frac{\partial\phi}{\partial Y}\right|^{m+1}_{\substack{\text{inner}\\ \text{wall}}} = \frac{\phi_2^{m+1}-\phi_1^{m+1}}{\Delta Y_1} \tag{E.1}$$

and

$$\left.\frac{\partial\phi}{\partial Y}\right|^{m+1}_{\substack{\text{outer}\\ \text{wall}}} = \frac{\phi_{N-1}^{m+1}-\phi_N^{m+1}}{\Delta Y_N} \tag{E.2}$$

The wall slope for the third degree polynomial fit is given by the

following four point difference scheme:

$$\left.\frac{\partial\phi}{\partial Y}\right|^{m+1}_{\substack{\text{inner}\\ \text{wall}}} = (PTA)\phi_1^{m+1} + (PTB)\phi_2^{m+1} + (PTC)\phi_3^{m+1} + (PTD)\phi_4^{m+1} \qquad (E.3)$$

and

$$\left.\frac{\partial\phi}{\partial Y}\right|^{m+1}_{\substack{\text{outer}\\ \text{wall}}} = (PSA)\phi_N^{m+1} + (PSB)\phi_{N-1}^{m+1} + (PSC)\phi_{N-2}^{m+1} + (PSD)\phi_{N-3}^{m+1} \qquad (E.4)$$

where

$$PTB = \frac{1+RS+RS^2}{\Delta Y_1 RS^2} \qquad (E.5)$$

$$PTC = -\frac{1+RS+RS^2}{\Delta Y_1 (1+RS) RS^3} \qquad (E.6)$$

$$PTD = \frac{1}{\Delta Y_1 (1+RS+RS^2) RS^3} \qquad (E.7)$$

$$PTA = -PTB - PTC - PTD \qquad (E.8)$$

Here RS is as defined in Eq. (3.16).

Similar relations hold for PSA, PSB, PSC and PSD.

XIV. APPENDIX F: FLUID PROPERTIES

The property relations employed to furnish the properties of the fluids used in the present study are given below.

A. Air and Nitrogen

1. Density

Density of both air and nitrogen can be calculated using the perfect gas law:

$$\frac{p}{\rho T} = R_g$$

or

$$\rho = \frac{p}{R_g T} \tag{F.1}$$

where

R_g = 287.7 joules/(kg °K) for air

= 296.9 joules/(kg °K) for nitrogen

2. Coefficient of thermal expansion

The coefficient of thermal expansion, β, can be calculated by use of perfect gas law, Eq. (F.1), as

$$\beta = \frac{1}{T} \frac{1}{°K} \tag{F.2}$$

3. Viscosity

For air viscosity can be calculated using the following relation [157]:

$$\mu = \frac{1.458 \times 10^{-6}\ T^{3/2}}{T + 110.4} \quad \text{kg/(m-sec)} \tag{F.3}$$

For nitrogen, a power law was employed,

$$\frac{\mu}{\mu_0} = \left(\frac{T}{T_0}\right)^{0.75} \tag{F.4}$$

where the exponent was determined using the data given in [160].

4. Thermal conductivity

Thermal conductivity can be given as [160]

$$\lambda = \frac{Z_1(T)^{1/2}}{1 + \frac{Z_2 + 10^{-Z_3/T}}{T}} \quad \text{W/(m °K)} \tag{F.5}$$

where, for air,

$$Z_1 = 2.646 \times 10^{-8}$$

$$Z_2 = 245.4$$

$$Z_3 = 12$$

and for nitrogen ($T < 300$ °K),

$$Z_1 = 2.527 \times 10^{-8}$$

$$Z_2 = 224$$

$$Z_3 = 12$$

For nitrogen, at $T > 300$ °K, the thermal conductivity can be calculated using the following expression [160]:

$$\lambda = Z_1(1 + Z_2\Pi - Z_3\Pi^2 + Z_4\Pi^3) \quad \text{W/(m °K)} \tag{F.6}$$

where

$$\Pi = T - 273.16$$

$$Z_1 = 2.41 \times 10^{-2}$$

$$Z_2 = 3.13 \times 10^{-3}$$

$$Z_3 = 1.33 \times 10^{-6}$$

$$Z_4 = 2.63 \times 10^{-10}$$

5. Specific heat

Specific heat at constant pressure can be calculated using a power law of the form

$$\frac{C_p}{C_{p_0}} = \left(\frac{T}{T_0}\right)^{Z_1} \tag{F.7}$$

where Z_1 can be found from the data given in [160].

B. Distilled Water

The property relations listed below are taken from [161] and correspond to a pressure of 1.38 bars.

1. Density

Equation:

$$\rho = 999.88 - 3.5019\Pi - 3.4895\Pi^2 + 0.17251\Pi^3 \text{ kg/m}^3 \tag{F.8}$$

where

$$\Pi = \frac{1.8T - 510}{50}$$

Temperature range: 284 - 366 °K

2. Coefficient of thermal expansion

Using Eq. (F.8), coefficient of thermal expansion can be written as

$$\beta = - \frac{-3.5019 - 6.979\Pi + 0.51753\Pi^2}{27.777(999.88 - 3.5019\Pi - 3.4895\Pi^2 + 0.17251\Pi^3)} \frac{1}{°K} \qquad (F.9)$$

where

$$\Pi = \frac{1.8T - 510}{50}$$

3. Viscosity

Equation:

$$\mu = 4.787 \times 10^{-6} \exp(5.6036 - 0.76097\Pi + 0.1245\Pi^2 - 0.01133\Pi^3) \quad kg/(m\text{-}sec) \qquad (F.10)$$

where

$$\Pi = \frac{1.8T - 510}{50}$$

Temperature range: 284 - 366 °K

4. Thermal conductivity

Equation:

$$\lambda = 0.58658 + 0.04756\Pi - 0.00588\Pi^2 \quad W/(m\ °K) \qquad (F.11)$$

where

$$\Pi = \frac{1.8T - 510}{50}$$

Temperature range: 284 - 366 °K

5. Specific heat

C_p can be calculated if the molecular Prandtl number is known,

$$Pr = \frac{\mu C_p}{\lambda}$$

where μ and λ are already known from Eqs. (F.10) and (F.11).

The Prandtl number is given as [161]

$$Pr = \exp(2.2279 - 0.84747\Pi + 0.14015\Pi^2 - 0.012083\Pi^3) \qquad (F.12)$$

where

$$\Pi = \frac{1.8T - 510}{50}$$

Temperature range: 284 - 366 °K

C. Ethylene Glycol

Property relations given below are taken from [161].

1. Density

Equation:

$$\rho = 1000/(0.924848 + 6.2796 \times 10^{-4}\Pi + 9.2444 \times 10^{-7}\Pi^2 + 3.057 \times 10^{-9}\Pi^3) \quad kg/m^3 \qquad (F.13)$$

where

$$\Pi = T - 338$$

Temperature range: 278 - 445 °K

2. Coefficient of thermal expansion

Using Eq. (F.13), coefficient of thermal expansion can be written as

$$\beta = \frac{6.2796\text{x}10^{-4} + 1.84888\text{x}10^{-6}\Pi + 9.171\text{x}10^{-9}\Pi^2}{0.924848 + 6.2796\text{x}10^{-4}\Pi + 9.2444\text{x}10^{-7}\Pi^2 + 3.057\text{x}10^{-9}\Pi^3} \frac{1}{°K} \qquad \text{(F.14)}$$

where

$$\Pi = T - 338$$

3. Viscosity

Equation:

$$\mu = 0.001 \exp(3.80666 - 1.79809\Pi + 0.38590\Pi^2 - 0.05878\Pi^3 + 0.004173\Pi^4) \text{ kg/(m-sec)} \qquad \text{(F.15)}$$

where

$$\Pi = \frac{1.8T - 500}{60}$$

Temperature range: 278 - 422 °K

4. Thermal conductivity

Equation:

$$\lambda = 0.3156 - 3.98\text{x}10^{-4}\Pi \text{ W/(m °K)} \qquad \text{(F.16)}$$

where

$$\Pi = 1.8T - 460$$

Temperature range: 277 - 450 °K

5. Specific heat

Equation:

$$C_p = 2313.7 + 173.64\Pi + 14.644\Pi^2 \text{ joules/kg-°K} \qquad \text{(F.17)}$$

where

$$\Pi = \frac{1.8T - 500}{80}$$

Temperature range: 277 - 422 °K

APPENDIX G: COMPUTER CODE "ANNULUS"

```
C*******************************PROGRAM ANNULUS*************************************
C**************MUJEEB MALIK****** IOWA STATE UNIVERSITY*************************
C     CALCULATES VARIABLE PROPERTY LAMINAR AND TURBULENT FLOW HEAT TRANSFER WITH
C     DEVELOPING OR FULLY DEVELOPED FLOW AT THE INLET
C     PROPERTY FUNCTIONS FOR THE FLUID USED SHOULD BE INPUT
C************INPUT DATA************
C     DENS = DENSITY AT THE INLET (LBM/FT3)
C     DENS = -(DENSITY) IF VARIABLE DENSITY USED
C     VISC = VISCOSITY AT THE INLET (LBM/FT-SEC)
C     VISC = -(VISCOSITY) IF VARIABLE VISCOSITY USED
C     USTART = VELOCITY AT THE INLET (FT/SEC)
C     USTART = -(MEAN VELOCITY) IF FULLY DEVELOPED FLOW
C     PSTART = INLET PRESSURE (PSF)
C     RAD1,RAD2 = RADIUS OF INNER AND OUTER WALLS RESPECTIVELY (FT)
C     H1 = VALUE OF INLET FREE STREAM TKE (K/U02)
C     H2 = 0.12 USED IN L MODEL
C     H3 = 0.92 USED IN L MODEL(FOR DEVELOPING FLOWS)
C     H3 = 1.1 (OR SOME OTHER CLOSE VALUE)USED IN FDVP
C     H4 = 0. IF TRANS. CURVATURE CORR. NOT REQUIRED
C     H4 = 0.1 IF TRANS. CURVATURE CORR. REQUIRED
C     H7 = 0. IF TKE USED
C     H7  .GE. 2. IF TKE USED AND SOLUTION STARTED AGAIN AFTER READING FROM DISK
C     H7  .LT. 0. TKE NOT USED
C     H7 = -2. IF BRIDGING EMPLOYED FOR FD FLOW
C     H5.H6,H9,H10   RESEARCH PARAMETERS NO LONGER USED
C     HTC < 0. IF NO HEAT TRANSFER
C     HTC > 0. IF HEAT TRANSFER ( =PRT FOR TURBULENT FLOWS)
C     DXF = RESEARCH PARAMETER USED IN PRESS (USE 4.)
C     DXFM = MAX DELX/DELTAO OR DELX/TBTHIC ALLOWED ;A VALUE OF 0.5-0.7 SUGGESTED
C            LOWER VALUE CAN BE USED BUT WILL RESULT IN MORE COMPUTER TIME
C     CJC = DELXF/DELXB ALLOWED; A MAX OF 1.05 RECOMMENDED
C     VJS,VJF = RESEARCH PARAMETERS NO MORE USED
C     RT = RATIO OF SUCCESSIVE CROSS STREAM GRID NEAR OUTER WALL( USE 1.07)
C     DELY = DELY NEAREST THE OUTER WALL FOR VARIABLE GRID (FT)
C     FCON = 0. IF NO BUOYANCY
C     FCON < 0. IF BOUSSINESQ'S APPROXIMATION USED IN THE BUOYANCY TERM
C     FCON > 0. IF DENSITY VARIABLE EVERYWHERE
C     GG= 1. FOR DOWNWARD FLOW
C     GG=-1. FOR  UPWARD FLOW
C     BETA = COEFFICIENT OF THERMAL EXPANSION AT INLET MEAN TEMP (1/R)
C     PREAD < 0. DATA NOT READ FROM THE DISK
C     PREAD > 0. DATA READ FROM THE DISK
C     PWRITE < 0. DATA NOT WRITTEN ON THE DISK
C     PWRITE > 0. DATA WRITTEN ON THE DISK
C     CHECK < 0. IF HEAT TRANSFER CALCULATIONS STARTED  AFTER SOLVING MOM EQN UP
C     TO CERTAIN DISTANCE
C     CHECK > 0. IF BOTH HYDRODYNAMIC AND THERMAL CALCULATIONS STARTED
C     SIMULTANEOUSLY
C     STLF > 0. STRAIGHT LINE FIT
C     STLF < 0. 3RD DEGREE POLYNOMIAL USED
C     NY = NO. OF Y SPACINGS (EVEN NUMBER)
C     NT = NO. OF PRINT STATIONS (ISTEP.LT.0)
C     NST =  MAX ICOUNT ALLOWED
C     ISTEP < 0 IF PRINT OUT ACCORDING TO DISTANCE
C     ISTEP = NO. OF CALCULATION STEPS AFTER WHICH SOLUTION SHOULD BE PRINTED
C     REPEATEDLY
C     LCASE < 0 IF LAST TEST CASE
C     LCASE > 0 IF MORE TEST CASES FOLLOW
C     LORT < 0 FOR LAMINAR FLOW
C     LORT =.-4 IF VAR GRID TO BE USED FOR LAMINAR FLOW
```

```
C     LORT > 0 FOR TURBULENT FLOWS ( = MAX NO. OF ITERATIONS FOR ITERATIVE
C     SHOOTING METHOD. IF  = 8 OR 9, SOME PARMETERS IN PRESS WILL BE PRINTED)
C     LOCPG < 0 NUSSELT NO.,CF, ETC. WILL NOT BE STORED ON THE DISK
C     LOCPG > 0 THESE PARAMETERS WILL BE STORED ON THE DISK
C     IPRINT < 0 PRINT OUT ACCORDING TO X/DH
C     IPRINT = 0 PRINT OUT ACCORDING TO X/DH*RED
C     IPRINT > 0 PRINT OUT ACCORDING TO X/DH*RED*PR
C     XTR1,XTR2 READ ONLY IF LORT > 0 ( SEE LISTING FOR EXPLANATION)
C     AP, VOKC = 26. AND 0.41 RESPECTIVELY
C     HTK = THERMAL CONDUCTIVITY (BTU/HR-FT-R)
C     HTK = -(THERMAL CONDUCTIVITY) IF VARIABLE
C     CPCON = SPECIFIC HEAT (BTU/HR-R)
C     CPCON = -(SPECIFIC HEAT ) IF VARIABLE
C     TO = INLET TEMP (R)
C     TW1 = 0 INNER WALL INSULATED
C     TW1 > 0,UWT = TW1
C     TW1 < 0, UHF = ABS(TW1)
C     TW2 = 0 OUTER WALL INSULATED
C     TW2 > 0, UWT = TW2
C     TW2 < 0, UHF= ABS(TW2)
C     CORIN = 0 BOTH WALLS HEATED
C     OORIN > 0 ONLY INNER WALL HEATED
C     OORIN < 0 ONLY OUTER WALL HEATED
C     OUT(K),K=1,NT  PRINT OUT STATIONS ACCORDING TO X/DH OR X/DH*RED
C     OR X/DH*RED*PR (DEPENDING UPON VALUE OF IPRINT)
      DIMENSION OUT(30),XDS(66),TITLE(20)
      COMMON/XKEN/XKN1(101),XKN2(101),XKN3(101),PK(101),KOI,NJ1,NJ2,XDH
      COMMON/XPR/PR
      COMMON/AHMADI/T1(101),T2(101),T3(101),TW2,TW1,JTDEL,TBTHIC,OORIN,
     $DTDYO,DTDYI,TCONV,XKCONV,TMEAN,XTMEAN,QCV,QCD,HAVE2,HAVE1
      COMMON/TRANS/XTR1,XTR2,XTRE1,XTRE2,REXTR1,REXTR2,XLMDA1,XLMDA2
      COMMON/MUX/JOI,UPC1,UPC2,UPC3
      COMMON/MTF/XM(101),XK(101),HTC
      COMMON/MOMENT/RETO,RETI,DISPTI,THETI,HHI,DISPTO,THETO,HHO
      COMMON/MPVX/U1(101),U2(101),U3(101),V(101),EV(101),EK(101),EVF(101
     *),EVB(101),EKF(101),EKB(101),D1(101),D2(101),D3(101),C(101),NS,
     $ICOUNT,DELXF,DELXB,DELXT,DELPP,PDROP,PO,PP
      COMMON/PROBE/PTA,PTB,PTC,PTD
      COMMON/UMM/FCON,GG,BETA,UGF,FDV
      COMMON/ENERGY/SQCV,SQCD,QI,TMEAN1,HAVE11,HAVE22
        COMMON/MF/DPD
      COMMON/MY/RT,RS,DELY
      COMMON/VMP/PI,XMASS,DELPT
      COMMON/DEL/JDEL,JDELI,JDELO,DELMIN,DELTAI,DELTAO,MN,DXF,VJS,VJF,
     $DXFM,CCC
      COMMON/STUPID/LORT,NSM1,PSA,PSB,PSC,PSD,XCONV,S1,S2
      COMMON/NAILA/THERK,CPVAR,DVAR,CVISC,DMEAN,CPMEAN,VMEAN,XKMEAN,
     $UC,VO,DO,TO,PSTART,HTK,CPCON
        COMMON/HHHH/H1,H2,H3,H4,H5,H6,H7,H8,H9,H10
      COMMON/LATE/M,MM,N,NM1,NM2,NY,R1,R2,DYB(101),DYF(101),DYT(101),
     $Y(101),YF(101),YB(101),R(101)
      COMMON/TURB/XL(101),TA(101),TV(101),POUT(101),UST1,UST2,GCON,DD1,
     $DD2,AP,VOKC,XDIST,DUDYC,DUDYI,TAU1,TAU2
      COMMON/XBIRTH/PREAD,PWRITE,STLF,XC1,XC2,DEL1,DEL2,UE,CHECK,RED
      COMMON/XNEW/TA1P,TA2P,HAVE1P,HAVE2P,T3PL1,T3PL2
      DATA XDS/.2,.3,.4,.5,.7,1.,1.5,2.,2.5,3.,3.5,4.,4.5,5.,5.5,6.,6.5,
     $7.,7.5,8.,8.5,9.,10.,11.,12.,13.,14.,15.,16.,17.,18.,19.,19.5,
     $20.,20.5,21.,21.5,22.,23.,24.,25.,26.,27.,28.,29.,30.,31.,32.,33.,
     $34.,35.,36.,37.,38.,39.,40.,41.,42.,43.,44.,45.,46.,47.,48.,49.,
     $50./
```

```
      INTEGER PS
      JDX=-1
      IGRAPH=1
      GCON=32.174
      PI=3.1415926
      RV=-1.
      XJC=778.0
 2002 CONTINUE
      XDH=0.
      JCI=0
      RETC=1.
      PS=1
      JDEL=2
      ICOUNT=0
      ISTAT=1
      XC1=-1.
      XTR1=0.
      XTR2=0.
      XTRE1=-1.0E20
      XTRE2=-1.0E20
      XLMDA1=-1.
      XLMDA2=-1.
      UPC1=1.
      UPC2=1.
      UPC3=1.
      TAU1=0.0
      DELPP=0.0
      PDROP=0.0
      FDV=-1.0
      CPVAR=-1.0
      DVAR=-1.0
      THERK=-1.0
      CVISC=-1.0
      PRP=-1.
      QCV=0.0
      QCD=0.0
         RETC=0.
       READ(5,1)TITLE
    1 FORMAT(20A4)
    2 FORMAT(10G13.4)
      WRITE(6,3)
    3 FORMAT('1',///)
       WRITE(6,1)TITLE
      READ(5,5)DENS,VISC,USTART,PSTART,RAD1,RAD2
    5 FORMAT(6G12.5)
      WRITE(6,5)DENS,VISC,USTART,PSTART,RAD1,RAD2
      READ(5,5)H1,H2,H3,H4,H5,H6,H7,H8,H9,H10
       WRITE(6,5)H1,H2,H3,H4,H5,H6,H7,H8,H9,H10
      READ(5,5)HTC,DXF,DXFM,CDC,VJS,VJF
      WRITE(6,5)HTC,DXF,DXFM,CDC,VJS,VJF
      READ(5,5)RT,DELY,FCON,GG,BETA
      WRITE(6,5)RT,DELY,FCON,GG,BETA
      READ(5,5)PREAD,PWRITE,CHECK,STLF
      WRITE(6,5)PREAD,PWRITE,CHECK,STLF
      READ(5,7)NY,NT,NST,ISTEP,LCASE,LORT,LOOPG,IPRINT
    7 FORMAT(8I10)
      WRITE(6,7)NY,NT,NST,ISTEP,LCASE,LORT,LOOPG,IPRINT
      IF(LORT.GT.0)READ(5,5)XTR1,XTR2,AP,VDKC
C     XTR1=XTR2=-1  IF FLOW IS ASSUMED TO BE FULLY TURBULENT
C      XTR1=XTR2=0     IF TRANSITION IS TO BE CALCULATED BY THE
```

```
C       PROGRAM
C       XTR1>0 &XTR2>0   ,  INPUT VALUES OF LOCATION OF TRANSITION
        IF(LCRT.GT.0)WRITE(6,5)XTR1,XTR2,AF,VDKC
        IF(HTC.LT.0.0)GO TO 801
        READ(5,5)HTK,CPCON,TO,TW1,TW2,OORIN
        WRITE(6,5)HTK,CPCON,TO,TW1,TW2,OORIN
        IF(HTK.LT.0.0)THERK=1.0
        IF(CPCON.LT.0.0)CPVAR=1.0
        IF(DENS.LT.0.0)DVAR=1.0
        IF(VISC.LT.0.0)CVISC=1.0
        IF(CVISC.GT.0..OR.THERK.GT.0.)PRP=1.
        IF(CPVAR.GT.0..OR.DVAR.GT.0.)PRP=1.
        IF(FCON.NE.0.)PRP=1.
        HTK=ABS(HTK)
        CPCON=ABS(CPCON)
        HTK=HTK/3600.0
  801 CONTINUE
        IF(ISTEP.GT.0)GO TO 26
        READ(5,5)(OUT(K),K=1,NT)
        WRITE(6,5)(OUT(K),K=1,NT)
   26 CONTINUE
        IF(LCRT.GT.0)GO TO 6161
        AA=1.
        DO 5190 J=1,66
        XDS(J)=XDS(J)/(2000.*AA)
        AA=0.965*AA
        IF(AA.LT.0.125)AA=0.125
 5190 CONTINUE
 6161 CONTINUE
        IF(USTART.LT.0.0)FOV=1.0
        IF(FOV.LT.0.)JCI=5
C    INITIALIZING AND CONVERSION FACTORS
        UC=ABS(USTART)
        VC=ABS(VISC)
        DC=ABS(DENS)
        PC=PSTART
        UCONV=UO
        XCONV=VO/(DC*UO)
        PCONV=(DO*UC*UO)/GCON
        VCONV=VC
        XMCONV=(VO*VO)/(DC*UO)
        DCONV=DO
        WRITE(6,6)UCONV,XCONV,PCONV,XMCONV,DCONV,VCONV
    6 FORMAT(//,5X,'UC=',G12.4,5X,'XC=',G12.4,5X,'PC=',G12.4,5X,'MC=',G1
      $2.4,5X,'DC=',G12.4,5X,'VC=',G12.4)
        IF(HTC)10,11,11
   10 HTK=VC
        CPCON=1.0
        CPCONV=CPCON
        XKCONV=VCONV
        PR=ABS(HTC)
        GO TO 12
   11 CPCONV=CPCON
        XKCONV=CPCON*VO
        TCONV=UO*UC/(GCON*XJC*CPCON)
        WRITE(6,811)CPCONV,XKCONV,TCONV
  811 FORMAT(//,4X,'CPC=',G12.4,5X,'KC=',G12.4,5X,'TC=',G12.4)
        CPMEAN=CPCON
        XKMEAN=HTK
        VMEAN=VO
```

```
      PR=VMEAN*CPMEAN/XKMEAN
   12 CONTINUE
      DMEAN=CO
      DMEAN1=DMEAN
      UMEAN1=UC
      UCF=GG*VC/(DC*UC**3)*GCON
C    Y-GRID
      N=NY+1
      NM1=N-1
      NM2=N-2
      M=NM1
      MM=NM2
      NS=2
      NSP=2
      MN=NS+NSP
      NSM1=NS-1
      DH=2.0*(RAD2-RAD1)
      R1=RAD1/XCONV
      R2=RAD2/XCONV
      Y(N)=R1
C     Y MEANS RADIAL COORDINATE
      DO 1006 J=1,N
      XM(J)=1.
 1006 XK(J)= HTK/XKCONV
      IF(FREAD.GT.0.)GO TO 1110
      CALL DELYR
      XMASS=CO*UC*PI*(RAD2**2.0-RAD1**2.0)/XMCONV
      REC=DC*UC*DH/VC
      DMASS=XMASS*XMCONV
      WRITE(6,19)REC,DMASS
   19 FORMAT(///,5X,'REC=',G12.5,5X,'MASS FLOW=',G12.5)
      DELMIN=DYF(1)
      DO 20 J=1,N
      D1(J)=CO/DCONV
      D2(J)=D1(J)
      JDELI=NM2
      JDELC=3
      D3(J)=D2(J)
      EV(J)=VC/VCONV
      EK(J)=HTK/XKCONV
      C(J)=CPCON/CPCONV
   20 V(J)=0.0
      U1(1)=0.0
      U1(N)=0.0
      U2(1)=0.0
      U2(N)=0.0
      U3(1)=0.0
      U3(N)=0.0
      IF(FDV.GE.0.0)GO TO 22
      DO 21 J=2,M
   21 U1(J)=UC/UCONV
      GO TO 24
   22 CALL FDVP
   24 CONTINUE
      IF(HTC.LT.0.0)GO TO 824
      DO 823 J=2,M
  823 T1(J)=TC/TCONV
      IF(TW2.LE.0.0)GO TO 815
      T1(1)=TW2/TCONV
      T2(1)=T1(1)
```

```
      T3(1)=T1(1)
      GO TO 816
  815 DTDYC=TW2*XCONV/(HTK*TCONV)
      T1(1)=(DTDYC-T1(2)*PSB-T1(3)*PSC-T1(4)*PSD)/PSA
  816 IF(TW1.LE.0.0)GO TO 817
      T1(N)=TW1/TCONV
      T2(N)=T1(N)
      T3(N)=T1(N)
      GO TO 818
  817 DTDYI=TW1*XCONV/(HTK*TCONV)
      T1(N)=(DTDYI-T1(NM1)*PTB-T1(NM2)*PTC-T1(N-3)*PTD)/PTA
  818 CONTINUE
      IF(CHECK.LT.0.)GO TO 101
  824 CONTINUE
      DELXF=1.0E-10
      XDIST=0.0
      WRITE(6,25)
   25 FORMAT(///,'1****BEGINING OF COMP LOOP***')
      GO TO 101
 1110 CONTINUE
C     START READING DATA FROM DISK
      READ(10)Y,R,U3,V,EV,EK,UST1,UST2,RED,N,JDELI,TA,U2,D1,D2,D3,C,
     $YF,YB,DYF,DYB,DYT,PSA,PSB,PSC,PSD,PTA,PTB,PTC,PTD,PDROP,DELTAI,
     $DELTAO,DELXF,XDIST,UPC1,UPC2,UPC3,XC1,XC2,DEL1,DEL2,UE,XMASS,
     $JDELO,ICOUNT,JOI,ICRAPH,U1,XTR1,XTR2,XTRE1,XTRE2,XLMDA1,XLMDA2,
     $REXTR1,REXTR2,XKN1,XKN2,XKN3,PK,TV,XL,KOI,NJ1,NJ2,PR,XDH,DPD
      IF(HTC.LT.0..OR.CHECK.LT.0.)GO TO 1015
      READ(10)T2,XM,XK,T1,T3(1),T3(N),TMEAN1,HAVE11,HAVE22,QI,SQCV,
     $SQCD,TETHIC
 1015   CONTINUE
      IF(CHECK.LT.0.)ICOUNT=0
      ISTAT=ICOUNT+1
      IF(CHECK.GT.0.)GO TO 101
      DO 9191 J=1,N
      IF(LORT.GT.0)EK(J)=XK(J)+(EV(J)-XM(J))/HTC
 9191 U1(J)=U2(J)
      GO TO 24
  101 ICOUNT=ICOUNT+1
      IF(PREAD.GT.0..OR.ICOUNT.EQ.1)GO TO 103
      IF(CVISC.LT.0.0.AND.LORT.LT.0)GO TO 825
  103 EVF(1)=EV(1)+EV(2)
      EVB(1)=EVF(1)
      EVB(N)=EV(N)+EV(N-1)
      EVF(N)=EVB(N)
      EKF(1)=EK(1)+EK(2)
      EKB(N)=EK(N)+EK(N-1)
      EKF(N)=EKB(N)
      DO 210 J=2,NM1
      EVB(J)=EVF(J-1)
      EVF(J)=EV(J)+EV(J+1)
      EKB(J)=EKF(J-1)
      EKF(J)=EK(J)+EK(J+1)
  210 CONTINUE
      PREAD=0.
  825 CONTINUE
C   CALCULATION OF DELTAX
      DELXB=DELXF
      CALL DELX
   45 XDIST=XDIST+DELXF
      OXDIST=XDIST*XCONV
```

```
      XDH=CXDIST/DH
C   CALCULATION OF PRESS GRAD AND AXIAL VELOCITY
      IF(FDV.GT.0..AND.PRP.LT.0.)GO TO 309
      CALL PRESS
      CALL UVEL
       GC TC 310
  309  DELPP=-DPD*DELXF
       DELPT=-DPD*DELXT
      PDROP=PDROP+DELPP
      PP=PC-PDROP
      GC TC 75
  310  CONTINUE
      IF(ICOUNT.GE.NS)GO TO 75
      DC 70 J=1,N
   70 U3(J)=U2(J)
   75 CONTINUE
      IF(PTC.LT.0.0)GC TC 831
C     CALCULATION OF T(J)
      CALL TEMP
      IF(PRP.GT.0.)CALL VPROP
  831 CONTINUE
      DUDYO=PSA*U3(1)+PSB*U3(2)+PSC*U3(3)+PSD*U3(4)
      TA2P=EV(1)*DUDYO*VCONV*UCONV/(XCONV*GCON)
C     ***ST LINE FIT***
      DUDYO=(U3(2)-U3(1))/DYF(1)
      TAU2=EV(1)*DUDYO*VCONV*UCONV/(XCONV*GCON)
      IF(STLF.LT.0.)TAU2=TA2P
      DUDYI=PTA*U3(N)+PTB*U3(NM1)+PTC*U3(NM2)+PTD*U3(N-3)
      TA1P=EV(N)*DUDYI*VCONV*UCONV/(XCONV*GCON)
      DUDYI=(U3(NM1)-U3(N))/DYB(N)
      TAU1=EV(N)*DUDYI*VCONV*UCONV/(XCONV*GCON)
      IF(STLF.LT.0.)TAU1=TA1P
      REX=DC*UCONV*U3(JDELO)*OXDIST/VO
      IF(FDV.GT.0..AND.PRP.LT.0.)GO TO 76
      IF(XTR1.LT.0..AND.XTR2.LT.0.)GO TO 4640
         IF(LORT.LT.C.OR.FDV.GT.0.)GO TO 4640
 6545 IF(ICOUNT.GT.5)GO TO 9321
      IF(XTR1.GE.0..AND.XTR2.GE.0.)GO TO 4641
      IF(XTR1.LT.0..AND.XTR2.LT.0.)GC TO 3452
 9321 KKC=JDELC-2
      WY=KKC
      WY1=WY/2.
      LWY=WY1
      WY2=LWY
        IF(WY1.EQ.WY2)KKC=KKC-1
      STC1=0.0
      SDC1=0.0
      VVV=0.
      WWW=0.
      DC 789 J=1,KKO,2
      WF2=DYT(J+1)/DYF(J+1)*(DYT(J+1)/3.0-DYB(J+1)/2.0)
      WF1=DYT(J+1)**2.0/(2.0*DYB(J+1))-WF2*DYT(J+1)/DYB(J+1)
      WF0=DYT(J+1)-WF1-WF2
      IF(JCI.LE.2)GO TO 788
      SD1=(1.-D3(J)*U3(J)/(U3(JDELO+1)*D3(JDELO+1)))*2.*Y(J)
      SD2=(1.-D3(J+1)*U3(J+1)/(U3(JDELO+1)*D3(JDELO+1)))*2.*Y(J+1)
      SD3=(1.-D3(J+2)*U3(J+2)/(U3(JDELO+1)*D3(JDELO+1)))*2.*Y(J+2)
      ST1=(1.-U3(J)/U3(JDELO+1))*2.*Y(J)*D3(J)*U3(J)/(U3(JDELO+1)*
     $D3(JDELO+1))
      ST2=(1.-U3(J+1)/U3(JDELO+1))*2.*Y(J+1)*U3(J+1)*D3(J+1)/(U3(JDELO+1
```

```
     $)*D3(JDELC+1))
      ST3=(1.-U3(J+2)/U3(JDELO+1))*2.*Y(J+2)*D3(J+2)*U3(J+2)/
     $(D3(JDELC+1)*U3(JDELO+1))
      GO TO 788
  788 SD1=(1.-D3(J)*U3(J)/(D3(JDELC)*U3(JDELO)))*2.*Y(J)
      SD2=(1.-D3(J+1)*U3(J+1)/(D3(JDELC)*U3(JDELC)))*2.*Y(J+1)
      SD3=(1.-D3(J+2)*U3(J+2)/(D3(JDELO)*U3(JDELO)))*2.*Y(J+2)
      ST1=(1.-U3(J)/U3(JDELC))*2.*Y(J)*D3(J)*U3(J)/(D3(JDELC)*U3(JDELC))
      ST2=(1.-U3(J+1)/U3(JDELO))*2.*Y(J+1)* D3(J+1)*U3(J+1)/(D3(JDELO)
     $*U3(JDELC))
      ST3=(1.-U3(J+2)/U3(JDELO))*2.*Y(J+2)* D3(J+2)*U3(J+2)/(D3(JDELO)
     $*U3(JDELO))
  786 SDC1=SDO1+WF0*SD1+WF1*SD2+WF2*SD3
  789 STC1=STO1+WF0*ST1+WF1*ST2+WF2*ST3
      IF(WY1.NE.WY2)GO TO 4444
      UUU=0.5*(U3(KKO+2)+U3(KKO+3))
      DDD=0.5*(D3(KKC+2)+D3(KKO+3))
      YYY=Y(KKC+2)+Y(KKC+3)
      IF(JCI.GT.2)GO TO 4455
      WWW=(1.-UUU*DDD/(D3(JDELO)*U3(JDELO)))*YYY*DYF(KKC+2)
      VVV=(1.-UUU/U3(JDELO))*YYY*DDD*UUU*DYF(KKC+2)
     $/(D3(JDELO)*U3(JDELO))
      GO TO 4444
 4455 WWW=(1.-UUU*DDD/(U3(JDELO+1)*D3(JDELO+1)))*YYY*DYF(KKO+2)
        VVV=(1.-UUU/U3(JDELO+1))*DDD*UUU*YYY*DYF(KKO+2)/(D3(JDELC+1)*
     $U3(JDELO+1))
 4444 CONTINUE
       SDC1=SDC1+WWW
      STC1=STC1+VVV
      DISPTO=R2-SQRT(R2**2-SDO1)
      THETC=R2-SQRT(R2**2-STO1)
      HPC=DISPTC/THETO
      RETC=DC*UCONV*U3(JCELO)*THETC*XCONV/VO
      DISPTO=2.*DISPTC/(R2-R1)
      THETC=2.*THETO/(R2-R1)
      KKI=N-JDELI-1
       WY=KKI
      WY1=WY/2.
      LWY=WY1
      WY2=LWY
      IF(WY1.EQ.WY2)KKI=KKI-1
      SDI1=0.0
      STI1=0.
      VVV=0.
      WWW=0.
      DO 791 J=1,KKI,2
      K=N-J+1
      KL1=K-1
      KL2=K-2
      WF2=DYT(KL1)/DYB(KL1)*(DYT(KL1)/3.0-DYF(KL1)/2.0)
      WF1=DYT(KL1)**2.0/(2.0*DYF(KL1))-WF2*DYT(KL1)/DYF(KL1)
      WF0=DYT(KL1)-WF1-WF2
      IF(JCI.LE.2)GO TO 793
      SD1=(1.-D3(K)*U3(K)/(D3(JDELI-1)*U3(JDELI-1)))*2.*Y(K)
      SD2=(1.-U3(KL1)*D3(KL1)/(U3(JDELI-1)*D3(JDELI-1)))*2.*Y(KL1)
      SD3=(1.-U3(KL2)*D3(KL2)/(U3(JDELI-1)*D3(JDELI-1)))*2.*Y(KL2)
      ST1=(1.-U3(K)/U3(JDELI-1))*2.*Y(K)*D3(K)*U3(K)/(D3(JDELI-1)*
     $U3(JDELI-1))
      ST2=(1.-U3(KL1)/U3(JDELI-1))*2.*Y(KL1)*D3(KL1)*U3(KL1)/(D3(JDELI-1
     $)*U3(JDELI-1))
```

```
      ST3=(1.-U3(KL2)/U3(JDELI-1))*2.*Y(KL2)*D3(KL2)*U3(KL2)/(D3(JDELI-1
     $)*U3(JDELI-1))
      GO TO 794
  793 SD1=(1.-D3(K)*U3(K)/(D3(JDELI)*U3(JDELI)))*2.*Y(K)
      SD2=(1.-D3(KL1)*U3(KL1)/(D3(JDELI)*U3(JDELI)))*2.*Y(KL1)
      SD3=(1.-D3(KL2)*U3(KL2)/(D3(JDELI)*U3(JDELI)))*2.*Y(KL2)
      ST1=(1.-U3(K)/U3(JDELI))*2.*Y(K)*D3(K)*U3(K)/(D3(JDELI)*U3(JDELI))
      ST2=(1.-U3(KL1)/U3(JDELI))*2.*Y(KL1)*D3(KL1)*U3(KL1)/(D3(JDELI)*
     $U3(JDELI))
      ST3=(1.-U3(KL2)/U3(JDELI))*2.*Y(KL2)*D3(KL2)*U3(KL2)/(D3(JDELI)*
     $U3(JDELI))
  794 SDI1=SDI1+WF0*SD1+WF1*SD2+WF2*SD3
  791 STI1=STI1+WF0*ST1+WF1*ST2+WF2*ST3
      IF(MY1.NE.MY2)GO TO 5555
      UUU=0.5*(U3(K-2)+U3(K-3))
      DDD=0.5*(D3(K-2)+D3(K-3))
      YYY=Y(K-2)+Y(K-3)
      IF(JCI.GT.2)GO TO 5544
      WWW=(1.-UUU*DDD/(U3(JDELI)*D3(JDELI)))*YYY*DYB(K-2)
      VVV=(1.-UUU/U3(JDELI))*DDD*UUU*YYY*DYB(K-2) /(D3(JDELI)*U3(JDELI))
      GO TO 5555
 5544 WWW=(1.-UUU*DDD/(U3(JDELI-1)*D3(JDELI-1)))*YYY*DYE(K-2)
      VVV=(1.-UUU/U3(JDELI-1))*DDD*YYY*UUU*DYB(K-2)/(D3(JDELI-1)*
     $U3(JDELI-1))
 5555 CONTINUE
      SDI1=SDI1+WWW
      STI1=STI1+VVV
      DISPTI=SQRT(SDI1+R1**2)-R1
      THETI=SQRT(STI1+R1**2)-R1
      HHI=DISPTI/THETI
      RETI= CO*UCONV*U3(JDELI)*THETI*XCONV/VO
      DISPTI=2.*DISPTI/(R2-R1)
      THETI=2.*THETI/(R2-R1)
      IF(XTR1.LT.0..AND.XTR2.LT.0.)GO TO 3452
      IF(XTR1.GT.0..AND.XTR2.GT.0.)GO TO 4540
      CALL TRANS1(REX,RETI,RETO,XDIST,OXDIST)
      IF(XTR1.EQ.0..AND.XTR2.EQ.0.)GO TO 4641
 4540 IF(XTRE1.LT.0..OR.XTRE2.LT.0.)CALL TRANS2(REX,RETI,RETO,XDIST,
     $OXDIST)
 4640 IF(LCRT.GT.0.)CALL VISC2
 4641 CONTINUE
 1515 CONTINUE
      RV=1.
C    CALCULATION OF V(J)
      CALL RADVEL
  752 CONTINUE
      IF(ICOUNT.EQ.NSM1)GO TO 76
      DO 80 J=1,N
      U1(J)=U2(J)
      IF(DVAR.LT.0.)GO TO 80
      D1(J)=D2(J)
      D2(J)=D3(J)
   80 U2(J)=U3(J)
   76 CONTINUE
      XPLUS=XDH/RED
      XPPLUS=XPLUS/PR
      IF(ISTEP.LT.0)GO TO 81
      IF(ICOUNT.EQ.ISTAT)GO TO 84
      GO TO 3000
   81 IF(IPRINT)871,873,875
```

```
 671 IF(XDH.GE.OUT(PS))GO TO 83
     GO TO 3000
 673 IF(XPLUS.GE.OUT(PS))GO TO 83
      GO TO 3000
 675 IF(XPPLUS.GE.OUT(PS))GO TO 83
      GO TO 3000
  83 PS=PS+1
     GO TO 86
  84 ISTAT=ISTAT+ISTEP
  86 JDX=1
     WRITE(6,151)
 151 FORMAT(//,'*********************************************************
    $*************************************************************
    $**********')
     WRITE(6,1)TITLE
     WRITE(6,152)
 152 FORMAT('*********************************************************
    $*************************************************************
    $*********',//)
3451 IF(XTR1.LT.0..AND.XTR2.LT.0.)GO TO 6545
3452 CONTINUE
     DO 85 J=1,N
  85 PCUT(J)=U3(J)*UCONV
     ODELXF=XCONV*DELXF
     OPDROP=PCONV*PDROP
     ODPDX=-PCONV*DELPP/ODELXF
     ODELPF=DELPF*PCONV
     PPLUS=GCON*CPDROP/(DO*UO*UO)
     SM1=0.0
     SU1=0.0
     DO 704 J=1,NM2,2
     WF2=DYT(J+1)/DYF(J+1)*(DYT(J+1)/3.0-DYB(J+1)/2.0)
     WF1=DYT(J+1)**2.0/(2.0*DYB(J+1))-WF2*DYT(J+1)/DYB(J+1)
     WF0=DYT(J+1)-WF1-WF2
     SUM1=D3(J)*Y(J)
     SUM2=D3(J+1)*Y(J+1)
     SUM3=D3(J+2)*Y(J+2)
     SUM11=SUM1*U3(J)
     SUM22=SUM2*U3(J+1)
     SUM33=SUM3*U3(J+2)
     SU1=SU1+WF0*SUM1+WF1*SUM2+WF2*SUM3
 704 SM1=SM1+WF0*SUM11+WF1*SUM22+WF2*SUM33
     XMASX=2.0*PI*SM1*XMCONV
     UMEAN=SM1/SU1*UCONV
     FAV=-GCON*DH*ODPDX/(2.0*DMEAN*UMEAN*UMEAN)
     FREDP=REC*FAV
     F2=2.0*GCON*TAU2/(DMEAN*UMEAN**2.0)
     F1=2.0*GCON*TAU1/(DMEAN*UMEAN**2.0)
     FTOTAL=2.0*GCON*(TAU1*R1/R2+TAU2)/((1.0+R1/R2)*DMEAN*UMEAN**2.0)
     IF(JDX.LT.0)GO TO  1030
     WRITE(6,90)ICOUNT,DXDIST,XPLUS,XPPLUS,PPLUS
  90 FORMAT(4X,'ICOUNT=',I4,5X,'XDIST=',G12.5,5X,'XPLUS=',G12.5,5X,'XPP
    $LUS=',G12.5,5X,'PPLUS=',G12.5)
     WRITE(6,91)ODELXF,ODPDX,OPDROP,ODELPP,XDH
  91 FORMAT(//,5X,'DELXF=',G12.4,5X,'DP/DX=',G12.4,5X,'PG-PX=',G12.4,5X
    *,'DELPF=',G12.4,5X,'X/DH=',G12.4)
     DELTI=XCONV*DELTAI
     DELTC=XCONV*DELTAC
     WRITE(6,165)UMEAN,JDELI,JDELO,DELTI,DELTO,XMASX
165 FORMAT(//,4X,'UMEAN=',G12.5,5X,'JDELI=',I3,5X,'JDELO=',I3,5X,'DELT
```

```
     $AI=',G12.5,5X,'DELTAO=',G12.5,5X,'MASSX=',G12.5)
      WRITE(6,167)FREDF,FAV,TAU2,TAU1,FICTAL,F1,F2
  167 FORMAT(//,4X,'FAPP*RED=',G12.5,5X,'FAV=',G12.5,5X,'TAU2=',G12.5,5X
     $,'TAU1=',G12.5,5X,'FICTAL=',G12.5,5X,//,5X,'F1=',G12.5,5X,'F2=',G1
     $2.5)
      IF(LORT.GT.0.AND.FCV.LT.0.)WRITE(6,5001)DISPTI,THETI,HHI,DISPTO,
     $THETC,HHC
 5001 FORMAT(//,5X,'DEL*I=',G12.4,5X,'THETAI=',G12.4,5X,'HI=',G12.4,5X,'
     $DEL*C=',G12.4,5X,'THETAO=',G12.4,//,5X,'HC=',G12.4)
      IF(LORT.GT.0)WRITE(6,626)UST1,UST2,REX,RETO,RETI
  626 FORMAT(//,5X,'UST1=',G12.4,5X,'UST2=',G12.4,5X,'REX=',G12.4,5X,
     $'RETHC=',G13.5,5X,'RETHI=',G13.5)
      WRITE(6,5)H1,H2,H3,H4,H5,H6,H7,H8,H9,H10
      WRITE(6,5)TA1P,TA2P
      WRITE(6,151)
      WRITE(6,95)
   95 FORMAT(//'****U(J)***',//)
      WRITE(6,2)(FOUT(K),K=1,N)
      IF(RV.LT.0.)GO TO 1030
      DO 96 J=1,N
   96 POUT(J)=V(J)*UCONV
      WRITE(6,97)
   97 FORMAT(//,'****V(J)***',//)
      WRITE(6,2)(POUT(K),K=1,N)
 1030 IF(HTC.LT.0.)GO TO 961
      IF(JDX.GT.0)WRITE(6,151)
      PRB=VMEAN*CPMEAN/XKMEAN
      TDELTA=TBTHIC*XCONV
      XNUD2=HAVE2*DH/XKMEAN
      ST2=HAVE2/(DMEAN*CPMEAN*UMEAN)
      XNUD1=HAVE1*DH/XKMEAN
      ST1=HAVE1/(DMEAN*CPMEAN*UMEAN)
      IF(JDX.LT.0.AND.LOCPG.GT.0)GO TO 3002
      WRITE(6,866)JTDEL,TDELTA,PRB,XTMEAN,XNUD1,ST1,HAVE1,XNUD2,ST
     $2,HAVE2,QCD,QCV,SQCD,SQCV
  866 FORMAT(//,5X,'JTDEL=',I4,5X,'TDELTA=',G12.4,5X,'PRANDTL NO.=',G12.
     $4,5X,'XMEAN=',G14.7,//,5X,'NUD1=',G12.4,5X,'STANTN1=',
     $        G12.4,5X,'HAVE1=',G12.4,5X,'NUD2=',G12.4,5X,'STANTON2=',G12
     $.4,5X,//,5X,'HAVE2=',G12.4,5X,'QCD=',G12.4,5X,'QCV=',G12.4,5X,
     $'SQCD=',G12.4,5X,'SQCV=',G12.4)
      REDM=DMEAN*UMEAN*DH/VMEAN
      WRITE(6,946)DMEAN,CPMEAN,XKMEAN,VMEAN,REDM
  946 FORMAT(//,3X,'DMEAN=',G12.4,5X,'CPMEAN=',G14.7,5X,'KMEAN=',G12.4,5
     $X,'VMEAN=',G12.4,5X,'REDM=',G12.4)
      WRITE(6,5)HAVE1P,HAVE2P,T3PL1,T3PL2
      IF(FCON.EQ.0.)GO TO 890
      IF(CORIN)8022,8023,8021
 8021 QQQ=RAD1*ABS(TW1)*DH/(2.*(XKMEAN*(RAD1+RAD2)))
      IF(TW1.GT.0.)QQQ=(T3(N)-T3(1))*TCONV
      GO TO 8315
 8022 QQQ=RAD2*ABS(TW2)*DH/(2.*(XKMEAN*(RAD1+RAD2)))
      IF(TW2.GT.0.)QQQ=(T3(1)-T3(N))*TCONV
      GO TO 8315
 8023 QQQ=(RAD1*ABS(TW1)+RAD2*ABS(TW2))*DH/(2.*(XKMEAN*(RAD1+RAD2)))
 8315 GR=QQQ*BETA*GCON*(DH/2.)**3*(DMEAN/VMEAN)**2
      WRITE(6,8316)GR
 8316 FORMAT(5X,'GR NO.=',G12.4)
  890 WRITE(6,151)
      DO 860 J=1,N
  860 POUT(J)=T3(J)*TCONV
```

```
      WRITE(6,861)
  861 FORMAT(//,'****T(J)***',//)
      WRITE(6,2)(POUT(K),K=1,N)
      IF(PRP.LT.0.)GO TO 865
      IF(CPVAR.LT.0.0)GO TO 952
      DO 950 J=1,N
  950 POUT(J)=C(J)*CPCONV
      WRITE(6,951)
  951 FORMAT(//,'****CP(J)***',//)
      WRITE(6,2)(POUT(K),K=1,N)
  952 CONTINUE
      IF(DVAR.LT.0.0)GO TO 955
      DO 953 J=1,N
  953 POUT(J)=D3(J)*DCONV
      WRITE(6,954)
  954 FORMAT(//,'****RHO(J)***',//)
      WRITE(6,2)(POUT(K),K=1,N)
  955 CONTINUE
      IF(THERK.LT.0.0)GO TO 961
      DO 959 J=1,N
  959 POUT(J)=EK(J)
      WRITE(6,960)
  960 FORMAT(//,'****K(J)***',//)
      WRITE(6,2)(POUT(K),K=1,N)
  961 IF(JDX.LT.0.AND.LOCPG.GT.0)GO TO 3002
  865 CONTINUE
      IF(CVISC.LT.0.0.AND.LCRT.LT.0.0)GO TO 966
      DO 964 J=1,N
  964 POUT(J)=EV(J)
      WRITE(6,965)
  965 FORMAT(//,'****MU(J)***',//)
      WRITE(6,2)(POUT(K),K=1,N)
      IF(LCRT.LT.0)GO TO 966
      IF(XTR1.EQ.0..AND.XTR2.EQ.0.)GO TO 966
      DO 675 J=JDELI,N
  675 POUT(J)=(Y(J)-R1)*CD1
      DO 676 J=1,JDELO
  676 POUT(J)=(R2-Y(J))*CD2
      WRITE(6,678)
  678 FORMAT(//,'****Y+(J)***',//)
      WRITE(6,2)(POUT(K),K=1,N)
      DO 651 J=JDELI,N
  651 POUT(J)=U3(J)*UCONV/UST1
      DO 652 J=1,JDELO
  652 POUT(J)=U3(J)*UCONV/UST2
      WRITE(6,654)
  654 FORMAT(//,'****U+(J)***',//)
      WRITE(6,2)(POUT(K),K=1,N)
      DO 661 J=1,N
  661 POUT(J)=XL(J)
      WRITE(6,662)
  662 FORMAT(//,'****XL(J)***',//)
      WRITE(6,2)(POUT(K),K=1,N)
      WRITE(6,665)
  665 FORMAT(//,'****TAU(J)***',//)
      WRITE(6,2)(TA(K),K=1,N)
      IF(H7.LT.0.)GO TO 966
      WRITE(6,4095)
 4095 FORMAT(//,'****KEN(J)***',//)
      WRITE(6,2)(XKN3(K),K=1,N)
```

```
  966 CONTINUE
 3000 IF(LCCFG.LT.0)GO TO 1001
      XDISK=XDH
      IF(LCRT.LT.0.)XDISK=XPPLUS
      IF(XDISK.GE.XDS(IGRAPH))GO TO 3001
      GO TO 1001
 3001 IGRAPH=IGRAPH+1
      IF(JDX.LT.0.)GO TO 3451
 3002 IF(HTC.LT.0.)WRITE(12)XDISK,FAV,FTOTAL,U3(JDELI),F1,F2,
     $DISPTI,DISPTO,THETI,THETO
      IF(HTC.GT.0..AND.FCV.LT.0.)WRITE(12)XDISK,FAV,FTOTAL,F1,F2,
     $U3(JDELI),ST1,ST2,XNUD1,XNUD2,T3(1),T3(N),DISPTI,DISPTO,THETI,
     $THETO
      IF(HTC.GT.0..AND.FCV.GT.0.)WRITE(12)XDISK,ST1,ST2,XNUD1,XNUD2,
     $T3(1),T3(N)
 1001 JDX=-1
      IF(ISTEP)1002,1002,1003
 1002 IF(ICOUNT-NST)2222,100,100
 2222 IF(PS-NT)101,101,100
 1003 IF(ICOUNT-NST)101,100,100
  100 IF(PWRITE.LT.0.)GO TO 1005
C     START WRITING DATA ON THE DISK
      WRITE(11)Y,R,U3,V,EV,EK,UST1,UST2,RED,N,JDELI,TA,U2,D1,D2,D3,C,
     $YF,YB,DYF,DYB,DYT,FSA,FSB,FSC,FSD,PTA,PTB,PTC,PTD,PDROP,DELTAI,
     $DELTAO,DELXF,XDIST,UPC1,UPC2,UPC3,XC1,XC2,DEL1,DEL2,UE,XMASS,
     $JDELC,ICOUNT,JOI,IGRAPH,U1,XTR1,XTR2,XTRE1,XTRE2,XLMDA1,XLMDA2,
     $REXTR1,REXTR2,XKN1,XKN2,XKN3,PK,TV,XL,KOI,NJ1,NJ2,PR,XDH,DPD
      WRITE(6,5)XDIST,XDH
      WRITE(6,7)IGRAPH
      IF(HTC.LT.0.)GO TO 1004
      WRITE(11)T2,XM,XK,T1,T3(1),T3(N),TMEAN1,HAVE11,HAVE22,QI,SQCV,
     $SQCD,TETHIC
 1004 CONTINUE
 1005 CONTINUE
      IF(LCASE.GT.0.)GO TO 2002
      STOP
      END
      SUBROUTINE DELX
C*************************************DELX*************************************
      DIMENSION SKCB(101),SKCF(101),SFMAX(101),SBMAX(101),COEFF(101),COE
     *FB(101)
      COMMON/XKEN/XKN1(101),XKN2(101),XKN3(101),PK(101),KOI,NJ1,NJ2,XDH
      COMMON/XBIRTH/PREAD,PWRITE,STLF,XC1,XC2,DEL1,DEL2,UE,CHECK,RED
      COMMON/XPR/PR
      COMMON/TURB/XL(101),TA(101),TV(101),POUT(101),UST1,UST2,GCON,DD1,
     $DD2,AP,VOKC,XDIST,CUDYO,DUDYI,TAU1,TA02
      COMMON/MPVX/U1(101),U2(101),U3(101),V(101),EV(101),EK(101),EVF(101
     *),EVB(101),EKF(101),EKB(101),D1(101),D2(101),D3(101),C(101),NS,
     $ICOUNT,DELXF,DELXB,DELXT,DELPP,PDROP,PO,PP
      COMMON/DEL/JDEL,JDELI,JDELO,DELMIN,DELTAI,DELTAO,MN,DXF,VJS,VJF,
     $DXFM,CCC
      COMMON/LATE/M,MM,N,NM1,NM2,NY,R1,R2,DYB(101),DYF(101),DYT(101),
     $Y(101),YF(101),YB(101),R(101)
      COMMON/STUPID/LORT,NSM1,FSA,FSB,FSC,FSD,XCONV,S1,S2
      COMMON/MTF/XM(101),XK(101),HTC
      COMMON/AHMAD1/T1(101),T2(101),T3(101),TW2,TW1,JTDEL,TBTHIC,DORIN,
     $DTDYO,DTDYI,TCONV,XKCONV,TMEAN,XTMEAN,QCV,QCD,HAVE2,HAVE1
      COMMON/UMM/FCON,GG,BETA,UGF,FDV
      IF(ICOUNT-NS)310,210,410
  310 IF(HTC.LT.0.)GO TO 207
```

```
      IF(CCFIN.LE.0.)GO TO 200
      IF(ICOUNT.EQ.1)JTDEL=NM2
      LI=MAXO(JTDEL,JDELI)
      LO=NM1
      GO TO 205
  200 IF(ICOUNT.EQ.1)JTDEL=3
      LI=2
      LO=MINO(JTDEL,JDELO)
      GO TO 205
  207 LI=JDELI
      LO=NM1
  205 DX3=0.0
      DO 206 J=LI,LO
      SKCB(J)=EKB(J)/C(J)
      SKCF(J)=EKF(J)/C(J)
      SFMAX(J)=AMAX1(EVF(J),SKCF(J))
      SBMAX(J)=AMAX1(EVB(J),SKCB(J))
      DX1=2.0*D1(J)*U1(J)*V(J)*DYT(J)
      COEFF(J)=YF(J)/(DX1*DYF(J))
      COEFB(J)=YB(J)/(DX1*DYF(J-1))
      VVPP=V(J)
      DX2=(ABS(VVPP))/(U1(J)*DYF(J-1))+COEFF(J)*SFMAX(J)+COEFB(J)*SBMAX(
     *J)
      DX3=AMAX1(DX2,DX3)
  206 CONTINUE
      DELXF=.5/DX3
      GO TO 41
  210 WRITE(6,35)ICOUNT
   35 FORMAT(///,'0***C-F EQNS AT ICOUNT=',I3)
  410 IF(ICOUNT.LT.MN)GO TO 41
      IF(LORT.GT.0)GO TO 42
      DPR=2.*(R2-R1)*PR*RED
      DXP=DELXF/DPR
      IF(DXP.GT.DXFM)GO TO 41
      DXF=DXF*CDC
      DELXF=DXP*DPR
      GO TO 41
   42 CONTINUE
      IF(FDV.GT.0..AND.FTC.GT.0.)GO TO 56
      DELXF=CDC*DELXB
      IF(DELXF/DELTAO.GT.DXFM)DELXF=DXFM*DELTAO
      GO TO 41
   56 DELXF=CDC*DELXB
C  MAY NEED TO CHANGE FOR BOTH WALLS HEATED
      IF(XCH.GT.2.)GO TO 50
      DDXY=0.5*DXFM
      IF(DELXF/TBTHIC.GT.DDXY)DELXF=DDXY*TBTHIC
      GO TO 41
   50 IF(DELXF/TBTHIC.GT.DXFM)DELXF=DXFM*TBTHIC
   41 DELXT=DELXF+DELXB
      RETURN
      END
      SUBROUTINE DELYR
C*************************************DELYR*****************************************
C** NY/2 GRIDS ON EACH SIDE OF THE CENTER OF THE GAP FOR LAMINAR FLOWS AND FOR
C  TURBULENT FLOWS WITH R*>0.8 ******FOR SMALLER RADIUS RATIOS(FOR TURB FLOWS)
C   NY/2 GRIDS ON EACH SIDE OF THE RADIUS OF MAX VEL DETERMINED BY KAYS-LEUNG*
      COMMON/PROBE/PTA,PTB,PTC,PTD
      COMMON/MY/RT,RS,DELY
      COMMON/LATE/M,MM,N,NM1,NM2,NY,R1,R2,DYB(101),DYF(101),DYT(101),
```

```
     $Y(101),YF(101),YE(101),R(101)
      COMMCN/STUPID/LORT,NSM1,PSA,PSB,PSC,PSD,XCCNV,S1,S2
      ABL=IABS(LORT)
      IF(LORT.GT.0.0.OR.ABL.EQ.4)GO TO 300
      RS=1.
      DELY=(R2-R1)/NY
      DO 8 J=1,N
      DYE(J)=DELY
      DYF(J)=DELY
    8 Y(J)=R2-(J-1)*DYF(J)
      GO TO 301
  300 DYF(1)=DELY/XCCNV
      I=0
       II=0
      DYE(1)=DELY/XCCNV
      Y(1)=R2
      Y(N)=R1
      NC=NY/10
      NY2=NY/2+1
      NNY=NY2-NC
      NNY1=NNY+1
      RRR=R1/R2
      IF(RRR.GT.0.8.OR.LORT.LT.0)GO TO 3500
      RM=RRR**0.343
       RMM=(R1+R2*RM)/(1.+RM)
        YR1=RMM-R1
       YR2=R2-RMM
       DYE(N)=DYF(1)*YR1/YR2
        DYF(N)=DYE(N)
       DR=YR2
      EGGR=-1.
      GO TO 404
 3500 NY21=NY2-1
      DR=(R2-R1)/2.
      EGGR=1.
  404 DO 406 J=2,NNY
      DYF(J)=RT*DYF(J-1)
      DYE(J)=DYF(J-1)
  406 Y(J)=Y(J-1)-DYF(J-1)
      DO 408 J=NNY1,NY2
      DYF(J)=DYF(NNY)
      DYE(J)=DYF(J-1)
  408 Y(J)=Y(J-1)-DYF(J-1)
      I=I+1
      DY=Y(1)-Y(NY2)
      IF(DY.GE.DR)GO TO 461
      RT=RT+0.005
      GO TO 404
  461 YRC=DR/DY
      DO 471 J=2,NY2
  471 Y(J)=R2-(R2-Y(J))*YRC
      DO 472 J=2,NY2
      DYF(J-1)=Y(J-1)-Y(J)
  472 DYE(J)=DYF(J-1)
      DYE(1)=DYF(1)
      WRITE(6,5)RT,I
    5  FORMAT(5X,G12.4,I10)
      RS=RT
      IF(EGGR.EQ.1.)GO TO 3600
       DR=YR1
```

```
 475   DO 480 J=2,NNY
       K=N-J+1
      DYF(K)=RS*DYF(K+1)
       DYB(K+1)=DYF(K)
 480  Y(K)=Y(K+1)+DYF(K)
       II=II+1
       DO 481 J=NNY1,NY2
       K=N-J+1
       DYF(K)=DYF(K+1)
       DYB(K+1)=DYF(K)
 481   Y(K)=Y(K+1)+DYF(K)
       DY=Y(NY2)-Y(N)
       IF(DY.GE.DR)GO TO 490
      RS=RS+.005
       GO TO 475
 490   YRC=DR/DY
       DO 492 J=2,NY2
       K=N-J+1
 492   Y(K)=R1+(Y(K)-R1)*YRC
       DO 495  J=2,NY2
       K=N-J+1
       DYF(K)=Y(K)-Y(K+1)
 495   DYB(K+1)=DYF(K)
       DYF(N)=DYB(N)
       LY1=NY2-ND-3
       LY2=NY2+ND-1
       DDDY=(Y(LY1)-Y(LY2))/(LY2-LY1)
       LYY2=LY2-1
       DO 221 J=LY1,LYY2
       DYF(J)=DDDY
       DYB(J)=DYF(J-1)
 221   Y(J+1)=Y(J)-DDDY
       DYB(LY2)=DYF(LYY2)
      WRITE(6,5)RS,II
      GO TO 301
3600  DYF(NY2)=DYB(NY2)
      DYB(N)=DYF(1)
        DYF(N)=DYB(N)
      DO 505 J=2,NY21
      K=N-J+1
      DYB(K)=DYF(J)
 505  DYF(K)=DYB(K+1)
      DO 506 J=2,NY21
      K=N-J+1
 506  Y(K)=Y(K+1)+DYB(K+1)
 301  DO 303 J=1,N
      DYT(J)=DYB(J)+DYF(J)
 303  R(J)=(Y(J)-Y(N))/(R2-R1)
      DO 13 J=1,N
  13  YF(J)=Y(J)*XCONV
      WRITE(6,15)
  15  FORMAT('CY(J)')
      WRITE(6,60)(YF(K),K=1,N)
      WRITE(6,17)
  17  FORMAT('CR(J)')
      WRITE(6,60)(R(K),K=1,N)
      YF(1)=Y(1)+Y(2)
      YB(1)=YF(1)
      YB(N)=Y(N)+Y(N-1)
      YF(N)=YB(N)
```

```
      DO 9 J=2,NM1
      YB(J)=YF(J-1)
    9 YF(J)=Y(J)+Y(J+1)
      WRITE(6,60)(DYF(K),K=1,N)
      WRITE(6,60)(DYB(K),K=1,N)
      WRITE(6,60)(DYT(K),K=1,N)
   60 FORMAT(1X,10G13.5)
      PSB=(1.+RT+RT**2)/(DYF(1)*RT**2)
      PSC=-(1.+RT+RT**2)/(DYF(1)*(1.+RT)*RT**3)
      PSD=1./(DYF(1)*(1.+RT+RT**2)*RT**3)
      PSA=-PSB-PSC-PSD
      WRITE(6,60)PSA,PSB,PSC,PSD
      PTB=(1.+RS+RS**2)/(DYB(N)*RS**2)
      PTC=-(1.+RS+RS**2)/(DYB(N)*(1.+RS)*RS**3)
      PTD=1./(DYB(N)*(1.+RS+RS**2)*RS**3)
      PTA=-PTB-PTC-PTD
      WRITE(6,60)PTA,PTB,PTC,PTD
      RETURN
      END
      SUBROUTINE FDVF
C*************************FDVF*************************************************
C***CALCULATES FULLY DEVELOPED VELOCITY PROFILE FOR LAMINAR OR TURBULENT FLOW***
      COMMON/VMP/FI,XMASS,DELPT
      COMMON/TURB/XL(101),TA(101),TV(101),POUT(101),UST1,UST2,GCON,DD1,
     $DD2,AP,VDKC,XDIST,DUDYO,DUDYI,TAU1,TAU2
      COMMON/LATE/M,MM,N,NM1,NM2,NY,R1,R2,DYB(101),DYF(101),DYT(101),
     $Y(101),YF(101),YB(101),R(101)
      COMMON/MPVX/U1(101),U2(101),U3(101),V(101),EV(101),EK(101),EVF(101
     *),EVB(101),EKF(101),EKB(101),D1(101),D2(101),D3(101),C(101),NS,
     $ICOUNT,DELXF,DELXB,DELXT,DELPP,PDROP,PO,PP
      COMMON/DEL/JDEL,JDEL1,JDELC,DELMIN,DELTAI,DELTAO,MN,DXF,VJS,VJF,
     $DXFM,CEC
      COMMON/STUPID/LORT,NSM1,PSA,PSB,PSC,PSD,XCONV,S1,S2
        COMMON/HHHH/H1,H2,H3,H4,H5,H6,H7,H8,H9,H10
      COMMON/NAILA/THERK,CPVAR,DVAR,CVISC,DMEAN,CPMEAN,VMEAN,XKMEAN,
     $UO,VO,DC,TC,PSTART,HTK,CPCON
      COMMON/MF/DPD
      COMMON/XBIRTH/PREAD,PWRITE,STLF,XC1,XC2,DEL1,DEL2,UE,CHECK,RED
      DOUBLE PRECISION XX,XY,XU,XU1,XF1,XF,A1,A2,A3,A4,B1,B2,B3,B4,
     $F(101),          FOLT(101),TA1,TA2,G,DABS,XU2,XF2,XM,XPM,XNM,A,B,C1
     $,C2,C3,C4,DLOG
      DIMENSION DXX(101)
      IF(LORT.GT.0.)GO TO 1202
      C1=R1
      C2=R2
      B=((C1/C2)**2-1.)/DLOG(C1/C2)
      A=1.-B+C1*C1/(C2*C2)
      DO 1205 J=2,NM1
      C3=Y(J)
      C4=2.*(1.+B*DLOG(C3/C2)-C3*C3/(C2*C2))/A
 1205 U1(J)=C4
      GO TO 1201
 1202 CONTINUE
      JK=0
      I=-1
       X1=0.
      XU=0.
       XU1=0.
      IJ=0
         N4=N/4
```

```
      GF=AP*(R1/R2)**H4
      BB=VDKC
      CC=AP
      DO 101 J=1,N
  101 DXX(J)=DYB(J)
      DPD=-0.067/((R2-R1)*R5D**0.25)
      RM=(R1/R2)**.343
      RMM=(R1+RM*R2)/(1.+RM)
  200 DO 201 J=1,N
      K=N-J+1
      YYY=RMM-Y(K)
      IF(YYY.LT.0.)GO TO 202
  201   CONTINUE
  202 JDELI=K
      YR1=RMM-Y(K+1)
      YR2=Y(K)-RMM
      IF(YR1.LT.YR2)JDELI=K+1
       DELTAI=Y(JDELI)-R1
        DELTAO=R2-Y(JDELI)
      JJJJJ=JDELI
  203 JDELO=JDELI
      TA1=-DPD*(Y(JJJJJ)**2-R1**2)/(2.*R1)
      TA2=-DPD*(R2**2-Y(JJJJJ)**2)/(2.*R2)
      F(N)=TA1
      F(1)=-TA2
      FOUT(N)=0.
    9 IJ=IJ+1
         XX=F(1)
         XY=F(N)
      DO 102 JJ=1,NM1
      J=N-JJ+1
      A1=DXX(J)*G(Y(J),F(J),DPD,XX,XY,R1,R2,DELTAI,DELTAO,JDELI,J,BB,
     $CC,GF)
      B1=DXX(J)*F(J)
      B2=DXX(J)*(F(J)+A1/2.)
      A2=DXX(J)*G(Y(J)+DXX(J)/2.,F(J)+A1/2.,DPD,XX,XY,R1,R2,DELTAI,DELTA
     $O,JDELI,J,BB,CC,GF)
      B3=DXX(J)*(F(J)+A2/2.)
      A3=DXX(J)*G(Y(J)+DXX(J)/2.,F(J)+A2/2.,DPD,XX,XY,R1,R2,DELTAI,DELTA
     $O,JDELI,J,BB,CC,GF)
      A4=DXX(J)*G(Y(J)+DXX(J),F(J)+A3,DPD,XX,XY,R1,R2,DELTAI,DELTAO,JDEL
     $I,J,BB,CC,GF)
      B4=DXX(J)*(F(J)+A3)
      F(J-1)=F(J)+(A1+2.*A2+2.*A3+A4)/6.
  102 FOUT(J-1)=FOUT(J)+(B1+2.*B2+2.*B3+B4)/6.
      XO=FOUT(1)
      XF=F(N)
      YO=F(1)
      IF(IJ.NE.1)GO TO 901
      XF2=XF
      XO2=XO
  901 CONTINUE
      IF(IJ.LE.2)GO TO 441
         DO 438 J=N4,NM2
        X=FOUT(J)/FOUT(J+1)
        IF(X.GE.1.)GO TO 440
  438   CONTINUE
  440    JDELO=J
         JDELI=JDELO
          DELTAO=R2-Y(JDELO)
```

```
      DELTA1=Y(JDELI)-R1
 441  CONTINUE
      WRITE(6,29)XU,YC,XF,DPD,JDELI
  29  FORMAT(5X,4G13.5,I10)
      IF(DABS(XU).LT.1.D-04)GO TO 25
      IF(IJ.GE.LCRT)GO TO 25
      IF(I.GT.0)GO TO 7
      IF(XU)3,25,4
   3  F(N)=TA1*H3
      F(1)=-TA2*(2.-H3)
        I=1
      GO TO 9
   4  F(N)=TA1*(2.-H3)
      F(1)=-TA2*H3
      I=1
      GO TO 9
   7  CONTINUE
      F(N)=XF2-XU2*(XF2-XF)/(XU2-XU)
      XU2=XU
      XF2=XF
      GO TO 9
  25   DO 301 J=1,N
 301   U1(J)=POUT(J)
1201  CONTINUE
      SM1=0.0
      SU1=0.0
       NM2=N-2
      DO 704 J=1,NM2,2
      WF2=DYT(J+1)/DYF(J+1)*(DYT(J+1)/3.0-DYB(J+1)/2.0)
      WF1=DYT(J+1)**2.0/(2.0*DYB(J+1))-WF2*DYT(J+1)/DYB(J+1)
      WF0=DYT(J+1)-WF1-WF2
      SUM1=Y(J)
      SUM2=Y(J+1)
       SUM3=Y(J+2)
        SUM11=SUM1*U1(J)
        SUM22=SUM2*U1(J+1)
       SUM33=SUM3*U1(J+2)
         SU1=SU1+WF0*SUM1+WF1*SUM2+WF2*SUM3
 704  SM1=SM1+WF0*SUM11+WF1*SUM22+WF2*SUM33
      UMEAN=SM1/SU1
      RED=RED*UMEAN
      XMASS=XMASS*UMEAN
      WRITE(6,31)RED,XMASS
      WRITE(6,31)(U1(K),K=1,N)
  31    FORMAT(5X,10G12.4)
      IF(LCRT.LT.0.)RETURN
       WRITE(6,31)(F(K),K=1,N)
      TAU1=DABS(F(N))
      TAU2=DABS(F(1))
      WRITE(6,30)IJ,XU,TA1,TA2,UMEAN,XF,DPD,RED
      DD1=DSQRT(DABS(F(N)))
      DD2=DSQRT(DABS(F(1)))
      UST1=DD1*UC
      UST2=DD2*UC
       JJ=JDELI-1
       DO 90 J=1,JJ
          POUT(J)=U1(J)/DD2
90       F(J)=(R2-Y(J))*DD2
        DO 91 J=JDELI,N
          POUT(J)=U1(J)/DD1
```

```
91    F(J)=(Y(J)-R1)*DD1
      WRITE(6,31)(F(K),K=1,N)
        WRITE(6,31)(PCUT(K),K=1,N)
     U1(1)=0.
       U1(N)=0.
       DO 815 J=1,N
       U2(J)=U1(J)
815    U3(J)=U1(J)
         CALL VISC2
     WRITE(6,31)(TV(K),K=1,N)
     WRITE(6,31)(XL(K),K=1,N)
     WRITE(6,31)(EK(K),K=1,N)
30      FORMAT(5X,I4,5G13.5)
     RETURN
     END
      FUNCTION G(Y,F,DPD,X1,XF,R1,R2,DELTAI,DELTAO,JDELI,J,BB,CC,GF)
       COMMON/HHHH/H1,H2,H3,H4,H5,H6,H7,H8,H9,H10
     COMMON/TURB/XL(101),TA(101),TV(101),POUT(101),JST1,JST2,GCON,DD1,
    $DD2,AP,VDKC,XDIST,DUDYC,DUDYI,TAU1,TAU2
     DOUBLE PRECISION F,     X1,XF,DXL,XM,G,XP,XP1,XPF,XL1,XL2,XPM,
    $XNM,GF,DEXP,DABS,DSQRT,DD,DMIN1,DLOG,SSDD
     XPF=1.
       DXL=0.
     XL1=0.06*(R2-R1)
     J1=JDELI+1
      IF(J.GE.J1)GO TO 35
     DD=DSQRT(DABS(X1))
      XF=R2-Y
      XP1=XF*DD/CC
     IF(XP1.GT.7.)GO TO 59
     XPF=1.-DEXP(-XP1)
59   XL2=BB*XP*XPF
     XM=DMIN1(XL1,XL2)
      IF(XM.EQ.XL2)DXL=-BB*XPF-BB*XF*DD*(1.-XPF)/CC
      GO TO 40
35 CONTINUE
     DD=DSQRT(DABS(XF))
      XP=Y-R1
      XP1=XF*DD/GF
     IF(XP1.GT.7.)GO TO 69
     XPF=1.-DEXP(-XP1)
69 XL2=BB*XP*XPF
     XM=DMIN1(XL1,XL2)
      IF(XM.EQ.XL2)DXL=BB*XP*DD*(1.-XPF)/GF+BB*XPF
40 CONTINUE
     XPM=XM*XM/Y+2.*XM*DXL
     XNM=1.+2.*XM*XM*DABS(F)
     G=(DPD-F/Y-XPM*F*DABS(F))/XNM
     RETURN
     END
     SUBROUTINE PRESS
     DIMENSION SUM1(101),SUM2(101)
     COMMON/LATE/M,MM,N,NM1,NM2,NY,R1,R2,DYB(101),DYF(101),DYT(101),
    $Y(101),YF(101),YE(101),R(101)
     COMMON/MPVX/U1(101),U2(101),U3(101),V(101),EV(101),EK(101),EVF(101
    *),EVB(101),EKF(101),EKB(101),D1(101),D2(101),D3(101),C(101),NS,
    $ICOUNT,DELXF,DELXB,DELXT,DELPP,PDROP,PO,PP
     COMMON/VMP/PI,XMASS,DELPT
     COMMON/DEL/JDEL,JDELI,JDELO,DELMIN,DELTAI,DELTAO,MN,DXF,VJS,VJF,
    $DXFM,CCC
```

```
      COMMON/STUPID/LORT,NSM1,PSA,PSB,PSC,PSD,XCONV,S1,S2
      COMMON/UNM/FCON,GC,BETA,UGF,FDV
      COMMON/AHMADI/T1(101),T2(101),T3(101),TW2,TW1,JTDEL,TBTHIC,OORIN,
     $DTCYO,CTCYI,TCONV,XKCONV,TMEAN,XTMEAN,QCV,QCD,HAVE2,HAVE1
      COMMON/NAILA/THERK,CPVAR,DVAR,CVISC,DMEAN,CPMEAN,VMEAN,XKMEAN,
     $UC,VC,CO,TC,PSTART,HTK,CPCON
      COMMON/TURB/XL(101),TA(101),TV(101),POUT(101),JST1,JST2,GCON,DD1,
     $DD2,AP,VCKC,XDIST,DUDYO,DUDYI,TAU1,TAU2
      COMMON/HHHH/H1,H2,H3,H4,H5,H6,H7,H8,H9,H10
      SUMP1=0.0
      SUMP2=0.0
      IF(ICOUNT.GE.NS)GO TO 305
C     STANDARD EXPL EQNS
      U1(1)=U1(2)/(1.0+(1.0-U1(2)/U1(3))*DYF(1)/DYF(2))
      IF(U1(1).EQ.0.0)U1(1)=1.0E-50
      SUM1(1)=(DELXF*YF(1)*EVF(1)/(2.0*DYT(1)*DYF(1)))*(U1(2)/U1(1)-1.0)
        IF(FCON.GT.0..AND.OORIN.LT.0.)SUM1(1)=SUM1(1)-DELXF*UGF*BETA*(T1
     $(1)-T1(N))*TCONV*Y(1)/U1(1)
      IF(FCON.LT.0.0)SUM1(1)=SUM1(1)+DELXF*UGF*D1(1)*Y(1)/U1(1)
      SUM2(1)=-Y(1)/U1(1)
      IF(R1.EQ.0.0)GO TO 300
      U1(N)=U1(N-1)/(1.0+(1.0-U1(N-1)/U1(N-2))*DYB(N)/DYB(N-1))
      IF(U1(N).EQ.0.0)U1(N)=1.0E-50
      SUM1(N)=(DELXF*YB(N)*EVB(N)/(2.0*DYT(N)*DYB(N)))*(U1(N-1)/U1(N)-1.
     *0)
        IF(FCON.GT.0.0.AND.OORIN.GT.0.)SUM1(N)=SUM1(N)-DELXF*UGF*BETA*(T1
     $(N)-T1(1))*TCONV*Y(N)/U1(N)
      IF(FCON.LT.0.0)SUM1(N)=SUM1(N)+DELXF*UGF*D1(N)*Y(N)/U1(N)
      SUM2(N)=-Y(N)/U1(N)
      IF(ABS(DXF).NE.4.)GO TO 300
      SUM1(1)=0.0
      SUM2(1)=0.0
      SUM1(N)=0.0
      SUM2(N)=0.0
  300 CONTINUE
      DO 301 J=2,NM1
      PF=2.0*Y(J)*DYT(J)*DYF(J)*DYB(J)
      PA=PF*U1(J)
      PE1=DELXF*DYB(J)*YF(J)*EVF(J)*(U1(J+1)-U1(J))
      PB2=YB(J)*EVB(J)*DYF(J)*DELXF*(U1(J-1)-U1(J))
      VVPP=V(J)
      HP= VVPP*(U1(J)-U1(J-1))/DYB(J)
      IF(VVPP.LT.0.0)HP=VVPP*(U1(J+1)-U1(J))/DYF(J)
      PB3=-PF*DELXF*D1(J)*HP
      PB4=PF*D1(J)*U1(J)*U1(J)
      PC=-PF
      IF(FCON)30,35,40
   30 PT=PF*DELXF*UGF*D1(J)
      GO TO 45
   35 PT=0.0
      GO TO 45
   40 PT=PF*DELXF*FCONVC(BETA,UGF,TO,N,J)
   45 SUM1(J)=(PE1+PE2+PE3+PB4+PT)*Y(J)/PA
      SUM2(J)=PC*Y(J)/PA
  301 CONTINUE
      IF(R1.NE.0.0)GO TO 304
      SUM1(N)=0.0
      SUM2(N)=0.0
  304 CONTINUE
      U1(1)=0.0
```

```
      IF(R1.GT.0.0)U1(N)=0.0
      GO TO 311
  305 CONTINUE
C     C-F EQNS
      BBB=2.*DELXB/DELXT
      DEN1=DELXT*(DYB(1)*YF(1)*EVF(1)+DYF(1)*YB(1)*EVB(1))*BBB
      SUM1(1)=2.0*DELXT*DYB(1)*EVF(1)*YF(1)*U2(2)*D2(1)*Y(1)/DEN1
      IF(FCON.GT.0.0.AND.DORIN.LT.0.)SUM1(1)=SUM1(1)-4.*Y(1)*DYT(1)*DYF(
     $1)*DYB(1)*DELXT*UGF*BETA*(T2(1)-T2(N))*TCONV*D2(1)*Y(1)/DEN1
      IF(FCON.LT.0.0)SUM1(1)=SUM1(1)+4.0*Y(1)*DYT(1)*DYF(1)*DYB(1)*DELXT
     $*UGF*D2(1)*D2(1)*Y(1)/DEN1
      SUM2(1)=-4.0*DYT(1)*DYF(1)*DYB(1)*D2(1)*(Y(1)**2.0)/DEN1
      IF(R1.EQ.0.0)GO TO 306
      DENN=DELXT*(DYB(N)*YF(N)*EVF(N)+DYF(N)*YB(N)*EVB(N))*BBB
      SUM1(N)=2.0*DELXT*DYF(N)*EVB(N)*YB(N)*U2(N-1)*D2(N)*Y(N)/DENN
       IF(FCON.GT.0.0.AND.DORIN.GT.0.)SUM1(N)=SUM1(N)-4.*Y(N)*DYT(N)*DYF
     $(N)*DYB(N)*DELXT*UGF*BETA*(T2(N)-T2(1))*TCONV*D2(N)*Y(N)/DENN
      IF(FCON.LT.0.0)SUM1(N)=SUM1(N)+4.0*Y(N)*DYT(N)*DYF(N)*DYB(N)*DELXT
     $*UGF*D2(N)*D2(N)*Y(N)/DENN
      SUM2(N)=-4.0*DYT(N)*DYF(N)*DYB(N)*D2(N)*(Y(N)**2.0)/DENN
      IF(ABS(DXF).NE.4.)GO TO 321
      SUM1(1)=0.0
      SUM2(1)=0.0
      SUM1(N)=0.0
      SUM2(N)=0.0
      GO TO 321
  306 U2(N+1)=U2(N-1)
  321 CONTINUE
      AAA=DELXF/DELXT
      DO 307 J=2,NM1
      PF=4.0*Y(J)*DYT(J)*DYF(J)*DYB(J)
      PA1=PF* D2(J)*U2(J)
      PA2=DELXT*DYB(J)*YF(J)*EVF(J)*BBB
      PA3=DELXT*DYF(J)*YB(J)*EVB(J)*BBB
      VVFF=V(J)
      PB1=-PF*DELXT*D2(J)*VVPP*(U2(J+1)-U2(J-1))/DYT(J)
      PB2=2.0*DELXT*DYB(J)*EVF(J)*(U2(J+1)-AAA*U1(J))*YF(J)
      PB3=2.0*DELXT*DYF(J)*EVB(J)*(U2(J-1)-AAA*U1(J))*YB(J)
      PB4=PF*D2(J)*U1(J)*U2(J)
      PC=-PF
      IF(FCON)60,65,70
   60 PT=PF*DELXT*UGF*D2(J)
      GO TO 75
   65 PT=0.0
      GO TO 75
   70 PT=PF*DELXT*FCONVC(BETA,UGF,TC,N,J)
   75 SUM1(J)=(PB1+PB2+PB3+PB4+PT)*D2(J)*Y(J)/(PA1+PA2+PA3)
       IF(IABS(LCRT).EQ.9.)WRITE(6,90)PA1,PA2,PA3,PB1,PB2,PB3,PB4,PT
  307 SUM2(J)=PC*D2(J)*Y(J)/(PA1+PA2+PA3)
  311 CONTINUE
   90 FORMAT(5X,10G13.5)
       IF(IABS(LCRT).EQ.9.)WRITE(6,90)(SUM1(K),K=1,N)
       IF(IABS(LCRT).EQ.9.)WRITE(6,90)(SUM2(K),K=1,N)
      DO 309 J=1,NM2,2
      WF2=DYT(J+1)/DYF(J+1)*(DYT(J+1)/3.0-DYB(J+1)/2.0)
      WF1=DYT(J+1)**2.0/(2.0*DYB(J+1))-WF2*DYT(J+1)/DYB(J+1)
      WF0=DYT(J+1)-WF1-WF2
      SUMP1=SUMP1+WF0*SUM1(J)+WF1*SUM1(J+1)+WF2*SUM1(J+2)
  309 SUMP2=SUMP2+WF0*SUM2(J)+WF1*SUM2(J+1)+WF2*SUM2(J+2)
      DPPP=(SUMP1-XMASS/(2.0*PI))/SUMP2
```

```
      IF(ICOUNT.GE.NS)GO TO 371
      DELPP=DPPPP
      GO TO 381
  371 DELPT=DPPPP
      DELPP=DELXP*DELPT/DELXT
  381 PDROP=PDROP+DELPP
      PP=PO-PDROP
      XDPD=DELPP/DELXP
      IF(IABS(LORT).EQ.8)WRITE(6,90)DELTAO,DELTAI,XDPD,XDIST
       IF(IABS(LORT).EQ.9.)WRITE(6,90)SUMP1,SUMP2
      RETURN
      END
      SUBROUTINE UVEL
C*************************************UVEL*************************************
      COMMON/XBIRTH/PREAD,PWRITE,STLP,XC1,XC2,DEL1,DEL2,UE,CHECK,RED
      COMMON/MOX/JOI,UPC1,UPC2,UPC3
      COMMON/MOMENT/RETO,RETI,DISPTI,THETI,HHI,DISPTO,THETO,HHO
        COMMON/HHHH/H1,H2,H3,H4,H5,H6,H7,H8,H9,H10
      COMMON/NAILA/THERK,CPVAR,DVAR,CVISC,DMEAN,CPMEAN,VMEAN,XKMEAN,
     $UO,VO,DO,TO,PSTART,HTK,CPCON
      COMMON/LATE/M,MM,N,NM1,NM2,NY,R1,R2,DYB(101),DYF(101),DYT(101),
     $Y(101),YF(101),YE(101),R(101)
      COMMON/DEL/JDEL,JDELI,JDELO,DELMIN,DELTAI,DELTAO,MN,DXF,VJS,VJF,
     $DXFM,CCC
      COMMON/MPVX/U1(101),U2(101),U3(101),V(101),EV(101),EK(101),EVF(101
     *),EVE(101),EKF(101),EKB(101),D1(101),D2(101),D3(101),C(101),NS,
     $ICOUNT,DELXF,DELXB,DELXT,DELPP,PDROP,PO,PP
      COMMON/VMP/PI,XMASS,DELPT
      COMMON/STUPID/LORT,NSM1,PSA,PSB,PSC,PSD,XCONV,S1,S2
      COMMON/UMM/FCON,GC,BETA,UGF,FDV
      COMMON/AHMADI/T1(101),T2(101),T3(101),TW2,TW1,JTDEL,TBTHIC,GORIN,
     $DTDYC,DTDYI,TCONV,XKCONV,TMEAN,XTMEAN,QCV,QCD,HAVE2,HAVE1
C    STAND EXFL EQNS
      IF(ICOUNT.GE.NS)GO TO 403
      IF(CHECK.GT.0.)GO TO 999
      IF(ICOUNT.EQ.1)UPC1=UPC2
      GO TO 1000
  999 CONTINUE
      IF(ICOUNT.EQ.1.AND.FDV.LT.0.)JOI=10
      IF(FDV.GT.0.0)JOI=0
      IF(ICOUNT.EQ.1)UPC1=1.
 1000 CONTINUE
      IF(JOI.GT.1)UPC2=UPC1+DELPP/UPC1
      IF(JOI.GT.1)UDEL=0.995*UPC2
       UPC3=UPC2
      LJI=-1
      LJO=-1
      DO 401 JJJ=2,NM1
      IF(JOI.LE.1)GO TO 611
      II=-1
      IF(LJI.GT.0.AND.LJO.GT.0)GO TO 809
      IF(LJO.GT.0)GO TO 680
  611 J=JJJ
      JPL=J+1
      JML=J-1
  620 DBY=Y(JML)-Y(J)
      DFY=Y(J)-Y(JPL)
      DTY=Y(JML)-Y(JPL)
      UF=2.0*Y(J)*DTY*DFY*DBY
      UA=UF*D1(J)*U1(J)
```

```
      UB1=DELXF*DBY*(Y(J)+Y(JPL))*(EV(J)+EV(JPL))*(U1(JPL)-U1(J))
      UB2=DELXF*DFY*(Y(J)+Y(JML))*(EV(J)+EV(JML))*(U1(JML)-U1(J))
      VVPP=V(J)
      HV=VVPP*(U1(J)-U1(JML))/DBY
      IF(VVPP.LT.0.0)HV=VVPP*(U1(JPL)-U1(J))/DFY
      UB3=-UF*DELXF*D1(J)*HV
      UB4=UF*D1(J)*U1(J)*U1(J)
      UC=-UF
      IF(FCON)30,35,40
   30 UT=UF*DELXF*UGF*D1(J)
      GO TO 45
   35 UT=0.0
      GO TO 45
   40 UT=UF*DELXF*FCONVC(BETA,UGF,TO,N,J)
   45 U2(J)=(UB1+UB2+UB3+UB4+UT)/UA-DELPF*UC/UA
      U3(J)=U2(J)
      IF(JOI.LE.1)GO TO 401
      IF(II.GT.0)GO TO 688
      IF(U2(J).GE.UDEL)LJO=J
      IF(LJO.GT.0)UUO=U3(LJO)
  680 IF(LJI.GT.0)GO TO 401
      J=N-JJJ+1
      JPL=J-1
      JML=J+1
      II=1
      GO TO 620
  688 IF(U2(J).GE.UDEL)LJI=J
      IF(LJI.GT.0)UUI=U3(LJI)
  401 CONTINUE
      IF(JOI.LE.1)GO TO 434
      GO TO 801
  403 CONTINUE
C     D-F EQNS
      IF(FDV.GT.0.)JOI=0
      IF(JOI.GT.1)UPC3=UPC1+DELPT/UPC1
      IF(JOI.GT.1)UDEL=0.995*UPC3
      LJI=-1
      LJO=-1
      AAA=DELXF/DELXT
      BBB=2.*DELXB/DELXT
      DO 405 JJJ=2,NM1
      IF(JOI.LE.1)GO TO 711
      II=-1
      IF(LJI.GT.0.AND.LJO.GT.0)GO TO 809
      IF(LJO.GT.0)GO TO 780
  711 J=JJJ
      JPL=J+1
      JML=J-1
  720 DBY=Y(JML)-Y(J)
      DFY=Y(J)-Y(JPL)
      DTY=Y(JML)-Y(JPL)
      UF=4.0*Y(J)*DTY*DFY*DBY
      UA1=UF*D2(J)*U2(J)
      UA2=DELXT*DBY*(Y(J)+Y(JPL))*(EV(J)+EV(JPL))*BBB
      UA3=DELXT*DFY*(Y(J)+Y(JML))*(EV(J)+EV(JML))*BBB
      VVPP=V(J)
      UB1=-UF*D2(J)*DELXT*VVPP*(U2(JPL)-U2(JML))/DTY
      UB2=2.0*DELXT*DBY*(EV(J)+EV(JPL))*(Y(J)+Y(JPL))*(U2(JPL)-AAA*U1(J)
     $)
      UB3=2.0*DELXT*DFY*(EV(J)+EV(JML))*(Y(J)+Y(JML))*(U2(JML)-AAA*U1(J)
```

```
     $)
      UB4=UF*D2(J)*U1(J)*U2(J)
      UC=-UF
      IF(FCCN)60,65,70
   60 UT=UF*DELXT*UGF*D2(J)
      GO TO 75
   65 UT=0.0
      GO TO 75
   70 UT=UF*DELXT*FCCNVC(BETA,UGF,TO,N,J)
   75 U3(J)=(UB1+UB2+UB3+UB4+UT)/(UA1+UA2+UA3)-DELPT*UC/(UA1+UA2+UA3)
      IF(JOI.LE.1)GO TO 405
      IF(II.GT.0)GO TO 785
      IF(U3(J).GE.UDEL)LJC=J
      IF(LJC.GT.0)UUC=U3(LJC)
  780 IF(LJI.GT.0)GO TO 405
      J=N-JJJ+1
      JPL=J-1
      JML=J+1
      II=1
      GO TO 720
  785 IF(U3(J).GE.UDEL)LJI=J
      IF(LJI.GT.0)UUI=U3(LJI)
      GO TO 405
  405 CONTINUE
      IF(JOI.LE.1)GO TO 434
  801 IF(LJI.EQ.LJO)U3(LJI)=(UUI+UUO)/2.
  809 JDELI=LJI
      JDELC=LJC
      JOI=JDELI-JDELC
      DELTAI=Y(JDELI)-R1
      DELTAO=R2-Y(JDELC)
      DELMIN=AMAX1(DELTAI,DELTAO)
      IF(JOI.LE.1)GO TO 407
      UU=(UUI+UUO)/2.
      L1=JDELC+1
      L2=JDELI-1
      DO 811 J=L1,L2
      IF(ICOUNT.LT.NS)U2(J)=UPC2
  811 U3(J)=UPC3
      IF(ICOUNT.NE.NSM1)UPC1=UPC2
      IF(ICOUNT.GE.NS)UPC2=UPC3
      GO TO 407
  434 DO 438 J=2,NM2
      K=N-J+1
      IF(JDELO.LT.0.0)GO TO 436
      X=U3(J)/U3(J+1)
      IF(X.GE..9999)JDELC=-J
  436 IF(JDELI.LT.0.0)GO TO 437
      Z=U3(K)/U3(K-1)
      IF(Z.GE..9999)JDELI=-K
  437 IF((JDELI.LT.0.0).AND.(JDELO.LT.0.0))GO TO 439
  438 CONTINUE
  439 JDELI=IABS(JDELI)
      JDELC=IABS(JDELO)
      DELTAI=Y(JDELI)-R1
      DELTAO=R2-Y(JDELO)
      DELMIN=AMIN1(DELTAI,DELTAO)
  407 CONTINUE
      JOI=JDELI-JDELC
      RETURN
```

```
      END
      FUNCTION FCONVC(BETA,UGF,TC,N,J)
      COMMON/MPVX/U1(101),U2(101),U3(101),V(101),EV(101),EK(101),EVF(101
     *),EVB(101),EKF(101),EKB(101),D1(101),D2(101),D3(101),C(101),NS,
     $ICOUNT,DELXF,DELXB,DELXT,DELPP,PDRCP,PC,PP
      COMMON/AHMADI/T1(101),T2(101),T3(101),TW2,TW1,JTDEL,TBTHIC,DORIN,
     $DTDYO,DTDYI,TCONV,XKCONV,TMEAN,XTMEAN,QCV,QCD,HAVE2,HAVE1
      IF(ICOUNT.EQ.1)T2(J)=T1(J)
      FCONVC=UGF*(1.-BETA*(T2(J)*TCONV-TC))
      RETURN
      END
      SUBROUTINE RADVEL
C*************************RADVEL*********************************************
      COMMON/NAILA/THERK,CPVAR,DVAR,CVISC,DMEAN,CPMEAN,VMEAN,XKMEAN,
     $UC,VC,DO,TC,PSTART,HTK,CPCON
      COMMON/LATE/M,MM,N,NM1,NM2,NY,R1,R2,DYB(101),DYF(101),DYT(101),
     $Y(101),YF(101),YB(101),R(101)
      COMMON/TURB/XL(101),TA(101),TV(101),POUT(101),UST1,UST2,GCON,DD1,
     $DD2,AP,VDKC,XDIST,DUDYO,DUDYI,TAU1,TAU2
      COMMON/MPVX/U1(101),U2(101),U3(101),V(101),EV(101),EK(101),EVF(101
     *),EVB(101),EKF(101),EKB(101),D1(101),D2(101),D3(101),C(101),NS,
     $ICOUNT,DELXF,DELXB,DELXT,DELPP,PDRCP,PO,PP
      COMMON/DEL/JDEL,JDELI,JDELO,DELMIN,DELTAI,DELTAC,MN,DXF,VJS,VJF,
     $DXFM,CCC
      COMMON/MTF/XM(101),XK(101),HTC
      DELXX=DELXT
      IF(ICOUNT.LT.NS)DELXX=DELXF
      KI=-1
      KO=-1
      JOI=JDELI-JDELO
      JC=JDELO+JOI/2
      JI=JC+1
      IF(HTC.LT.0.)JO=JDELO+1
      IF(HTC.LT.0.)JI=JDELI-1
      DO 50 JJJ=1,N
      IF(KI.GT.0.AND.KO.GT.0)GO TO 750
      ILL=-1
      IF(KO.GT.0)GO TO 3001
 3000 J=JJJ
      JLL=J+1
      IF(JOI.GE.2.AND.JLL.EQ.JO)KO=1
      IF(JOI.LT.2.AND.JLL.EQ.JDELO)KO=1
 3002 VA1=(Y(J)+Y(JLL))*(Y(J)-Y(JLL))  *(D3(JLL)*U3(JLL)+D3(J)*U3(J))
      VA2=(Y(J)+Y(JLL))*(Y(J)-Y(JLL))  *(D1(JLL)*U1(JLL)+D1(J)*U1(J))
      VA3=4.0*DELXX*D3(J)*V(J)*Y(J)
      VB1=4.0*DELXX*D3(JLL)*Y(JLL)
      V(JLL)=(VA3+VA2-VA1)/VB1
      IF(JOI.EQ.0.AND.KI.GT.0)VVI=V(JLL)
      IF(ILL.GT.0)GO TO 50
      IF(JOI.EQ.0.AND.KO.GT.0)VVO=V(JLL)
 3001 J=N-JJJ+1
      IF(KI.GT.0)GO TO 50
      ILL=1
      JLL=J-1
      IF(JOI.GT.2.AND.JLL.EQ.JI)KI=1
      IF(JOI.LE.2.AND.JLL.EQ.JDELI)KI=1
      GO TO 3002
   50 CONTINUE
  750 CONTINUE
      IF(JOI.EQ.0)V(JDELI)=(VVI+VVO)/2.
```

```
      RETURN
      END
      SUBROUTINE VISC2
C**********************VISC2*************************************************
C     CALCULATES TURBULENT DIFFUSIVITIES USING LENGTH SCALE MODEL
C     CAN ALSO USE K-L MODEL
C     BRDGING CAN BE USED ONLY WITH L MODEL FOR FULLY DEVELOPED FLOW
      COMMON/XKEN/XKN1(101),XKN2(101),XKN3(101),PK(101),KOI,NJ1,NJ2,XDH
      COMMON/TRANS/XTR1,XTR2,XTRE1,XTRE2,REXTR1,REXTR2,XLMDA1,XLMDA2
      COMMON/MUX/JCI,UPC1,UPC2,UPC3
      COMMON/AHMAD1/T1(101),T2(101),T3(101),TW2,TW1,JTDEL,TBTHIC,DORIN,
     $DTDYC,DTDYI,TCONV,XKCONV,TMEAN,XTMEAN,QCV,QCD,HAVE2,HAVE1
      COMMON/MTF/XM(101),XK(101),HTC
      COMMON/UMM/FCON,GG,BETA,UGF,FDV
        COMMON/HHHH/H1,H2,H3,H4,H5,H6,H7,H8,H9,H10
      COMMON/TURB/XL(101),TA(101),TV(101),POUT(101),UST1,UST2,GCON,DD1,
     $DD2,AP,VDKC,XDIST,DUDYC,DUDYI,TAU1,TAU2
      COMMON/LATE/M,MM,N,NM1,NM2,NY,R1,R2,DYB(101),DYF(101),DYT(101),
     $Y(101),YF(101),YB(101),R(101)
      COMMON/MPVX/U1(101),U2(101),U3(101),V(101),EV(101),EK(101),EVF(101
     *),EVB(101),EKF(101),EKB(101),D1(101),D2(101),D3(101),C(101),NS,
     $ICOUNT,DELXF,DELXB,DELXT,DELPP,PDROP,PC,PP
      COMMON/DEL/JDEL,JDELI,JDELO,DELMIN,DELTAI,DELTAO,MN,DXF,VJS,VJF,
     $DXFN,CCC
      COMMON/STUPID/LORT,NSM1,PSA,PSB,PSC,PSD,XCONV,S1,S2
      COMMON/NAILA/THERK,CPVAR,DVAR,CVISC,DMEAN,CPMEAN,VMEAN,XKMEAN,
     $UG,VG,DG,TC,PSTART,HTK,CPCON
      COMMON/XBIRTH/PREAD,PWRITE,STLF,XC1,XC2,DEL1,DEL2,UE,CHECK,RED
      SSSS=0.1E4
      GAMAT1=1.
      GAMAT2=1.
      IF(FDV.GT.0.)GO TO 903
      IF(XTR1.LT.0..AND.XTR2.LT.0.)GO TO 4640
      IF(XDIST.GT.ABS(XTRE1).AND.XDIST.GT.ABS(XTRE2))GO TO 4640
      IF(XTR1.GE.0..OR.XTR2.GE.0.)CALL GMTRAN(XDIST,U3(JDELO),
     $GAMAT1,GAMAT2,XM(JDELI),XM(JDELO),D3(JDELI),D3(JDELO),DG,VG)
4640  IF(XC1.LT.0.)GO TO 901
      XC1=XC1+DELXF*XC1*UST1/(H3*UE*DEL1*DEL1*UC)*(DEL1-XC1)
      XC2=XC2+DELXF*XC2*UST2/(H3*UE*DEL2*DEL2*UC)*(DEL2-XC2)
      XL1=H2*XC1
      XL11=H2*XC2
      IF(JCI.GT.0)GO TO 903
       XL1=(XL1+XL11)/2.
      XL11=XL1
      GO TO 903
901   XL1=.085*DELTAI
      XL11=.085*DELTAO
      XC2=XL11/H2
      XC1=XL1/H2
 903  CONTINUE
      IF(ICOUNT.LT.1)GO TO 1001
      UST1=SQRT(GCON*TAU1/(D3(N)*DC))
      UST2=SQRT(GCON*TAU2/(D3(1)*DC))
      DD1=XCONV*UST1*D3(N)*DC/(XM(N)*VG)
      DD2=XCONV*UST2*D3(1)*DC/(XM(1)*VG)
      IF(FDV.GT.0.)GO TO 1001
      GO TO 1002
1001  XL1=H2*(R2-R1)/2.
      XL11=XL1
1002  CONTINUE
```

```
      IF(H7.LT.2.)GO TO 8005
      DO 8160 J=1,N
8160  TA(J)=XL(J)
8005  CONTINUE
      JK=-1
      KJ=-1
      JM=-1
      JN=-1
      IF(FDV.GT.0.)JM=1
      IF(FDV.GT.0.)JN=1
      DO 410 J=2,NM1
      IF(KJ.GT.0.AND.JK.GT.0)GO TO 411
      IF(KJ.GT.0)GO TO 401
      K=N-J+1
      R1K=Y(K)-R1
      Y1P=R1K*DD1
      AP1=AP*(R1/R2)**P4
      XL2=VOKC*R1K*(1.-EXP(-Y1P/AP1))
      XL(K)=AMIN1(XL1,XL2)
      IF(XTR1.GE.0.)GO TO 400
      IF(JM.GT.0)GO TO 400
      IF(Y1P.LE.50..AND.XL2.GT.XL1)GO TO 333
      GO TO 400
 333  XL1=VOKC*(1.-EXP(-50./AP1))*50./DD1
      XL(K)=XL2
      JM=1
      XC1=0.085*DELTAI/H2
 400  IF(K.LE.JDELI.OR.XL(K).EQ.XL1)KJ=K
 401  IF(JK.GT.0)GO TO 410
      R2J=R2-Y(J)
      Y2P=R2J*DD2
      XL2=VOKC*R2J*(1.0-EXP(-Y2P/AP))
      XL(J)=AMIN1(XL11,XL2)
      IF(XTR2.GE.0.)GO TO 409
      IF(JN.GT.0)GO TO 409
      IF(Y2P.LE.50..AND.XL2.GT.XL11)GO TO 433
      GO TO 409
 433  XL11=VOKC*(1.-EXP(-50./AP))*50./DD2
      XL(J)=XL2
      JN=1
      XC2=0.085*DELTAO/H2
 409  IF(J.GE.JDELO.OR.XL(J).EQ.XL11)JK=J
 410  CONTINUE
 411  JK1=JK+1
      KJ1=KJ-1
      DO 418 J=JK1,JDELO
 418  XL(J)=XL(JK)
      DO 419 J=JDELI,KJ1
 419  XL(J)=XL(KJ)
      XL(1)=0.
      XL(N)=0.
      IF(JDI.LE.1)GO TO 435
      JJI=JDELI-1
      JJO=JDELO+1
      XLM=(XL(JK)+XL(KJ))/2.
      DO 430 J=JJO,JJI
 430  XL(J)=XLM
 435  CONTINUE
      DO 431 J=2,NM1
 431  POUT(J)=C3(J)*XL(J)*XL(J)*ABS((U3(J+1)-U3(J-1))/DYT(J))
```

```
      PCUT(1)=0.0
      PCUT(N)=0.0
      IF(H7.LT.2.)GO TO 5000
      IF(KCI.LE.1)GO TO 3500
      XKG=H1*U3(JDELC+1)**2
 3500 LJI=-1
      LJC=-1
      AAA=DELXF/DELXT
      BBB=2.*DELXB/DELXT
      NJK1=NJ1-1
      NJK2=NJ2+1
      DO 405 JJJ=NJK2,NJK1
      IF(KCI.LE.1)GO TO 711
      II=-1
      IF(LJI.GT.0.AND.LJC.GT.0)GO TO 801
      IF(LJO.GT.0)GO TO 780
  711 J=JJJ
      JPL=J+1
      JML=J-1
  720 DBY=Y(JML)-Y(J)
      DFY=Y(J)-Y(JPL)
      DTY=Y(JML)-Y(JPL)
      EF=4.*Y(J)*DTY*DFY*DBY
      EA1=EF*D2(J)*U2(J)
      EA2=DELXT*DBY*(Y(J)+Y(JPL))*(PK(J)+PK(JPL))*BBB
      EA3=DELXT*DFY*(Y(J)+Y(JML))*(PK(J)+PK(JML))*BBB
      VVPP=V(J)
      EB1=-EF*C2(J)*DELXT*VVPP*(XKN2(JPL)-XKN2(JML))/DTY
      EB2=2.*DELXT*DBY*(Y(J)+Y(JPL))*(PK(J)+PK(JPL))*(XKN2(JPL)-AAA*
     $XKN1(J))
      EB3=2.*DELXT*DFY*(Y(J)+Y(JML))*(PK(J)+PK(JML))*(XKN2(JML)-AAA*
     $XKN1(J))
      EB4=EF*D2(J)*U2(J)*XKN1(J)
      XKKK=SQRT((DBY*XKN2(JPL)+DFY*XKN2(JML))/DTY)
      EG=-EF*DELXF*D2(J)*STLF*XKN1(J)*XKKK/TA(J)
      ET=EF*DELXB*D2(J)*STLF*XKKK/TA(J)
      ET1=EF*DELXT*TV(J)*(ABS(U2(JPL)-U2(JML))/DTY)**2
      XKN3(J)=(EB1+EB2+EB3+EB4+EG+ET1)/(EA1+EA2+EA3+ET)
      IF(KCI.LE.1)GO TO 405
      IF(II.GT.0)GO TO 785
      IF(XKN3(J).LE.XKG)LJO=J
      IF(LJO.GT.0)XKN3(J)=XKG
      IF(LJO.GT.0)EEO=XKN3(LJO)
  780 IF(LJI.GT.0)GO TO 405
      J=NJK2+NJK1-JJJ
      JPL=J-1
      JML=J+1
      II=1
      GO TO 720
  785 IF(XKN3(J).LE.XKG)LJI=J
      IF(LJI.GT.0)XKN3(J)=XKG
      IF(LJI.GT.0)EEI=XKN3(LJI)
  405  CONTINUE
      IF(KCI.LE.1)GO TO 407
      IF(LJI.EQ.LJO)XKN3(LJI)=(EEI+EEO)/2.
  801 KDELI=LJI
      KDELO=LJO
      KCI=KDELI-KDELO
      IF(KCI.LE.1)GO TO 407
      L1=KDELO+1
```

```
      L2=KDELI-1
      DO 811 J=L1,L2
  811 XKN2(J)=XKC
  407 XKN2(NJ1)=   (XL(NJ1)*ABS(U3(NJ1+1)   U2(NJ1 1))/(DY1(NJ1)*5555
     $**(1./3.))**2
      XKN2(NJ2)=   (XL(NJ2)*ABS(U3(NJ2+1)-U3(NJ2-1))/(DY1(NJ2)*5555
     $**(1./3.))**2
      DO 4400 J=NJK2,NJK1
      XKN1(J)=XKN2(J)
      XKN2(J)=XKN3(J)
 4400 POUT(J)=STLF**(1./3.)*U3(J)*XKN3(J)**0.5*XL(J)
      XKN1(NJ1)=XKN2(NJ1)
      XKN1(NJ2)=XKN2(NJ2)
      XKN2(NJ1)=XKN3(NJ1)
      XKN2(NJ2)=XKN3(NJ2)
 5000 CONTINUE
      DO 432 J=2,NM1
  432 TV(J)=0.5*(POUT(J)+(DYB(J)*POUT(J+1)+DYF(J)*POUT(J-1))/DYT(J))
      TV(1)=0.
      TV(N)=0.
      DO 2331 J=2,JDELO
 2331 TV(J)=TV(J)*GAMAT
      DO 2333 J=JDELI,NM1
 2333 TV(J)=TV(J)*GAMAT1
      IF(H7.NE.-2..AND.REV.LT.0.)GO TO 8890
C       CHECKING FOR FULLY DEVELOPED FLOW
      JBO=-1
      JB1=-1
      JKOM=JDELI+6
      DO 9981 J=2,NM1
      IF(JBO.GT.0)GO TO 7897
      IF(TV(J).LE.TV(J-1))JBO=J-1
 7897 IF(J.LE.JKOM)GO TO 9981
      IF(JB1.GT.0)GO TO 9981
      IF(TV(J).LT.TV(J-1))JB1=J-2
 9981 CONTINUE
      DELY=(TV(JBO-1)-TV(JB1+1))/(Y(JBO-1)-Y(JB1+1))
      DO 9009 J=JBO,JB1
 9009 TV(J)=TV(JBO-1)+DELY*(Y(J)-Y(JBO-1))
 8890 CONTINUE
      DO 521 J=2,NM1
      EV(J)=TV(J)+XM(J)
  521 TA(J)=EV(J)*(U3(J+1)-U3(J-1))/DYT(J)
      IF(H7.LT.0.)GO TO 6000
      IF(H7.GE.2.)GO TO 9500
      IF(XDIF.LT.0.3)GO TO 6000
      Y1P=(Y(JDELI)-R1)*CD1
      Y2P=(R2-Y(JDELI))*CD2
      IF(Y1P.LT.150..OR.Y2P.LT.150.)GO TO 6000
      H7=H7+1.
      XKC=H1*U3(JDELI+1)**2
      IF(H7.GT.1.)GO TO 3001
      NJ2=-1
      NJ1=-1
      DO 7001 J=1,JDELO
      Y2P=(R2-Y(J))*CD2
      IF(Y2P.GE.70.)GO TO 7002
 7001 CONTINUE
 7002 NJ2=J
      DO 7003 J=JDELI,N
```

```
      Y1P=(Y(J)-R1)*CC1
      IF(Y1P.LE.70.)GC TC 7004
 7003 CCNTINUE
 7004 NJ1=J
      WRITE(6,1108)NJ1,NJ2
 1108 FCRMAT(5X,'AB',5I1C)
      DC 3005 J=2,NM1
      XKN1(J)=POUT(J)*ABS(U3(J+1)-U3(J-1))/(DYT(J)*SSSS**(2./3.)*D3(J))
 3005 IF(XKN1(J).LT.XKG)XKN1(J)=XKG
      KCI=10
      XKN1(1)=0.
      XKN1(N)=0.
      XKN2(1)=0.
      XKN2(N)=0.
      XKN3(1)=0.
      XKN3(N)=0.
      PK(1)=0.
      PK(N)=0.
      WRITE(6,4900)(XKN1(K),K=1,NM1)
 4900 FCRMAT(10G13.5)
      GC TC 5500
 3001 DC 3006 J=2,NM1
      XKN2(J)=POUT(J)*ABS(U3(J+1)-U3(J-1))/(DYT(J)*SSSS**(2./3.)*D3(J))
      IF(XKN2(J).LT.XKG)XKN2(J)=XKG
 3006 XKN3(J)=XKN2(J)
      WRITE(6,4900)(XKN2(K),K=1,NM1)
 5500 DC 5600 J=NJ2,NJ1
 5600 PK(J)=XM(J)+TV(J)/1.47
 6000 CCNTINUE
      IF(ICCUNT.LT.1)GC TO 20
      TA(1)=TAU2*CCCN/(DC*UC**2)
      TA(N)=-TAU1*TA(1)/TAU2
         GC TC 21
   20    TA(N)=TAU1
         TA(1)=TAU2
   21    CCNTINUE
      IF(HTC.LT.0.)GC TC 500
      DC 502 J=2,NM1
      EK(J)=XK(J)+TV(J)*C(J)/HTC
  502 CCNTINUE
  500 CCNTINUE
      IF(JCI.GT.1)UE=UPC3
      IF(JDI.LE.1)UE=U3(JDELC)
      DEL1=DELTAI
      DEL2=DELTAC
      RETURN
      END
      SUBRCUTINE TRANS1(REX,RETI,RETC,XDIST,OXDIST,H1)
C*********************TRANSITION CALCULATICNS**********************************
      COMMCN/TRANS/XTR1,XTR2,XTRE1,XTRE2,REXTR1,REXTR2,XLMDA1,XLMDA2
      IF(REX.LT.H1)RETURN
      RTHTR=1.174*(1.+22400./REX)*REX**0.46
      IF(XTR1.GT.0.)GC TC 10
      RTHR =RETI /RTHTR
      IF(RTHR .GE.0.99)XTR1=XDIST
      IF(XTR1.GT.0.)REXTR1=REX
      IF(XTR1.GT.0.)WRITE(6,40)OXDIST,REXTR1
   40 FCRMAT(10X,'TRANSITICN AT  INNER WALL =',2G15.6)
   10 IF(XTR2.GT.0.)RETURN
      RTHR =RETO /RTHTR
```

```
      IF(RTHR.GE.0.99)XTR2=XDIST
      IF(XTR2.GT.0.)REXTR2=REX
      IF(XTR2.GT.0.)WRITE(6,50)OXDIST,REXTR2
   50 FORMAT(10X,'TRANSITION AT OUTER WALL =',2G15.6)
      RETURN
      END
      SUBROUTINE TRANS2(REX,RETI,RETO,XDIST,OXDIST)
      COMMON/TRANS/XTR1,XTR2,XTRE1,XTRE2,REXTR1,REXTR2,XLMDA1,XLMDA2
      IF(XTRE1.GT.0.)GO TO 10
      XTRE1=XTR1+5.*(XDIST/REX)*REXTR1**0.8
   10 IF(XTRE2.GT.0.)RETURN
      XTRE2=XTR2+5.*(XDIST/REX)*REXTR2**0.8
      RETURN
      END
       SUBROUTINE GMTRAN(XDIST,UE,GAMAT1,GAMAT2,XME1,XME2,DE1,DE2,
     $DC,VC)
      COMMON/TRANS/XTR1,XTR2,XTRE1,XTRE2,REXTR1,REXTR2,XLMDA1,XLMDA2
      GAMAT1=0.
      GAMAT2=0.
      IF(XTR1.EQ.0.)GO TO 22
      IF(XDIST.GT.XTRE1)GO TO 22
      IF(XLMDA1.LT.0.)XLMDA1=(XTRE1-XTR1)*0.2115
      GAMAT1=1.-EXP(-0.412*((XDIST-XTR1)/XLMDA1)**2)
   22 IF(XTR2.EQ.0.)RETURN
      IF(XDIST.GT.XTRE2)RETURN
      IF(XLMDA2.LT.0.)XLMDA2=(XTRE2-XTR2)*0.2115
      GAMAT2=1.-EXP(-0.412*((XDIST-XTR2)/XLMDA2)**2)
      RETURN
      END
      SUBROUTINE GMTRAN(XDIST,UE,GAMAT1,GAMAT2,XME1,XME2,DE1,DE2,
     $DC,VC)
      COMMON/TRANS/XTR1,XTR2,XTRE1,XTRE2,REXTR1,REXTR2,XLMDA1,XLMDA2
      GAMAT1=0.
      IF(XDIST.LE.XTR1)GO TO 10
      IF(XLMDA1.LT.0.)XLMDA1=(XTRE1-XTR1)*0.2115
      GAMAT1=1.-EXP(-0.412*((XDIST-XTR1)/XLMDA1)**2)
   10 WRITE(6,7)XLMDA1,GAMAT1,XTR1,XTRE1
    7 FORMAT(4G13.5)
      RETURN
      END
      SUBROUTINE VPROP
C*************************VARIABLE PROPERTIES************************************
      COMMON/VMP/PI,XMASS,DELPT
      COMMON/TURB/XL(101),TA(101),TV(101),POUT(101),UST1,UST2,GCON,DD1,
     $DD2,AP,VDKC,XDIST,DUDYO,DUDYI,TAU1,TAU2
      COMMON/MTF/XM(101),XK(101),HTC
      COMMON/AHMADI/T1(101),T2(101),T3(101),TW2,TW1,JTDEL,TBTHIC,DORIN,
     $DTDYO,DTDYI,TCONV,XKCONV,TMEAN,XTMEAN,QCV,QCD,HAVE2,HAVE1
      COMMON/UMM/FCON,GG,BETA,UGF,FDV
      COMMON/STUFID/LORT,NSM1,PSA,PSB,PSC,PSD,XCONV,S1,S2
      COMMON/NAILA/THERK,CPVAR,DVAR,CVISC,DMEAN,CPMEAN,VMEAN,XKMEAN,
     $UC,VO,CO,TC,PSTART,HTK,CPCON
         COMMON/HPPH/P1,P2,H3,H4,H5,H6,H7,H8,H9,H10
      COMMON/LATE/M,MM,N,NM1,NM2,NY,R1,R2,DYB(101),DYF(101),DYT(101),
     $Y(101),YF(101),YB(101),R(101)
      COMMON/MPVX/U1(101),U2(101),U3(101),V(101),EV(101),EK(101),EVF(101
     *),EVB(101),EKF(101),EKB(101),D1(101),D2(101),D3(101),C(101),NS,
     $ICOUNT,DELXF,DELXB,DELXT,DELPP,PDROP,PC,PF
      COMMON/XBIRTH/PREAD,PWRITE,STLF,XC1,XC2,DEL1,DEL2,UE,CHECK,RED
      IJ=N-JTDEL+1
```

```
      IF(CORIN.LT.0.)IJ=JTDEL
      IF(CVISC.LT.0.)GO TO 51
      VMEAN=VISC(TMEAN,TCONV,TO,VO)*VC
      DO 1 J=1,N
      IF(CORIN.NE.0..AND.J.GT.IJ)GO TO 51
      K=N-J+1
      IF(CORIN.LE.0.)K=J
    1 XM(K)=VISC(T3(K),TCONV,TO,VO)
   51 IF(THERK.LT.0.)GO TO 101
      XKMEAN=THCNL(TMEAN,TCONV,TC,XKCONV)*XKCONV
      DO 55 J=1,N
      IF(CORIN.NE.0..AND.J.GT.IJ)GO TO 101
      K=N-J+1
      IF(CORIN.LE.0.)K=J
   55 XK(K)=THCNL(T3(K),TCONV,TC,XKCONV)
  101 IF(DVAR.LT.0.)GO TO 201
      DMEAN=RHO(TMEAN,TCONV,TC,DO)*DO
      DO 110 J=1,N
      IF(CORIN.NE.0..AND.J.GT.IJ)GO TO 201
      K=N-J+1
      IF(CORIN.LE.0.)K=J
  110 D3(K)=RHO(T3(K),TCONV,TC,DO)
  201 IF(CPVAR.LT.0.)GO TO 301
      CPMEAN=CP(TMEAN,TCONV,TO,CPCON)*CPCON
      DO 251 J=1,N
      IF(CORIN.NE.0..AND.J.GT.IJ)GO TO 301
      K=N-J+1
      IF(CORIN.LE.0.)K=J
  251 C(K)=CP(T3(K),TCONV,TO,CPCON)
  301 CONTINUE
      IF(FCON.NE.0.)BETA=FBETA(TMEAN,TCONV,TC)
      PR=VMEAN*CPMEAN/XKMEAN
      REO=2.*XMASS*VC/(PI*(R1+R2)*VMEAN)
      IF(LORT.LT.0)GO TO 501
      EV(1)=XM(1)
      EV(N)=XM(N)
      EK(1)=XK(1)
      EK(N)=XK(N)
      GO TO 502
  501 CONTINUE
      DO 499 J=1,N
      IF(CORIN.NE.0..AND.J.GT.IJ)GO TO 502
      K=N-J+1
      IF(CORIN.LE.0.)K=J
      EV(K)=XM(K)
  499 EK(K)=XK(K)
  502 CONTINUE
      RETURN
      END
      SUBROUTINE TEMP
C*************************TEMP FOR GASES  ************************************
      COMMON/XKEN/XKN1(101),XKN2(101),XKN3(101),PK(101),KOI,NJ1,NJ2,XDH
        COMMON/HHHH/H1,H2,H3,H4,H5,H6,H7,H8,H9,H10
      COMMON/XBIRTH/PREAD,PWRITE,STLF,XC1,XC2,DEL1,DEL2,UE,CHECK,REO
      COMMON/XNEW/TA1P,TA2P,HAVE1P,HAVE2P,T3PL1,T3PL2
      COMMON/PROBE/PTA,PTB,PTC,PTD
      COMMON/LATE/M,MM,N,NM1,NM2,NY,R1,R2,DYB(101),DYF(101),DYT(101),
     $Y(101),YF(101),YE(101),R(101)
      COMMON/MPVX/U1(101),U2(101),U3(101),V(101),EV(101),EK(101),EVF(101
     *),EVB(101),EKF(101),EKB(101),D1(101),D2(101),D3(101),C(101),NS,
```

```
      $ICCUNT,DELXF,DELXE,DELXT,DELPP,PDRCP,PC,PF
       COMMCN/VMP/PI,XMASS,DELPT
       COMMCN/AHMADI/T1(101),T2(101),T3(101),TW2,TW1,JTDEL,TBTHIC,DDRIN,
      $DTDYD,DTDYI,TCCNV,XKCCNV,TMEAN,XTMEAN,QCV,QCD,HAVE2,HAVE1
       COMMCN/DEL/JDEL,JDELI,JDELC,DELMIN,DELTAI,DELTAO,MN,DXF,VJS,VJF,
      $DXFM,CDC
       COMMCN/NAILA/THERK,CPVAR,DVAR,CVISC,DMEAN,CPMEAN,VMEAN,XKMEAN,
      $UO,VO,DO,TC,PSTART,HTK,CPCCN
       COMMCN/STUPID/LURT,NSM1,PSA,PSB,PSC,PSD,XCCNV,S1,S2
       COMMCN/UMM/FCCN,GG,BETA,UGF,FDV
       COMMCN/ENERGY/SQCV,SQCD,QI,TMEAN1,HAVE11,HAVE22
C    CALCULATES TEMP PRCFILE FOR THE BOUNDARY CONDITION OF ALL   KINDS
       IF(ICCUNT.NE.1)GC TO 202
       QI=0.
       SQCV=0.0
       SQCD=0.0
       TMEAN1=TC/TCCNV
       HAVE11=0.01
       HAVE22=0.01
       IF(DDRIN.LT.0.)HAVE11=0.
       IF(DDRIN.GT.0.)HAVE22=0.
       IF(TW1.LT.0.0)HAVE11=ABS(TW1)/((T1(N)-TMEAN1)*TCCNV)
       IF(TW2.LT.0.0)HAVE22=ABS(TW2)/((T1(1)-TMEAN1)*TCCNV)
   202 CCNTINUE
       IF(ICCUNT.GE.NS)GC TO 550
C    STAND EXPL EQNS
       DO 505 JJJ=2,NM1
       IF(DDRIN.LE.0.)GO TO 720
       J=N-JJJ+1
       JPL=J-1
       JML=J+1
       GC TC 722
   720 J=JJJ
       JPL=J+1
       JML=J-1
   722 DFY=Y(J)-Y(JPL)
       DBY=Y(JML)-Y(J)
       DTY=Y(JML)-Y(JPL)
       TF=2.0*Y(J)*DFY*DEY*DTY
       TA=TF*D1(J)*U1(J)*C(J)
       TB1=DELXF*   DBY          *(Y(J)+Y(JPL))*(EK(J)+EK(JPL))*(T1(JPL)-T1(
      $J))
       TB2=DELXF*    DFY         *(Y(J)+Y(JML))*(EK(J)+EK(JML))*(T1(JML)-T1(
      $J))
       VVPP=V(J)
       TB3=TF*DELXF*D1(J)*VVPP*C(J)*(T1(JML)-T1(J))/DBY
       TB4=TA*T1(J)
       TC1=-TF*U1(J)*DELPP
       TC2=TF*DELXF*EV(J)*(ABS((U1(J)-U1(JML))/DBY))**2
       T2(J)=(TB1+TB2+TB3+TB4+TC1+TC2)/TA
       T3(J)=T2(J)
        IF(DDRIN.EG.0.)GC TO 505
       IF(J.EG.2.CR.J.EG.NM1)GO TO 505
       X=T2(J)/T2(JML)
       IF(X.GE.0.99999)GC TO 574
   505 CCNTINUE
       GC TC 784
   550 CCNTINUE
C    C-F EQNS
       BBB=2.*DELXB/DELXT
```

```
      AAA=2.*DELXF/DELXT
      DO 560 JJJ=2,NM1
      IF(ICCRIN.LE.0.)GO TO 740
      J=N-JJJ+1
      JPL=J-1
      JML=J+1
      GO TO 742
  740 J=JJJ
      JPL=J+1
      JML=J-1
  742 DFY=Y(J)-Y(JPL)
      DBY=Y(JML)-Y(J)
      DTY=Y(JML)-Y(JPL)
      TF=4.0*Y(J)*DFY*DBY*DTY
      TA1=TF*D2(J)*U2(J)*C(J)
      TA2=DELXT*(Y(J)+Y(JPL))*(EK(J)+EK(JPL))*DBY*BBB
      TA3=DELXT*(Y(J)+Y(JML))*(EK(J)+EK(JML))*DFY*BBB
      TB1=DELXT*(Y(J)+Y(JPL))*(EK(J)+EK(JPL))*   DBY          *(2.0*T2(JPL)
     *-T1(J)*AAA)
      TB2=DELXT*(Y(J)+Y(JML))*(EK(J)+EK(JML))*    DFY         *(2.0*T2(JML)
     $-T1(J)*AAA)
      VVFF=V(J)
      TB3=DELXT*D2(J)*VVFP*C(J)*TF*(T2(JML)-T2(JPL))/DTY
      TB4=TA1*T1(J)
      TC1=-TF*U2(J)*DELFT
      TC2=TF*DELXT*EV(J)*(ABS((U2(JPL)-U2(JML))/DTY))**2
      T3(J)=(TB1+TB2+TB3+TB4+TC1+TC2)/(TA1+TA2+TA3)
       IF(ICCRIN.EG.0.)GO TO 560
      IF(J.EQ.2.OR.J.EQ.NM1)GO TO 560
      IF(TETHIC.GE.0.8*(R2-R1))GO TO 560
      X=T3(J)/T3(JML)
      IF(X.GE.0.99999)GO TO 574
  560 CONTINUE
  784 JTDEL=J
      TBTHIC=(R2-R1)
      GO TO 599
  574 JTDEL=J
      IF(ICCRIN.LT.0.0)GO TO 760
      TBTHIC=Y(JTDEL)-R1
      JJ=JTDEL-1
      DO 575 J=2,JJ
      IF(ICCUNT.LT.NS)T2(J)=TC/TCONV
  575 T3(J)=TC/TCONV
      GO TO 599
  760 JTDEL=J
      TBTHIC=R2-Y(JTDEL)
      JJ=JTDEL+1
      DO 580 J=JJ,NM1
      IF(ICCUNT.LT.NS)T2(J)=TC/TCONV
  580 T3(J)=TC/TCONV
  599 CONTINUE
      IF(ICCUNT.EQ.NSM1)GO TO 828
      DO 830 J=2,NM1
      T1(J)=T2(J)
  830 T2(J)=T3(J)
  828 IF(TW2.GT.0.0)GO TO 829
      DTDYO=TW2*XCONV/(EK(1)*XKCONV*TCONV)
      IF(ICCUNT.GE.NS)T1(1)=T2(1)
      T3(1)=(DTDYO-T3(2)*PSB-T3(3)*PSC-T3(4)*PSD)/PSA
      T3FL2=T3(1)
```

```
C     ***ST LINE FIT***
      T3(1)=T3(2)-DTDYO*DYF(1)
      T3SL2=T3(1)
      IF(STLF.LT.0.)T3(1)=T3PL2
      IF(STLF.LT.0.)T3PL2=T3SL2
      T2(1)=T3(1)
      IF(ICOUNT.LT.NSM1)T1(1)=T2(1)
  825 IF(TW1.GT.0.0)GO TO 831
      DTDYI=TW1*XCONV/(EK(N)*XKCONV*TCONV)
      IF(ICOUNT.GE.NS)T1(N)=T2(N)
      T3(N)=(DTDYI-T3(NM1)*PTB-T3(NM2)*PTC-T3(N-3)*PTD)/PTA
      T3PL1=T3(N)
C     ***ST LINE FIT***
      T3(N)=T3(NM1)-DTDYI*DYE(N)
      T3SL1=T3(N)
      IF(STLF.LT.0.)T3(N)=T3PL1
      IF(STLF.LT.0.)T3PL1=T3SL1
      T2(N)=T3(N)
      IF(ICOUNT.LT.NSM1)T1(N)=T2(N)
  831 CONTINUE
      S1=0.0
      S2=0.0
      DO 900 J=1,NM2,2
      WF2=DYT(J+1)/DYF(J+1)*(DYT(J+1)/3.0-DYB(J+1)/2.0)
      WF1=DYT(J+1)**2.0/(2.0*DYB(J+1))-WF2*DYT(J+1)/DYB(J+1)
      WF0=DYT(J+1)-WF1-WF2
      SUM1=C(J)*D3(J)*U3(J)*Y(J)
      SUM2=C(J+1)*D3(J+1)*U3(J+1)*Y(J+1)
      SUM3=C(J+2)*D3(J+2)*U3(J+2)*Y(J+2)
      SUM11=SUM1*T3(J)
      SUM22=SUM2*T3(J+1)
      SUM33=SUM3*T3(J+2)
      S1=S1+WF0*SUM1+WF1*SUM2+WF2*SUM3
  900 S2=S2+WF0*SUM11+WF1*SUM22+WF2*SUM33
      TMEAN=S2/S1
      XTMEAN=TMEAN*TCONV
      QC=2.0*PI*S2
      IF(TW2.LT.0.0)HAVE2=ABS(TW2)/((T3(1)-TMEAN)*TCONV)
      IF(TW2.LT.0.)HAVE2P=ABS(TW2)/((T3PL2-TMEAN)*TCONV)
      IF(TW2.EQ.0.)HAVE2=0.
      IF(TW2.EQ.0.)HAVE2P=0.
      IF(TW2.LE.0.0)GO TO 903
      DTDYO=PSA*T3(1)+PSB*T3(2)+PSC*T3(3)+PSD*T3(4)
      HAVE2P=-EK(1)*XKCONV*DTDYO/(XCONV*(T3(1)-TMEAN))
C     ***ST LINE FIT***
      DTDYO=(T3(2)-T3(1))/DYF(1)
      HAVE2=-EK(1)*XKCONV*DTDYO/(XCONV*(T3(1)-TMEAN))
      HAVE2S=HAVE2
      IF(STLF.LT.0.)HAVE2=HAVE2P
      IF(STLF.LT.0.)HAVE2P=HAVE2S
      IF(HAVE2.LT.0.0)HAVE2=0.0
  903 CONTINUE
      IF(TW1.LT.0.0)HAVE1=ABS(TW1)/((T3(N)-TMEAN)*TCONV)
      IF(TW1.LT.0.)HAVE1P= ABS(TW1)/((T3PL1-TMEAN)*TCONV)
      IF(TW1.EQ.0.)HAVE1=0.
      IF(TW1.EQ.0.)HAVE1P=0.
      IF(TW1.LE.0.0)GO TO 902
      DTDYI=PTA*T3(N)+PTB*T3(NM1)+PTC*T3(NM2)+PTD*T3(N-3)
      HAVE1P=-EK(N)*XKCONV*DTDYI/(XCONV*(T3PL1-TMEAN))
C     ***ST LINE FIT***
```

```
      DTDYI=(T3(NM1)-T3(N))/DYB(N)
      HAVE1=-EK(N)*XKCONV*DTDYI/(XCONV*(T3(N)-TMEAN))
      HAVE1S=HAVE1
      IF(STLF.LT.0.)HAVE1=HAVE1P
      IF(STLF.LT.0.)HAVE1P=HAVE1S
      IF(HAVE1.LT.0.0)HAVE1=0.0
  902 CONTINUE
      QW2=(HAVE2+HAVE22)*(T3(1)+T1(1)-TMEAN-TMEAN1)*R2
      QW1=(HAVE1+HAVE11)*(T3(N)+T1(N)-TMEAN-TMEAN1)*R1
      QCV=(GC-GI)*XKCONV*XCONV*TCONV
      QCD=PI*DELXF*(QW1+QW2)*TCONV*XCONV*XCONV/2.0
      IF(ICOUNT.EQ.1)QCV=QCD
      SQCV=SQCV+QCV
      SQCD=SQCD+QCD
      HAVE11=HAVE1
      HAVE22=HAVE2
      QI=QC
      TMEAN1=TMEAN
      RETURN
      END
      FUNCTION FBETA(TT,TCONV,TO)
C     BETA FOR AIR
C      UNITS 1/F
      FBETA=1./(TT*TCONV)
      RETURN
      END
      FUNCTION THCNL(TT,TCONV,TO,XKCONV)
C**   THERMAL CONDUCTIVITY FOR AIR
C       UNITS=DIMENSIONLESS
      DATA Z1,Z2,Z3/1.52518E-03,245.4,12./
      T=TT*TCONV/1.8
      THCNL=Z1*SQRT(T)/((1.+Z2*10.**(-Z3/T)/T)*3600.*XKCONV)
      RETURN
      END
      FUNCTION RHO(TT,TCONV,TC,DO)
C **  DENSITY OF AIR
C       UNITS=DIMENSIONLESS
      RHO=TC/(TT*TCONV)
      RETURN
      END
      FUNCTION VISC(TT,TCONV,TO,VO)
C  ****  VISCOSITY OF AIR
C       UNITS=DIMENSIONLESS
      DATA Z1,Z2/0.97569E-06,110.4/
      T=TT*TCONV/1.8
      VISC=Z1*SQRT(T)/((1.+Z2/T)*VO)
      RETURN
      END
      FUNCTION CP(TT,TCONV,TC,CPCON)
C  ***** SPECIFIC HEAT OF AIR
C       UNITS=DIMENSIONLESS
      DATA Z1/0.05/
      CP=(TT*TCONV/TC)**Z1
      RETURN
      END
      SUBROUTINE TEMP
C*************************TEMP FOR ETHYLENE  GLYCOL*******************************
      COMMON/XKEN/XKN1(101),XKN2(101),XKN3(101),PK(101),KOI,NJ1,NJ2,XDH
        COMMON/HHHH/H1,H2,H3,H4,H5,H6,H7,H8,H9,H10
      COMMON/XBIRTH/PREAD,PWRITE,STLF,XC1,XC2,DEL1,DEL2,UE,CHECK,RED
```

```
      COMMON/XNEW/TA1P,TA2P,HAVE1P,HAVE2P,T3PL1,T3PL2
      COMMON/PRCBE/PTA,PTE,PTC,PTD
      COMMON/LATE/M,MM,N,NM1,NM2,NY,R1,R2,DYB(101),DYF(101),DYT(101),
     $Y(101),YF(101),YE(101),R(101)
      COMMON/MPVX/U1(101),U2(101),U3(101),V(101),EV(101),EK(101),EVF(101
     *),EVE(101),EKF(101),EKB(101),D1(101),D2(101),D3(101),C(101),NS,
     $ICOUNT,DELXF,DELXB,DELXI,DELPP,PDRCP,PC,PP
      COMMON/VMP/PI,XMASS,DELPT
      COMMON/AHMADI/T1(101),T2(101),T3(101),TW2,TW1,JTDEL,TBTHIC,DORIN,
     $DTDYC,DTDYI,TCONV,XKCONV,TMEAN,XTMEAN,GCV,QCD,HAVE2,HAVE1
      COMMON/DEL/JDEL,JDEL1,JDELC,DELMIN,DELTAI,DELTAG,MN,DXF,VJS,VJF,
     $DXFM,CDC
      COMMON/NAILA/THERK,CPVAR,DVAR,CVISC,DMEAN,CPMEAN,VMEAN,XKMEAN,
     $UO,VO,DO,TC,PSTART,HTK,CPCON
      COMMON/STUPID/LORT,NSM1,PSA,PSE,PSC,PSD,XCONV,S1,S2
      COMMON/UNM/FCON,GC,BETA,UGF,FDV
      COMMON/ENERGY/SQCV,SQCD,QI,TMEAN1,HAVE11,HAVE22
C   CALCULATES TEMP PROFILE FOR THE BOUNDARY CONDITION OF ALL   KINDS
      IF(ICOUNT.NE.1)GO TO 202
      QI=0.
      SQCV=0.0
      SQCD=0.0
      TMEAN1=TC/TCONV
      HAVE11=0.01
      HAVE22=0.01
      IF(DORIN.LT.0.)HAVE11=0.
      IF(DORIN.GT.0.)HAVE22=0.
      IF(TW1.LT.0.0)HAVE11=ABS(TW1)/((T1(N)-TMEAN1)*TCONV)
      IF(TW2.LT.0.0)HAVE22=ABS(TW2)/((T1(1)-TMEAN1)*TCONV)
  202 CONTINUE
      IF(ICOUNT.GE.NS)GO TO 550
C   STAND EXPL EQNS
      DO 505 JJJ=2,NM1
      IF(DORIN.LE.0.)GO TO 720
      J=N-JJJ+1
      JPL=J-1
      JML=J+1
      GO TO 722
  720 J=JJJ
      JPL=J+1
      JML=J-1
  722 DFY=Y(J)-Y(JPL)
      DBY=Y(JML)-Y(J)
      DTY=Y(JML)-Y(JPL)
      TF=2.0*Y(J)*DFY*DBY*DTY
      TA=TF*D1(J)*U1(J)*C(J)
      TB1=DELXF*   DBY          *(Y(J)+Y(JPL))*(EK(J)+EK(JPL))*(T1(JPL)-T1(
     $J))
      TB2=DELXF*    DFY         *(Y(J)+Y(JML))*(EK(J)+EK(JML))*(T1(JML)-T1(
     $J))
      VVPP=V(J)
      TB3=TF*DELXF*D1(J)*VVPP*C(J)*(T1(JML)-T1(J))/DBY
      TB4=TA*T1(J)
      TC1=0.
      TC2=TF*DELXF*EV(J)*(ABS((U1(J)-U1(JML))/DBY))**2
      T2(J)=(TB1+TB2+TB3+TB4+TC1+TC2)/TA
      T3(J)=T2(J)
       IF(DORIN.EQ.0.)GO TO 505
      IF(J.EQ.2.OR.J.EQ.NM1)GO TO 505
      X=T2(J)/T2(JML)
```

```
      IF(X.GE.0.99999)GO TO 574
  505 CONTINUE
      GO TO 784
  550 CONTINUE
C     C-F EQNS
      BBB=2.*DELXB/DELXT
      AAA=2.*DELXF/DELXT
      DO 560 JJJ=2,NM1
      IF(CORIN.LE.0.)GO TO 740
      J=N-JJJ+1
      JPL=J-1
      JML=J+1
      GO TO 742
  740 J=JJJ
      JPL=J+1
      JML=J-1
  742 DFY=Y(J)-Y(JPL)
      DBY=Y(JML)-Y(J)
      DTY=Y(JML)-Y(JPL)
      TF=4.0*Y(J)*DFY*DEY*DTY
      TA1=TF*D2(J)*U2(J)*C(J)
      TA2=DELXT*(Y(J)+Y(JPL))*(EK(J)+EK(JPL))*DEY*BBB
      TA3=DELXT*(Y(J)+Y(JML))*(EK(J)+EK(JML))*DFY*BBB
      TB1=DELXT*(Y(J)+Y(JPL))*(EK(J)+EK(JPL))*  DBY          *(2.0*T2(JPL)
     *-T1(J)*AAA)
      TB2=DELXT*(Y(J)+Y(JML))*(EK(J)+EK(JML))*    DFY        *(2.0*T2(JML)
     $-T1(J)*AAA)
      VVPP=V(J)
      TB3=DELXT*D2(J)*VVPP*C(J)*TF*(T2(JML)-T2(JPL))/DTY
      TB4=TA1*T1(J)
      TC1=0.
      TC2=TF*DELXT*EV(J)*(ABS((U2(JPL)-U2(JML))/DTY))**2
      T3(J)=(TB1+TB2+TB3+TB4+TC1+TC2)/(TA1+TA2+TA3)
       IF(CORIN.EQ.0.)GO TO 560
      IF(J.EQ.2.OR.J.EQ.NM1)GO TO 560
      IF(TETHIC.GE.0.8*(R2-R1))GO TO 560
      X=T3(J)/T3(JML)
      IF(X.GE.ABS(VJS))GO TO 574
  560 CONTINUE
  784 JTDEL=J
      TETHIC=(R2-R1)
      GO TO 599
  574 JTDEL=J
      IF(CORIN.LT.0.0)GO TO 760
      TETHIC=Y(JTDEL)-R1
      JJ=JTDEL-1
      DO 575 J=2,JJ
      IF(ICOUNT.LT.NS)T2(J)=TC/TCONV
  575 T3(J)=TC/TCONV
      GO TO 599
  760 JTDEL=J
      TETHIC=R2-Y(JTDEL)
      JJ=JTDEL+1
      DO 580 J=JJ,NM1
      IF(ICOUNT.LT.NS)T2(J)=TC/TCONV
  580 T3(J)=TC/TCONV
  599 CONTINUE
      IF(ICOUNT.EQ.NSM1)GO TO 828
      DO 830 J=2,NM1
      T1(J)=T2(J)
```

```
  830 T2(J)=T3(J)
  828 IF(TW2.GT.0.0)GO TO 829
      DTDYC=TW2*XCONV/(EK(1)*XKCONV*TCONV)
      IF(ICOUNT.GE.NS)T1(1)=T2(1)
      T3(1)=(DTDYC-T3(2)*PSB-T3(3)*PSC-T3(4)*PSD)/PSA
      T3PL2=T3(1)
C     ***ST LINE FIT***
      T3(1)=T3(2)-DTDYC*DYF(1)
      T3SL2=T3(1)
      IF(STLF.LT.0.)T3(1)=T3PL2
      IF(STLF.LT.0.)T3PL2=T3SL2
      T2(1)=T3(1)
      IF(ICOUNT.LT.NSM1)T1(1)=T2(1)
  829 IF(TW1.GT.0.0)GO TO 831
      DTDYI=TW1*XCONV/(EK(N)*XKCONV*TCONV)
      IF(ICOUNT.GE.NS)T1(N)=T2(N)
      T3(N)=(DTDYI-T3(NM1)*PTB-T3(NM2)*PTC-T3(N-3)*PTD)/PTA
      T3PL1=T3(N)
C     ***ST LINE FIT***
      T3(N)=T3(NM1)-DTDYI*DYB(N)
      T3SL1=T3(N)
      IF(STLF.LT.0.)T3(N)=T3PL1
      IF(STLF.LT.0.)T3PL1=T3SL1
      T2(N)=T3(N)
      IF(ICOUNT.LT.NSM1)T1(N)=T2(N)
  831 CONTINUE
      DO 800 J=1,N
      TT=(T3(J)*TCONV-520.)/80.
  800 XKN3(J)=(27.4786+44.24*TT+1.66*TT**2+0.09333*TT**3)/(TCONV*CPCON)
      S1=0.0
      S2=0.0
      DO 900 J=1,NM2,2
      WF2=DYT(J+1)/DYF(J+1)*(DYT(J+1)/3.0-DYB(J+1)/2.0)
      WF1=DYT(J+1)**2.0/(2.0*DYB(J+1))-WF2*DYT(J+1)/DYB(J+1)
      WF0=DYT(J+1)-WF1-WF2
      SUM1=D3(J)*U3(J)*Y(J)
      SUM2=D3(J+1)*U3(J+1)*Y(J+1)
      SUM3=D3(J+2)*U3(J+2)*Y(J+2)
      SUM11=SUM1*XKN3(J)
      SUM22=SUM2*XKN3(J+1)
      SUM33=SUM3*XKN3(J+2)
      S1=S1+WF0*SUM1+WF1*SUM2+WF2*SUM3
  900 S2=S2+WF0*SUM11+WF1*SUM22+WF2*SUM33
      HBULK=S2/S1
      XHBULK=HBULK*TCONV*CPCON
      H3=XHBULK
      A1=1.66/0.09333
      A2=44.24/0.09333
      A3=(27.4786-XHBULK)/0.09333
      QQ=(3.*A2-A1**2)/9.
      RR=(9.*A1*A2-27.*A3-2.*A1**3)/54.
      DS=SQRT(QQ**3+RR**2)
      SS=(DS+RR)**(1./3.)
      TT=-(DS-RR)**(1./3.)
      XTT=SS+TT-A1/3.
      XTMEAN=XTT*80.+520.
      TMEAN=XTMEAN/TCONV
      QQ=2.0*PI*S2
      IF(TW2.LT.0.0)HAVE2=ABS(TW2)/((T3(1)-TMEAN)*TCONV)
      IF(TW2.LT.0.)HAVE2F=ABS(TW2)/((T3PL2-TMEAN)*TCONV)
```

```
      IF(TW2.EQ.0.)HAVE2=0.
      IF(TW2.EQ.0.)HAVE2P=0.
      IF(TW2.LE.0.0)GO TO 903
      DTDYO=PSA*T3(1)+PSB*T3(2)+PSC*T3(3)+PSD*T3(4)
      HAVE2P=-EK(1)*XKCONV*DTDYO/(XCONV*(T3(1)-TMEAN))
C     ***ST LINE FIT***
      DTDYO=(T3(2)-T3(1))/DYF(1)
      HAVE2=-EK(1)*XKCONV*DTDYO/(XCONV*(T3(1)-TMEAN))
      HAVE2S=HAVE2
      IF(STLF.LT.0.)HAVE2=HAVE2P
      IF(STLF.LT.0.)HAVE2P=HAVE2S
      IF(HAVE2.LT.0.0)HAVE2=0.0
  903 CONTINUE
      IF(TW1.LT.0.0)HAVE1=ABS(TW1)/((T3(N)-TMEAN)*TCONV)
      IF(TW1.LT.0.)HAVE1P= ABS(TW1)/((T3PL1-TMEAN)*TCONV)
      IF(TW1.EQ.0.)HAVE1=0.
      IF(TW1.EQ.0.)HAVE1P=0.
      IF(TW1.LE.0.0)GO TO 902
      DTDYI=PTA*T3(N)+PTB*T3(NM1)+PTC*T3(NM2)+PTD*T3(N-3)
      HAVE1P=-EK(N)*XKCONV*DTDYI/(XCONV*(T3PL1-TMEAN))
C     ***ST LINE FIT***
      DTDYI=(T3(NM1)-T3(N))/DYB(N)
      HAVE1=-EK(N)*XKCONV*DTDYI/(XCONV*(T3(N)-TMEAN))
      HAVE1S=HAVE1
      IF(STLF.LT.0.)HAVE1=HAVE1P
      IF(STLF.LT.0.)HAVE1P=HAVE1S
      IF(HAVE1.LT.0.0)HAVE1=0.0
  902 CONTINUE
      QW2=(HAVE2+HAVE22)*(T3(1)+T1(1)-TMEAN-TMEAN1)*R2
      QW1=(HAVE1+HAVE11)*(T3(N)+T1(N)-TMEAN-TMEAN1)*R1
      QCV=(GC-GI)*XKCONV*XCONV*TCONV
      QCD=PI*DELXF*(QW1+QW2)*TCONV*XCONV*XCONV/2.0
      IF(ICOUNT.EQ.1)QCV=QCD
      SQCV=SQCV+QCV
      SQCD=SQCD+QCD
      HAVE11=HAVE1
      HAVE22=HAVE2
      QI=QO
      TMEAN1=TMEAN
      RETURN
      END
      FUNCTION FBETA(TT,TCONV,TO)
C             COEFFICIENT OF THERMAL EXPANSION AS A FUNCTION OF
C             TEMPERATURE (F) FOR ETHELENE GLYCOL
C                       UNITS 1/F
      DATA X1,X2,X3,X4 /0.924848,6.2796E-04,9.2444E-07,3.057E-09/
      TC=(TMEAN*TCONV-492.)/1.8
      DT   = TC-65.00
      VOL  =((X4*DT+X3)*DT+X2)*DT+X1
      DVOL = (3.0*X4*DT+2.0*X3)*DT+X2
      FBETA= DVOL/(1.8*VOL)
      RETURN
      END
      FUNCTION THCNL(TT,TCONV,TO,XKCONV)
C             THERMAL CONDUCTIVITY AS A FUNCTION OF TEMPERATURE (F)
C                       UNITS = DIMENSIONLESS
      DATA X1,X2 /0.1825,-2.3E-04/
      T=TT*TCONV-460.
      THCNL =(X1+X2*T)/(XKCONV*3600.)
      RETURN
```

```
      END
      FUNCTION RHO (TT,TCONV,TO,DO)
C             DENSITY AS A FUNCTION OF TEMPERATURE (F) FOR ETHELENE GLYCOL
C                        UNITS = DIMENSIONLESS
      DATA X1,X2,X3,X4 /0.924846,6.2796E-04,9.2444E-07,3.057E-09/
      TC=(TT*TCONV-492.)/1.8
      DT   = TC-65.0
      VOL  =((X4*DT+X3)*DT+X2)*DT+X1
      RHO  = 62.43/(VOL*DO)
      RETURN
      END
      FUNCTION VISC (TT,TCONV,TC,VO)
C             VISCOSITY AS A FUNCTION OF TEMPERATURE (F) FOR
C             ETHELENE GLYCOL
C                        UNITS = DIMENSIONLESS
      DATA X1,X2,X3,X4,X5 /3.80666,-1.798086,0.385912,-0.05878,0.004173/
     1,TO,DT /40.0,60.0/
      THETA=(TT*TCONV-460.-TC)/DT
      VISC  = 2.42*EXP((((X5*THETA+X4)*THETA+X3)*THETA+X2)*THETA+X1)/
     $(VC*3600.)
      RETURN
      END
      FUNCTION  CP(TT,TCONV,TO,CPCON)
C   SPECIFIC  HEAT AS A FUNCTION OF TEMPERATURE(F) FOR  FLUID
C                              ETHYLENE GLYCOL
C                        UNITS = DIMENSIONLESS
      ETA=(TT*TCONV-520.)/80.
      CP=(0.953+0.0415C*ETA+0.0035*ETA*ETA)/CPCON
      RETURN
      END
```

XVI. APPENDIX H: TABULATION OF SOME TYPICAL TEST CASES

Table H.1. Prediction of flow development in an annulas ($r^* = 0.99$, $D_h = 24.38$ mm) at $Re = 2 \times 10^5$ using Model A

$\frac{x}{D_h}$	$\frac{u}{u_b}$	$C_f \times 10^3$	$\frac{4\delta^*}{D_h}$	$\frac{4\theta}{D_h}$
0.5	1.012	4.607	0.0116	0.0060
1.0	1.019	4.402	0.0181	0.0106
2.0	1.031	4.130	0.0297	0.0190
3.0	1.042	3.994	0.0400	0.0266
4.0	1.052	3.928	0.0492	0.0335
5.0	1.062	3.884	0.0582	0.0403
6.0	1.071	3.864	0.0663	0.0465
7.0	1.080	3.852	0.0742	0.0526
8.0	1.089	3.849	0.0817	0.0583
9.0	1.097	3.853	0.0883	0.0635
10.0	1.105	3.859	0.0954	0.0690
11.0	1.114	3.870	0.1021	0.0743
12.0	1.122	3.883	0.1084	0.0792
13.0	1.129	3.898	0.1141	0.0837
14.0	1.132	3.914	0.1202	0.0885
15.0	1.145	3.936	0.1263	0.0934
16.0	1.152	3.954	0.1320	0.0980
17.0	1.159	3.976	0.1359	0.1012
18.0	1.164	3.994	0.1410	0.1052

Table H.1 (Continued)

$\frac{x}{D_h}$	$\frac{u}{u_b}$	$C_f x 10^3$	$\frac{4\delta^*}{D_h}$	$\frac{4\theta}{D_h}$
19.0	1.164	4.018	0.1411	0.1056
20.0	1.162	4.043	0.1399	0.1051
21.1	1.160	4.068	0.1382	0.1042
22.1	1.157	4.091	0.1360	0.1029
23.0	1.154	4.116	0.1336	0.1014
24.0	1.150	4.140	0.1311	0.0999
25.0	1.147	4.159	0.1287	0.0984
26.2	1.144	4.181	0.1262	0.0967
28.6	1.138	4.216	0.1216	0.0937
32.0	1.133	4.248	0.1174	0.0909
35.1	1.130	4.264	0.1152	0.0894
40.1	1.127	4.277	0.1134	0.0882
46.8	1.126	4.283	0.1126	0.0876

Table H.2. Prediction of local Stanton number for hydrodynamically developed flow through an annulus ($r^* = 0.68$, $D_h = 12.2$ mm) for Re = 20000, $\dot{q}_1 = 2582$ W/m^2, $\dot{q}_2 = 0$

$\frac{x}{D_h}$	St x 10^3	
	Model A	Model B
1.0	5.900	5.901
2.0	5.134	5.144
3.0	4.825	4.871
4.0	4.665	4.704
5.0	4.550	4.596
6.0	4.446	4.501
7.0	4.380	4.422
8.0	4.315	4.352
9.0	4.255	4.298
10.0	4.195	4.252
11.0	4.147	4.201
12.0	4.094	4.161
13.0	4.052	4.124
14.0	4.014	4.092
15.0	3.979	4.063
16.0	3.943	4.036
18.0	3.886	3.992
20.0	3.835	3.962
22.0	3.785	3.940

Table H.2 (Continued)

$\frac{x}{D_h}$	St x 10^3	
	Model A	Model B
25.0	3.725	3.916
30.0	3.638	3.888
35.0	3.571	3.875

Table H.3 Predicted temperature profile in an annulus ($r^* = 0.556$, $D_h = 76.2$mm) at $x/D_h = 33$ using Model B; Re = 32285, $\dot{q}_1 = 0$, $\dot{q}_2 = 1220\ W/m^2$, inlet temperature = 36.31°C.

$\frac{r-r_1}{r_2-r_1}$	Temperature (°C)	$\frac{r-r_1}{r_2-r_1}$	Temperature (°C)
0.0	40.73	0.4683×10^{-1}	40.90
0.6989×10^{-3}	40.73	0.5338×10^{-1}	40.90
0.1485×10^{-2}	40.73	0.6075×10^{-1}	40.95
0.2370×10^{-2}	40.73	0.6904×10^{-1}	41.01
0.3365×10^{-2}	40.73	0.7837×10^{-1}	41.06
0.4485×10^{-2}	40.73	0.8887×10^{-1}	41.12
0.5745×10^{-2}	40.73	0.1007	41.17
0.7162×10^{-2}	40.73	0.1140	41.23
0.8756×10^{-2}	40.73	0.1289	41.34
0.1055×10^{-1}	40.73	0.1457	41.40
0.1257×10^{-1}	40.73	0.1646	41.56
0.1484×10^{-1}	40.73	0.1859	41.73
0.1739×10^{-1}	40.73	0.2098	41.90
0.2026×10^{-1}	40.78	0.2368	42.17
0.2350×10^{-1}	40.78	0.2637	42.51
0.2713×10^{-1}	40.78	0.2941	42.90
0.3122×10^{-1}	40.78	0.3246	43.34
0.3582×10^{-1}	40.84	0.3550	43.78
0.4100×10^{-1}	40.84	0.3855	44.34

Table H.3 cont.

$\frac{r-r_1}{r_2-r_1}$	Temperature (°C)	$\frac{r-r_1}{r_2-r_1}$	Temperature (°C)
0.4159	44.90	0.9305	63.67
0.4464	45.56	0.9390	64.56
0.4768	46.23	0.9465	65.56
0.5073	46.95	0.9531	66.56
0.5377	47.73	0.9590	67.62
0.5682	48.56	0.9643	68.78
0.5986	49.45	0.9690	70.06
0.6291	50.40	0.9731	71.45
0.6595	51.40	0.9768	72.95
0.6900	52.45	0.9801	74.56
0.7204	53.51	0.9830	76.34
0.7509	54.67	0.9856	78.28
0.7813	55.84	0.9879	80.28
0.8118	57.06	0.9900	82.45
0.8334	58.01	0.9918	84.67
0.8526	58.78	0.9934	86.78
0.8697	59.56	0.9949	88.84
0.8849	60.34	0.9962	90.73
0.8984	61.17	0.9973	92.40
0.9104	61.95	0.9983	93.90
0.9210	62.78	0.9992	95.23
		1.000	96.40

Table H.4 Predicted fully developed velocity profile in an annulus ($r^* = 0.25$, $D_h = 170.4$ mm) using Model B; Re = 215,000, $u_b = 21.22$ m/sec

$\frac{r-r_1}{r_2-r_1}$	$\frac{u}{u_b}$	$\frac{r-r_1}{r_2-r_1}$	$\frac{u}{u_b}$
0.0000	0.0000	0.9655×10^{-2}	0.7484
0.1157×10^{-3}	0.0310	0.1117×10^{-1}	0.7681
0.2481×10^{-3}	0.0665	0.1291×10^{-1}	0.7869
0.3998×10^{-3}	0.1070	0.1489×10^{-1}	0.8050
0.5743×10^{-3}	0.1528	0.1717×10^{-1}	0.8226
0.7723×10^{-3}	0.2039	0.1977×10^{-1}	0.8397
0.1000×10^{-2}	0.2592	0.2275×10^{-1}	0.8563
0.1261×10^{-2}	0.3164	0.2617×10^{-1}	0.8728
0.1559×10^{-2}	0.3728	0.3008×10^{-1}	0.8889
0.1901×10^{-2}	0.4261	0.3456×10^{-1}	0.9049
0.2292×10^{-2}	0.4750	0.3968×10^{-1}	0.9205
0.2740×10^{-2}	0.5192	0.4555×10^{-1}	0.9360
0.3253×10^{-2}	0.5587	0.5227×10^{-1}	0.9511
0.3841×10^{-2}	0.5942	0.5997×10^{-1}	0.9660
0.4513×10^{-2}	0.6261	0.6878×10^{-1}	0.9807
0.5283×10^{-2}	0.6548	0.7887×10^{-1}	0.9949
0.6165×10^{-2}	0.6811	0.9042×10^{-1}	1.0087
0.7175×10^{-2}	0.7051	0.1036	1.0222
0.8331×10^{-2}	0.7275	0.1188	1.0351

Table H.4 cont.

$\frac{r-r_1}{r_2-r_1}$	$\frac{u}{u_b}$	$\frac{r-r_1}{r_2-r_1}$	$\frac{u}{u_b}$
0.1361	1.0475	0.7605	0.9956
0.1560	1.0598	0.7915	0.9771
0.1787	1.0725	0.8226	0.9573
0.2014	1.0832	0.8452	0.9423
0.2325	1.0953	0.8650	0.9284
0.2636	1.1048	0.8882	0.9148
0.2946	1.1117	0.8973	0.9010
0.3257	1.1161	0.9104	0.8871
0.3567	1.1184	0.9219	0.8728
0.3878	1.1187	0.9320	0.8586
0.4188	1.1170	0.9407	0.8442
0.4499	1.1136	0.9484	0.8297
0.4810	1.1082	0.9551	0.8151
0.5120	1.1013	0.9609	0.8003
0.5431	1.0929	0.9660	0.7855
0.5741	1.0830	0.9705	0.7704
0.6052	1.0716	0.9744	0.7553
0.6362	1.0588	0.9778	0.7400
0.6673	1.0449	0.9807	0.7243
0.6984	1.0297	0.9833	0.7084
0.7294	1.0133	0.9856	0.6920

Table H.4 cont.

$\frac{r - r_1}{r_2 - r_1}$	$\frac{u}{u_b}$	$\frac{r - r_1}{r_2 - r_1}$	$\frac{u}{u_b}$
0.9876	0.6749	0.9977	0.4010
0.9893	0.6571	0.9981	0.3522
0.9908	0.6381	0.9985	0.2983
0.9921	0.6179	0.9988	0.2412
0.9933	0.5959	0.9991	0.1841
0.9943	0.5719	0.9994	0.1301
0.9951	0.5442	0.9996	0.0811
0.9959	0.5158	0.9998	0.0379
0.9966	0.4823	1.0000	0.0000
0.9972	0.4442		

Table H.5 Predicted distribution of skin-friction parameter for upward laminar flow of ethylene glycol in an annulus ($r^* = 0.99$, $D_h = 22.23$ mm) with inner wall heated ($Gr/Re^2 = 110$)

x_b^+	$\frac{C_{f_1} Re_b}{24}$	$\frac{C_{f_2} Re_b}{24}$	$\frac{C_f Re_b}{24}$
0.0001	1.104	0.958	1.030
0.0002	1.153	0.937	1.048
0.0005	1.269	0.894	1.081
0.001	1.388	0.840	1.113
0.002	1.571	0.753	1.161
0.005	1.999	0.543	1.269
0.007	2.233	0.423	1.326
0.01	2.644	0.202	1.420